Lodz University of Technology

Faculty of Civil Engineering, Architecture and Environmental Engineering
Department of Structural Mechanics

DOCTORAL THESIS

Probabilistic analysis of composite materials with hyperelastic components

Probabilistyczna analiza materiałów kompozytowych
o składnikach hipersprężystych

Damian Sokołowski, M.Sc. Eng.
author

Marcin Kamiński, Prof. Ph.D. M.Sc. Eng.
scientific supervisor

Lodz, August 2021

I would like to acknowledge support provided by my Supervisor
Prof. Ph.D. M.Sc. Eng. Marcin Kamiński in all stages of this work
and recognize His excellent guidance not only during the doctoral studies
but also the earlier stages of my Higher Education.
He accepted me as His individual student, assisted in my personal development
and encouraged to strive persistently for the chosen goals.
He inspired me to go off the beaten path
and to reach beyond the well understood.
I consider myself lucky to have such an excellent scientist on my side and
appreciate everything I have learned from him both personally and scientifically.

I am very grateful to my beloved Wife Paulina, who always stands by me.
Her support is invaluable and care immense.
I appreciate the warmth of her feeling and encouragement to go on.
Thank You, my dear.

I would like to thank my Grandma Alicja
for incessant belief in my abilities and encouragement for further development.
She gave me so much more than She was ever supposed to …
and continues to do so.

I would like to recognize the support of my closest family
dearest Parents, lovely Siblings, Aunts and Grandparents.
They always back up my aspirations and offer aid whenever I need it.
Their influence is inestimable, although not straightforward. They overlook my
faux pas, tolerate persistent lack of time and encourage to achieve my personal goals.
This is simply more than I deserve.

Abstract

A major topic of this dissertation is determination of the effective material parameters of composites with stochastic interface defects in their hyperelastic mode of strains. This is done with a joint usage of specially designed laboratory experiments and probabilistic homogenization. For this purpose a theoretical introduction is provided and suitable computational algorithms are proposed. These are applied and validated for the objective composite under uniaxial stretch. The objective composite consists of high density polyurethane matrix made of Laripur LPR 5020 and 5% of carbon black F60 reinforcement. The proposed approach is designed for an arbitrary isotropic hyperelastic potential and is validated with success for the Mooney-Rivlin, Arruda-Boyce and Neo-Hookean constitutive models. It introduces a concept of the augmented material model, which describes dependency of the effective material parameters on an extent of the stochastic interface defects. It is described by their volume fraction, which is also the only input random variable in this study; it has a Gaussian distribution. Further, the modeling strategy for mechanical properties of the hyperelastic interphase in direct neighborhood of the CB particles is proposed. It is used in verification of an influence of the input random variable on the composite effective material parameters, effective strain energies and effective stress under uniaxial stretch; this is done in the deterministic and stochastic context. Next, a computational algorithm for determination of statistical estimators of the input random variable is introduced and applied for the objective composite. Numerical calculus is made in a hybrid approach within a framework of the stochastic finite element method. The deterministic part is computed in the FEM system ABAQUS on the basis of a cubic Representative Volume Element and the probabilistic calculus is performed symbolically in the computer algebra system MAPLE 2018. Probabilistic part is computed with use of three independent methods, which are the generalized iterative stochastic perturbation technique, the crude Monte-Carlo simulation and probabilistic semi-analytical method. Probabilistic characteristics are computed for the composite state variables. They include the expected values, coefficients of variation, skewness and kurtosis.

Keywords: probabilistic homogenization; hyperelasticity; particulate composite; particle-reinforced composite; stochastic perturbation technique; Monte-Carlo simulation; semi-analytical method; interphase; interface defects; multiscale approach;

Streszczenie

Głównym celem dysertacji jest określenie efektywnych parametrów materiałowych kompozytów ze stochastycznymi defektami międzyfazowymi w hipersprężystym zakresie odkształceń. W tym celu przeprowadzono specjalnie zaprojektowane eksperymenty laboratoryjne użyte w algorytmach homogenizacji probabilistycznej. Powyższe zagadnienie zostało sformułowane teoretycznie, a algorytmy zastosowano i zweryfikowano dla przedmiotowego kompozytu poddanego osiowemu odkształceniu wzdłużnemu. Kompozyt składa się z matrycy z poliuretanu wysokiej gęstości Laripur LPR 5020 zbrojonej cząsteczkami węgla (fullerenami F60) o objętości 5%. Proponowane rozwiązanie zagadnienia zaprojektowano dla dowolnego izotropowego potencjału hipersprężystego i użyto z sukcesem dla modeli konstytutywnych Mooney-Rivlina, Arruda-Boycea oraz Neo-Hooka. Wprowadza ono koncept rozszerzonego modelu materiałowego, który uwzględnia zależność parametrów materiałowych na objętość stochastycznych defektów międzyfazowych. Są one przedstawione jednoparametrowo jako frakcja objętościowa defektów w interfazie; stanowi ona jedyny wejściowy parametr losowy rozważany w niniejszej dysertacji oraz posiada rozkład typu Gaussa. Następnie zaproponowano sposób modelowania właściwości materiałowych hipersprężystej interfazy znajdującej się w bezpośrednim sąsiedztwie zbrojenia. Został on użyty do weryfikacji wpływu wejściowej zmiennej losowej na efektywne parametry materiałowe, efektywną energię odkształcenia oraz efektywne naprężenie kompozytu poddanego rozciąganiu wzdłużnemu; przyjęto podejście deterministyczne oraz stochastyczne. Kolejno, zaproponowano algorytm numeryczny do określenia estymatorów statystycznych wejściowej zmiennej losowej; został on zastosowany z sukcesem dla przedmiotowego kompozytu. Badania numeryczne przeprowadzone zostały w sposób hybrydowy, z użyciem stochastycznej metody elementów skończonych. Część deterministyczną obliczono za pomocą metody elementów skończonych na podstawie sześciennego reprezentatywnego elementu objętościowego. Część probabilistyczną obliczono symbolicznie w systemie algebry komputerowej MAPLE 2018. Probabilistyka wykonana została przy użyciu trzech niezależnych metod, iteracyjnej techniki perturbacji stochastycznej, symulacji Monte-Carlo oraz probabilistycznej metody pół-analitycznej. W analizie ujęte zostały pierwsze cztery charakterystyki losowe efektywnych własności kompozytu, tj. wartość oczekiwana, współczynnik wariancji, skośność oraz kurtoza.

Słowa kluczowe: wielo-skalowa technika homogenizacji; hipersprężystość; technika perturbacji stochastycznej; symulacja Monte-Carlo; metoda pół-analityczna; interfaza; defekty międzyfazowe; homogenizacja probabilistyczna;

Table of contents

1. Introduction

1.1. Subject of dissertation

Elastomers and other rubber-like materials have a wide range of industrial and engineering applications, such as tires, engine mounts, seals, conveyor belts, base isolations energy dampers, automotive suspension bushings or high-performance adhesives, to mention a few; their properties are considered for example in [1]. Due to their numerous applications, rubber mechanics has become a very active field of research in last several decades. The emerging field of numerical techniques, especially the finite element method (FEM), enables researchers to design and analyze complex large strain three-dimensional elastomeric components to be an integral part of the design process. One of their examples is polyurethane, especially in its thermoplastic version (TPU). Polyurethanes have relatively high tensile and flexural properties, are resistant to tear, have good electrical isolation properties and high resiliency range. Lastly, they are highly active chemically, which is accompanied with strong bonding properties to multiple materials. Their properties could be further modified by various fillers and additives [2,3,4]. An introduction to their analysis could be found in [5,6].

One of the fillers that affect physical properties of polyurethane is the carbon black [7]. It influences its thermal and electrical conductivity, improves impact strength and tribolgical properties. It is used for various polymers to adapt them to a wide range of applications including fuel and solar cells, sensors, detectors, supercapacitors, electromagnetic interference shielding, and coatings. Its application not always come in pair with an increase of stiffness and ultimate strength of these polymers. This is frequently caused by the interface defects that form on particle-matrix transition. Such defective interfaces significantly affect mechanical properties of polymer based composites. Their existence contradicts the strengthening potential of the CB that is indicated in many studies focused solely on its theoretical limit upon homogenization. Their effect is well studied in the reversible elastic mode of composites. It is, however, not well known for their hyperelastic mode, which is relevant for majority of industrial applications. This fact becomes even more involving when coupled with an abundance of available constitutive models of hyperelastic materials. Unlike in reversible elasticity, each of them have their own set of assumptions as well as material properties and none

is perfectly suited for all applications. These are one of the main reasons why a topic of interface defects is covered in this dissertation. One of its major objectives is proposition of a way to determine the effective material properties of such composites that works for all the isotropic hyperelastic constitutive models.

Interface defects are decisive for (not only) mechanical properties of the composite. Still, they are not easily detected by laboratory experiments because of their very small dimensions and highly random character. They are also not easily incorporated to the contemporary numerical solvers. This is because their existence changes the properties of interface between the particle and the matrix in a fine-grained manner. Instead of considering them separately, special methods are commonly applied to consider their common influence. One of these approaches incorporate them into a separate scale in the composite, which is next homogenized to form an interphase. This interphase includes the effect of interface defects and enables further homogenization of composite microstructure that finally returns their macroscopic properties. Such an approach is proposed in this dissertation as an extension to previous considerations in the reversible elastic mode.

Random character of interface defects is exemplified by a fluctuating number, shape and dimensions of the defects for each particle. All these factors influence the composite mechanical properties, but analysis of their separate impact in hyperelastic mode of deformations is very difficult even for common computational machines. It is also not too much conclusive on the macroscopic level because they simply cannot be steered during manufacturing process or precisely measured by laboratory experiments. This is the reason why they were replaced here by a single parameter of interface defects volume fraction. Such a choice enables augmentation of an arbitrary hyperelastic constitutive model with an additional variable describing the extent of interface defects. Such extended constitutive model is aimed for prediction of the macroscopic properties of defective particulate composites; it is called further the **augmented material model** (AMM). Since the interface defects are random, such are also the effective properties of the composite. This has been documented by specially designed laboratory experiments comparing randomness of uniaxial stretch in the virgin homogeneous polymer and the same polymer filled with CB particles. They proved similarity in their randomness, especially the coefficient of random dispersion having close relation to strain with an almost constant offset. This offset

is assumed to be an effect of stochastic interface defects. Laboratory experiments verify the expectations, standard deviations and coefficients of variation of stress of the composite and the virgin homogeneous material under uniaxial single and cyclic stretch. They were not available previously and may serve as an input data for other stochastic and deterministic studies of this composite per se.

Results of these experiments have been used jointly with the proposed **probabilistic homogenization** to determine the statistical estimators of the interface defects volume fraction. Probabilistic homogenization of composites with stochastic interface defects is designed especially for determination of randomness in the effective state variables of the composite with stochastic interface defects; they are the effective (hyperelastic) material properties, effective deformation energies and effective stresses. This resulting randomness is induced solely by a single source of uncertainty, the stochastic interface defects. The resulting random effective material properties could be included directly in macroscopic constitutive model of the composite together with other uncertainty sources. Characteristics determined relative to the input volume fraction of interface defects are the expectations, coefficients of random dispersion, skewness and kurtosis. In turn, stochastic characteristics of the effective stresses are used in an algorithm for determination of the statistical estimators of the **interface defects volume fraction**. Importantly, these stochastic characteristics are determined independently by three probabilistic methods, which serves for their simultaneous verification.

Relation between the state variables of the composite with stochastic interface defects and the input random variable is not available. Thus, two methods are used here for their recovery. They are the response function method and its generalized version - the **response surface method**. The first of those can be used when the state variable is a function of a single parameter. It is used frequently in stochastic calculations and their effectiveness is very well known. The response surface could be used for state variables dependent on multiple parameters or variables. It has not been used previously in connection with the stochastic finite element method. This is proposed here together with an algorithm for its optimization. Finally, accuracy of this method is verified for the effective deformation energy and the effective stress of composite with stochastic interface defects.

1.2. Motivation

The leading motivation for this thesis is a lack of reliable method to define the effective probabilistic properties of particulate composites with defective interfaces and hyperelastic components. Such method is introduced for a hyperelastic regime of this composite; it is supported by laboratory tests of uniaxial tension. If available at all, the existing methods focus purely on a theoretical constitutive model and/or numerical implementation of a fictitious material. They also typically limit themselves to a single hyperelastic potential and single probabilistic approach, which does not allow for reliable verification of its results. A secondary motivation for this work is an aspiration to extend and verify applicability of the hybrid probabilistic homogenization for problems outside linear elasticity. Former usage of this method was applied to composites with purely linear components and simple composition of phases, which is extended here for hyperelastic components. Further, a choice of interface defects as a random parameter is motivated by their high influence on effective probabilistic properties of the composite despite their small volume. It was already proven for linear-elastic case but not yet for the hyperelastic composite, which is verified in this thesis. Finally, a computational algorithm to determine statistical estimators of volume fraction of interface defects is introduced. It is a first approach known to the author that successfully quantifies interface defect stochastic characteristics in a joint computational-experimental way. This is impossible when using laboratory tests by only because of the size of interface defects, their variable amount and size around each particle.

1.3. Thesis and hypotheses

Thesis is composed of four major parts proved in successive sections of this dissertation. They are following:

(1) It is possible to formulate theoretically the deformation process of particulate composites with random interface defects in its hyperelastic regime. **(2)** The proposed augmented material model could be applied with success to the real case scenario basing on the selected hyperelastic formulations. **(3)** A proposed algorithm allows determination of the statistical estimators of the normally distributed volume fraction of interface defects in this composite. **(4)** It is possible to determine the effective material properties of the composite with stochastic interface defects together with their stochastic characteristics for the selected hyperelastic constitutive models. They may be used for a wide range of defects volume fraction in the range of $[0.09 - 0.95]$.

The main thesis is supported with additional hypotheses that are following:

Hypothesis 1. Existence and increase of volume fraction of interface defects reduce (a) the effective material properties, (b) the effective stress and (c) the effective deformation energy of the hyperelastic composite. Their uncertain character causes a considerable stochastic scatter of these effective parameters and their resulting probabilistic density is not Gaussian. These characteristics fluctuate together with an increase of strain.

Hypothesis 2. Proposed stochastic homogenization scheme enables an effective determination of stress in the selected particulate composite with interface defects, i.e. Laripur LPR 5020 reinforced with 5% carbon black particles F60 (HDPU-CB).

Hypothesis 3. Generalized iterative stochastic perturbation method allows a precise determination of random characteristics of effective stress and deformation energy in hyperelastic particulate composites with uncertain interface defects. It also offers a considerable reduction of computational time and resources in relation to an alternative Monte-Carlo simulation assuring a comparable precision of results. The semi-analytical method is not perfectly suited to this kind of problems.

Hypothesis 4. Stiffness and effective stress of the objective composite (HDPU-CB) subjected to uniaxial stretch is lower with respect to the virgin homogeneous material and the coefficient of variation of the effective stress is higher. Difference between these coefficients of variation stabilizes with an increase of strain.

Hypothesis 5. (a) Stochastic characteristics of the effective material properties of the composite with stochastic interface defects could be computed independently of strain level in hyperelastic regime of this composite. (b) It is not possible for the effective stress and deformation energy because their variation with strain is not negligible.

Hypothesis 6. (a) The response surface method is accurate in approximation of the effective deformation energy and effective stress in the objective composite for all the considered hyperelastic constitutive models. (b) A relative error is also very low for approximation of the effective material properties by the response function method.

Hypothesis 7. (a) The proposed augmented material constitutive model allows accurate modeling of the effective deformation energy of the objective composite. (b) It can also capture degradation of stress in the objective composite under uniaxial stretch with respect to the virgin homogeneous material.

1.4. Aim and scope of dissertation

A general research objective is verification of the thesis that is connected to theoretical formulation and numerical verification of the deformation process of composites with random variable in their nonlinear-elastic (hyperelastic) regime. It is done with use of the generalized iterative stochastic finite element method (SFEM) for the composite made of high density polyuretane (HDPU) matrix and carbon black (CB) nanoparticle reinforcement. This composite is made of Laripur 5020 and it is reinforced with fullerenes F60; it is further called the objective composite. Strategic goals are as follows: (a) proposition of the way to model mechanical properties of the hyperelastic interphase forming in the direct neighborhood of CB particles in the HDPU-CB composite and (b) determination of the effective material properties of this composite, (c) determination of the influence of uncertain volume fraction of interface defects on these effective properties and the general deformation process of such composites in their hyperelastic regime and (d) determination of statistical estimators of the volume fraction of interface defects in the objective composite. This is done with support of laboratory tests performed by the author that have been used in algorithms proposed by him; state functions analyzed for the deformation process are the effective stress and the effective deformation energy; they accompany a set of state functions describing the effective material properties for the selected hyperelastic augmented material models.

Additional **accompanying objectives** are following:

Obj. 1. Introduction of the response surface method for the ISFEM as an extension of the response function method. It enables stochastic calculations of implicit objective functions that depend on more than one variable and whose relation with this function is unknown; it could include one or more random input variables (section 3.2.2).

Obj. 2. Theoretical formulation of the probabilistic homogenization problem (section 3.1).

Obj. 3. Proposition of the algorithm to determine the effective state functions of composites with stochastic interface defects together with their stochastic characteristics and independent from the underlying hyperelastic formulation (section 4.1).

Obj. 4. Introduction of a single-valued parameter defining the extent of stochastic interface defects called interface defect volume fraction. Proposition of a method to determine its statistical estimators in hyperelastic composites with stochastic interface defects independently from the underlying hyperelastic formulation (section 4.1).

Obj. 5. Execution of laboratory experiments including single and cyclic uniaxial stretch of the virgin homogeneous material (Laripur LPR 5020) and the objective composite (section 5).

Obj. 6. Determination and analysis of the first two stochastic characteristics of the stress in the virgin homogeneous material and the objective composite relative to the level of the strain based on laboratory experiments (section 5.3); characteristics include expectation and coefficient of variation computed from results of laboratory experiments.

Obj. 7. Verification of the type of relation between the coefficient of variation of the virgin homogeneous material and the objective composite judging from the results of laboratory experiments (section 5.2).

Obj. 8. Selection of the best fitting hyperelastic constitutive models of the virgin homogeneous material for further usage in numerical part of this dissertation (Appendix A).

Obj. 9. Analysis of the effective material properties of the objective composite for the three selected hyperelastic material formulations and for an increasing volume fraction of interface defects (section 6.1.1).

Obj. 10. Determination of statistical estimators of the volume fraction of interface defects for the objective composite (section 6.1.2).

Obj. 11. Calculation of stochastic characteristics of the effective material properties for an increasing volume fraction of interface defects (section 6.1.3) and verification of effectiveness of an algorithm for its response function optimization (Appendix B).

Obj. 12. Determination and analysis of stochastic characteristics of the effective material parameters for optimized statistical estimators of the input random parameter (section 6.1); they may be used directly in probabilistic analysis of the objective composite.

Obj. 13. Proposition of a procedure for optimization of the response surface for the effective deformation energy in the objective composite under uniaxial stretch. Verification of its effectiveness (Appendix C).

Obj. 14. Verification of an influence of the volume fraction of interface defects on the effective deformation energy (section 6.2.1) and the effective stress (section 6.3.2) in the objective composite under uniaxial stretch.

Obj. 15. Computational determination of the first four stochastic characteristics of the effective deformation energy (section 6.2.3) and the effective stress (section 6.3.2) in the objective composite; determination of an influence of the strain level jointly with an influence of the coefficient of variation of the input uncertain variable - the volume fraction of interface defects.

Obj. 16. Analysis of dependence of the first four stochastic characteristics of the effective deformation energy (section 6.2.3) and the effective stress (section 6.3.2) on the strain. Determination if this parameter could be dropped in further stochastic calculations or not.

Obj. 17. Verification of the proposed algorithm for determination of the volume fraction of interface defects statistical estimators; introduction of a concept of the augmented material model for composites with stochastic interface defects. Verification is done for uniaxial stretch of this composite (section 6.3.3).

Obj. 18. Determination of the augmented material model for the objective composite approximated by the selected underlying hyperelastic formulations; verification of its usefulness for the effective deformation energies (section 6.2.2) and the effective stresses (section 6.3.1) of the objective composite under uniaxial stretch.

Obj. 19. Comparison of effectiveness of the three selected methods for determination of stochastic characteristics of the effective material properties (section 6.1.2), the effective deformation energy (section 6.2.3) and the effective stress (sections 6.3.2 and 6.3.3); these are the generalized iterative stochastic perturbation, semi-analytical and crude Monte-Carlo simulation methods.

Obj. 20. Verification if the proposed algorithm could be applied for different hyperelastic material formulations and comparison of its results obtained for the three selected underlying material formulations (sections 6.1 and 6.3).

Scope of the thesis includes (a) uniaxial stretch laboratory tests of the matrix and composite, its further usage in (b) numerical analysis of the effective state functions in hyperelastic regime of composite with stochastic interface defects and (c) theoretical introduction of a probabilistic hyperelastic homogenization problem for the above mentioned composites.

One of the most important concepts in this dissertation is proposition of the way to estimate the stochastic interface defects in particulate composites. This original idea introduced by the author was developed by him through all its phases beginning from the early concept phase, through the phase of theoretical consideration and computational analysis up to its verification for a real hyperelastic composite. The most unique feature of this approach is a joint usage of laboratory experiments with computational analyses that, supported by a new theoretical concept, allows determination of the stochastic interface defects in the objective composite. The author came up with the above idea, conducted both, laboratory and computational experiments, proposed the necessary algorithms and, together with his Supervisor, introduced the theoretical introduction of connected probabilistic homogenization problem (section 3.1). Current proposition is valid for the Gaussian distribution of an input variable of the interface defects volume fraction; it requires determination of two statistical estimators. This approach may, however, be relatively easily extended for different distributions of the input variable.

A second innovation proposed here is introduction of a way to compute the effective material properties of composites with stochastic interface defects by the augmented material model. This concept introduces a new variable in the original constitutive formula for hyperelastic materials and provides an algorithm for its determination independent of the underlying hyperelastic formulation. This variable is denoted as the volume fraction of interface defects. Its introduction allows to determine the deformation process of composite with interface defects. It weakens the material parameters and exemplify the extent of interface degradation in the composite. It also allows to convert the uncertainty introduced by the interface defects directly into the hyperelastic material parameters. They may be next easily incorporated into probabilistic calculations of the macroscopic structures.

This dissertation also proposes the probabilistic homogenization scheme for composites with stochastic interface defects and nonlinear (hyperelastic) components. It is much

more demanding than the one previously proposed for the linear reversible components because of variability of hyperelastic formulations. Unlike in linear elasticity, these formulations end up with a unique set of material parameters that relate the state functions to the invariants or the strains. This is also the main reason why the author decided to disconnect the proposed homogenization algorithm from the underlying hyperelastic material. Selection of this constitutive model is still an important step, but each isotropic model is eligible.

Innovation is proposed in the SFEM also. The main novelty in this context is introduction of the response surface method, which opens the possibility to quantify the stochastic characteristics for implicit objective functions that cannot be reduced to single variable polynomials. It considerably widens the applicability of the SFEM. This extension also provides a first step to consider multiple, correlated input uncertain variables in stochastic calculations by the SFEM. The response surface method is first introduced, then the optimization algorithm is proposed and approximation error verified and then the optimal surface is used in the SFEM calculations.

This dissertation also introduces the concept of input uncertain variable in the SFEM. The traditional SFEM or probabilistic problem uses one or more random parameters whose stochastic characteristics are all known a priori. Alternatively, the effect of coefficient of random dispersion is verified for isolated random parameter. In contrast to them, in this dissertation the expected value and the coefficient of random dispersion of the input variable is unknown. It is determined in an inverse problem, where laboratory experiments are used for calibration and validation of the probabilistic homogenization problem for real, and not theoretically idealized composite. Importantly, computed state functions cannot be simplified to functions of only single random variable. Instead, they are a cross product of this random variable and the level of applied strain.

This dissertation includes only one uncertain parameter, which is the interface defects volume fraction. This choice follows an extensive research of uncertainty in particulate composites conducted by the author in his previous works for their reversible linear and hyperelastic regimes. In these works various kinds of random parameters were considered. Examples include imperfect particle geometry [8], uncertain ellipsoidal shape of particles [9], material parameters of the matrix [10], particle placement and agglomeration and also interface defects [11]. The interface defects are by far most

influencing the effective response of the composite in stochastic and deterministic contexts. A volume fraction of interface defects is preferred over alternative input random variables because it neatly encapsulates the interface defects by a single parameter that is easy to understand, compare and represent. It is introduced here because it is practically impossible to determine the number of interface defects of real nanacomposites with use of currently available laboratory equipment and use it for statistical consideration. It would be much easier to distinguish the radius of matrix affected by these defects that strictly relates to the volume of the interphase and consider solely the volume of the defects. Yet, such tests are not in scope of this thesis.

An input uncertain parameter is considered here to be exclusively Gaussian. This assumption is proposed especially because there exist no evidence of non-Gaussian character of the interface defects and also

- Gaussian distribution is considered as one of the most important theoretical probability distributions in statistics [12],
- distributions close to normal are frequently existing in nature, which is proved by Lindeberg-Lévy [13] theorem,
- characteristics of normal distributions make probabilistic methods based on it relatively easy; they are frequently used as a first step for analysis of complex distributions; normal distribution includes only two parameters in its definition (mean and standard deviation). It has a null skewness and kurtosis,
- a Gaussian distribution enables composition of a relatively easy relation of the result to a given coefficient of variation of input uncertain parameter. This is because this parameter is inherently included in definition of this distribution. Magnitude of this parameter differs significantly for certain unknowns, as for example in [14].

This dissertation consists of 7 chapters and 4 appendices. They cover the following topics:

Chapter 1 contains an introduction to all the main concepts contained in this dissertation. It describes the subject of this dissertation, presents the main motivation for selecting it and highlights the main features contained in it. In this chapter the thesis is formulated and supplementary hypotheses are presented. It also describes the aim and scope of this work.

Chapter 2 contains the review of literature in fields relevant for this dissertation. It covers the topics of hyperelastic materials, probabilistic analysis, multiscale analysis and homogenization method. It also provides a review of common ways to introduce the interface defects and explains a concept of the interphase. Finally, it brings closer a notion of the effective response of a medium and describes why it is commonly used in the SFEM and other stochastic/probabilistic computations.

Chapter 3 includes the theoretical background relevant for further numerical analysis. It provides mathematical formulation of the probabilistic homogenization problem for composites with stochastic interface defects. It also brings closer methods used to approximate the effective response of the objective composite.

Chapter 4 is dedicated to explanation of details of computer analysis. It is composed of three sections. The first one presents details of the selected Representative Volume Element and the finite element method solver. The second one describes specifics of methods used for determination of stochastic characteristics of the state functions. The third section explains the major algorithms proposed in this dissertation. They serve for determination of the effective state functions and volume fraction of interface defects in particulate composites and also for computation of their stochastic characteristics. The lesser algorithms and concepts used in different steps of the probabilistic homogenization algorithm are described in chapter 6 prior to their results.

Chapter 5 contains description, results and conclusions coming from laboratory experiments conducted for the virgin homogeneous material and the objective composite. They include uniaxial stretch of 10 specimens under single and cyclic loading. Considered statistical estimators include the mean, expected value, standard deviation and coefficient of variation of stress for variable strain. This chapter confronts the results for virgin homogeneous material and the objective composite; it also indicates their similarities as well as differences. Observations coming from this analysis are strictly relevant for further numerical experiments.

Chapter 6 is fully dedicated to the numerical experiments. It is composed of three parts and provides major results of this dissertation. The first part is dedicated to the effective material properties. The second part describes computations of the effective deformation energy and the third – of the effective stress.

The first section dedicated to the effective material properties firstly determines dependence of these parameters on the volume fraction of interface defects. Then, it presents an analysis of stochastic characteristics of the interface defects volume fraction and of the effective material properties recovered for the objective composite. This is done separately for all the three selected underlying hyperelastic constitutive models. At the end these stochastic characteristics are tabularized and described.

The second section firstly provides results of the effective deformation energy relative to the input uncertain parameter and verifies the effectiveness of the two alternative methods of its approximation. Next, it analyzes the stochastic characteristics of the effective deformation energy w.r.t. the coefficient of variation of the interface defects volume fraction and provides final conclusions.

The third section is dedicated to the effective stress of the objective composite under uniaxial stretch. Firstly, it provides details how this state function was computed and analyzes the relation of the effective stress to the strain and variable interface defects volume fraction. Then it provides analysis and interprets results of stochastic characteristics of this stress for the three selected underlying material formulations. Finally it verifies effectiveness of the proposed approach for determination of the effective stress of the objective composite against the results coming from the laboratory experiments. This is done on the basis of uniaxial stretch and two statistical estimators, i.e. expected value and coefficient of variation and relative to the applied strain.

All stochastic calculations are made by the three independent methods, i.e. the stochastic perturbation and semi-analytical methods as well as the crude Monte-Carlo simulation. Stochastic characteristics are computed for three selected underlying constitutive models. An exception is the effective deformation energy, which was determined for the Arruda-Boyce by only.

Chapter 7 includes summary, conclusions and future prospects for the conducted research.

Appendix A summarizes a selection process for hyperelastic constitutive models of the matrix.

Appendix B explains optimization procedure of the response function used for approximation of the effective material properties of the objective composite. It also provides optimization and verification of accuracy of the applied response function.

Appendix C explains optimization procedure of the response surface used for approximation of the effective deformation energy and the effective stress of the objective composite.

Appendix D includes a scheme of probabilistic homogenization algorithm.

2. Review of literature

Computational analysis of materials is crucial for design of contemporary appliances, mechanical parts and bearing systems. Its introduction changed entire design process supplementing its traditional cycle of conceptualizing and laboratory testing with a swift computer modeling. It cuts down the design time and provides tools for a very optimized or complex solutions unavailable by a sole analytical approach. All computations base on constitutive models of materials, defining their behavior under different mechanical, thermal [15], electrical [16], magnetic and coupled [17] conditions. They are well defined for relatively simple continua [18,19,20], but are still challenging for composites outside of elastic region. In this thesis a hyperelastic response of complex continuum is studied. It is highly useful for predicting the behavior of rubber-like composites with polymeric matrix. Their main strengths include the ease of usage and calibration, computational efficiency and also flexibility of usage and accessibility in commercial code. They could also be quite easily augmented to capture hysteresis in cyclic loading. Application of hyperelastic constitutive models ranges from tire industry to biological tissues, such as human arteries [21] and polymers.

2.1. Hyperelastic materials

An early motivation for theoretical formulation of hyperelastic materials was lack of existence of large-strain models capturing deformations accounting for its non-linearity above infinitesimal level. Such materials can deform largely and nonlinearly upon loading without breaking and then return to its initial configuration. Such rubber elasticity is achieved due to very flexible long-chain molecules and a three-dimensional network structure that is formed via cross-linking or entanglements between molecules. This behavior characterizes a wide range of continua, including rubber-like materials, polymers [22] and elastomers [23]. Its implementation in the finite element framework requires two important ingredients to solve a boundary value problem. They are the stress tensor and the consistent fourth-order tangent operator; the latter is the result of linearization of the former. Rubber-like materials are generally modeled as being homogeneous, isotropic, incompressible or nearly incompressible, geometrically and physically nonlinear hyper- or visco- elastic solids [24,25,26,27,28] and visco-plastic solids [29]. Their models are commonly supported by experimental data. The most

common tests involve the uniaxial stretch, biaxial stretch and pure shear. Some models consider also aging [30,31], Mullins effect [32,33,34], hysteresis [35] or failure of rubber-like materials [36,37]. In this dissertation, hyperelastic constitutive models are selected. Their theoretical introduction is available for example in [38,39,40,41] and examples of its FEM formulation are [42,43,44,45].

Classical hyperelastic constitutive models include Mooney-Rivlin [46,47], Neo-Hookean [48,49], Yeoh [50], Arruda-Boyce [51] and Gent [52]. They have been developed in mid and late 1900s and all provide analytical solutions for an isotropic single phase medium. Number of parameters included in their equations is small, which enables their analytical treatment for simple engineering problems. Contemporary models introduce more parameters that increase flexibility and accuracy of calculations. The trade-off is a considerable increase of calibration and computation efforts that makes them preferable for large scale computer simulations and not for analytical calculus. One of the modern formulations of hyperelastic material is the Extended Tube model [53] including 5 parameters. It focus on the molecular-statistical approach for polymer networks. The other provides solution for hyperelastic anisotropy [54]. One of the popular ways to categorize the hyperelastic constitutive models is their phenomenological or micromechanical character [55] (see Fig. 2.1). The micromechanical models are based on the analysis of networks of cross-linked long-chain molecules. Some examples include 3-chain [56], 8-chain [57], full-network [58], Flory-Erman [59], unit sphere [60], tube [43] and extended tube models. Phenomenological models are further subdivided into the invariant or principal stretch based macroscopic continuum formulations. They are generally based on polynomials that usually lack a firm physical interpretation of the governing parameters in deformation energy function. The invariant based continua are much more common. Some examples include the classical models mentioned before, i.e. Mooney-Rivlin, Neo-Hookean, Yeoh, Arruda-Boyce and Gent. Some more contemporary approaches are Pucci-Saccomandi [61], Lopez-Pamies [62] or Alexander models. They incorporate a logarithmic or an exponential term in their energy functions that allows a better estimation of deformation in uniaxial stretch and equibiaxial stretch. Principal stretch based models include for example Attard and Hunt [25] or Shariff [13] and Ogden [14] implementations. A comparison of various mentioned hyperelastic constitutive models is available in [63]; some other models use neural networks also [64]. The author

decided to select among the classical invariant-based models, because they are widespread, easy to implement in the finite element code (unlike the stretch based models) and allow a satisfactory convergence of the Newton algorithm; they are bolded on Fig. 2.1. The modern micromechanical models were not selected because of a limited availability of laboratory equipment and the filler.

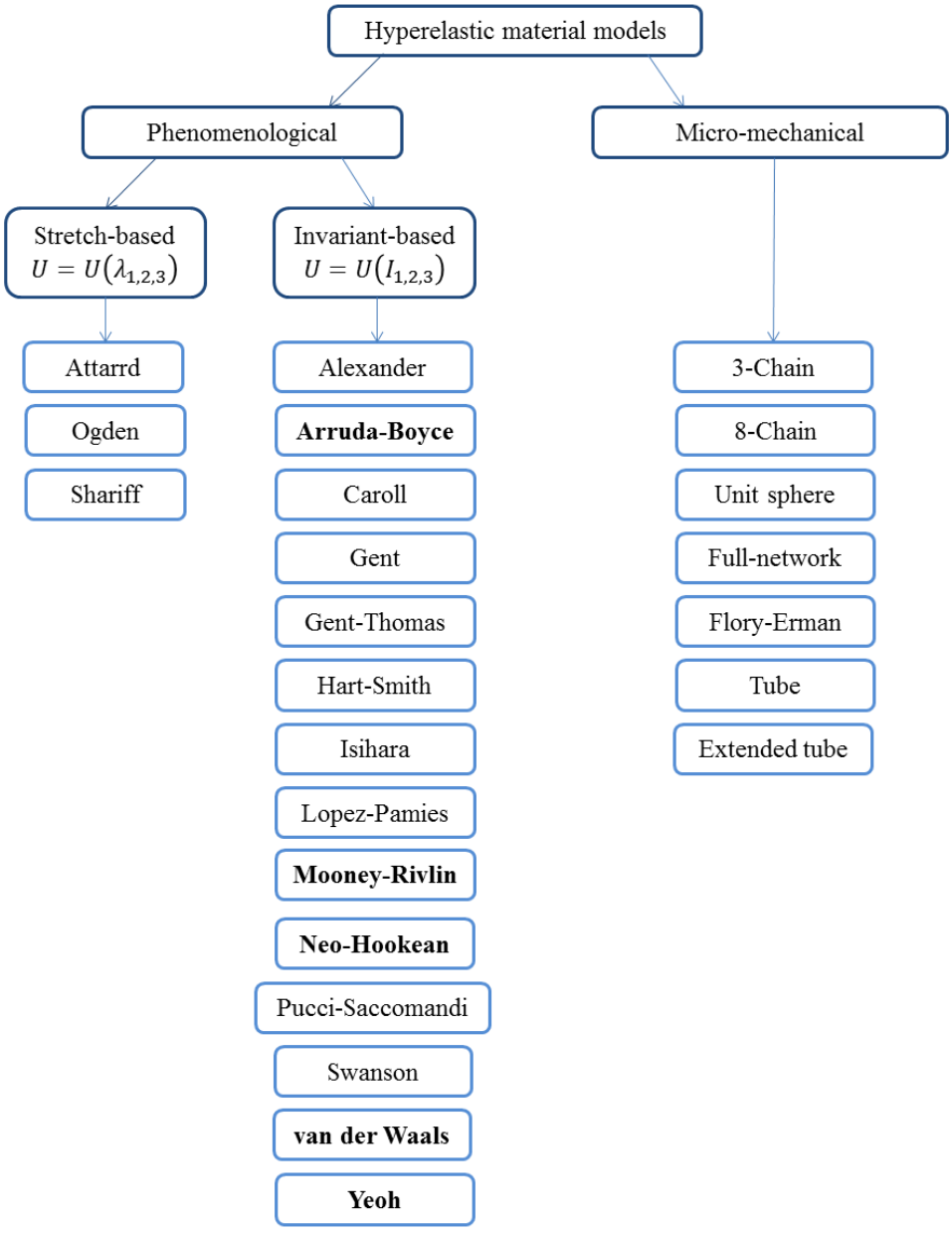

Fig. 2.1 Different constitutive models of hyperelastic materials.

Only recently efforts have been put to define the hyperelastic behavior of multi-phase materials. This is because of high complexity of calculations and unavailability of analytical solutions. This problems are leveled by a rapid increase in computational resources allowing an iterative solution. Some examples of contemporary studies

include [65,66,67,68,69,70,71,72,73,74]. They are available also for visco-elastic regime [75]. A demand of extensive hyperelastic constitutive models is stimulated by biotechnological industry, where mechanics of biological tissue [76] and its interaction with artificial appliances is studied [21]. They are also required in aerial, textile and automotive industries and are used for example in tires or various shock absorbers.

Unlike in linear small strain elasticity all the models provide their own set of assumptions prescribed during the derivation process and are not necessarily easily interchangeable with others. This introduces challenges in description of their stochastic nature because material parameters are no more a good choice for overall stochastic unknowns. Such choice would bound the analysis to a specific constitutive model, which is highly undesirable. Instead, some more generic parameters or variables should be preferred, for example a defects volume fraction, that stays unique for all constitutive models. Random (effective) material coefficients should rather be a derivative of other random sources. Such an approach is proposed here in Section 6.1.

Stochastic or probabilistic studies are quite well documented in the reversible elastic regime of composites [77,78]. This is not true for the inelastic regime. One of the main reasons is the above mentioned lack of generality of various laws and complexity of their numerical solution already in the deterministic case. Stochastic hyperelasticity or visco-elasticity of composites is considered only in a limited number of studies; some examples include [79,80,81,82]. Researchers usually focus on a certain hyperelasticity potential, for example the Ogden [83,84,85], Neo-Hookean [62,86] or van der Waals model [70]; some of them compare also the results of several potentials, as in [87] or propose a specific solution techniques [80,88]. There, however, is a lack of studies concerning the composites that include interface defects in the nonlinear regime. This is especially true for the joint deterministic and stochastic analysis coupled with a verification of multiple hyperelastic potentials. This dissertation is intended to cover this topic. Unlike majority of the stochastic considerations it is additionally based on the set of laboratory tests performed specially for the computational part, for which the numerical response of the matrix is fitted with use of the Least Squares algorithm. The proposed approach specifically tackles the problem of lack of generality of hyperelastic laws by introduction of a probabilistic homogenization algorithm. It enables computation of random effective material parameters for an arbitrary

isotropic hyperelastic potential with a specified source of uncertainty (random parameter or variable). This source is here the volume fraction of interface defects.

2.2. Probabilistic analysis

Behavior of materials and structures in civil engineering and mechanical design is defined by models with specific assumptions. Traditionally they have a certain set of parameters to fit them into a response of material in well-known tests. These parameters are always exposed to some scatter. It comes from various sources of randomness such as morphology of the material, tolerances in manufacturing and measurements, accuracy of conversions or other unknown origins impossible to quantify during measurement.

Probabilistic analysis is an approach that tackles this problem directly by augmenting deterministic mathematical models with random parameters or variables representing sources of uncertainty. It allows much more precise estimation of behavior of analyzed system. In addition to the mean, characteristic or design values obtained in most engineering calculations it outputs also the expected value, coefficient of variation, and other specific information of the results uncertainty. It further allows to compute directly and optimize the structural safety margin in certain load conditions. This margin may be represented for example as reliability index or probability of survival. Probabilistic analysis may be applied in structural analyses at various levels of design, i.e. level of material, structural element or even at the level of entire structure. Examples include heat transfer [89,90], fatigue [91,92], stiffness [93], failure [94,95].

Probabilistic approach encompass all the methods based on probability calculus leading to calculation of material or structural response with input uncertainties. This response is commonly represented as random moments or characteristics, such as expected value (E), coefficient of variation (α), skewness (β) or kurtosis (κ). One of the common representations of statistical distribution is the probability density function (PDF), but it is also the most demanding in terms of computational resources. It is preferable also because it ensures a continuous representation of probability density. This is why in most cases the characteristics are preferable, as in this study. The most widespread methods allowing probabilistic design are direct derivation methods, simulation methods, spectral methods and perturbation methods.

Direct derivation methods [96,14] use integral calculus to derive random characteristics of the response with a known PDF of the input random variables. In its classical form, this approach takes a direct relation of the structural response and the random parameter; it is commonly called as analytical method (AM). In many cases such relation is not known, cannot be derived analytically or a symbolic solution for known relation simply does not exist. An approximation of this relation is obtained with various numerical techniques that is commonly referred as a response function or a response surface. Such an approach is called a semi-analytical method (SAM) [97,96] and is applied in this study. Alternatively, approximate or bounded integration may also be used. The disadvantage of such approximation may be requirement to set an input CoV to correctly set its bounds. Furthermore, its direct consequence is a loss of continuous relation of the uncertain material response. Continuous representation is important for numerical part of this dissertation and thus approximations were not used.

Simulation methods [98,99,100,14,101,102,103] substitute integration with a finite number of deterministic realizations, which are next subjected to statistical estimation. They are used in many technical, financial and engineering areas [104,105,106,107,98,100,108]. Realizations are made with sets of parameters obtained from random or pseudo random generation according to their predefined PDFs; they are all referred as Monte-Carlo simulation (MCS) methods [107,98,109]. They have several advantages, i.e. ease of implementation and avoidance of integration, but they all also have important disadvantages. Major drawback of this approach is a vast number of realizations required to reach a satisfactory result convergence that is guaranteed only with their infinite number [110,98]. This problem is partially covered in more modern approaches, such as importance sampling [111], stratified sampling [112], or latin hypercube sampling [113,114] techniques; they all attempt to lower the required sampling number. A second disadvantage is poor scaling for increasing number of unknowns. The last and deciding disadvantage is an inherent discrete character of MCS disallowing retrieval of continuous probabilistic characteristics or measures of reliability.

Spectral method [115,116,117,90] describes a Gaussian random field with use of Karhunen-Loève expansion. Structural response is emulated by expansion into a polynomial chaos [118]. The biggest problem of this methodology is very low number

of terms in the series that usually does not exceed two [119]. Because of this, the result may be inadequate and quite far from the exact solution, especially when a second order polynomial is used (which is commonly done). For them to obtain satisfactory accuracy a high number of elements may oftentimes be required. Additional problem is connected to Karhunen-Loève expansion itself, which does not have a solution for certain problems [120,121]. The one especially important is reliable calculation of higher order probabilistic characteristics [97], which prevents it from being considered in this thesis.

Perturbation methods [96,122,123] describe the structural response as spread around its mean value with a small perturbation. They expand the response function into a Taylor series around the expected values of random variables. The order of this method depends on the number of terms of applied expansion. One term in first order, two terms in second order etc. One of its topics is convergence of the Taylor series, which is not always guaranteed. This problem is even more complex when response function is not known and must be approximated, which is the case for this dissertation. For this reason a most suitable function is verified here according to algorithm presented in section 3.2. The response function is selected from a set of polynomial functions, for which a convergence of Taylor series is mathematically proved. Major advantages of this method are swift execution, relative ease of implementation and continuous character of the results. It also substitutes integrals by derivatives and overcomes a problem of lack of solution that exists in the AM and SAM. The biggest drawback is unproved convergence for certain types of functions and requirement of high order expansion to reach a high accuracy for input random variables with a high CoV. Nevertheless, ability to reach a very high level of accuracy for polynomial based response function was recently proved numerically in [124].

The leading probabilistic method used in this thesis is the stochastic perturbation method, because of already mentioned relative ease of its implementation, continuous character (ability to output continuous probabilistic characteristics) and lack of derivation problems. Monte Carlo and semi-analytical methods serve here as reference methods for verification of the results of the ISPT.

Relation of the result and the input random variable is usually unknown prior to probabilistic analysis. Its analytical derivation is available only for relatively simple, well known problems. In other cases this relation is sought with use of numerical

methods, such as the finite element method, boundary element method, finite difference method. Joining their output with probabilistic analysis results in stochastic finite element method (SFEM) [116,125,126,127,128,129,130], stochastic boundary element method (SBEM) [131,132] and stochastic finite difference method (FFDM) [96,133]. Such a fusion creates a powerful tool for probabilistic design and stochastic computations but it does not provide a new probabilistic method itself. In this thesis SFEM is preferred. This is because of convenience in solving the homogenization problem and availability of software for FEM computations. The ones looking for a comprehensive introduction to the finite element method shall refer to [134].

It is worth to mention that the results of probabilistic analysis serves further for reliability verification of materials and structures. They, however, form a separated group of methods using theory of reliability. Their specifics are described well in following works [135,136,14,137,138,139,140,141,142,143]. This dissertation does not focus on them directly, because it is rather devoted to a level of material and its effective representation and not on structural analysis itself. The author, however, already have focused his research attentions on reliability problems in corrugated-web I beams. Interested readers could refer to [144,145,146,147,148,149,150,151].

2.3. Interphase and interface defects

An interphase is an additional phase of the composite formed during its manufacturing process or exploitation. It exists in-between two phases of the composite, commonly between the matrix and the filler. Its mechanical [152], thermal, electrical, thermo-mechanical [153] and physical characteristics differ from the ones of the two surrounding phases. Its volume is much lower than the other phases, yet it highly influences behavior of an entire composite. This is because the interphase effectively encapsulates the filler and prevents a direct interaction in-between the composite constituents. As it has been documented, an interphase affects significantly the effective material properties of multiple isotropic, cubic and anisotropic composites in a deterministic [154,155,156,157,158] and also stochastic context [159,8,11,160,161]. It either decreases them in an existence of defects [162] or increases, when the two phases are chemically bound [163,164,165,166]. Its influence is so high, that considerable research attention has been put for its tuning and tweaking to improve key properties of composites or adjust their performance for special purposes [167,168].

Interphase is extremely difficult to define in laboratory tests. This is because its thickness is very small (in order of μm) and its characteristics differ for each particle or fiber in the same sample of the composite. Despite an existence of multiple surface agents applied on the phases, interphase around each of filler particles or fibers has unique thermo-electro-mechanical conditions in which it forms. This effectively makes its geometry, thickness and properties random. An exemplary interphase formed between the glass fiber and the polypropylene matrix is shown in Fig. 2.2. Its morphology is clearly different than both adjacent phases and transition is sharp.

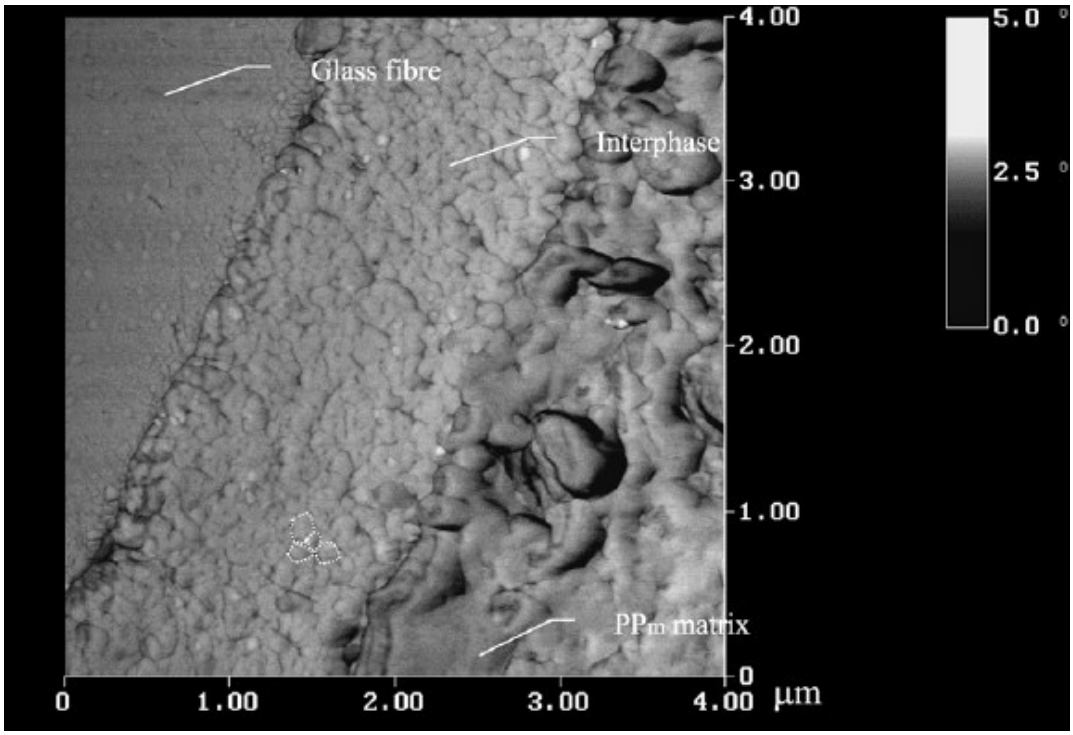

Fig. 2.2 AFM of an interphase between the polypropylene matrix and glass fiber [169].

Interface defects encompass all the inclusions, voids, discontinuities and inaccuracies that exists on the transition of the two phases in a composite. They reflect frequent manufacturing imperfections, following remarkable residual thermal stresses for instance, and can be treated during numerical simulation as geometrical imperfections in composite materials [170]. Their occurrence majorly affects response and properties of the composite despite its extremely small volume, which is a fraction of a volume of an interphase. Interface defects prove to be crucial for many properties of a composite including its durability [171], reliability [172], thermal conductivity [173] and even failure [167,174,175,176] of these materials. Defects and inclusions also

cause a high microscopic stress concentration [177]. Some studies are devoted to the defects by only [178].

An interphase with interface defects forms an imperfect interface. Its usage in realistic prediction of composites behavior dates back many years [179,180,181,182,183]. Analysis of composites having imperfect interfaces is performed primarily with use of three techniques 1. an insertion of interphase in-between the main composite constituents [184,185,186,187,180,188], 2. usage of special contact finite elements [189,190] or 3. an introduction of a system of springs [191] that may also be supplemented with dumpers.

In this dissertation the first approach has been selected, because it best represents the real phase that exists in between the main constituents of the composite. Interface defects of spherical shape are artificially smeared in the interphase domain. It is done by a statistical spatial averaging of interphase hyperelastic properties. Geometrical idealization of such defects has been provided in homogenization based studies, i.e. with the use of semi-circular or semi-spherical shapes and it follows the well-known cavitation phenomenon for a variety of matrices [192,174].

2.4. Multiscale analysis and homogenization

Multiscale analysis represents a style of modeling in which system is described simultaneously by multiple constitutive models at different scales of resolution. Models at each scale may originate from physical laws of different nature, for example continuum mechanics in macroscale [193] and molecular dynamics in atomistic scale. They are required because certain phenomena visible on one scale cannot be described accurately without supplementary information from a different scale from which they originate. Some of the examples include (1) brittle failure of reinforced concrete beam, which is caused by micro-cracks in concrete microstructure in-between the cement and grains, (2) plastic elongation of steel caused by a slip between its grains or (3) macroscopic properties of composites affected by microstructural defects. Alternatively, they are used because purely macroscale constitutive models are not accurate enough and lower scale models offer too much information or require too high computational power to be executed. Multiscale approach aims at achieving a compromise between accuracy an efficiency and frequently provides solutions to problems otherwise unsolvable in a reasonable time span.

Multiscale analysis comprise three major components: multiscale models, multiscale analysis tools and multiscale algorithms. Multiscale algorithms are the ideas of how to use a multiscale analysis tools to bridge the scale and connect different multiscale models at different levels.

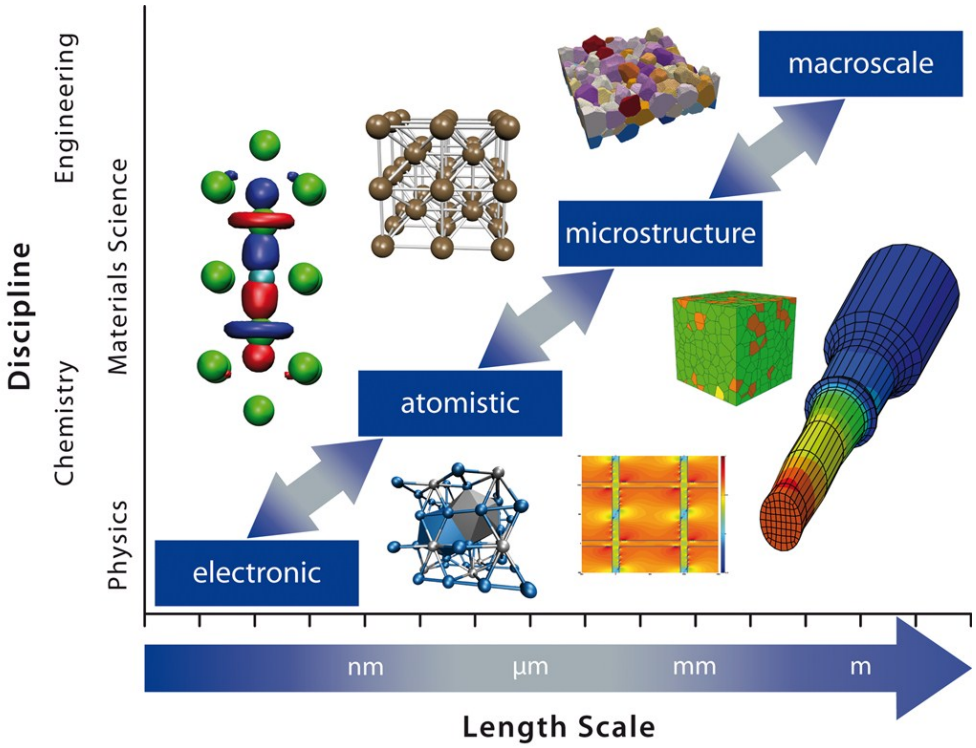

Fig. 2.3 Different length scales in multiscale analysis [N5].

The mostly used scales are depicted on Fig. 2.3. In statics they mainly depend on dimensions and are following: macroscale, mesoscale (level of microstructure), atomistic scale and electronic scale. Interestingly, each of this scales falls into a different discipline, for example macroscale into civil and mechanical engineering, mesoscale – materials science and electronic scale into physics. Thus, multiscale design frequently requires bridging different disciplines to be solved. Connection in between the constitutive models is either ensured analytically or numerically [194,195,196] and bridging between different scales is either done sequentially or concurrently. In sequential approach certain characteristics used in macroscopic constitutive models are precomputed. Usually only limited number of parameters (or variables) is passed to a different scale, but in some sparse representations even as much as six variables can be passed with success [197,198]. In concurrent alternative the macroscale constitutive model variables are computed on-the-fly during simulation. Its major advantage is that a much smaller domain of macroscopic variables must be computed in different scale.

On the other hand, a complexity of numerical algorithm solving macroscale increases. Concurrent methods are especially not well suited to problems in which parameters are passed to the FEM-based code, where each element would potentially require a separate set of parameters.

Traditional structural analysis preferred in civil engineering does not involve a multiscale approach because it tends to limit calculations to a linear range of material deformation, where simple empirical constitutive laws are sufficient. The additional margin of nonlinear structural response is frequently used as a safety margin. A good example is a design of structures made from constructional steel, for which the engineering codes, such as Eurocodes [N1], [N2], [N3], [N4] usually prefer to stay in linear elasticity. Calculations became much more involving even for steel when a localized phenomena must be taken into consideration, such as strain localization [199] or crystal plasticity [200]. For them, a macroscale constitutive model must be supplemented or interchanged with macroscopic structure. In multiscale design information may be passed from higher scale into lower scale (top-down way) or from lower to higher scale (bottom up way). Process of crossing a certain scale is called a scale bridging. Example of top-down bridging is passing boundary conditions for each element of FEM analysis into a mesoscale constitutive model and a bottom-up a intra-grain bonding conditions coming from an atomistic scale.

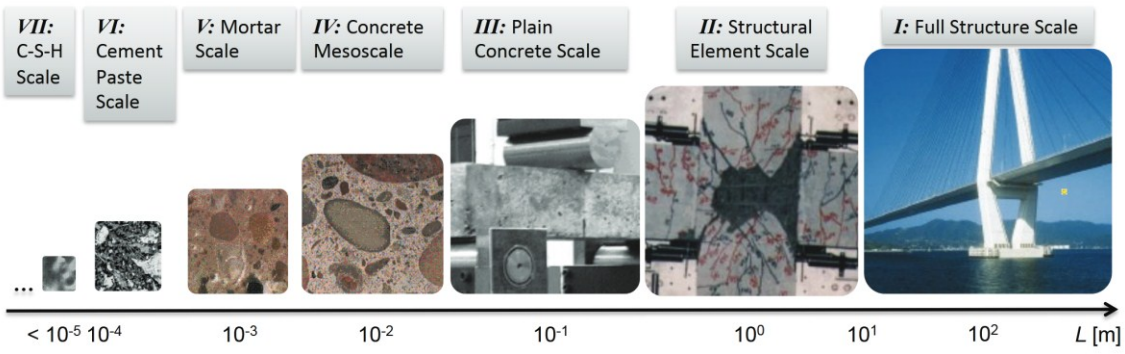

Fig. 2.4 Different scales of concrete [201].

A multiscale approach, yet indirectly, is already used on a structural design level for reinforced concrete. Calculation of ultimate limit state of this composite already requires some supplementary information apart from the scale of structural element. Specifically, precise information of steel rebars positioning is required even when all the macroscopic properties of concrete and steel are already known. These properties

already depend on information coming from four lower scales, i.e. C-S-H, cement paste, mortar and concrete mesoscale scales (see Fig. 2.4).

There are multiple methods and algorithms that allow solving multiscale problems. They focus on algebraic, numerical or hybrid solutions and usually are aimed on certain problem domains. Their comprehensive review is available in [202]. Some examples include the multi-grid methods aimed at solving a large system of algebraic equations [203] with some alteration in equation-free method [204], heterogeneous multiscale method where a preconceived macroscale constitutive model with missing components is assembled and missing data is found with use of microscale constitutive models or matched asymptotics approach [205,206,207]. Some other methods include averaging and tolerance averaging methods [208,209,210] hydrodynamic limit methods [211], the Mori-Zwanzing formalism [212], renormalization group methods [213], variational methods [214] and homogenization methods [215,216,217,218]. Multiscale approach is very frequently used for determination of the macroscopic (or effective) properties of composites, also in the stochastic context [219]. Some introduction to their theory is available for example in [220,221]. In this study a homogenization method has been selected because of its relative ease of application to the FEM systems. It is described in more detail in the next paragraph.

Homogenization method is frequently referred as a process of replacement of an equation with highly oscillatory coefficient with one having a homogenous coefficient. Initially used in studying partial differential equations (PDEs) [222,215], this concept proved to be suitable for solving a problem of inhomogeneous microstructure of continuum, such as composites. This is because the macroscale boundary conditions, such as loadings or supports usually is much bigger than the length scale of the microstructure.

The classical problem is formed in a following way

$$\nabla\left(A\left(\frac{\vec{x}}{\tau}\right)\nabla u_\tau\right)=f \tag{2.1}$$

with τ being a very small parameter and $A(\vec{g})$ being a 1-periodic coefficient $A(\vec{g}+\vec{e}_i)=A(\vec{g})$, i=1, …, n. It may be modified to the following form

$$\nabla\left(\widetilde{A}\nabla u\right)=f \tag{2.2}$$

where $\widetilde{A}$ is a constant tensor coefficient representing the effective property of a material. This property could be computed as

$$\widetilde{A}_{ij}=\int_{(0,1)^n} A(\vec{g})\left(\nabla w_j(\vec{g})+\vec{e}_j\right)\vec{e}_i dy_1\ldots dy_n, \qquad i,j=1,\ldots,n \tag{2.3}$$

in which 1-periodic w_j satisfies $\nabla_y\left(A(\vec{g})\nabla w_j\right)=-\nabla_y\left(A(\vec{g})\vec{e}_j\right)$. One equation may be replaced by another if τ is small enough to satisfy $u_\tau\approx u$ and when $u_\tau\rightarrow u$ at $\tau\rightarrow 0$. In the continuum concept an analogue of the differential element is the Representative Volume Element (RVE) in 3D problems or the representative surface element (RSE) in 2D problems. The RVE is considered representative of the medium and it should be selected in a way to contain all the relevant statistical information about an inhomogeneous medium. With such an assumption, averaging over this element results in an effective property of the medium defined as $\widetilde{A}$ above. A key problem in such formulation is assumption of such an RVE to be solvable and contain as much information about the microstructure as possible. This also holds for stochastic calculations where, in addition to the RVE selection also uncertain parameters must be selected in a way to catch the best representation of most important randomness sources and still remain simple enough to be solved.

In its early approaches homogenization was used in a purely analytical [218,223] way and thus microstructure was very simple and range of applications limited. This obstacle was overcome with incorporation of the FEM, where the RVE is modeled and solved. Rapid evolution of the FEM academic and commercial software that started in early 2000s, supported researchers in discretization and visualization of the RVE. A simultaneous revolution in computational power of personal computers made accessible solution of more complex problems. All of these allowed homogenization to become one of the most widespread methods used to solve the multiscale problems in materials science, especially those connected to meso- and micro- scale of inhomogeneous materials, see e.g. [224,225,226,227]. The topic of a correct RVE is so important that some studies treat it as a research problem connected with its generation [228], size or scale effect [229,230,231,232,233] and validity of applied random microstructure [234]. Some other works review existing and introduce

stochastic boundary conditions [235] or propose formulation of finite elements for the hyperelastic case [236]. The FEM is commonly included in approaches aimed at decrease of problem size or computation time, which is done on the expense of accuracy. These propose usage of the artificial neural networks and machine learning approaches [237,238,239], divide the heterogeneous medium to several subdomains [83], use manifold-learning method to reduce dimensions of microscopic strain fields [240], utilize orthogonal decomposition R3M [241] or aim to apply a reduced database model [242]. The FEM is, of course, not the only possibility. There also exist some alternative methods such as mesh-free formulations [243], gradient approach [244], the fast Fourier Transform based methods (FFT) [245], transformation field [246], or the discrete element method [247], perfect for densely packed solids. In this study a nonlinear response of material is studied, for which exist some approaches to homogenization, such as the ones in [248,249,250,251]. In many cases they include specific a-priori assumptions connected to the stress or strain fields, see e.g. [252,253,254].

Probabilistic homogenization adds to homogenization yet one more level of abstraction. It introduces uncertain parameters and variables in the lower scale of homogenization, usually in the material microstructure. Some examples include [255,256,257,258,259,97,260,261]. Similarly to the probabilistic analysis in macroscopic calculations, it quantifies the influence of an input uncertainty on the response of the medium. The difference lays in the source of uncertainty, which cannot be included in a macroscopic level, yet cause randomness in engineering structures. Common problems for which probabilistic homogenization is applied include uncertain phase properties, interface defects, geometric uncertainty or inclusions. Uncertainty may be included in one phase or in in the various characteristics of the RVE, for example the reinforcement positioning. They all result in an uncertain stiffness tensor or parameters leading the material constitutive relation.

Probabilistic homogenization of composites is especially interesting when it is coupled with a problem of interface defects. Analytical solution of this problem can only be obtained for elastic composites and a simple RVE, which was proposed by M.M. Kamiński in [262]. A more in-depth analysis of stiffness tensor even in elastic regime requires usage of numerical solvers. The author proposed such an approach [188], verified it with analytical solution and, further, studied a fully anisotropic response of

a homogenized composite [159]. Results proved, that particle clustering and uneven particle distribution affects anisotropy of the composite and has a high influence on components of its stiffness tensor. In his other work [8], the author verified a numerical solution of a composite with uncertain reinforcing particle radius with an analytical solution and studied influence of an uncertain aspect ratio [263] on the effective stiffness tensor of a composite.

This thesis presents an extension of the previous research into a hyperelastic regime of the composite. In the first phase, an uncertain hyperelastic response of homogeneous medium was considered [82] and then a problem of stochastic hyperelastic response of composites with hysteresis [70] and with stochastic interface defects [264,265] was solved. It has been decided to limit considerations of this thesis to a problem of hyperelastic composite with stochastic interface defects to keep it concise and cover all the aspects of the problem.

2.5. Effective response of medium

Effective response of a medium is a relation of objective function with uncertain parameters or variables. In structural design the objective function could be defined as a limit function. In homogenization it usually is an effective property of a medium, such as the stiffness tensor, bulk modulus, effective stress or strain energy. In majority of homogenization problems (and also in most structural engineering problems) such relation cannot be analytically determined. This is a reason why the objective function is commonly computed with use of discrete numerical procedures. In SPT this is frequently done using a response function method (RFM) [266,267,268,269,144] or response surface method (RSM) [270,271,113], when more variables are considered. An alternative of direct differentiation method (DDM) is rarely selected because it requires at least an intervention into a source code of discrete numerical solver. In the worst case, writing a complete solver algorithm is required. This is because deterministic values used by these programs must be substituted with their stochastic counterparts.

Response function and response surface methods both aim to approximate the real relations of the objective function with use of a surrogate model (also called as a metamodel [272,273]) having an uncertain variable. This is done on the basis of a carefully selected set of discrete numerical (or laboratory) experiments performed for

different values of input variables [274,275]. Their major advantage is ease of application and disconnection of the metamodel fitting from the stochastic procedure, which allows simple analysis of fitting error. Surrogate models are commonly applied from a subset of polynomial functions and also their fractions or other rational functions [276,277]. A little less common is usage of B-splines, logarithmic, exponential or hyperbolic functions, as in [278,279], for instance.

The main difference between the response function and response surface methods is number of variables included in it. While the former holds only a single variable, the latter depends from at least two (or more). This, in turn, limits usage of the response function to a single source of uncertainty, while the response surface may be used for unlimited number of input random (or deterministic) variables. The two methods also majorly differ in cost of their fitting and the amount of discrete experiments required. This amount increases exponentially together with a number of input variables (or dimensions) n in a rate of n^v, where n denotes the number of realizations around the expected value of each uncertain variable (assuming this number is equal for all of variables). Fitting of the response function is commonly done by the least squares algorithm, which is very well performing for single variable polynomials. It is not the case of multivariate functions, including the polynomials.

In general, optimization problems are commonly divided to three major categories, i.e. the linear programming (LP), quadratic programming (QP) and nonlinear programming (NP) problems.

- linear programming problem is the one in which the objective function and all of the constraints are linear functions of the decision variables. It always has either (a) one or more equivalent globally optimal solution, (b) has an unbounded objective or (c) no feasible solution. It is convex and have at most one feasible region with ‘flat faces’ (i.e. no curves) on its outer surface. Its optimal solution (if available) lays at a ‘corner point’ on this surface that is represented by constraints. A solver may work point wise and solution is fast. Common solvers include families of the simplex technique [280,281] in its primal [282] or dual [283] version and interior point [284,285] technique. Fitting is usually done with linear or (sometimes) nonlinear least squares.
- quadratic programming problem has an objective function which is a quadratic function of the decision variables and constraints which are all linear functions

of the variables. They have only one feasible region with 'flat faces' on its surface (due to the linear constraints), but the optimal solution may be found anywhere within this region or on its surface. Objective function may be convex or non-convex. The convex functions have either positive definite or semi-definite Hessians, and non-convex - an indefinite Hessian and a saddle-shape. It is usually out of scope for QP solvers. Typical solvers include simplex extension to the QP, active set and working set method variations [286,287,286], interior point [288,289,290] or Newton-barrier methods [291,292,293,294].

- nonlinear programming problem is the most difficult for optimization. Objective function is generally a nonlinear function of the decision variables and usually has many locally optimal solutions. A global minimum is very difficult to find [295]. Common solvers include the augmented Lagrangian methods [296,297], sequential quadratic programming [298,299] and reduced gradient methods [300,301,302].

Optimization of the response function and the response surface performed in this dissertation falls into the quadratic programming class of problems. A more detailed introduction for algorithms used in recovery of an effective response of the composite is available in section 3.2.

3. Theoretical background

This section consists of two main parts. In the first one (section 3.1) the probabilistic homogenization used in numerical part of this dissertation is introduced. In the second one (section 3.2) the selected methods to recover the effective response of the medium are presented. The first section is based on previously published works by the author, namely [264,265].

3.1. Probabilistic homogenization

Probabilistic homogenization serves for determination of the random effective material parameters of the composite with stochastic interface defects for the specified hyperelastic potential. In this section, theoretical formulation of this problem is provided.

3.1.1. Multiscale composition of the composite

Let me introduce a heterogeneous and continuous solid body representing a particle-reinforced composite in 3D Euclidean space Ω presented on Fig. 3.1.

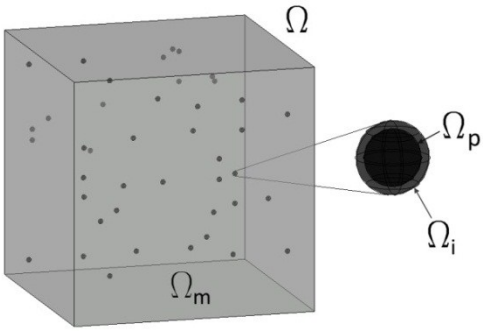

Fig. 3.1 A heterogeneous body under consideration. Ω - heterogeneous solid body, Ω_i – hyperelastic interphase, Ω_m - hyperelastic matrix, Ω_p – linear elastic reinforcing particles [265].

This body is composed by three distinct phases — a linear elastic reinforcing particle filling the region Ω_p, a hyperelastic matrix in domain of Ω_m and hyperelastic interphase in the region of Ω_i, as in the following equation

$$\Omega=\Omega_m \cup \Omega_p \cup \Omega_i \tag{3.1}$$

Contact in-between the subsets is considered to be perfect and load-independent in further deformation process (no slip or damage occurs). The interphase and a particle

does not intersect the other surfaces of the RVE $\partial\Omega$ so that $\Omega_p \cap \partial\Omega = \varnothing$. The RVE contains k non-intersecting non-uniformly distributed reinforcing particles with the same distribution of defects. The domain of the defects is composed of the series of disjoint single semi-bubbles as follows

$$\Omega_d = \bigcup_{j=1}^{r} \bigcup_{i=1}^{n} \Omega_{d(i,j)} \tag{3.2}$$

Each interface defect $\Omega_{d(i,j)}$ is localized on the given particle surface, has semi-spherical shape and is directed outwards from the particle center; this is visualized on Fig. 3.2. Defect number on the given particle-matrix interface is denoted by i, $1 \le i \le n$ and $j = 1,...,r$ stands for the particle number. All the interface defects are statistically dispersed according to the Gaussian distribution radius $R_{(i,j)}$. It is defined by its expected value $E\left(R_{(i,j)}\right)$ and variance $Var\left(R_{(i,j)}\right)$ on each particle-matrix interface.

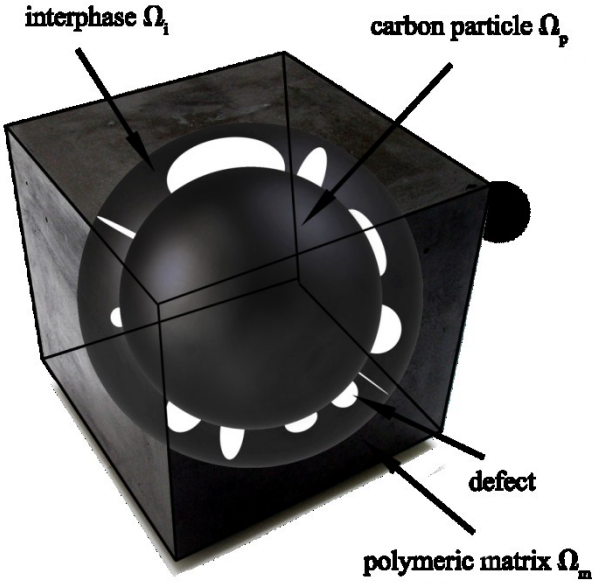

Fig. 3.2 Internal composition of the composite.

Multiscale homogenization framework consists of the micro-contact and micro-scale. It is proposed by three subsequent steps

- reconstruction of the interphase as the new artificial material that fully separates the two other domains – the particle and the matrix,

- probabilistic averaging of the defects throughout the interphase; defects belong to the micro-contact scale,
- probabilistic homogenization of the composite consisting of three components – the matrix, particles and interphases belonging to the micro-scale.

The interphase is considered to be a thin layer around any particle, whose constant thickness equals to an upper bound on statistical population of the defects radii according to the well-known three sigma rule [159]

$$\Delta_j = E\left(R_{(j)}\right) + 3\sqrt{\mathrm{Var}\left(R_{(j)}\right)}, \quad j=1,\ldots,r \tag{3.3}$$

Effective stress of the interphase is recovered by the probabilistic averaging method as the volumetric average of stress of the defects σ^d and stress of the matrix σ^m belonging to its volume Ω_i

$$\sigma^{int}(\varepsilon_i) = \frac{\Omega_i - \Omega_d}{\Omega_i}\sigma^m(\varepsilon_i) + \frac{\Omega_d}{\Omega_i}\sigma^d(\varepsilon_i) \tag{3.4}$$

The first two moments of variable σ^{int} can be simplified to

$$E[\sigma^{int}] = (1 - E[w])\sigma^m(\varepsilon_i);\ \mathrm{Var}[\sigma^{int}] = \mathrm{Var}(w)\sigma^m(\varepsilon_i)^2 \tag{3.5}$$

assuming that $\sigma^d(\varepsilon_i)=0$ for the defects and substituting their volume ratio the interphase as the parameter w. First two moments of the interface defects radius ($E(R)$ and $Var(R)$) are assumed according to Appendix of [159], while $E(w)$ and $Var(w)$ are calculated analytically using statistical parameters of R. Such an assumption is applied intentionally to make the solution independent from the underlying hyperelastic law applied for the matrix. This enables a direct comparison of the results for different potentials, which would be otherwise extremely difficult. This is because each of the hyperelastic formulations has its own set of properties to be defined that are variable in length and not interchangeable, especially in the stochastic case.

Next, I introduce a weakening coefficient w equivalent to the volume fraction of interface defects as

$$w = \frac{V^d}{V^m + V^d} = \frac{V^d}{V^{int}}. \tag{3.6}$$

Volume of the defects V^d is uniquely defined by their number and radii as $V^d=k\frac{2}{3}\sum_{i=1}^{n}\pi r_1^n r_2^n r_3^n$, while volume of the matrix could be computed as $V^m=V^{int}-V^d=k\frac{4}{3}\pi\left(R_i^3-R_p^3\right)-V^d$; V^{int} denotes the volume of the interphase and k stands for the number of particles inside the RVE. Volume of the RVE is unitary, thus V^{int} directly represents a volume fraction of interface in the entire composite. The above introduced weakening coefficient is a single-parameter representation of the defects intensity on the matrix-particle interface. Such a defective interface is used in consequent stochastic homogenization limited to the range of strain considered in laboratory tests (here $\varepsilon_{11}\in(0,0.275)$). The weakening coefficient is sampled in an equidistant manner in a range of $w\in(0.05,0.9)$ so that $V^d/V^{int}\in[0.00, 0.005, \ldots., 0.9]$. It also serves for the input random variable in the stochastic studies and, together with the strain level, as a variable in the deterministic analysis. This coefficient remains constant through an entire deformation process. This means that all defects follow the deformation of the interphase (their radius increases or decreases together with interphase thickness and shape changes). An alternative evolution of this parameter may be considered also, for example an assumption of a constant shape of the defects regardless the strain level. It is not applied here. In further chapters the weakening coefficient is also referred as the volume fraction of interface defects.

3.1.2. Hyperelastic formulation of the matrix

Let me further assume the deformation gradient of hyperelastic matrix as $\mathbf{F}=\partial\mathbf{x}/\partial\mathbf{X}$, with $\mathbf{x}$ referring to the spatial and $\mathbf{X}$ the reference configuration, the right Cauchy-Green deformation tensor $\mathbf{C}$ as $\mathbf{C}=\mathbf{F}^T\mathbf{F}$ and the Finger tensor $\mathbf{b}$ as $\mathbf{b}=\mathbf{F}\mathbf{F}^T$. For hyperelastic materials with no hysteresis mechanical behavior is independent of the history of loading and the strain energy is only a function of the elastic deformation. There holds

$$U^m=U^m(\mathbf{C})=U^m(\mathbf{b}),\ C=\phi(\mathbf{g})=\mathbf{F}^T\mathbf{g}\mathbf{F}. \tag{3.7}$$

The second Piola-Kirchhoff stress tensor $\mathbf{S}$ of such a material is following

$$\mathbf{S}=\frac{\partial U^m}{\partial\mathbf{E}}=\frac{2\partial U^m}{\partial\mathbf{C}}, \tag{3.8}$$

where $\mathbf{E}$ is connected with $\mathbf{C}$ by the Langrangian strain tensor as $\mathbf{E}=1/2(\mathbf{C}-\mathbf{1})$; $\mathbf{1}$ is the second order identity tensor. Let me also introduce the metric tensor as $\mathbf{g}=\mathbf{F}^{-T}\mathbf{C}\mathbf{F}^{-1}$, the

Eulerian strain tensor as $\mathbf{e}=1/2\left(\mathbf{g}-\mathbf{b}^{-1}\right)$ and the volumetric change with a reference to material configuration as J=det(**F**). The Cauchy stress tensor **σ** and the Kirchoff stress tensor could be defined in the following way:

$$\boldsymbol{\tau}=\frac{\partial U^m}{\partial \mathbf{e}}=\frac{2\partial U^m}{\partial \mathrm{g}},\ \boldsymbol{\sigma}=\frac{1}{\mathbf{J}}\boldsymbol{\tau}=\frac{1}{\mathbf{J}}\mathbf{F}\mathbf{S}\mathbf{F}^{\mathrm{T}} \tag{3.9}$$

Time derivatives of the second Piola-Kirchhoff stress tensor $\dot{\mathbf{S}}$ and the Langrangian strain tensor $\dot{\mathbf{E}}$ can be calculated as $\dot{\mathbf{S}}=\mathrm{J}\mathbf{F}^{-1}\boldsymbol{\sigma}^{0}\mathbf{F}^{-\mathrm{T}}$ and $\dot{\mathbf{E}}=\mathbf{F}^{\mathrm{T}}\mathbf{D}$. In these relations $\boldsymbol{\sigma}^{0}=\dot{\boldsymbol{\sigma}}-\mathbf{L}\boldsymbol{\sigma}-\boldsymbol{\sigma}\mathbf{L}^{\mathrm{T}}+(\mathrm{tr}\,\mathbf{D})\boldsymbol{\sigma}$ is the Truesdell rate of Cauchy stress tensor, **D** is the deformation rate tensor and **L** represents the velocity gradient. Taking into consideration the above relations the fourth order elasticity tensor C is linked with the Piola-Kirchhoff stress in the following way

$$\dot{\mathbf{S}}=\mathrm{C}:\dot{\mathbf{E}}. \tag{3.10}$$

Upon some substitutions of the above relations, Truesdell rate of Cauchy stress tensor could be expressed as

$$\boldsymbol{\sigma}^{0}=\frac{1}{\mathrm{J}}\mathbf{F}\left[\mathrm{C}:\left(\mathbf{F}^{\mathrm{T}}\mathbf{D}\mathbf{F}\right)\right]\mathbf{F}^{\mathrm{T}}=\mathbf{c}:\mathbf{D}. \tag{3.11}$$

The fourth order elasticity tensor C could be finally expressed as

$$\mathrm{c}_{\mathrm{ijkl}}=\frac{1}{\mathrm{J}}\mathrm{F}_{\mathrm{iI}}\mathrm{F}_{\mathrm{jJ}}\mathrm{F}_{\mathrm{kK}}\mathrm{F}_{\mathrm{lL}}\mathrm{C}_{\mathrm{IJKL}} \tag{3.12}$$

Let me further decompose the strain energy into the isochoric and volumetric parts. With such an assumption, isochoric part of hyperelastic strain energy is a function of the first and the second invariant of the right Cauchy-Green deformation tensor **C** (I_1, I_2) and the volumetric part – only function of J. These invariants are defined here as $\mathrm{I}_1=\mathrm{tr}\mathbf{C}$ and $\mathrm{I}_2=\frac{1}{2}\left\{(\mathrm{tr}\mathbf{C})^2-\mathrm{tr}\mathbf{C}^2\right\}$.

In this light expression for **C** can be recalled as

$$\mathbf{C}=\mathbf{F}^{\mathrm{T}}\mathbf{F} \tag{3.13}$$

and J=det(**F**)=1 also holds (volume is preserved in loaded configuration).

With above assumptions, the second Piola-Kirchhoff stress simplifies to

$$\mathbf{S}=2\left(\frac{\partial U^m}{\partial \mathrm{I}_1}\frac{\partial \mathrm{I}_1}{\partial \mathbf{C}}+\frac{\partial U^m}{\partial \mathrm{I}_2}\frac{\partial 2}{\partial \mathbf{C}}+\frac{\partial U^m}{\partial \mathrm{I}_3}\frac{\partial \mathrm{I}_3}{\partial \mathbf{C}}\right). \tag{3.14}$$

Let me further define a following operation $\mathbf{K'}=\mathbf{K}-\frac{1}{3}\mathrm{tr}\left(\mathbf{K}^{\mathrm{T}}\mathbf{C}\right)\mathbf{C}^{-1}$ for the arbitrary second order tensor **K** and introduce derivatives of the invariants in reference to the right Cauchy-Green deformation tensor $\partial \mathrm{I}_1/\partial\mathbf{C}=\mathrm{J}^{-\frac{2}{3}}\mathbf{1'}$, $\mathrm{I}_2/\partial\mathbf{C}=\mathrm{J}^{-\frac{2}{3}}(\mathrm{I}_1\mathbf{1'}-\mathbf{C'})$ and $\partial \mathrm{J}/\partial\mathbf{C}=\mathbf{1/2}\mathrm{J}\mathbf{C}^{-1}$. The second Piola-Kirchhoff stress tensor can be now further simplified to

$$\mathbf{S}=2\left(\mathrm{J}^{-\frac{2}{3}}\left(\frac{\partial \mathrm{U^m}}{\partial \mathrm{I}_1}+\frac{\partial \mathrm{U^m}}{\partial \mathrm{I}_2}\right)\mathbf{1'}-\mathrm{J}^{-\frac{2}{3}}\frac{\partial \mathrm{U^m}}{\partial \mathrm{I}_2}\mathbf{C'}+\frac{\mathbf{1}}{\mathbf{2}}\mathrm{J}\frac{\partial \mathrm{U^m}}{\partial \mathrm{J}}\mathbf{C}^{-1}\right) \tag{3.15}$$

and the Cauchy stress tensor may be expressed as

$$\boldsymbol{\sigma}=2\left(\frac{1}{\mathrm{J}}\left(\frac{\partial \mathrm{U^m}}{\partial \mathrm{I}_1}+\frac{\partial \mathrm{U^m}}{\partial \mathrm{I}_2}\right)\mathbf{b''}-\frac{1}{\mathrm{J}}\frac{\partial \mathrm{U^m}}{\partial \mathrm{I}_2}\mathbf{b''b''}+\frac{1}{2}\frac{\partial \mathrm{U^m}}{\partial \mathrm{J}}\mathbf{1}\right) \tag{3.16}$$

where **K''** is a following operation applied on the arbitrary second order tensor related to its origin $\mathbf{K''}=\mathbf{K}-\frac{1}{3}(\mathrm{tr}\ \mathbf{K})\mathbf{1}$; it is done for the Finger tensor **b**. The invariants for this constitutive model and boundary conditions used to fitting the model curve to the laboratory tests for the uniaxial stretch are given as follows: $\mathrm{I}_1=\lambda^{4/3}+2\lambda^{-2/3}$, $\mathrm{I}_2=2\lambda^{2/3}+2\lambda^{-4/3}$, $\mathrm{J}=\lambda$.

An alternative formulation of the hyperelastic strain energy function is available, where the isochoric and volumetric parts are both dependent on all three invariants (I_1, I_2, I_3) and on their cross-products also; the number of invariants taken into consideration may even be increased. Derivation of strain energy in such a general case would be very demanding, but under an assumption of vanishing cross-products is much easier [249]. Strain energy has a two-parametric description in this constitutive model, i.e. the isochoric one dependent form $(\mathrm{I}_1,\mathrm{I}_2)$ and the volumetric one dependent only from J so that

$$U^m=U^m_{iso}(\mathrm{I}_1,\mathrm{I}_2)+U^m_v(\mathrm{J}). \tag{3.17}$$

The simplest functions depend on (I_1,J) by only [49,303]

$$U^m=\sum_{i=1}^{D}(I_1-3)^i+U_v^m(J). \tag{3.18}$$

The volumetric strain energy for the compressible hyperelastic materials may be computed with the following equation [304]:

$$U_v^m=\frac{K_1}{2}(\ln J)^2+\frac{K_2}{2}(J-1)^2+K_3(J-\ln J-1). \tag{3.19}$$

In further analysis the incompressible case is assumed so that $U_v^m(J)=0$.

A formulation of strain energy based on the first invariant only is quite straightforward but has limited applicability for multi-axial loading. An example of such a formulation is the Neo-Hookean model [49] and it defines the strain energy (incompressible case) as

$$U_{NH}^m=C_{1,NH}^m(I_1-3); \tag{3.20}$$

it includes a single material parameter $C_{1,NH}^m$ only. There holds for this constitutive model in case of the uniaxial stretch

$$\sigma_{NH}^m=2C_{1,NH}^m\left(\lambda-\frac{1}{\lambda^2}\right). \tag{3.21}$$

The approaches based on two invariants are much more versatile [305], where most probably the simplest one is the Mooney-Rivlin model. It defines the strain energy for an incompressible material as [46,47]

$$U_{MR}^m=C_{1,MR}^m(I_1-3)+C_{2,MR}^m(I_2-3), \tag{3.22}$$

where two independent empirical constants are $C_{1,MR}^m$ and $C_{2,MR}^m$. The unidirectional engineering stress under uniaxial stretch can be described as

$$\sigma_{MR}^m=\left(2C_{1,MR}^m+\frac{2C_{2,MR}^m}{\lambda}\right)\left(\lambda^2-\frac{1}{\lambda}\right), \tag{3.23}$$

where λ denotes the specimen (or RVE) elongation. This elongation is connected to the strain with $\varepsilon_{11}=\lambda-1$. A more general form of the strain energy represent various polynomial formulations, where the strain energy is a function of the first and second invariant of the isochoric right Cauchy-Green deformation tensor, so that

$$U^m_{p,ij}=\sum_{i=1}^{o}\sum_{j=1}^{p} C_{ij}(I_1-3)^i\,(I_2-3)^j+U^m_v(J). \tag{3.24}$$

The last considered here formulation is the Arruda-Boyce [51] model that defines the strain energy as

$$\begin{aligned} U^m_{AB}=C^m_{1,AB}&\left(\begin{array}{c}\left(\frac{1}{2}I_1-3\right)+\frac{1}{20(\lambda^m_A)^2}+\frac{1}{1050(\lambda^m_A)^4}\left(I_1^3-27\right)+\\ \frac{19}{7000(\lambda^m_A)^6}\left(I_1^4-81\right)+\frac{519}{673750(\lambda^m_A)^8}\left(I_1^5-243\right)\end{array}\right)\\ &=C^m_{1,AB}\sum_{i=1}^{5}\alpha_i\hat{\beta}^{i-1}\left(I_1^i-3^i\right)\end{aligned} \tag{3.25}$$

where λ^m_A stands for the stretch at which polymer chain networks becomes locked and $C^m_{1,AB}$ is an additional material parameter. In an alternative form $\hat{\beta}=\frac{1}{(\lambda^m_A)^2}$ and α_i defines the consecutive coefficients before $(\lambda^m_A)^{2x}$. The unidirectional engineering stress is described as follows

$$\sigma^m_{AB}=2C^m_{1,AB}\left(\lambda-\frac{1}{\lambda^2}\right)\left(\begin{array}{c}\frac{1}{2}+\frac{2}{20(\lambda^m_A)^2}\left(I_1-9\right)+\frac{3}{1050(\lambda^m_A)^4}\left(I_1^2-27\right)+\\ \frac{4\cdot19}{7000(\lambda^m_A)^6}\left(I_1^3-81\right)+\frac{5\cdot519}{673750(\lambda^m_A)^8}\left(I_1^4-243\right)\end{array}\right). \tag{3.26}$$

More hyperelastic formulations can be found e.g. in [306]. They are also listed in the Introduction.

3.1.3. Homogenization method

Next, the homogenization method is introduced. Firstly the expected value of the uniaxial stress in the matrix coming from laboratory tests is recovered w.r.t. the strain level $[\sigma^m(\varepsilon_{11})]=\frac{1}{M}\sum_{i=1}^{M}\sigma^m(\varepsilon_{11})^{(i)}$. Subsequently, it is fitted to it the response of 10 different hyperelastic formulations. Specifically the parameters of these constitutive models $C^m_{k,\xi}$ are optimized to minimize the least squares total error for all the stress-strain data points. Next, the 3 best potentials are selected that have the lowest overall fitting error. Then, the sets of material parameters $C^{int}_{i,\xi}$ of the defected interphase are recovered for each constitutive model denoted by ξ with use of the least squares

method (LSM) so that they minimize the error of the LSM for $\sigma^{int}(\varepsilon_{11})$. Recalling eqn (3.4) such optimization problem could be defined as

$$C_{i,\xi}^{int} \rightarrow \sum_{k=1}^{Y} \left(\frac{\Omega_k - \Omega_d}{\Omega_k} \sigma^m(\varepsilon_1, w_i) - \sigma^{int}\left(\varepsilon_1, C_{i,\xi,l}^{int}\right) \right) = \min \tag{3.27}$$

where k denotes the different magnitudes of the interface defects volume fraction and l different levels of stretch. In each constitutive model considered here the physical meaning (if at all available) and number of parameters is completely different and therefore directly averaging the material properties of the hyperelastic interphase would bound it to a concrete model, which is strictly limiting. An alternative approach of averaging an entire stress-strain relation of the interphase $\sigma^{int}(\varepsilon_{11})$ that is proposed here enables comparison of all possible constitutive models and additionally makes it straightforward. For the simpler, elastic case the situation is totally different, because all the isotropic materials (applied as the composite phases) expose only two constants – the Young modulus and the Poisson ratio; they may be directly averaged as in [159] and compared for different materials or composites; anisotropy is usually considered only in the macro level available upon homogenization [307,308].

These parameters $C_{i,\xi}^{int}$ are used next for a definition of artificial interface material in the FEM and they are found thanks to spatial averaging. This step involves also a composition of the RVE and computation of the effective strain energy $U_{\xi}^{eff,FEM}$ (strain energy for the homogenized composite) with use of the FEM solver. This is done for various volume fractions of interface defects w dispersed in the range of $w \in (0.05, 0.9)$, which serves further for determination of the composite effective material parameters.

The effective strain energy may be represented for each constitutive model ξ as the following function of the invariants and the interface defects volume fraction w:

$$U_{\xi}^{eff} = \mathrm{f}_{\xi}^{\mathrm{U}}(\lambda, \mathrm{I}_1, \mathrm{I}_2, w) \cong U_{\xi}^{m} + U_{\xi}^{int} + U_{\xi}^{p}, \tag{3.28}$$

where only the coefficients of the selected potential $C_{i,\xi}^{eff}$ depend on w (i denoting coefficient number). This assumption focus the application to incompressible hyperelastic composites with very stiff particles, such as polymers or rubber that is reinforced by carbon black. For this case the deformation of stiff particles in the stretch

is very small and their volume fraction also so that $U_{\xi}^{p} \lll U_{\xi}^{m}, U_{\xi}^{int}$. Further, mechanical properties of the defects (semi-spherical voids) are negligible and close to zero. Because of this they produce zero strain energy. Following from above, it is assumed that the composite is effectively governed by hyperelastic phases with a relatively small error. Hyperelastic material coefficients $C_{i,\xi}^{eff}(w)$ will, of course, be different than the ones for the virgin homogeneous material $C_{i,\xi}^{m}$ or the interphase $C_{i,\xi}^{int}$ and will depend on the number and radii of the interface defects represented by w.

Let me focus on example based on the Mooney-Rivlin potential. Effective strain energy of the composite is governed by a following relation $U_{MR}^{eff,LSM}=C_{1,MR}^{eff}(w)\cdot(\mathrm{I}_1-3)+C_{2,MR}^{eff}(w)\cdot(\mathrm{I}_2-3)$. Dependence of the material coefficients is calculated in a two-step procedure. Firstly, sets of material parameters are recovered for all the FEM simulations with respect to w and the selected hyperelastic constitutive models. In the case of Mooney-Rivlin they are $C_{1,MR}^{eff}(w_\mathrm{i})$ and $C_{2,MR}^{eff}(w_\mathrm{i})$. Secondly, these sets are further used as an input to the LSM approximation. This approximation recovers a continuous polynomial function of material parameters with respect to w. For Mooney-Rivlin it is $C_{1,MR}^{eff}(w)$ and $C_{2,MR}^{eff}(w)$. Optimum order of this polynomial is recovered by a triple criterion, i.e. minimization of the LSM error and variance, as well as maximization of correlation of the lab test results and the stress-strain relation for the considered potential.

$$C_{i,\xi}^{eff}(w)=\mathrm{a}_{i,j}w^{j}, \quad i=0,\ldots,\mathrm{n}, j=0,\ldots,\mathrm{m}_i, \tag{3.29}$$

where i is the i^{th} material coefficient of the hyperelastic constitutive model ξ and m_i is the polynomial order of the i^{th} material coefficient. Following the example of Mooney-Rivlin potential, polynomial representations of its material coefficients are defined as

$$C_{1,MR}^{eff}(w)=\mathrm{a}_{1,j}w^{j},\ C_{2,MR}^{eff}(w)=\mathrm{a}_{2,j}w^{j}, \quad j=0,\ldots,\mathrm{m}_i \tag{3.30}$$

where m_i stand for the optimum order of the polynomials equivalent to $\mathrm{m}_i=5$ (6 or 7). The error of such approximation is relatively small and response is always continuous in the (w, ε_{11}) range. The number of polynomials required for fitting strictly follows the number of material parameters and the number of the FEM realizations required

as an input increases together with a range of w analyzed. This means that each material parameter may have a different dependence on this w.

Next, an effective stress of the composite σ^{eff} is calculated as

$$\sigma^{eff}_{\xi,AMM}=f^{\sigma}_{\xi,\mathrm{AMM}}(\lambda,I_1,I_2,w), \tag{3.31}$$

where $f^{\sigma}_{\xi,\mathrm{LSM}}$ is some function of the invariants, the stretch and interface defects volume fraction. It is based on the hyperelastic constitutive model applied for the matrix for the same reason as the effective strain energy of the composite is. For example, for the Mooney-Rivlin the effective uniaxial stress of the composite could be represented by a following formula

$$\sigma^{eff}_{MR,AMM}=\left(2C^{eff}_{1,MR}(w)+\frac{2C^{eff}_{2,MR}(w)}{\lambda}\right)\left(\lambda^2-\frac{1}{\lambda}\right), \tag{3.32}$$

where $C^{eff}_{1,MR}(w)$ and $C^{eff}_{2,MR}(w)$ are already recovered from the effective strain energies. This approximation is called an augmented material model and denoted by the lower index AMM. The second, alternative, approximation of the effective stress directly relates it to the interface defects volume fraction and strain with a polynomial $f^{\sigma}_{\xi,\mathrm{Approx}}$. polynomial representations of its components are found numerically, e.g.

$$\sigma^{eff}_{MR,Approx}(w)=f^{\sigma}_{\mathrm{MR,Approx}}=a^{\mathrm{MR}}_{\mathrm{Approx,i}}w^{\mathrm{i}}\varepsilon^{\mathrm{j}}_{11}, \qquad \mathrm{i}=0,\ldots,\mathrm{s},\ \mathrm{j}=0,\ldots,\mathrm{t} \tag{3.33}$$

Deformations applied for the RVE for an uniaxial stretch can be applied with a following deformation gradients

$$F_{x_1}=\begin{bmatrix}\lambda & 0 & 0\\ 0 & 1 & 0\\ 0 & 0 & 1\end{bmatrix},\ F_{x_2}=\begin{bmatrix}1 & 0 & 0\\ 0 & \lambda & 0\\ 0 & 0 & 1\end{bmatrix},\ F_{x_3}=\begin{bmatrix}1 & 0 & 0\\ 0 & 1 & 0\\ 0 & 0 & \lambda\end{bmatrix} \tag{3.34}$$

for the three directions x_1, x_2 and x_3, where the deformations on diagonal represent the elongations and apart from diagonal – shears.

These equations have been derived assuming that each particle is surrounded by the interphase of the same thickness and the same elastic properties reduction parameter w. This thickness does not appear as an explicit additional parameter here but affects computational FEM experiments leading to the specific LSM approximation of

the effective elasticity tensor. It is possible to insert different Gaussian random variables w_i here, whose basic probabilistic moments may be different for various particles interphases or insert the w_i into each particle that follows a specific probability density but for it to be reliable would require thousands or at least several hundreds of particles in the RVE that are surrounded by a thin interphases. This is unavailable from the computational point of view, for which a set of nonlinear analyses would be required with billions of finite elements each. Current considerations include at most 150 particles that are treated deterministically and they do not have the interphase at all, whose small thickness majorly increases computational complexity.

3.1.4. Mechanical problem formulation

Next, an uncoupled mechanical problem of static or quasi-static large deformations is formulated in the heterogeneous domain composed of two disjoint constituents. The main aim here is to find an equivalent medium having the same deformation energies under uniaxial, biaxial and shear deformations. Homogenization of a composite occupying a volume $\Omega \in \Re^3$ with linear elastic components in large deformation state is rewritten for stresses $\sigma_{ij}(\mathbf{x})$, strains $\varepsilon_{ij}(\mathbf{x})$ and displacements $u_i(\mathbf{x})$ functions as

$$\sigma_{ij,j}(\mathbf{x})+\rho f_i(\mathbf{x})=0, \tag{3.35}$$

$$\sigma_{ij}(\mathbf{x})=C_{ijkl}(\mathbf{x})\varepsilon_{kl}(\mathbf{x}), \tag{3.36}$$

$$\varepsilon_{kl}(\mathbf{x})=\frac{1}{2}\left(u_{k,l}(\mathbf{x})+u_{l,k}(\mathbf{x})+u_{k,i}(\mathbf{x})u_{l,i}(\mathbf{x})\right) \tag{3.37}$$

$$\sigma_{ij}(\mathbf{x})n_j=0,\ \mathbf{x}\in\partial\Omega_\sigma, \tag{3.38}$$

$$u_j(\mathbf{x})=\hat{u}_j(\mathbf{x}),\ \mathbf{x}\in\partial\Omega_u \tag{3.39}$$

where both $\partial\Omega_\sigma$ and $\partial\Omega_u$ represent some subsets of the outer faces of the given RVE. Combination of the virtual work principle corresponding to the original composite deformations $\varepsilon_{kl}(\mathbf{x})$ and these obtained for the homogenized composite $\varepsilon'_{kl}(\mathbf{x})$ under the same Dirichlet boundary conditions specified above with the equity of deformation energies in these two cases leads to

$$C_{ijkl}^{(eff)} \int_{\Omega} \varepsilon'_{ij}(\mathbf{x})\, \varepsilon'_{kl}(\mathbf{x}) d\Omega = C_{ijkl}^{(p)} \int_{\Omega_p} \varepsilon_{ij}(\mathbf{x})\, \varepsilon_{kl}(\mathbf{x}) d\Omega + C_{ijkl}^{(i)} \int_{\Omega_i} \varepsilon_{ij}(\mathbf{x})\, \varepsilon_{kl}(\mathbf{x}) d\Omega + C_{ijkl}^{(m)} \int_{\Omega_m} \varepsilon_{ij}(\mathbf{x})\, \varepsilon_{kl}(\mathbf{x}) d\Omega \tag{3.40}$$

where constitutive tensors $C_{ijkl}^{(p)}$, $C_{ijkl}^{(i)}$, $C_{ijkl}^{(m)}$ correspond to the particle, interphase and the matrix, respectively. Imposition of the unit deformations $\varepsilon'_{ij}(\mathbf{x})$, $\varepsilon'_{kl}(\mathbf{x})$ enables for an analytic calculations of the effective tensor components using deformation energy stored in the original composite. Hyperelastic homogenization problem solution needs an incremental version of the boundary value problem constituted by Eqns (3.35) - (3.39) and it can be proposed in the following form:

$$\Delta\sigma_{ij,j}(\mathbf{x}) + \rho f_i(\mathbf{x}) = 0, \tag{3.41}$$

$$\Delta\sigma_{ij}(\mathbf{x}) = C_{ijkl}(\mathbf{x}) \Delta\varepsilon_{kl}(\mathbf{x}), \tag{3.42}$$

$$\Delta\varepsilon_{kl}(\mathbf{x}) = \frac{1}{2}\left(\Delta u_{k,l}(\mathbf{x}) + \Delta u_{l,k}(\mathbf{x}) + \Delta u_{k,i}(\mathbf{x}) \Delta u_{l,i}(\mathbf{x})\right), \tag{3.43}$$

$$\sigma_{ij}(\mathbf{x}) n_j = 0, \ \mathbf{x} \in \partial\Omega_\sigma, \tag{3.44}$$

$$u_j(\mathbf{x}) = \hat{u}_j(\mathbf{x}), \ \mathbf{x} \in \partial\Omega_u. \tag{3.45}$$

Hence, the effective tensor components are determined from the following equation:

$$C_{ijkl}^{(eff)} \int_{\Omega} \Delta\varepsilon'_{ij}(\mathbf{x})\, \Delta\varepsilon'_{kl}(\mathbf{x}) d\Omega = C_{ijkl}^{(p)} \int_{\Omega_p} \Delta\varepsilon_{ij}(\mathbf{x})\, \Delta\varepsilon_{kl}(\mathbf{x}) d\Omega + C_{ijkl}^{(i)} \int_{\Omega_i} \Delta\varepsilon_{ij}(\mathbf{x})\, \Delta\varepsilon_{kl}(\mathbf{x}) d\Omega + C_{ijkl}^{(m)} \int_{\Omega_m} \Delta\varepsilon_{ij}(\mathbf{x})\, \Delta\varepsilon_{kl}(\mathbf{x}) d\Omega. \tag{3.46}$$

Money-Rivlin, Neo-Hookean and Arruda-Boyce constitutive tensors have been adopted in this analysis at the right hand side of this equation to determine its effective characteristics.

In the presence of random parameter w defined for any $\mathbf{x}\in\Omega_i$ in this RVE one rewrites above relation as

$$C_{ijkl}^{(eff)}(w)\int_{\Omega}\Delta\varepsilon'_{ij}(\mathbf{x})\,\Delta\varepsilon'_{kl}(\mathbf{x})d\Omega=C_{ijkl}^{(p)}\int_{\Omega_p}\Delta\varepsilon_{ij}(w;\mathbf{x})\,\Delta\varepsilon_{kl}(w;\mathbf{x})d\Omega$$
$$+C_{ijkl}^{(i)}(w)\int_{\Omega_i}\Delta\varepsilon_{ij}(w;\mathbf{x})\,\Delta\varepsilon_{kl}(w;\mathbf{x})d\Omega+C_{ijkl}^{(m)}\int_{\Omega_m}\Delta\varepsilon_{ij}(w;\mathbf{x})\,\Delta\varepsilon_{kl}(w;\mathbf{x})d\Omega. \tag{3.47}$$

So that, the goal of further numerical experiments is to compute an incremental function of the homogenized characteristics for the given composite using its strain energy U^{eff} as

$$C_{ijkl}^{(eff)}(w,\boldsymbol{\varepsilon}')=U^{eff}\left(C_{ijkl}^{(p)},C_{ijkl}^{(i)}(w),C_{ijkl}^{(m)},\boldsymbol{\varepsilon}(w,\mathbf{x})\right). \tag{3.48}$$

and its basic probabilistic characteristics by using the stochastic finite element method.

Further probabilistic analysis undergoes with the following discretization of a displacement field in this composite computed at some increment r:

$$u_k^{(r)}=N_{i\alpha}q_\alpha^{(r)}=N_{i\alpha}D_{\alpha j}^{(r)}w^j. \tag{3.49}$$

Where $N_{i\alpha}$ denote the shape functions, while $D_{\alpha j}^{(r)}$ are the coefficients for the polynomial bases of independent random variable w. Quite similarly one discretizes the strain and the stress tensors at the same increment:

$$\varepsilon_{ij}^{(r)}=B_{ij\alpha}q_\alpha^{(r)}=B_{ij\alpha}D_{\alpha j}^{(r)}w^j, \tag{3.50}$$

$$\sigma_{ij}^{(r)}=C_{ijkl}^{(r)}\varepsilon_{kl}^{(r)}=C_{ijkl}^{(r)}B_{kl\alpha}q_\alpha^{(r)}=C_{ijkl}^{(r)}B_{kl\alpha}D_{\alpha m}^{(r)}w^m, \tag{3.51}$$

where $B_{kl\alpha}$ is the matrix of the shape functions spatial derivatives. Let us adopt classical FEM notation, where the composite global stiffness matrix is $K_{\alpha\beta}$ for α, β indexing all degrees of freedom available in the RVE, Δq_β includes increments of displacements for all DOFs, while ΔQ_α combines the external nodal forces increments.

Then, static equilibrium equations being solved for the state functions and their increments is

$$K_{\alpha\beta}\Delta q_{\beta} = \Delta Q_{\alpha}. \tag{3.52}$$

The left hand side here depends upon the input random variable w, so that final solution for the displacements can be recovered as

$$\Delta q_{\beta}(w)=\left[K_{\alpha\beta}^{(m)}+K_{\alpha\beta}^{(i)}(w)+K_{\alpha\beta}^{(p)}\right]^{-1}\Delta Q_{\alpha}. \tag{3.53}$$

Random polynomial basis is found from the series of solutions of the above equation when w having the basic moments equal to $E(w)$, $\mathrm{SD}(w)$ takes the trial deterministic values in the interval $[E(w)-3\sigma(w),E(w)+3\sigma(w)]$. It enables the least squares method approximations of the polynomial bases.

3.1.5. Stochastic perturbation solution

Stochastic perturbation method is of the non-statistical nature and it uses analytical formulas describing probabilistic moments of the structural response rewritten for the continuous distributions. It is used for probabilistic analysis in multiple fields [309,310,311,312,313,309]. The expected value as well as higher order central probabilistic moments of the mth order of structural response $\mathbf{u}(w)$ can be described as

$$E\left(\mathbf{u}(w)\right)=\int_{-\infty}^{+\infty}\mathbf{u}(w)\cdot p(w)\mathrm{d}w,\ \mu_m\left(\mathbf{u}(w)\right)=\int_{-\infty}^{+\infty}\left(\mathbf{u}(w)-E\left(\mathbf{u}(w)\right)\right)^m\cdot p(w)\mathrm{d}w, \tag{3.54}$$

where $p(w)$ is its probability density function (PDF). Determination of these characteristics undergoes by the use of Taylor expansion of the given order n, which guarantees sufficient numerical accuracy while comparing with some referencing analysis like Monte-Carlo simulation strategy, for instance. The ISPT uses the following expansion about the mean value w^0 [96,266,314,315]:

$$\mathbf{u}\left(w\right)=\mathbf{u}\left(w^0\right)+\sum_{m=1}^{n}\frac{\varepsilon^m}{m!}\left.\frac{\partial^m\mathbf{u}\left(w\right)}{wb^m}\right|_{w=w^0}(\Delta w)^m. \tag{3.55}$$

where $\Delta w=w-w^0$ is a first order variation of variable w and ε is a positive definite perturbation parameter [316,96]. It is most frequently adopted as $\varepsilon=1$, as in this study (after [122]), and vanish for further equations. Partial derivatives of the function $\mathbf{u}(w)$

with respect to input parameter w are calculated from the approximating polynomial. Equation (3.55) is valid for the ISPT only when $w^0 = E(w)$, which is the case of Gaussian PDF applied here. Otherwise the expected value shall replace the mean value. Further calculations need also higher central probabilistic moments of the parameter w provided that it has Gaussian PDF, so that one obtains for its standard deviation $\sigma(w)$

$$\mu_m(w) = \int_{-\infty}^{+\infty} \left(w - w^0\right)^m \cdot p(w)\, dw = \begin{cases} 1 & when\ m = 0 \\ (m-1)!!\left(\sigma(w)\right)^m & when\ 2 \mid m \\ 0 & otherwise \end{cases} \tag{3.56}$$

where

$$p(w) = \frac{1}{\sigma(w) \cdot \sqrt{2\pi}} \exp\left(-\frac{\left(w - E(w)\right)^2}{2\sigma^2(w)} \right). \tag{3.57}$$

The following relations for the first four probabilistic moments of the structural response $\mathbf{u}(w)$ may be relatively easily derived with the tenth order expansion assuming that higher than the order selected for the Taylor series terms simply vanish according to the least squares method fittings included in the next section. One obtains

$$\begin{aligned} E\left[\mathbf{u}(w)\right] = u^0\left(w^0\right) + \frac{1}{2}\frac{\partial^2 \mathbf{u}(w)}{\partial w^2}\bigg|_{w=w^0} \alpha^2(w)\left(w^0\right)^2 + \frac{1}{8}\frac{\partial^4 \mathbf{u}(w)}{\partial w^4}\bigg|_{w=w^0} \alpha^4(w)\left(w^0\right)^4 + \\ + \frac{1}{48}\frac{\partial^6 \mathbf{u}(w)}{\partial w^6}\bigg|_{w=w^0} \alpha^6(w)\left(w^0\right)^6 \end{aligned} \tag{3.58}$$

$$\begin{aligned} Var\left(\mathbf{u}(w)\right) &= \alpha^2(w)\left(w^0\right)^2 D_{[1,1]}\mathbf{u} + \alpha^4(w)\left(w^0\right)^4 \left\{ \frac{1}{2} D_{[2,2]}\mathbf{u} + D_{[1,3]}\mathbf{u} \right\} \\ &+ \alpha^6(w)\left(w^0\right)^6 \left\{ \frac{5}{12} D_{[3,3]}\mathbf{u} + \frac{1}{2} D_{[2,4]}\mathbf{u} + \frac{1}{4} D_{[1,5]}\mathbf{u} \right\} + \\ &+ \alpha^8(w)\left(w^0\right)^8 \left\{ \frac{1}{6} D_{[4,4]}\mathbf{u} + \frac{7}{24} D_{[3,5]}\mathbf{u} + \frac{1}{8} D_{[2,6]}\mathbf{u} \right\} \\ &+ \alpha^{10}(w)\left(w^0\right)^{10} \left\{ \frac{21}{320} D_{[5,5]}\mathbf{u} + \frac{5}{48} D_{[4,6]}\mathbf{u} \right\} \end{aligned} \tag{3.59}$$

$$\mu_3\left(\mathbf{u}(w)\right)=\int_{-\infty}^{+\infty}\left(\mathbf{u}(w)-E\left[\mathbf{u}(w)\right]\right)^3\,p(w)\,dw=$$
$$=3D_{[1,1,2]}u\;\alpha^4(w)\left(w^0\right)^4+\alpha^6(w)\left(w^0\right)^6\left\{D_{[2,2,2]}\mathbf{u}+\frac{3}{2}D_{[1,1,4]}\mathbf{u}+6D_{[1,2,3]}\mathbf{u}\right\}$$
$$+\alpha^8(w)\left(w^0\right)^8\left\{\frac{3}{8}D_{[1,1,6]}\mathbf{u}+\frac{9}{4}D_{[2,2,4]}\mathbf{u}+\frac{15}{4}D_{[2,3,3]}\mathbf{u}+4D_{[1,3,4]}\mathbf{u}+\frac{9}{4}D_{[1,2,5]}\mathbf{u}\right\} \tag{3.60}$$
$$+\alpha^{10}(w)\left(w^0\right)^{10}\left\{\frac{3}{4}D_{[2,2,6]}\mathbf{u}+2D_{[2,4,4]}\mathbf{u}+\frac{25}{8}D_{[3,3,4]}\mathbf{u}\right\}$$
$$+\alpha^{10}(w)\left(w^0\right)^{10}\left\{\frac{15}{8}D_{[1,4,5]}\mathbf{u}+\frac{5}{4}D_{[1,3,6]}\mathbf{u}+\frac{7}{2}D_{[2,3,5]}\mathbf{u}\right\}$$

$$\mu_4\left(\mathbf{u}(w)\right)=\int_{-\infty}^{+\infty}\left(\mathbf{u}(w)-E\left[\mathbf{u}(w)\right]\right)^4\,p(w)\,dw=$$
$$=3\alpha^4(w)\left(w^0\right)^4D_{[1,1,1,1]}\mathbf{u}+\alpha^6(w)\left(w^0\right)^6\left\{10D_{[1,1,1,3]}\mathbf{u}+15D_{[1,1,2,2]}\mathbf{u}\right\}$$
$$+\alpha^8(w)\left(w^0\right)^8\left\{39D_{[1,2,2,3]}\mathbf{u}+21D_{[1,1,2,4]}\mathbf{u}+\frac{35}{2}D_{[1,1,3,3]}\mathbf{u}+\frac{15}{4}D_{[2,2,2,2]}\mathbf{u}+\frac{7}{2}D_{[1,1,1,5]}\mathbf{u}\right\} \tag{3.61}$$
$$+\alpha^{10}(w)\left(w^0\right)^{10}\left\{9D_{[1,1,4,4]}\mathbf{u}+\frac{35}{2}D_{[1,3,3,3]}\mathbf{u}+\frac{27}{2}D_{[2,2,2,4]}\mathbf{u}+\frac{125}{4}D_{[2,2,3,3]}\mathbf{u}+67D_{[1,2,3,4]}\mathbf{u}\right\}$$
$$+\alpha^{10}(w)\left(w^0\right)^{10}\left\{\frac{75}{4}D_{[1,2,2,5]}\mathbf{u}+\frac{63}{4}D_{[1,1,3,5]}\mathbf{u}+\frac{27}{4}D_{[1,1,2,6]}\mathbf{u}\right\}.$$

The following notation for the derivatives products evaluated at the mean value of the parameter w has been adopted:

$$\begin{cases} D_{[i,j]}\mathbf{u}(w)=\dfrac{\partial^i\mathbf{u}(w)}{\partial w^i}\dfrac{\partial^j\mathbf{u}(w)}{\partial w^j} \\ D_{[i,j,k]}\mathbf{u}(w)=\dfrac{\partial^i\mathbf{u}(w)}{\partial w^i}\dfrac{\partial^j\mathbf{u}(w)}{\partial w^j}\dfrac{\partial^k\mathbf{u}(w)}{\partial w^k} \qquad , \quad i,j,k,l\in\aleph \\ D_{[i,j,k,l]}\mathbf{u}(w)=\dfrac{\partial^i\mathbf{u}(w)}{\partial w^i}\dfrac{\partial^j\mathbf{u}(w)}{\partial w^j}\dfrac{\partial^k\mathbf{u}(w)}{\partial w^k}\dfrac{\partial^l\mathbf{u}(w)}{\partial w^l} \end{cases} \tag{3.62}$$

A procedure concerning determination of the basic moments of the effective tensor is almost the same – one replaces structural response $\mathbf{u}(w)$ with $C_{ijkl}^{(eff)}(w)$ and global approximation is used instead of the local one presented above. It should be noticed also that theoretical probabilistic convergence analysis for these moments has been provided in [96]. Probabilistic semi-analytical method uses the same definitions and the same

polynomial bases, but the resulting moments are derived symbolically using MAPLE 2017 by random polynomials integration; the resulting formulas are omitted here for a brevity of the presentation.

At this point part (1) of the thesis is confirmed. Deformation process of particulate composites with random interface defects is formulated in its hyperelastic regime.

In this thesis order of perturbation was limited till the tenth, depending on the response function or response surface for each numerical example. Procedure of its optimization is introduced in Section 3.2.

A truncated version of the ISPT called TISPT is not used here principally because the physical bound of an input variable considered here as random (volume fraction of interface defects) is not symmetric for all the selected expected values (despite $E(w)$=0.5) and secondly because a precise verification of an effect of inclusion of this bound into a stochastic calculation was not provided. It was also not tested at all for the response surface method, which is used here in a considerable part of numerical experiments.

Two other methods serving here as reference are the Monte-Carlo simulation and the direct derivation method. They both have been selected in their classical form to omit the error introduced in their modified or approximate solutions mentioned in section 2.2, such as a midpoint Riemann Sum [317]. Classical derivation of probabilistic characteristics according to the DDM could be found for example in [110,318,319,138,320], while Monte-Carlo simulation method introduction could be found for example in [100,107].

3.2. Effective response of a medium

Exact relation between objective function f and random variable b can rarely be found. This is why f(b) must be obtained as a result of some approximate procedure. It is frequently done with a joint use of discrete numerical experiments or laboratory tests together with curve fitting algorithms. Discrete points obtained from these experiments are approximated with some continuous function that satisfies differentiability and continuity requirements of the SPT or is integrable with a chosen PDF, when the SAM is preferred. Numerical determination of this function is called either a response function method (RFM), when it relates a single variable to the objective function f(b), or a response surface method (RSM), when two or more random input

variables are related to this function f(***b***) or some other not random input variables are also involved f(b, **x**). The objective function obtained with this procedure is commonly referred as the effective response or effective function of the medium. Please note, that in this section the random variable is referred as b to indicate that it is referring to an arbitrary random variable. In contrast, w refers to interface defects volume fraction – the input variable used specifically in this dissertation.

Discrete experiments are performed repeatedly around a mean b^0 or expected value $E(b)$ of random input variables in a range corresponding to a region where PDF of these variables are not null. Since multiple popular PDFs defining $p(b)$ are absolutely continuous and have a very limited range where $p(b) \gg 0$, a region of sampling is typically limited to $\left[b^0-\Delta b_\mathrm{l}, b^0+\Delta b_\mathrm{h}\right]$ for which $p(b)\big|_{b^0-\Delta_\mathrm{l}}^{b^0+\Delta_\mathrm{h}} \approx 1$. Likelihood of occurrence of b outside this region, i.e. $b \in \left(-\infty, b-\Delta b_\mathrm{l}\right) \cup \left(b+\Delta b_\mathrm{h}, +\infty\right)$ should be close to zero. The lower Δb_l and higher Δb_h bounds correspond to the PDF. They remain symmetric to b^0 for symmetric distributions of b, such as Gaussian distribution. In case of unsymmetrical or multimodal distributions, they may not. A range of discrete sampling shall correspond to the domain of density of occurrence of b so that an objective function is known in all the regions where $p(b) \gg 0$.

This is visualized for a Gaussian PDF on Fig. 3.3, where a response is sampled in a neighborhood of 3 standard deviations of the input. With such an assumption 0.997 of the occurrences of input random parameter are guaranteed to be inside this interval [321]. This property of a Gaussian PDF is also known as a three-sigma rule. In this thesis all the considered input random variables are Gaussian an thus $\Delta b_\mathrm{h}=\Delta b_\mathrm{l}=\Delta b$. A ratio of $\Delta b/b^0$ varies in literature [322,323,324] and here two approaches were proposed: 1. a traditional Dirac-like sampling in 20% neighborhood of b^0 and $\Delta b/b^0=0.05$ used for RFM and 2. a holistic approach, where a single multivariate function is selected for all of considered mean values of $\boldsymbol{b}^0$; it is used in the RSM and corresponds to an increasing volume fraction of interface defects. More detailed introduction to both methods is available in Sections 3.2.1 and 3.2.2.

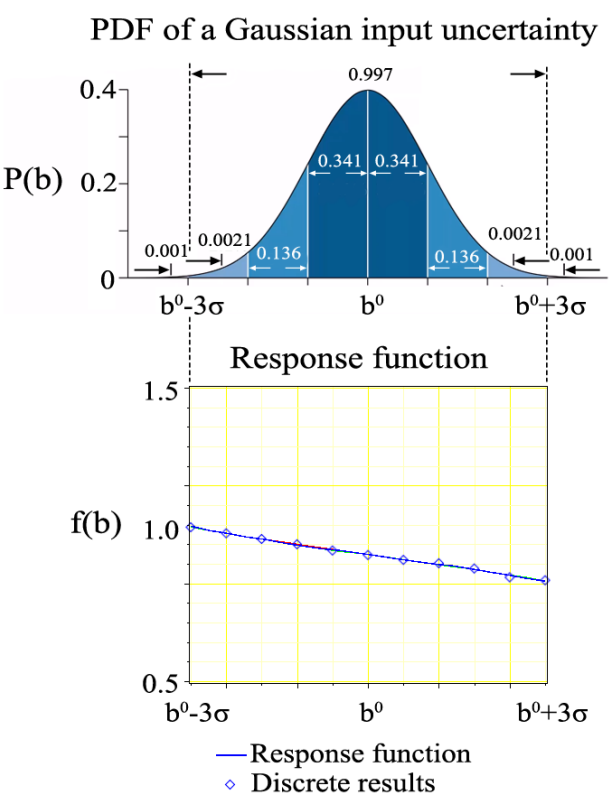

Fig. 3.3 Graphical representation of response approximation in a domain of random variable occurrence.

3.2.1. Response function method

The response function method applied here for determination of the effective material properties of the composite base on usage of the weighted least squares method (WLSM). Polynomial representation of the s[th] order is sought (indexed by β here) from n distinct pairs of $\left(b_{i,\xi}^{\alpha}, u_{i,\xi}^{(\alpha)}\right)$ for α=1,...,n. It relates each effective material coefficient of the composite $C_{i,\xi}^{eff}$ distinguished by i to the volume fraction of interface defects w for each probed hyperelastic potential ξ. These pairs come from a set of numerical experiments, whose arguments belong to the vicinity of the expected value of b; a following polynomial approximation is used

$$C_{i,\xi}^{eff}(w) \cong u_{i,\xi}\left(b_{i,\xi}, w\right) \cong D_{i,\xi}^{(\beta)}(w) b_{i,\xi}^{\beta} = f\left(\mathbf{D}, b_{i,\xi}\right) \qquad \beta = 1, \ldots, s;\ s < n,\ i = 1,\ldots,o, \xi = 1,\ldots,p. \tag{3.63}$$

An algebraic condition for these expansion coefficients is calculated at each trial point in a following way

$$r_{(\alpha),i,\xi} = u_{i,\xi}^{(\alpha)} - f\left(\mathbf{D}, b_{i,\xi}^{\alpha}\right) \quad \alpha = 1, \ldots, n,\, i = 1,\ldots,o,\, \xi = 1,\ldots,p. \tag{3.64}$$

Minimization of the weighted residuals functional is made as follows:

$$S_{i,\xi} = \sum_{\alpha=1}^{n} w_{\alpha\alpha,i,\xi} r_{(\alpha),i,\xi}^{2} \quad \alpha = 1, \ldots, n,\, i = 1,\ldots,o,\, \xi = 1,\ldots,p \tag{3.65}$$

so that

$$\frac{\partial S_{i,\xi}}{\partial D_{i,\xi}^{(\beta)}} = -2\sum_{\alpha=1}^{n} w_{\alpha\alpha,i,\xi} r_{(\alpha),i,\xi} \frac{\partial f\left(\mathbf{D}, b_{i,\xi}^{\alpha}\right)}{\partial D_{i,\xi}^{(\beta)}(w)} \quad \beta = 1, \ldots, s,\, i = 1,\ldots,o,\, \xi = 1,\ldots,p. \tag{3.66}$$

This derivative is further simplified as

$$\mathbf{J} = J_{\alpha\beta,i,\xi} = \frac{\partial f\left(\mathbf{D}_{i,\xi}, b_{i,\xi}^{\alpha}\right)}{\partial D_{i,\xi}^{(\beta)}(w)} \quad \alpha = 1, \ldots, n; \quad \beta = 1, \ldots, s,\, i = 1,\ldots,o,\, \xi = 1,\ldots,p \tag{3.67}$$

modified in a following way

$$\sum_{\alpha=1}^{n}\sum_{\beta=1}^{s} J_{\alpha\beta,i,\xi} w_{\alpha\alpha,i,\xi} J_{\alpha\beta,i,\xi} D_{i,\xi}^{(\beta)}(w) = \sum_{\alpha=1}^{\mathrm{n}} J_{\alpha\beta,i,\xi} w_{\alpha\alpha,i,\xi} u_{i,\xi}^{(\alpha)} \qquad \alpha = 1, \ldots, \mathrm{n};\, \beta = 1, \ldots, s,\, i = 1,\ldots,o,\, \xi = 1,\ldots,p \tag{3.68}$$

and converted into the regular matrix equations

$$\left(\left(\mathbf{J}\right)^{T} \mathbf{w}\, \mathbf{J}\right)\mathbf{D} = \left(\mathbf{J}\right)^{T} \mathbf{w}\, \mathbf{u}. \tag{3.69}$$

Such a system of equations (with the dimensions *n x s*) is solved symbolically in MAPLE 2018 for each effective material coefficient *i* and each hyperelastic potential.

There exist several important aspects of this approach to follow. The foremost is the closeness of the sampling to the results of a response function, which is covered by an algebraic fitting. It also prevents underfitting of the discrete data. Two additional factors include complexity of the predictor function (response function) and a course of function just outside the sampling region. In this thesis polynomial response function

is applied and thus complexity of response function mainly depends on the number of terms of this polynomial and its rank. Typically together with an increase of these two factors, the fitting gets closer to perfect. The course of function, however, tends to go through all the points with an increasing fluctuation between them causing so called overfitting.

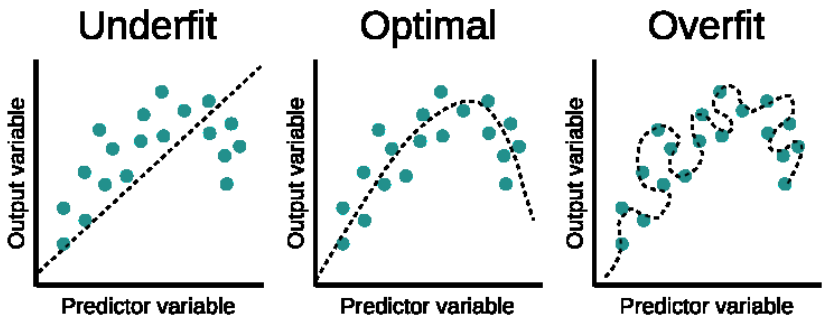

Fig. 3.4 Response function complexity related to under- and overfitting [N6].

This is presented on Fig. 3.4, where the optimal predictor function lays somewhere between the under- and overfitted predictions. Underfitting is treated perfectly well by a proposed triple criterion, while overfitting is prevented by a visual elimination of response functions. In practice, the optimal response function is selected as a polynomial having the highest rank and not yet with fluctuation representing overfitting. Such an approach is also applied here.

Course of function outside of sampling region is important, yet not always properly treated factor for a choice of the response function. Even if statistically a density of results therein is irrelevant, a high gradient of change just after the sampling region may influence the results of stochastic computations. This especially affects the unbounded formulations used here. Such a response function is presented on Fig. 3.5, where it decreases with a very high rate on both ends of sampling region; this is frequently a feature of overfitted samples but can also happen for these considered optimal from the previous step of response function optimization.

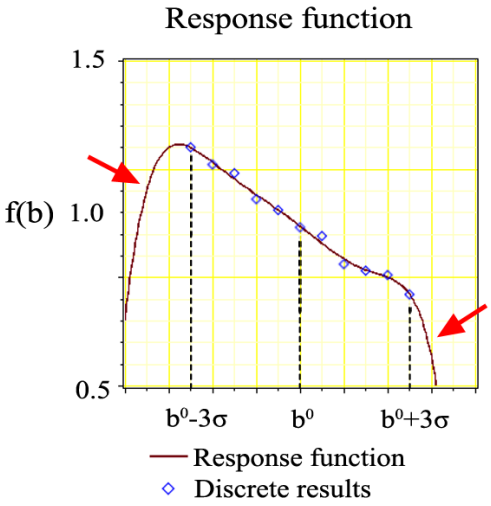

Fig. 3.5 An example of a weak response function.

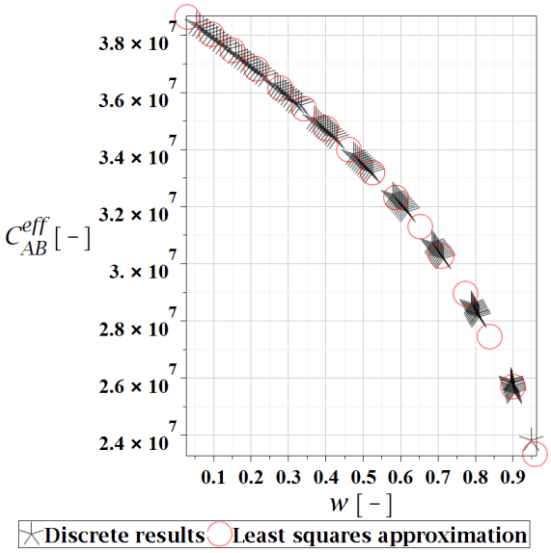

Fig. 3.6 Extended sampling of the objective variable to an input uncertain parameter.

Such a problem was treated here by usage of a sampling region much wider than the three-sigma rule suggests. Instead of treating separately each considered expected value of input volume fraction of interface defects w, a single function covering all the sampling regions is recovered. Such an approach eliminated the above deficiency of a closely-sampled response function, still preserving a very high precision of approximation for each sampling region; it is used here for determination of the effective material properties of the composite. An exemplary fitting using this approach is presented on Fig. 3.6 and a detailed consideration of approximation accuracy for numerical experiments is presented in Appendix B.

3.2.2. Response surface method

A response surface method is an extension of the response function method. It is introduced for all the objective functions that depend on more than one input variable and whose exact relation cannot be determined. Specifically, this method must be used when relation of this function to the target random variable cannot be derived independently of other variables. Otherwise the response function could be used. These additional dependencies can be either random or deterministic. Such conditions apply for the effective stress and effective deformation energy considered in this thesis. They are both functions of the volume fraction of interface defects w and also of the invariants (see for example eqn. (6.6) or eqn. (6.15)). These invariants are further

converted to strains; this is required to confront the results of numerical experiments with these coming from laboratory tests. In contrast, the effective material coefficients could all be approximated by the response functions. This is valid, because they are functions of input random variable and independent from other variables in the proposed constitutive model.

The response surface method aims to optimize coefficients of the multivariate polynomial $a_{i,j}$ (decision variables) in form of

$$u(b_1,b_2)=\sum_{i=1}^{m}\sum_{j=1}^{n} a_{i,j} b_1^{\,j} b_2^{\,i}, \tag{3.70}$$

where b_i, i=1,2 is a set of 2 dependent variables. They may be any combination of random and deterministic variables.

They are recovered by minimization of square residuals coming from all the discrete data points recovered from simulations so that

$$\sum_{i=1}^{n}\left(u\left(b_{1,i},b_{2,i}\right)_i - u_i^{\text{exact}}\right)^2 = \min, \tag{3.71}$$

where n denotes the number of observations; these discrete results come from the FEM realizations. Minimization is done using the iterative active-set method, which ensures an accurate solution for the quadratic programming (QP) problem posed here. The optimization task is quadratic in decision variables because polynomial coefficients are independent of each other and their square product is optimized. Please note, that a weighting scheme could also be introduced by multiplication of the residual by weight W_i variable for each observation

$$\sum_{i=1}^{n} W_i\left(u\left(b_{1,i},b_{2,i}\right)_i - u_i^{\text{exact}}\right)^2 = \min \tag{3.72}$$

that is the objective of the weighted least squares. It is not proposed here, because selected discretization scheme already favors results close to expectations of the input random variable. One may also opt to minimize the sum of absolute differences, which

simplifies the optimization and places it in the linear programming (LP) domain, but this option is not selected frequently.

The proposed concept may be generalized to any other multivariate polynomial with n variables and their cross-products, for example

$$\sum_{i=1}^{n} W_i \left(\left(\sum_{i=1}^{m} \sum_{j=1}^{n} a_{1,i,j} b_i^j + \sum_{i=1}^{m} \sum_{j=1}^{n} a_{2,i,j} b_i \right)_i - u_i^{exact} \right)^2 = \min. \tag{3.73}$$

The only requirement for this polynomial is to have uncorrelated coefficients $a_{x,i,j}$. The type of response function cannot be freely chosen to remain in QP optimization problem. A complex function may bound the decision variables that would place optimization in the nonlinear programming (NP) domain. This kind of optimization problem is not easily solved and very frequently only a local optimum can be sought; it may be very far from the global solution. A closed-form solution is generally not available. There are two main reasons for selecting polynomials as function class for the response surface. First of all, their coefficients are independent of each other, which is required for smoothness of optimization problem. Secondly, they are easily integrable and differentiable. This is relevant for two methods used in the stochastic calculus, the semi-analytical method and the generalized iterative stochastic perturbation method. The iterative active-set method is preferred over the other available method families, for example Interior Point or Newton-Barrier Method, because during optimization it also eliminates the irrelevant decision variables from the objective function. This is especially profitable for higher order polynomials with hundreds of decision variables that not necessarily contribute to the objective function in its considered domain.

In its multivariate version, a polynomial representation of the s^{th} order is sought from n distinct pairs of $\left(\boldsymbol{b}_\alpha, u^{(\alpha)}\right)$ for α=1,...,n, where $\boldsymbol{b}$ is a vector of independent variables. Polynomial approximation of the objective surface follows equation (3.70) and it may be further modified to a following form

$$u(b) \cong \sum_{\beta=1}^{s} \sum_{\gamma=1}^{s} D^{(\beta\gamma)} b_1^{\beta} b_2^{\gamma} = f(\mathbf{D}, \boldsymbol{b}) \quad s < n. \tag{3.74}$$

A residual at each trial point is calculated as

$$r_{(\alpha)} = u^{(\alpha)} - f\left(\mathbf{D}, \boldsymbol{b}_{\alpha}\right) \quad \alpha = 1, \ldots, n. \tag{3.75}$$

and a square residual follows equation (3.65). Derivative with respect to the decision variables is following:

$$\frac{\partial S}{\partial D^{(\beta)}} = -2\sum_{\alpha=1}^{n} w_{\alpha\alpha} r_{(\alpha)} \frac{\partial f\left(\mathbf{D}, \boldsymbol{b}_{\alpha}\right)}{\partial D^{(\beta)}} \quad \beta = 1, \ldots, s. \tag{3.76}$$

It can be next simplified to

$$\mathbf{J} = J_{\alpha\beta} = \frac{\partial f\left(\mathbf{D}, \boldsymbol{b}_{\alpha}\right)}{\partial D^{(\beta)}} \quad \alpha = 1, \ldots, n; \quad \beta = 1, \ldots, s, \tag{3.77}$$

and converted to equation (3.68), which finally gives regular matrix equations of

$$\left(\left(\mathbf{J}\right)^{T} \mathbf{w}\, \mathbf{J}\right)\mathbf{D} = \left(\mathbf{J}\right)^{T} \mathbf{w}\, \mathbf{u}. \tag{3.78}$$

They are similar to the ones in the response function method with an exception that they are driven by two (or more) independent variables ***b*** and much more decision variables **D**; it is not important how many random and deterministic variables are involved. However, discretization of the objective function should span at least the domain of occurrence of the random variables and also the one of the deterministic variables. Type of probability density of the decision variables should also be reflected in pattern of this discretization. A detailed consideration of approximation accuracy of the applied method for numerical experiments is presented in section 6.2.2 and optimization procedure of the response surface is included in Appendix C.

4. Computational implementation

In this section procedure of numerical analysis and general technical details are provided. It includes definition of the constitutive model, discretization details of the FEM, solution procedure of the deterministic and stochastic experiments as well as details of analysis relevant to all numerical experiments. At the end, computational algorithms used in numerical experiments are provided.

4.1. Finite element method solution details

The finite element method simulations are all solved for the RVE of the composite in the FEM system ABAQUS. Its discretization is always the same, but material parameters are updated for each characteristic value of volume fraction of interface defects w. FEM realizations of the cell problem are performed in the domain of (ε_{11},w) around nine expected values of w in the range of $E(w)\in[0.1,\ 0.2,\ \ldots\ 0.9]$. Eleven numerical experiments are performed in their 10% vicinity at 1% difference. For each volume fraction of interface defects considered and each potential used a separate FEM solution was performed with a total of 297 FEM computations. The processor used is Intel i7 6900k with eight cores, wall clock time of each FEM solution is approx. 11000 seconds and RAM required approx. 9 GB.

A direct sparse solver with multi-front technique is used and implemented together with the full Newton algorithm. Interpolation between increments is linear and in each increment the displacement of composite outer edges is increased. Deformation of the RVE is shown in Fig. 4.1.

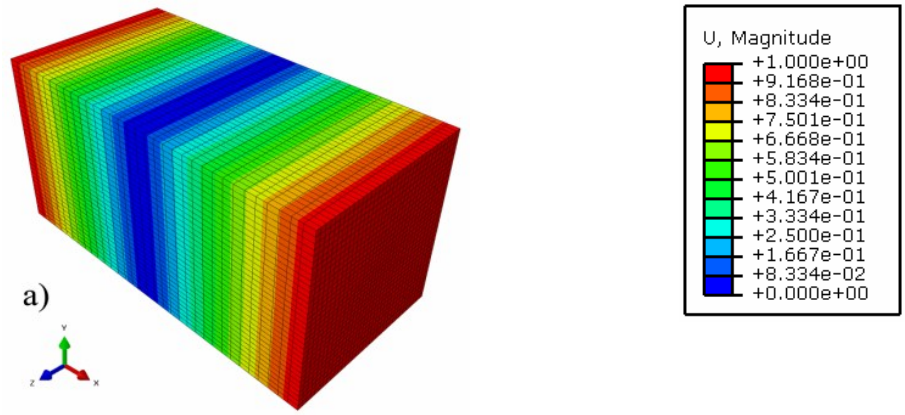

Fig. 4.1 Deformation for uniaxial stretch used in numerical analysis.

An initial increment size is 0.0005, minimum allowed increment size - 10^{-5} and maximum increment size - 0.005. The field and history outputs are written in an equidistant manner at each 0.005 strain increment, which gives 55 read-outs for each realization for the considered domain $\varepsilon_{11} \in (0.00, 0.275)$. Such range of strains is selected to reproduce the laboratory experiments included in section 5. The total number of increments is much higher but their output is not relevant for further fitting of the response function, where too many sample points with different strain spacing would result in a worse approximation than the regular ones due to non-equal weighing of the sampled domain of interest. The algorithm for strain increment determination is following:

1. Solver starts with an initial increment.
2. The next increment is always determined by number of iterations required to solve the last increment
   a. if solution is found within 4-10 iterations– next increment is equal to the previous/initial one.
   b. If number of iterations is smaller than 4, next increment is increased by a factor of 1.5.
   c. if more than 10 iterations are required for current increment - next increment is reduced by factor of 0.75.
   d. If a severe discontinuity is found for the current increment, current increment is reduced by a factor of 0.5 up to 10 times. On 11^{th} reduction the analysis is aborted with an error.

Once the time for next increment gets close to the next fixed read-out interval, it is reduced so that analysis passes exactly at this fixed time (understood here as the strain point in analysis). Please note that this algorithm is sensitive to a sharp increases of stiffness in the strain domain, which require a very close incrementation. This analysis may be further extended to higher strain rates, but at strains close to 0,4 mesh recalculation is already advised due to its excessive distortion. It is not done here to avoid extrapolation of the results coming from laboratory experiments.

The finite element method discretization of the entire RVE has been prepared with the use of 20-node three-dimensional iso-parametric finite elements in three-dimensional physical space. The particle is discretized with regular full-integration elements called C3D20 in ABAQUS, while the interphase and the matrix with hybrid,

linear pressure elements (C3D20H in ABAQUS) convenient to model material incompressibility. The first of these elements is discretized as

$$x^i = \sum_{k=1}^{20} N_{k\alpha} \bar{x}_k^i \; ; \; i, j = 1,2,3 \tag{4.1}$$

where the global coordinate system is given as (x^1,x^2,x^3) and the local normalized coordinate system as (ξ^1,ξ^2,ξ^3). Upon deformation, global coordinates of the i-th node are defined as $\bar{x}_i^1,\bar{x}_i^2,\bar{x}_i^3$ and local ones as $(\xi_k^1, \xi_k^2, \xi_k^3)$. Shape functions are defined as N_k for all nodes in a following way

- corner nodes:

$$N_{k1}(\xi^1,\xi^2,\xi^3) = \frac{1}{8}(1+\xi^1\xi_k^1)(1+\xi^2\xi_k^2)(1+\xi^3\xi_k^3)(\xi^1\xi_k^1+\xi^2\xi_k^2+\xi^3\xi_k^3-2) \tag{4.2}$$

- side nodes:

$$N_{k2}(\xi^1,\xi^2,\xi^3) = \frac{1}{4}\left(1+(\xi^1)^2\right)(1+\xi^2\xi_k^2)(1+\xi^3\xi_k^3) \quad \text{for } \xi_k^1=0,\xi_k^2=\pm1,\xi_k^3=\pm1 \tag{4.3}$$

$$N_{k3}(\xi^1,\xi^2,\xi^3) = \frac{1}{4}\left(1+(\xi^2)^2\right)(1+\xi^1\xi_k^1)(1+\xi^3\xi_k^3) \quad \text{for } \xi_k^2=0,\xi_k^1=\pm1,\xi_k^3=\pm1 \tag{4.4}$$

$$N_{k4}(\xi^1,\xi^2,\xi^3) = \frac{1}{4}\left(1+(\xi^3)^2\right)(1+\xi^1\xi_k^2)(1+\xi^2\xi_k^2) \quad \text{for } \xi_k^3=0,\xi_k^1=\pm1,\xi_k^2=\pm1 \tag{4.5}$$

The normalized local coordinate system is visualized in Fig. 4.2, separately for each node.

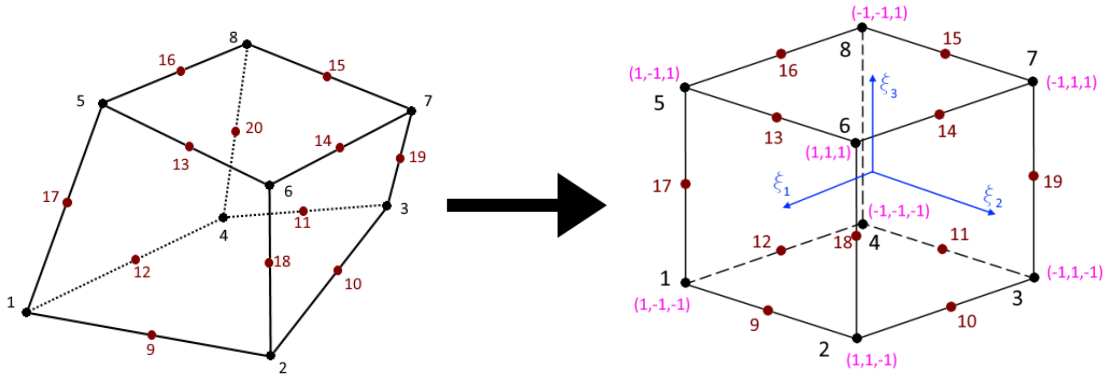

Fig. 4.2 Iso-parametric 20-noded 3D finite element: physical configuration – left graph, normalized local coordinate system – right graph [265].

Selection of an iso-parametric finite element allows usage of the same shape functions from eqns (5.2-5.5) in description of displacement increments

$$\Delta\mathbf{u}(X_1,X_2,X_3)=\mathbf{N}(X_1,X_2,X_3)\,\Delta\mathbf{q}, \tag{4.6}$$

in which $\Delta\mathbf{q}$ represents a vector with the increments of the given DOFs (degrees of freedom).

Increments of strain tensor $\Delta\boldsymbol{\varepsilon}$ could be calculated with use of formula (5.6) as

$$\Delta\boldsymbol{\varepsilon}=\mathbf{B}\Delta\mathbf{q}\ ; \tag{4.7}$$

where the strain tensor is given as

$$\varepsilon_{ij}=\frac{1}{2}\left(\frac{\partial u_i}{\partial X_j}+\frac{\partial u_j}{\partial X_i}+\frac{\partial u_k}{\partial X_i}\frac{\partial u_k}{\partial X_j}\right),\ i, j = 1,2,3 \tag{4.8}$$

and matrix **B** contains spatial derivatives of shape functions **N**. Increments of the stress tensor could be calculated in a following form

$$\Delta\boldsymbol{\sigma}=\mathbf{C}(\boldsymbol{\varepsilon})\mathbf{B}\Delta\mathbf{q} \tag{4.9}$$

where $\mathbf{C}(\boldsymbol{\varepsilon})$ is a matrix of functions dependent on the strain tensor $\boldsymbol{\varepsilon}$. A parameterization of this FEM model with respect to the interphase parameter *w* necessary in further stochastic finite element method implementation proceeds by a selection of the set of its real values taken from a certain neighborhood of its mean value, sequential recalculation of several FEM models with varying *w* and the least squares method approximation of approximating polynomials independently for strains, stresses and energies.

Hybrid elements include an additional degree of freedom that determines the pressure stress in the element directly. The nodal displacements are used only to calculate the deviatoric (shear) strains and stresses. Formulation of virtual work for these elements could be found for example in [N7]. A total amount of the finite elements used here is over 150 000; their type and amount has been selected to obtain the best possible quality of the results for acceptable computational effort via the error analysis with respect to the discretization intensity and processor computing time. Discretization of the RVE is given on Fig. 4.3.

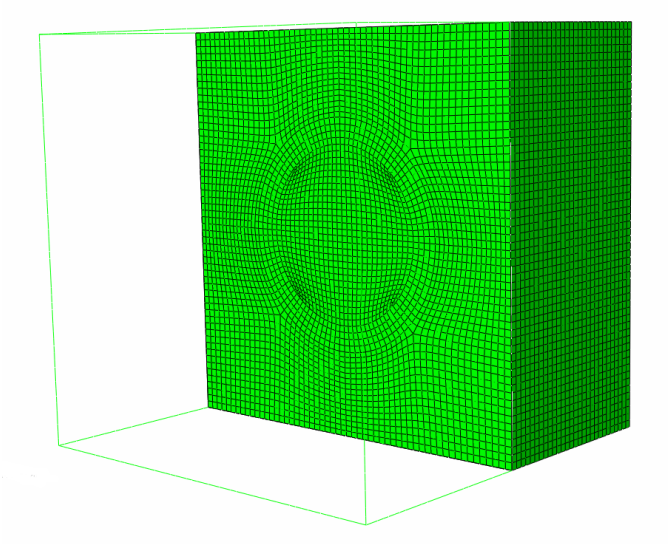

Fig. 4.3 Representative Volume Element of the composite.

This discretization has been optimized during the initial numerical error verification to minimize the computational effort necessary for satisfactory efficiency of the resulting deformation energies obtained in the FEM. An extensive analysis of relative error of various finite element types in its linear region of deformations has been performed by the author in [188].

The volume of the filler (CB particles) follows the one of laboratory experiments, which is 5%. The assigned volume of interphase is also 5% so that its thickness is much lower than the particle radius. It is visible as the ring around particle on Fig. 4.3.

4.2. Stochastic computations details

Stochastic procedures are all programmed in algebra system MAPLE 2018. They include the expectations, coefficients of random dispersion, skewness and kurtosis of effective characteristics of the objective composite. Skewness is output distribution asymmetry measure and kurtosis is output distribution concentration measure. Effective characteristics include the material coefficients, deformation energy and stress. They are determined with three independent methods, which are the generalized iterative stochastic perturbation, Monte-Carlo simulation and semi-analytical method; effective deformation energy is determined only by the first two methods. Separate calculation is done for the three selected hyperelastic formulations. An input uncertain variable is always volume fraction of interface defects w, whose randomness is exclusively Gaussian. Reasons for this choice are given in the introduction

(section 1). Its physical limitations are w, $E(w)\in(0.0, 1.0)$; its mean w is always equal to its expectation $E(w)$. Calculations are done on the full domain of w, no truncation is provided. Please note, that 0.997 of occurrences of this input random parameter are guaranteed to lay inside a the three standard deviations interval (as visualized previously on Fig. 3.3). Since its sampling region included here is very wide, i.e. $w\in(0.06, 0.96)$, an influence of the outsiders on a measure of stochastic characteristics is very limited. An additional gain of truncation would not be very meaningful and it must be non-symmetric for all the expectations of w except for $E(w)=0.05$ because of its physical limitations. The applied order of the ISPT as well as number of samples for the MCS is always given in sections dedicated to each state variable. It varies for different analyses. This is because computational requirements for the MCS and its required discretization density vary for different effective characteristics. The order of the ISPT is selected after the rank of the response function; it is never below the 6^{th} order. Calculations are based on a single- or bi-variate polynomial representation of the effective characteristics w.r.t. the input uncertain parameter. Its coefficients are optimized with use of the WLSM of equal weights and optimum rank is selected among first ten ranks for the effective stress and deformation energy and twenty ranks for the effective material parameters. Maximum allowed rank of the latter is higher because a single polynomial has much less terms than the bivariate polynomial. Equal weighing is preferred over Dirac weighting scheme because the expected value of w differs among realizations and its sampling is already denser close to these expectations. This already puts a higher weight to a close neighborhood of each $E(w)$. This polynomial response is retrieved from a series of FEM experiments using the WLSM technique. They are next integrated together with the Gaussian PDF in a semi-analytical method, inserted into n^{th} order Taylor expansions in stochastic perturbation-based approach and finally subjected to a discrete Monte-Carlo sampling for an increasing $\alpha(w)$ and ε_{11}. Symbolic calculations in MAPLE always have precision of 12 digits to avoid an additional calculation inaccuracy. Each analysis is made for nine expectations of the input uncertain variable $E(w)\in[0.1,\ 0.2, \ldots, 0.9]$. Only three of them are presented for each of the effective characteristic; it is done for the brevity of the results. The only exception are the sections 6.1.3 and 6.3.3. The first of these instead of $E(w)=0.9$ presents them for $E(w)$ optimized for each of the potential and the second mentioned

section strictly focuses on the optimized solution for the objective composite tested in the laboratory.

Stochastic analysis has three important parts. They are following:

1. Determination of the optimized expectation and coefficient of variation of stochastic volume fraction of interface defects $\left(E(w),\alpha(w)\right)$ for all the selected potentials provided in section 6.1.2.
2. determination of statistical disorder of the composite effective characteristics $(.)^{eff}$ to random variability in the volume fraction of interface defects w; it is provided in sections 6.1.3, 6.2.3 and 6.3.2.
3. verification of efficiency of a) the algorithm proposed for determination of $\left(E(w),\alpha(w)\right)$ and b) the augmented formulation of the selected potentials for composites with stochastic interface defects. Verification is based on the laboratory experiments and provided in section 6.3.3.

Analyses are done w.r.t. the coefficient of variation of this random parameter $\alpha(w)\in(0, 0.25)$ [$\alpha(w)\in(0, 0.15)$ for the effective material parameters], for its increasing expected value $E(w)$ and for an increasing strain in the range of $\varepsilon_{11}\in(0, 0.275)$. The maximum input dispersion analyzed here is relatively high and higher than the typical ones presented in stochastic studies especially using the ISPT. Such a spectrum of $\alpha(w)$ is selected because of a high variability in the defects dimensions and volume for each particle and also to extend applicability of this study above the standard level of uncertainty. A crude version of Monte-Carlo simulation is selected to avoid any loss of accuracy or initial assumptions accompanied with them. For the same reason a full integration procedure is applied in the SAM and not some approximation, such as a midpoint Riemann Sum [317], for example. They both serve as reference method for verification of ISPT accuracy and thus should not include any simplifications. If one aims to exclusively focus on any of these methods, some of their augmented variations are listed in section 2.2.

4.3. Computational algorithm

Algorithm for determination of basic probabilistic characteristics for the effective material properties of hyperelastic composites with stochastic interface defects is presented in this section. This approach could be applied for various hyperelastic potentials, and resulting uncertainty in material properties is aimed for direct usage in

the macro-scale computations of reliability in composite structures. Numerical analysis is delivered for the high density polyurethane Laripur LPR5020 filled with 5% of fullerenes F60. Laboratory tests include uniaxial stretch of virgin homogeneous material and a filled composite, which serves for a verification of efficiency of the proposed numerical approach in practical case study. Hyperelastic potentials selected for definition of this composite include Arruda-Boyce, Mooney-Rivlin, and also Neo-Hookean constitutive models. Numerical experiments are completed using homogenization method implemented for a cubic single-particle RVE of this composite using the FEM system ABAQUS. This homogenization scheme is based on numerical investigation of the strain energy density accumulated in the RVE under uniaxial stretches. The particle is spherical, remains in linear elastic regime, is centrally located in this RVE and perfectly surrounded by hyperelastic matrix. The interphase is a thin layer around particle that has elastic properties weaker than the matrix, because of the defects located on the particle-matrix transition; these defects are considered as the semi-spherical voids. A constitutive relation of the matrix is recovered experimentally in the uniaxial stretch test and approximated computationally by the best fitting hyperelastic constitutive model. Uncertainty of the voids volume fraction is modeled using Gaussian distribution with an increasing mean value and coefficient of variation not larger than 0.15 or 0.25 (depending on analysis type). A relation of the effective properties to this uncertain parameter is recovered via the response function method (RFM) and by the least squares method (LSM). The RFM polynomial order is optimized by simultaneous maximization of correlation and minimization of the LSM error and variance. Probabilistic calculus is carried out using three independent approaches, the generalized iterative stochastic perturbation, the crude Monte-Carlo simulation and the semi-analytical method. Probabilistic characteristics include expected values, coefficients of variation, skewness and kurtosis of the effective material properties. It is investigated numerically how the proposed algorithm works for the objective composite and how a fluctuation of the voids volume fraction affects the effective composite properties and state functions in the context of probabilistic analysis.

4.3.1. Stochastic characteristics of the interface defects

Stochastic interface defects characteristics are determined computationally using the results coming from laboratory experiments and from probabilistic homogenization of

this composite. It is firstly assumed that it is possible to find such a pair of expected value and coefficient of variation of volume fraction of interface defects $\exists\, E(w)$, $\alpha(w)$ which will ensure equality of expectations of the effective stress coming from the laboratory experiments $\left(\sigma^{m}_{lab\ CB\ 5\%}\right)$ and these retrieved from probabilistic homogenization $E\left(\sigma^{eff}_{\xi,w=5\%}\right)$ of this composite for all levels of the applied strain ε_l.

$$E\left(\sigma^{eff}_{\xi,w=5\%}\right) \cong E\left(\sigma^{m}_{lab\ CB\ 5\%}\right)(\varepsilon_l). \tag{4.10}$$

Secondly, it is assumed that the only new source of uncertainty in laboratory experiments of this composite with respect to the tests of virgin homogeneous material are the uncertain interface so that

$$\begin{gathered}\alpha(\sigma^{m}_{lab\ CB\ 5\%})(\varepsilon_l)\cong\alpha(\sigma^{m}_{lab\ CB\ 0\%})(\varepsilon_l)\\ +\alpha\left(\sigma^{eff}_{\xi,w=5\%}\right)(\varepsilon_l) - 2\mathrm{Cor}\left(\sigma^{m}_{lab\ CB\ 0\%},\sigma^{eff}_{\xi,w=5\%}\right)(\varepsilon_l).\end{gathered} \tag{4.11}$$

This condition is also valid for the sought pair of $E(w)$, $\alpha(w)$. It means that the coefficient of variation of the composite filled with 5% CB $\alpha\left(\sigma^{m}_{lab\ CB\ 5\%}\right)(\varepsilon_l)$ differs from the one for the virgin homogeneous material $\alpha\left(\sigma^{m}_{lab\ CB\ 0\%}\right)(\varepsilon_l)$ only with a coefficient of variation of volume fraction of interface defects $\alpha\left(\sigma^{eff}_{\xi,w=5\%}\right)(\varepsilon_l)$ and two correlations between these two. With such an assumption one could consider the uncertainty of the effective stress to be following

$$\begin{gathered}\alpha\left(\sigma^{eff}_{\xi,w=5\%}\right)(\varepsilon_l)=\\ \alpha\left(\sigma^{m}_{lab\ CB\ 5\%}\right)(\varepsilon_l) - \alpha\left(\sigma^{m}_{lab\ CB\ 0\%}\right)(\varepsilon_l)+2\mathrm{Cor}\left(\sigma^{m}_{lab\ CB\ 0\%},\sigma^{eff}_{\xi,w=5\%}\right)(\varepsilon_l),\end{gathered} \tag{4.12}$$

where correlation between all the sources of uncertainty in the laboratory tests of virgin homogeneous material and the defects volume fraction can be considered null and expectations of w are contained in an interval $\langle 0,1\rangle$ (physical restrictions)

$$\begin{gathered}\mathrm{Cor}\left(\sigma^{m}_{lab\ CB\ 0\%},\sigma^{eff}_{\xi,\ w=5\%}\right)\cong 0,\\ E(w)\in\langle 0,1\rangle.\end{gathered} \tag{4.13}$$

Correlation is assumed null because the formulation of interface defects occurs at manufacturing time and they are not altered afterwards. This is confirmed by the results of laboratory experiments, where $\alpha\left(\sigma^{m}_{lab\ CB\ 5\%}\right)(\varepsilon_l) - \alpha\left(\sigma^{m}_{lab\ CB\ 0\%}\right)(\varepsilon_l)$ is very weakly dependent on ε_l; its magnitude stabilize at a constant level of approx. 0.05 despite some initial fluctuation for small levels of strain (see Fig. 5.8).

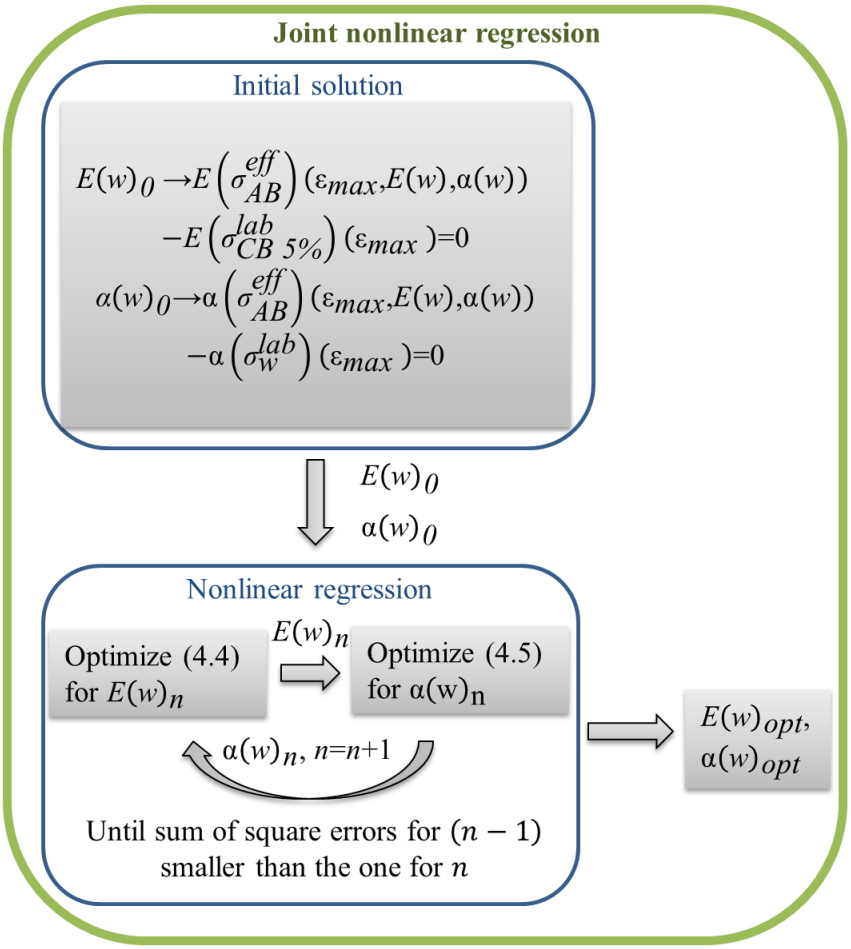

Fig. 4.4**.** Joint nonlinear regression algorithm.

A final optimization problem includes minimization of two objective functions that are tied together by $E(w)$ and $\alpha(w)$

$$E(w) \rightarrow \sum_{l=1}^{Y}\left(E\left(\sigma^{eff}_{\xi,w=5\%}\right)(\varepsilon_l, E(w), \alpha(w)) - E\left(\sigma^{m}_{lab\ CB\ 5\%}\right)(\varepsilon_l)\right)^2 = \min, \tag{4.14}$$

$$\alpha(w) \rightarrow \sum_{l=1}^{Y}\left(\alpha\left(\sigma^{eff}_{\xi,w=5\%}\right)(\varepsilon_l, E(w), \alpha(w)) - \alpha\left(\sigma^{m}_{lab\ CB\ w}\right)(\varepsilon_l)\right)^2 = \min \tag{4.15}$$

This coupled problem is solved iteratively using a joint linear regression algorithm that is based on a nonlinear regression solver provided by the NonlinearFit tool in Statistics package of MAPLE software. It consists of two consecutive steps presented in Fig. 4.4.

Firstly, an initial guess of $E(w)_0$ and $\alpha(w)_0$ is provided. Then the nonlinear regression is applied iteratively. It starts with determination of a first approximation of $E(w)_1$ using an initial value of $\alpha(w)_0$. Then $\alpha(w)_1$ is sought by the second criterion substituting $E(w)_0$ to eqn. (4.15). This iteration of nonlinear regression is repeated n times until the remainder of eqns (4.14) and (4.15) for the previous iteration is smaller than the one for the current iteration or a maximum allowed number of iterations (400) is reached. In this work the initial values are read out from figures included in section 6.3.2 presenting the results of previous steps in the probabilistic homogenization algorithm. This approach proved to be enough accurate, especially because the results of numerical experiments show a weak dependence of $E\left(\sigma_{\xi,w}^{eff}\right)$ on $\alpha(w)$ and also $\alpha\left(\sigma_{\xi,w}^{eff}\right)$ on ε_l. For composites in which these values are more tightly related, a larger number of initial guesses should be considered and convergence of their solution verified. The minimization is done using the continuous characteristics returned by the ISPT. Alternatively, they may also be calculated upon the results of the SAM or any response function fitted to the discrete results of the MCS. This is not proposed here, because all the stochastic methods return highly converging expectations and coefficients of variation, which are almost perfectly coincident close to the determined sets of $\{E(w),\ \alpha(w)\}$. This algorithm is repeated for all three selected hyperelastic potentials and for each of them result set may be slightly different. This is because the stochastic characteristics returned by the ISPT, MCS and SAM depend on an initial choice of hyperelastic potential especially for higher order stochastic characteristics and high levels of $\alpha(w)$.

4.3.2. Probabilistic homogenization algorithm

A probabilistic homogenization algorithm for computations performed in this dissertation is presented in Fig. D.1. It primarily aims to determine the expectation and the coefficient of variation of interface defects volume fraction. It allows to fully define the effective uncertain response of a selected composite with spherical reinforcement and stochastic interface defects. A secondary objective in this algorithm is determination of uncertainty in the effective material parameters of such a composite.

They can be further used in structural level of analysis without any need to consider the uncertain defects. In its intermediate steps, this algorithm also defines the deterministic and stochastic relations of the composite effective deformation including the effective deformation energy and effective stress in an uniaxial stretch. It also provides the effective material characteristics for each of the selected hyperelastic constitutive models. They are retrieved for an increasing level of strain and an increasing random dispersion of the defects volume fraction (stochastic characteristics) or expected value of the defects volume fraction (deterministic results). This algorithm includes four major consecutive steps (named in green on the graph) that are further decomposed to smaller procedures (provided in blue on the graph). Each step ends with a certain characteristic of this composite that are given in black in Fig. D.1. These characteristics could be used to define the response of this composite and are used in further steps. They are following:

1. laboratory experiments of uniaxial stretch for two sets of samples. The first set for a virgin homogeneous material and the second set with n% of carbon black particles; here 5% is selected. Experiments produce the rough data to feed the computational part of this algorithm. Their analysis includes expected values of stress under known boundary conditions $E\left(\sigma^{m}_{lab\ CBn\%}\right)$ together with its coefficient of variation $\alpha\left(\sigma^{m}_{lab\ CBn\%}\right)$; they are presented in section 5. These relations for the virgin homogeneous material serve for selection of the best constitutive law to approximate the composite behavior. Results for the filled composite are used in the final procedure for determination of statistical estimators the input uncertain parameter, i.e. the interface defects volume fraction; they are expectation and coefficient of variation. This procedure is explained in section 4.3.1.
2. Definition of computational model for composite phases. It contains two major parts
   a) selection of the constitutive models best approximating the matrix in uniaxial stretch (after laboratory experiments) together with their material parameters $C^{m}_{\xi,i}$ through fitting algorithm; it is described in Appendix A.
   b) determination of the interphase constitutive model and variables $C^{int}_{\xi,i}(w)$ defined according to the selected interphase constitutive model given in section 3.1.3.

      In this analysis the CB particle stays in its linear elastic reversible range, while the interphase and the matrix – in a hyperelastic mode.

3. Nonlinear probabilistic homogenization that presents the effective material coefficients of the defective composite together with its state variables, i.e. deformation energy and stress. It contains three major parts
   a) pointwise homogenization, which recovers the discrete relation of the effective deformation energy and the volume fraction of interface defects $U^{eff}_{\xi,x}\left(\lambda_x, I_{1,x}, I_{2,x}, w_x\right)$ through FEM experiments; its details could be found in section 4.1 and 4.2.
   b) determination of continuous representation of the effective material coefficients $C^{eff}_{\xi,i}\left(E(w)\right)$, effective deformation energy $U^{eff}_{\xi}\left(E(w)\right)$ and effective stress $\sigma^{eff}_{\xi}\left(E(w)\right)$ w.r.t. the expectation of the interface defects volume fraction; it is also denoted as w since the mean, expected and characteristic values of this Gaussian parameter are equal.
   c) determination of the four stochastic characteristics of the three above variables, i.e. $\zeta_4\left(C^{eff}_{\xi,i}\left(\zeta_2(w)\right)\right)$, $\zeta_4\left(U^{eff}_{\xi}\left(\zeta_2(w)\right)\right)$, $\zeta_4\left(\sigma^{eff}_{\xi}\left(\zeta_2(w)\right)\right)$ w.r.t. the expected value and coefficient of variation of the interface defects volume fraction $E(w)$, $\alpha(w)$; they are computed for an increasing level of the applied strain; $\zeta_n(.)$ denotes the first n stochastic characteristics of a certain random parameter or variable. Characteristics are expected value, coefficient of variation, skewness and kurtosis.

      Deterministic relations and stochastic characteristics of these variables are recovered in sections 6.1 (effective material coefficients), 6.2 (effective deformation energy) and 6.3 (effective stress under uniaxial stretch).
4. Final computation of the effective composite response with $E(w)$, $\alpha(w)$ found through application of the joint regression algorithm explained in section 4.3.1. It consists of two major tasks
   a) computation of the expected value and coefficient of variation of the volume fraction of interface defects $E(w)$, $\alpha(w)$ for the objective composite with stochastic interface defects. It is included in section 6.1.2.
   b) determination of the first four stochastic characteristics of the effective material coefficients for each of the selected constitutive models $\zeta_4\left(C^{eff}_{\xi,i}\left(\zeta_2(w)\right)\right)$, of the effective deformation energy $\zeta_4\left(U^{eff}_{\xi}\left(\zeta_2(w)\right)\right)$ and of the effective stress

$\zeta_4\left(\sigma_\xi^{eff}\left(\zeta_2(w)\right)\right)$; the stress is presented together with the relations obtained in laboratory experiments to verify this algorithm.

Results of this step are included in sections 6.1.3, 6.1.4, (effective material coefficients), 6.2.3 (effective deformation energy), 6.3.2 and 6.3.3 (effective stress).

Intentionally, this algorithm is kept independent from the underlying hyperelastic potential denoted as ξ. This is especially important because all of these potentials have some specific range of applications and material parameters differ for all of them. Some of the parameters have a strict physical meaning, as the λ_m in Arruda-Boyce constitutive model. The others are purely numerical, for example the coefficients in various polynomial approaches. As documented in section 6.1, a classical approach for stochastic analysis and homogenization using scatter of the material coefficients ties the analysis to a specific potential. Such an approach leaves limited possibilities for result verification and interchangeability. Variation of material parameters in hyperelastic regime should rather be perceived as a derivative of the randomness in material response and not otherwise, especially when these parameters are purely phenomenological. This is even more important for multi-phase composites, where each phase could work in different regime and be governed by a different law.

Please note that this algorithm is designed for an arbitrary volume fraction of the filler, which can be either spherical compound (it is not at all limited to carbon black). Such procedure may also be performed for non-isotropic composites, even the fully anisotropic ones. In this case, however ,the number of laboratory tests required will be much higher than in the isotropic case. It will work also for different than Gaussian type of uncertainty in defects volume fraction, but will require a much higher number of samples in sets of laboratory experiments than these for the Gaussian parameter. This is because a precise determination of skewness, kurtosis and even higher stochastic characteristics will be potentially required for determination of the input uncertain variable PDF.

The proposed algorithm enables determination of the effective uncertain response of a given composite with interface defects for a selected hyperelastic potential. Its major advantage is lack of requirement for prior information of the defects formed on its interface. This algorithm also returns an estimate of the volume fraction of this defects together with a coefficient of its dispersion. It further allows to incorporate the returned

uncertainty in material parameters of the selected constitutive model into the macromolecular analysis; their randomness intrinsically accounts for the uncertain interface defects. All of this is possible with a limited need of costly laboratory experiments; only two sets of relatively simple tests are required.

5. Laboratory experiments

5.1. Objectives of laboratory experiments

The principal objective of laboratory experiments is recovery of the stress-strain relation of the selected high density polyurethane (HDPU) composite together with its first two stochastic characteristics. They are used at various stages of numerical experiments (presented in section 6) for their calibration and verification. Specifically, they support selection of the matrix constitutive relation, are fundamental in numerical determination of the volume fraction of interface defects in this composite (its expected value and coefficient of variation) and serve for the final verification of applicability of the proposed stochastic algorithm.

5.2. Material preparation and test bench

Laboratory tests include classical uniaxial stretch and cyclic uniaxial stretch. They have been done a) for the high density polyurethane Laripur LPR 5020 and b) a composite with matrix made from this material reinforced with 5% carbon black particles F60. Each test consisted of a set of 10 samples with height of 14±2 mm and thickness equal to 4.7±0.6 mm. They have been prepared from granulate, which was melt and formed into a thin cuboid of constant thickness 0.95±0.5 mm and cut out to the required shape. Their geometrical dimensions were measured with a digital caliper having accuracy of $\pm 20\ \mu m$. Stretch has been applied as vertical elongation (Fig. 5.1 c) with deformation rate of 10 mm/minute for all tests. All of them have been made for a range of strain of $\varepsilon_{11} \in (0.00, 0.275)$. Strain cycle consisted of 10 consecutive increases of strain till $\varepsilon_{11}=0.275$ followed by relaxation to near zero strain. Experiments have been performed on INSTRON 5582 machine (Fig. 5.1 a) at room temperature. Samples were clamped at both ends during the entire analysis. No onset of damage was observed; samples were neither necking nor cracking. A result of experiments was engineering stress σ_{lab}^{m} and corresponding engineering strain ε_{11}.

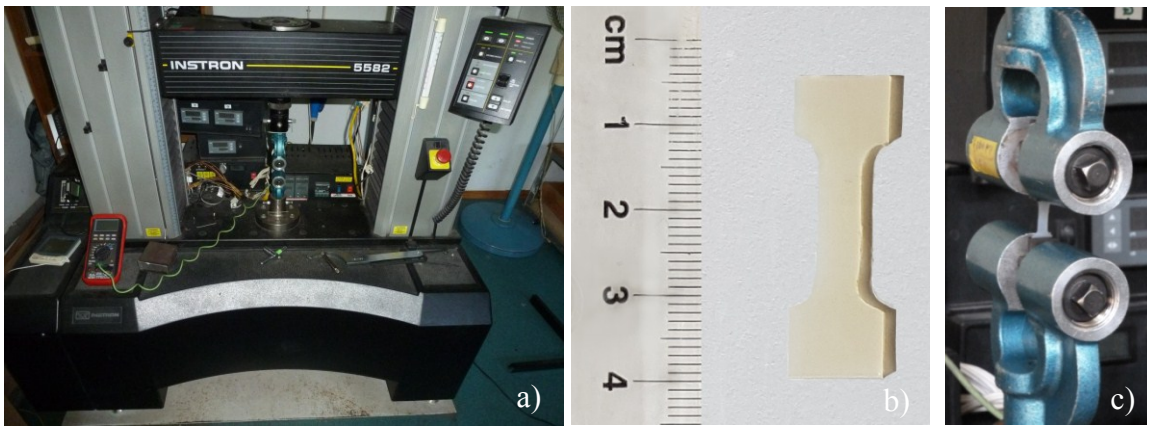

Fig. 5.1 Test bench (a) test specimens (b) and zoom on the test specimen (c) used for uniaxial stretch of high density polyurethane Laripur LPR 5020.

An exemplary sample is presented on Fig. 5.1 b), set of samples for virgin homogeneous material is shown on Fig. 5.2 and set for samples reinforced with 5% carbon black is presented on Fig. 5.3.

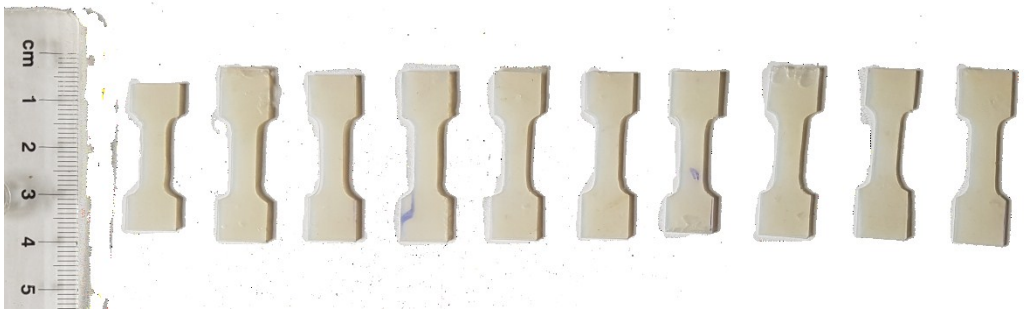

Fig. 5.2 Samples of virgin homogeneous material made from Laripur LPR 5020 high density polyurethane (HDPU).

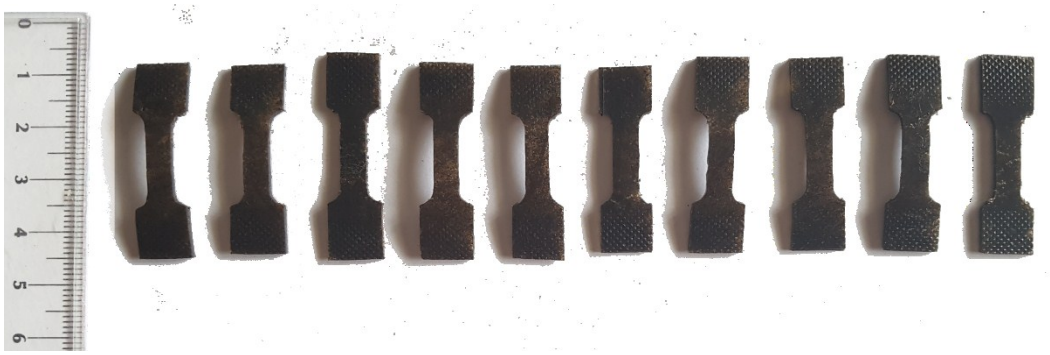

Fig. 5.3 Samples of composite made from Laripur LPR 5020 reinforced with 5% particles of carbon black.

5.3. Results

5.3.1. Single stretch

The stress-strain curves coming from a single stretch of the virgin homogeneous material Laripur LPR 5020 are shown on Fig. 5.4. They present all 10 experiments distinguished by colors that all have close loading curves. Linear-elasticity region ranges $\varepsilon_{11} \in (0.00, 0.027)$. It is followed by a local softening at $\varepsilon_{11} \in (0.03, 0.07)$ with corresponding stress of $\sigma^m_{lab} \in (4.4, 4.9)$ MPa. The stress difference between the experiments increases a little together with an increase of ε_{11} up to 10% of the expected value for the highest strain level.

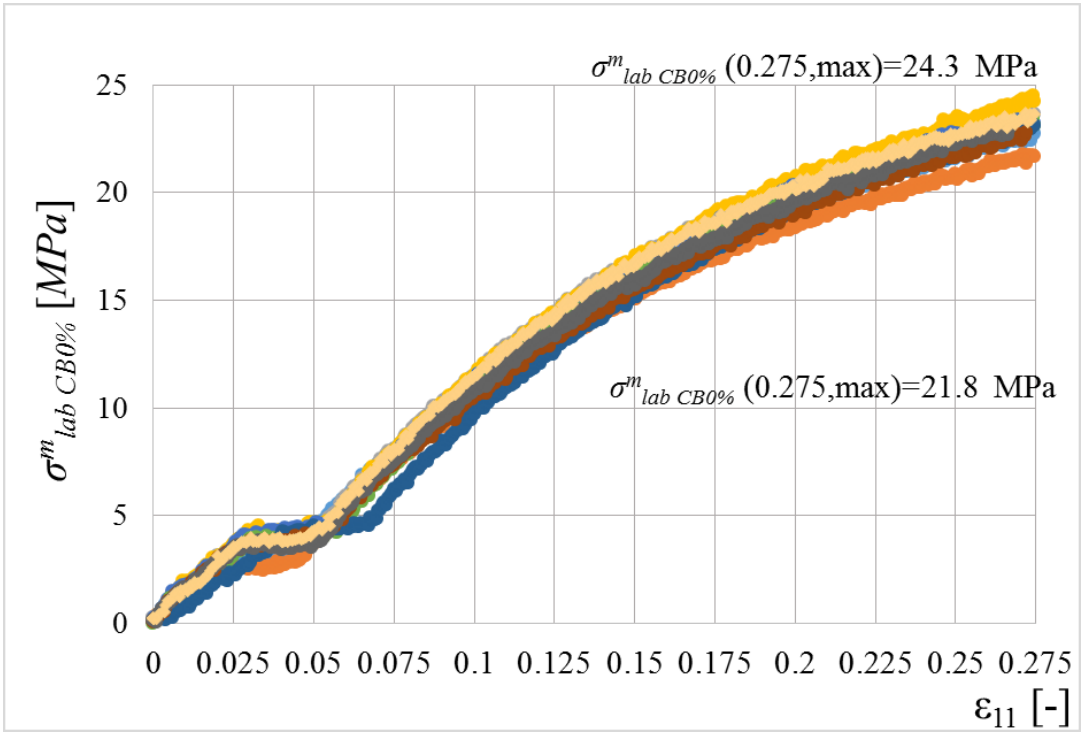

Fig. 5.4 Experimental stress-strain relation for the 10 specimens of Laripur LPR 5020 under an uniaxial stretch.

The composite (Laripur filled with 5% CB) is much softer than the virgin homogeneous material. This is because of the defects that form on the particle-matrix interface. Its stress-strain curve under uniaxial stretch is presented on Fig. 5.5 for 10 specimens. The maximum stress is much lower than the one for the pure material - $\sigma^m_{lab\ CB5\%}|_{\varepsilon_{11}=0.275}$=19 MPa and also scatter of results for consecutive specimens is much bigger.

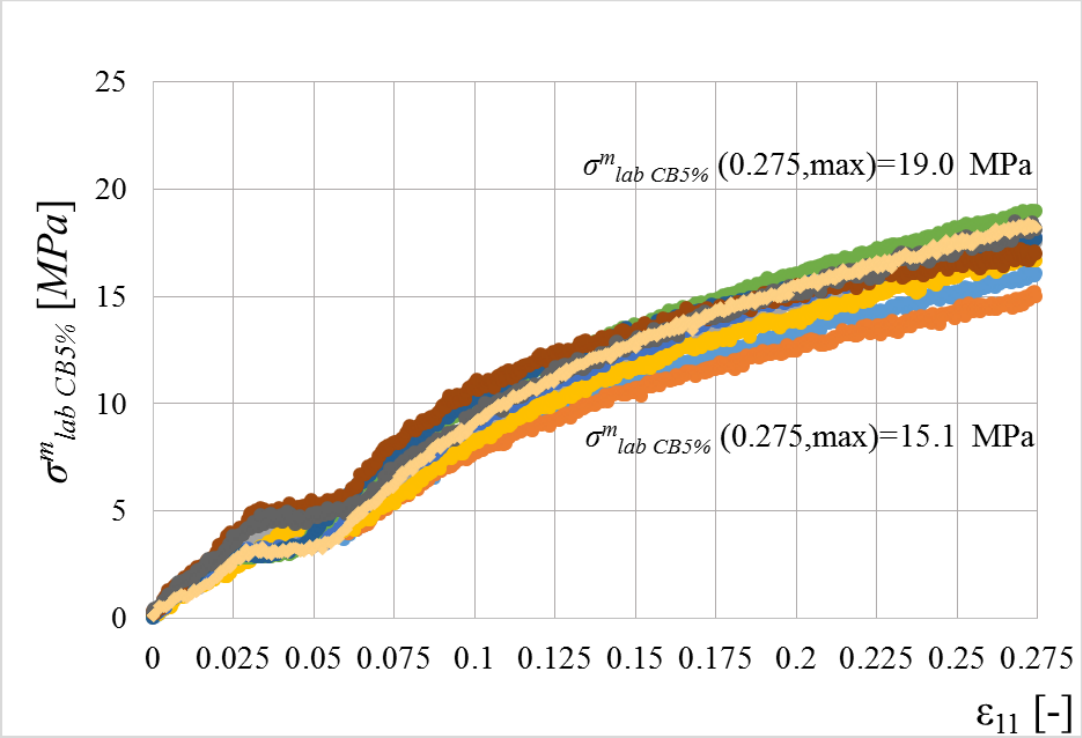

Fig. 5.5 Experimental stress-strain relation for the 10 specimens of Laripur LPR 5020 under uniaxial stretch.

This is exemplified on Fig. 5.6, where the ratio between expected values of these stresses is plotted w.r.t. the strain (blue curve, right axis). Upon initial variation at low strains $\varepsilon_{11} \in (0.0, 0.06)$ it increases to a little over 1.4 and stabilizes. The two expected values are also plotted on this graph (gray and black curves, left axis), which further proves that a character of deformation is retained in-between the filled composite and the virgin homogeneous material.

Coefficient of variation corresponding to a single uniaxial stretch laboratory tests $\alpha(\sigma^m_{lab,s})$ is presented on Fig. 5.7 for both, the virgin homogeneous material (gray) and the composite (black). It firstly shows that it is not constant with respect to the strain level. It is the highest for strains close to zero ($\varepsilon_{11} \approx 0$) and then decreases together with an increase of strain; difference between these two extremes is almost tenfold. A strong variation of $\alpha(\sigma^m_{lab,s})$ is observed in the region of local softening with a peak of $\alpha(\sigma^m_{lab,s})$=0.018 for the virgin homogeneous material and a little over $\alpha(\sigma^m_{lab,s})$=0.02 for the composite.

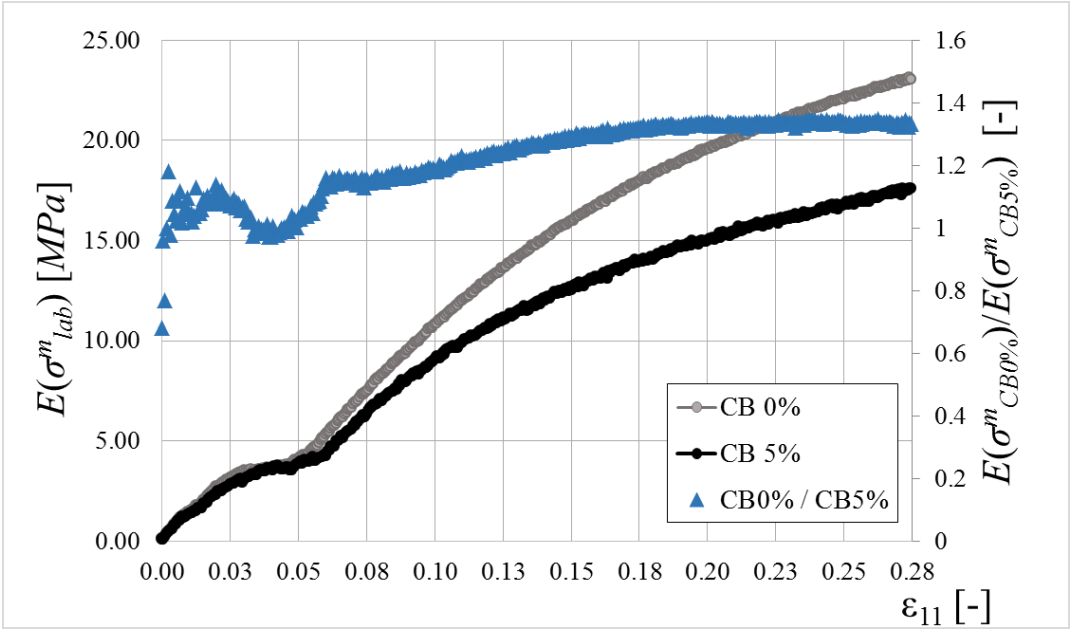

Fig. 5.6 Comparison of the stress-strain relation for the pure Laripur LPR 5020 material and the objective composite under uniaxial stretch.

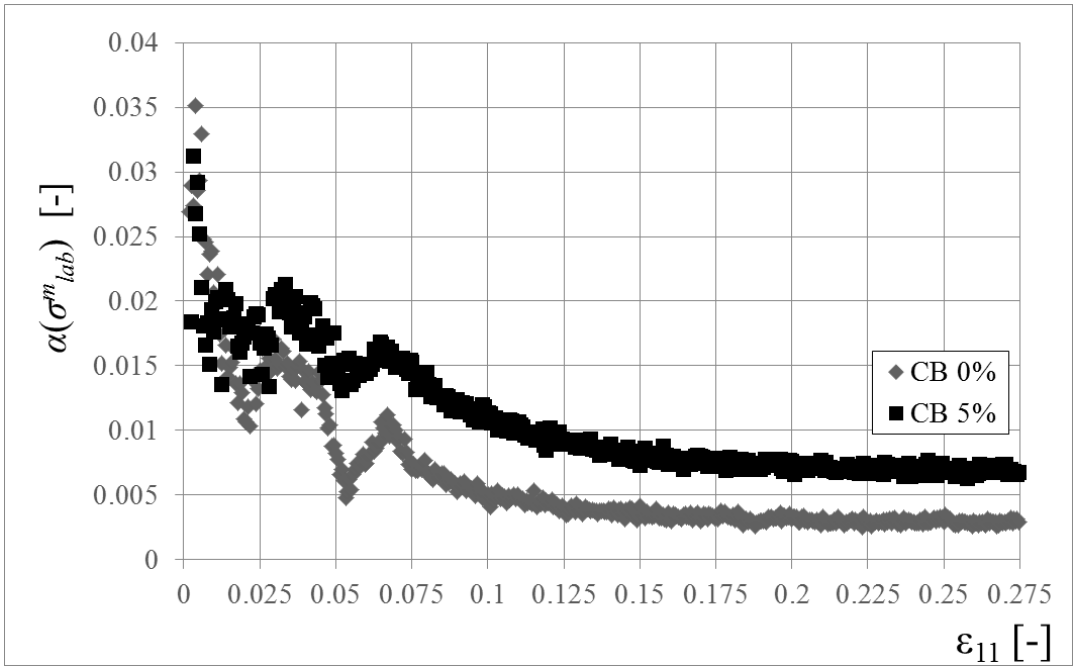

Fig. 5.7 Coefficient of variation of stress w.r.t. the strain ε_{11}.

Coefficient of variation of virgin homogeneous material is lower than the one of the composite, but they both have a very similar relation to the strain. Since $\alpha(\sigma^m_{lab,s})$ is clearly not constant for different levels of strain, so is the randomness of $\sigma^m_{lab,s}$; this also holds for the cycling loading (see Fig. 5.13). It indicates that application of a probability density function (PDF) independent from strain may be suboptimal for this material and

other hyperelastic continua also. This conclusion is the principal reason for including the strain level in further stochastic experiments performed in the numerical part of this thesis. Such an approach considerably increases complexity of calculations but it enables a check of the effective characteristics for desired uncertainty level and a level of the strain. It is especially affecting the Monte-Carlo simulations, because they must be repeated for different strain levels in relatively close intervals, unlike the stochastic perturbation or semi-analytical approach.

The last graph presented on Fig. 5.8 shows a difference of coefficient of variation of stress in uniaxial stretch between the pure material and the composite. Upon a small variation for the low strains, this difference stabilizes with magnitude of approximately 0.005. Such behavior indicates that an addition of the filler and subsequent generation of the interface defects introduce additional dispersion of stress that has a rather constant character for higher strains. This conclusion is especially important for the algorithm proposed in section 4.3.1, because it constitutes one of its conditions; this algorithm determines the statistical estimators of input uncertain variable.

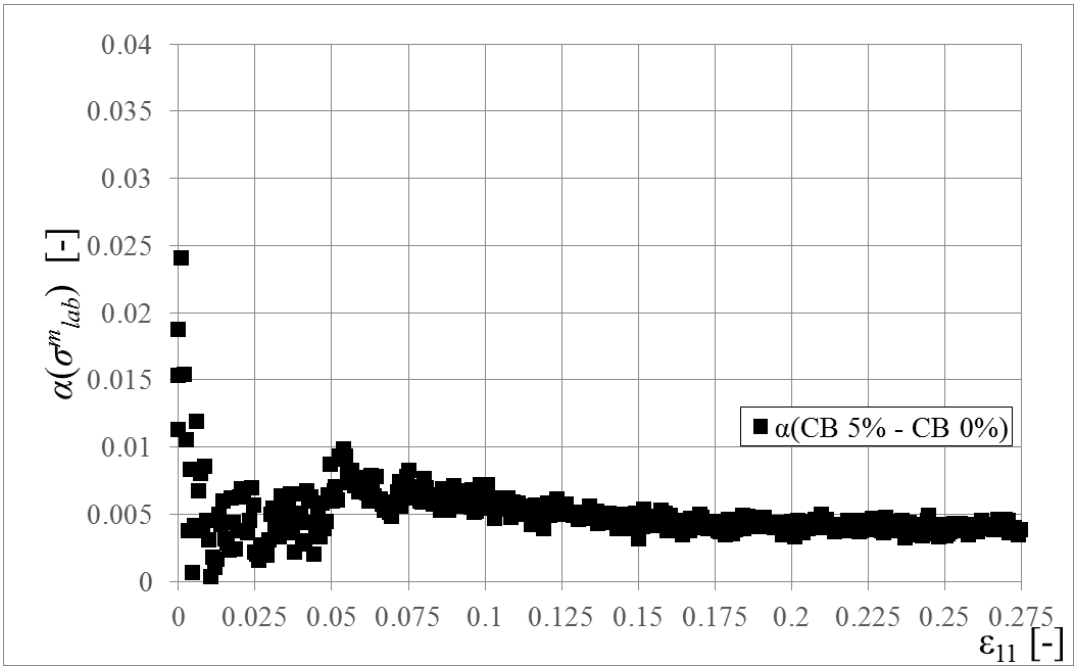

Fig. 5.8 A difference of coefficient of variation of stress in uniaxial stretch between the pure material and the objective composite w.r.t. the strain ε_{11}.

It is assumed here that the only source of uncertainty in the filled elastomer additional to the ones already present in the pure material are the interface defects. Thus, this graph is considered to directly represent their influence on uncertainty of deformation of

the filled material; this assumption is further used in numerical part of this dissertation. It is plausible firstly because a) treatment of all the specimens, both filled and unfilled, was always the same, b) they were tested on the same test bench in short span of time (environmental conditions did not change for different sets of experiments) and also because all the experiments were performed and samples prepared by the same person. Of course, the matrix of the composite is made with the same batch of Laripur as pure material samples. Number of samples in set may be considered too small for determination of statistical estimators, but please remember that each experiment consist of approximately 500 of read-outs by the test bench for single stretch case so that total number of trials is around 5 000 and not 10.

At this point Hypothesis 4 is confirmed. Stiffness and effective stress of the objective (HDPU-CB) composite subjected to uniaxial stretch is lower with respect to the virgin homogeneous material and the coefficient of variation of the effective stress is higher. Difference between these coefficients of variation stabilizes with an increase of strain.

5.3.2. Cyclic tests

Cyclic tests have been performed (a) for the virgin homogeneous material made from Laripur LPR 5020 (Fig. 5.9) and (b) for a composite filled with 5% carbon black fullerenes (Fig. 5.10). Their results show that the virgin homogeneous material has a little higher stiffness and much smaller dispersion than the composite. This indicates that the bond between reinforcement and the matrix is defective, because carbon black has a higher stiffness than the matrix. Both graphs clearly indicate a stiff first loading curve followed by an unloading curve and consecutive always softer loading/unloading curves. This holds for all ten realizations distinguished by colors. In first cycle the linear-elasticity is kept until $\varepsilon_{11} \approx 0.03$ above which material undergoes a local softening till around $\varepsilon_{11} \approx 0.05 - 0.07$.

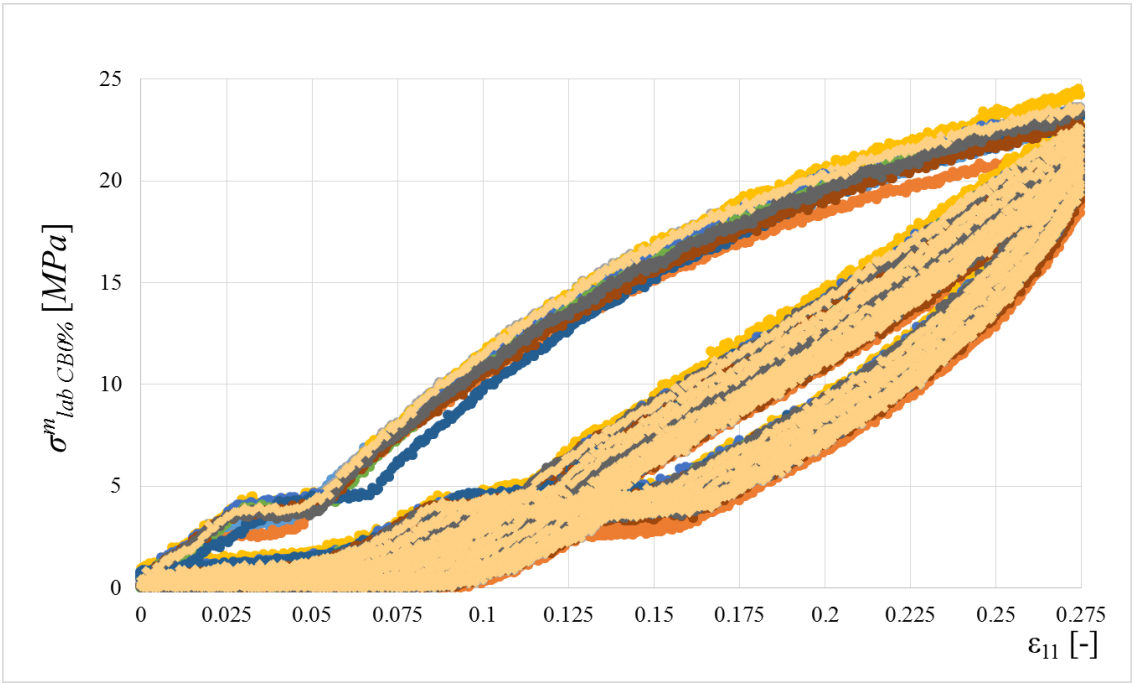

Fig. 5.9 Stress-strain relation of Laripur LPR 5020 under cyclic uniaxial stretch.

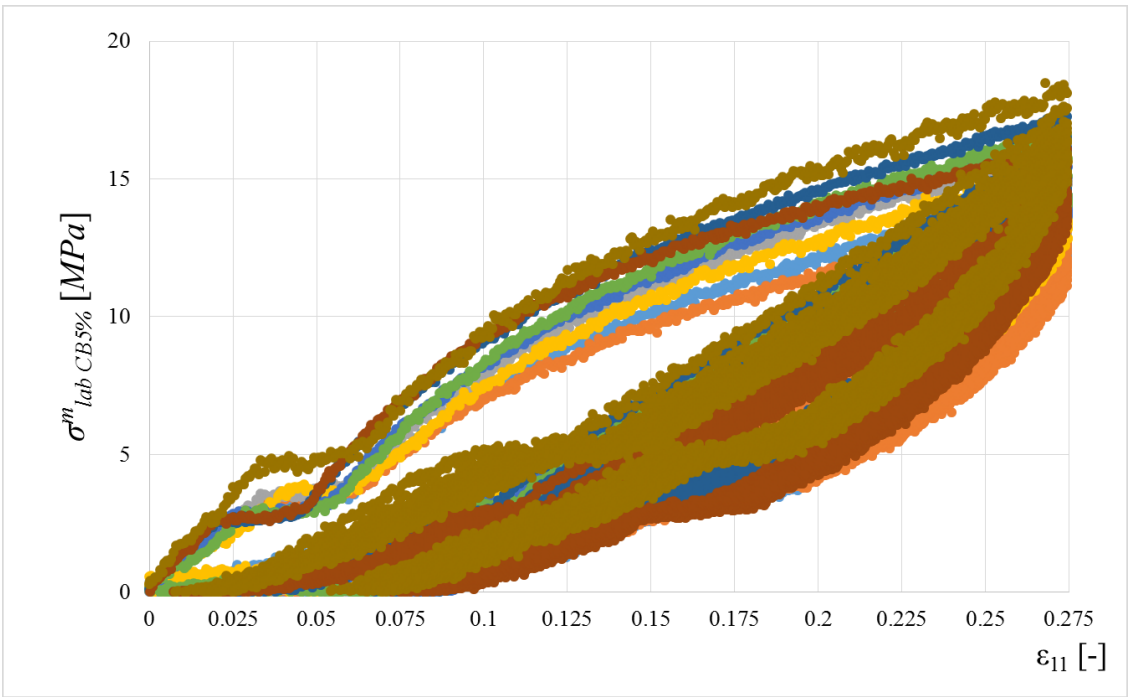

Fig. 5.10 Stress-strain relation of Laripur LPR 5020 filled with 5% carbon black under cyclic uniaxial stretch.

Above softening material regains stiffness close to the linear-elasticity that decreases together with an increase of strain and allow an increase of applied stress until the end of the loading phase. During first unloading material returns to near zero strain with a

lower curve. In the second and above cycle the loading curve follows previous unloading curve and the unloading is a little softer than the previous loadings. The highest loss of stiffness is observed for the first unloading. Softening occurs at higher stress and has smaller strain range for pure material than for the composite.

Expected value of stress w.r.t. applied strain is presented on Fig. 5.11. It firstly shows that on average the virgin homogeneous material sustains much higher stress - σ^m_{lab} =23.6 MPa vs σ^m_{lab} =17.4 MPa and has a little higher loss of stiffness from the first unloading. It also quite clearly presents an exponential character of stress curve, much more evident than for the composite.

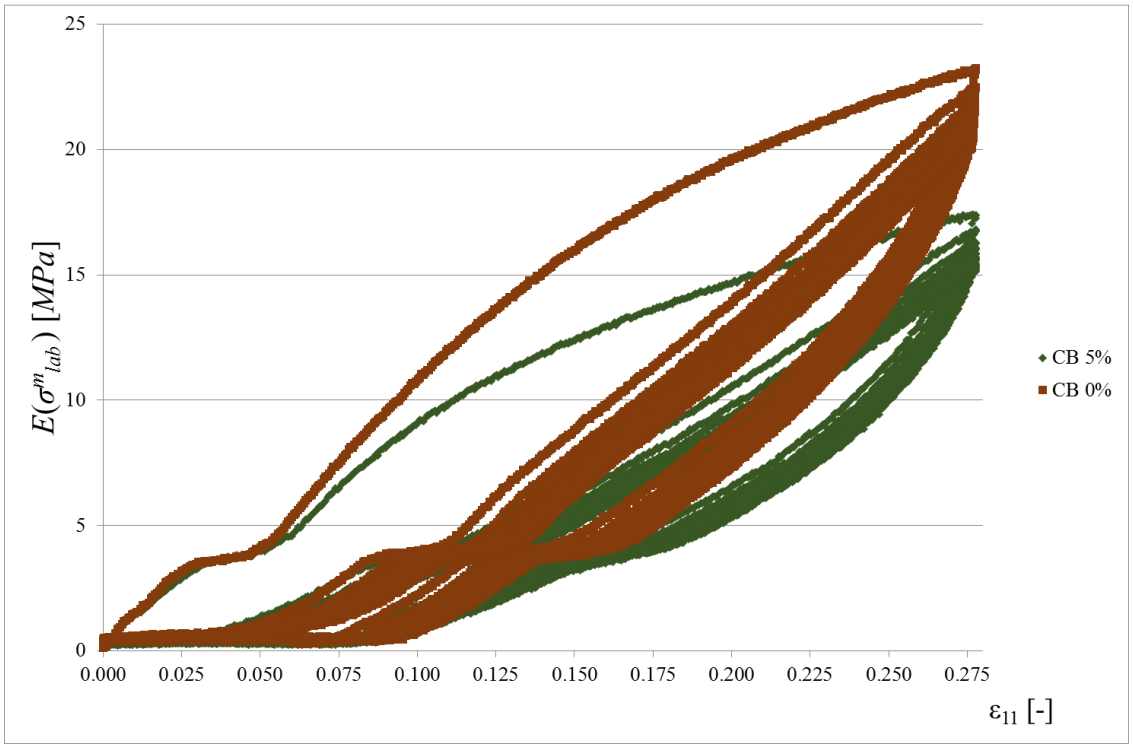

Fig. 5.11 Expected value of stress coming from experimental tests w.r.t. strain level.

Next, the stress envelope is presented on Fig. 5.12 with minimum, maximum and mean loading curves for both sets of experiments. The envelope of loading and unloading is a little narrower for the virgin homogeneous material than for the composite. The situation is the same for the absolute difference between the highest stress and the lowest at ε_{11}=0.275, which is much smaller for the pure material. Next, standard deviation of the cyclic lading experiments is presented on Fig. 5.13. It is much higher for the composite than for the pristine material and clearly is not constant for different levels of strain. It has a considerable difference in-between the loading-unloading cycles

and always increases together with an increase of strain. It reaches 1.6 MPa for the composite and almost 1.1 MPa for the pure material.

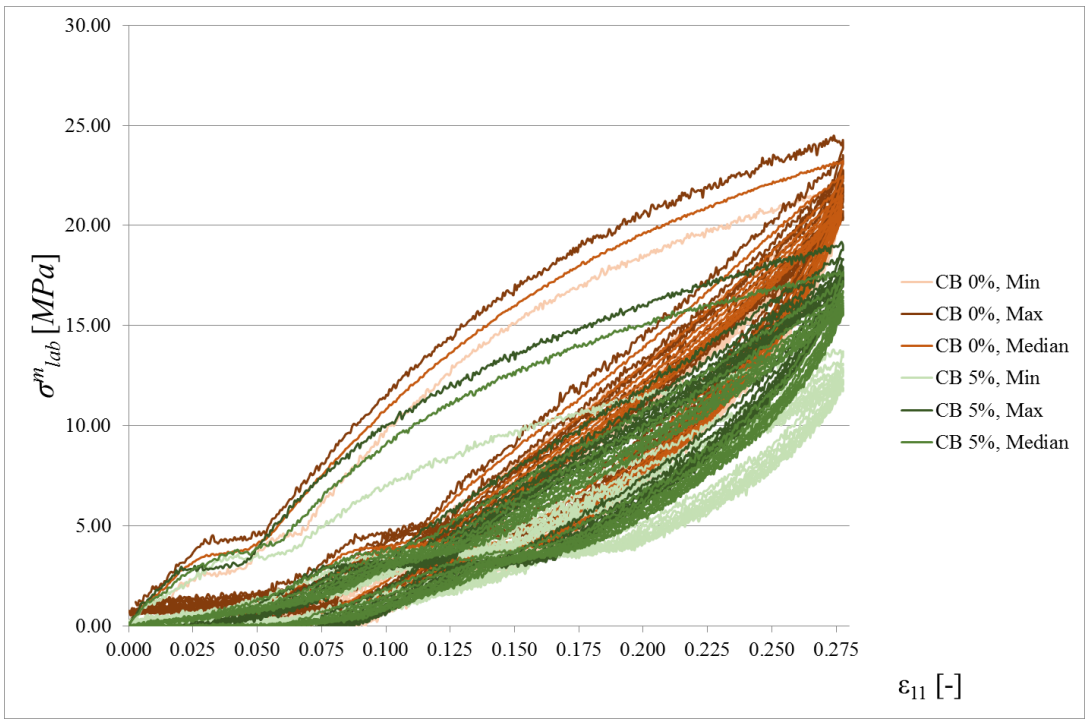

Fig. 5.12 Maximum, mean and minimum values of stress curves coming from experimental tests w.r.t. strain level.

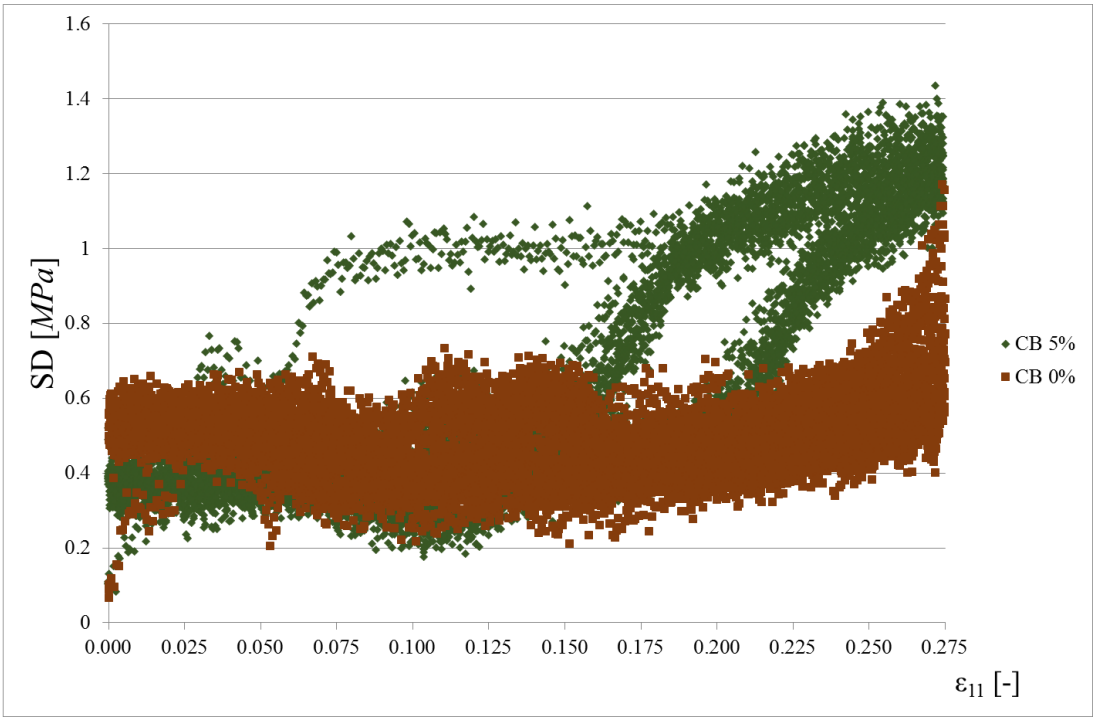

Fig. 5.13 Standard deviation of stress coming from experimental test w.r.t. strain level.

6. Numerical experiments

Numerical experiments consists of three main parts presenting results for different state variables; each of them is focused on different aspect of the composite effective response in deterministic and stochastic context. In section 6.1, the effective properties of the composite are calculated. In section 6.2, the effective deformation energy is verified and in section 6.3 the effective stress is determined. Results of numerical analysis are not fully presented in an order of the probabilistic homogenization algorithm. Instead, they are grouped into sections focused on each considered effective state variable of the composite. Firstly, the deterministic results are provided and then the stochastic results are presented. These results always include the expected values, coefficients of variation, skewness and kurtosis of the state variables.

Graphs of the following sections commonly include multiple colors and symbols. They are used to differentiate the results of the alternative methods or approaches. Legends included in these graphs commonly use abbreviations. They are all summarized here to avoid their repetitive introduction in following sections. Potentials include the Mooney-Rivlin 'MR', Arruda-Boyce 'AB' and Neo-Hookean 'NH'. Methods used for computation of stochastic characteristics are the generalized iterative stochastic perturbation 'ISPT', the Monte-Carlo simulation 'MCS' and the semi-analytical approach 'SAM'. Graphs connected to deterministic experiments denote discrete FEM results as 'FEM', the augmented material model as 'AMM' and the bivariate polynomial approximation as 'BPO'. Graphs connected to stochastic experiments commonly include $E(w)=0.(.)$, which always denote the expected value of volume fraction of interface defects w, for which they were calculated. The above mentioned abbreviations are commonly concatenated on the legend joining by a space. For example, 'ISPT MR' means that this result was obtained with use of the generalized iterative stochastic perturbation method and the Mooney-Rivlin constitutive model for matrix (and the interphase as well, see section 3.1.1, eqn (3.4)). There also exist additional abbreviations used locally in the legends, which are described once the figure is mentioned in the text. The different approaches, methods or parameters are always differentiated on these graphs by colors or/and symbols. Specifics of this division are inherent to each graph or group of graphs; they are included in description of each section.

Numerical experiments report results for three alternative potentials of the matrix and the interphase of the composite denoted by ξ. This has been done to verify effectiveness of the proposed computation algorithm independently from them. Such an approach has only been waived for consideration of stochastic characteristics of the effective deformation energy. This is because coincidence of their deterministic results is very high and does not provide significant addition to the observables coming from analysis of the effective stress.

6.1. Effective material properties of the composite

In this part of research the effective material properties of the defective composite are computed under uncertain volume fraction of interface defects w (alternatively called as the weakening coefficient) together with their stochastic characteristics. It presents these effective properties together its first four stochastic characteristics relative to the variable volume fraction of interface defects w. Their characteristic values given in the deterministic analysis are intended to directly serve for inclusion in simulations of this composite on the structural level. The exact values for the known volume of interface defects could be simply read-out from the below graphs. If this volume is not known a-priori, it may be computed according to the algorithm proposed in section 4.3.1. Next, stochastic characteristics of the interface defects are recovered with use of this algorithm and at the end they are used to recover the uncertainty in material coefficients of the objective composite tested in laboratory experiments.

6.1.1. Deterministic experiments

Deterministic experiments contain results of the effective material parameters of the composite with interface defects. They are presented relative to the volume fraction of interface defects w. Computation follows the procedure explained in Appendix B. It is done for all the three selected hyperelastic potentials of the matrix and the interphase. Results are ordered on separate graphs for each potential, because they all have a distinct set of parameters. They are presented on the below figures, which distinct the discrete FEM results with black asterisk and their optimized polynomial representation with red circles. These graphs are plotted w.r.t. the volume fraction of interface defects in a range of $w \in (0.06, 0.96)$. Effective parameters exclusively dictate the response of this composite for all deformations and for a variable interface defects intensity.

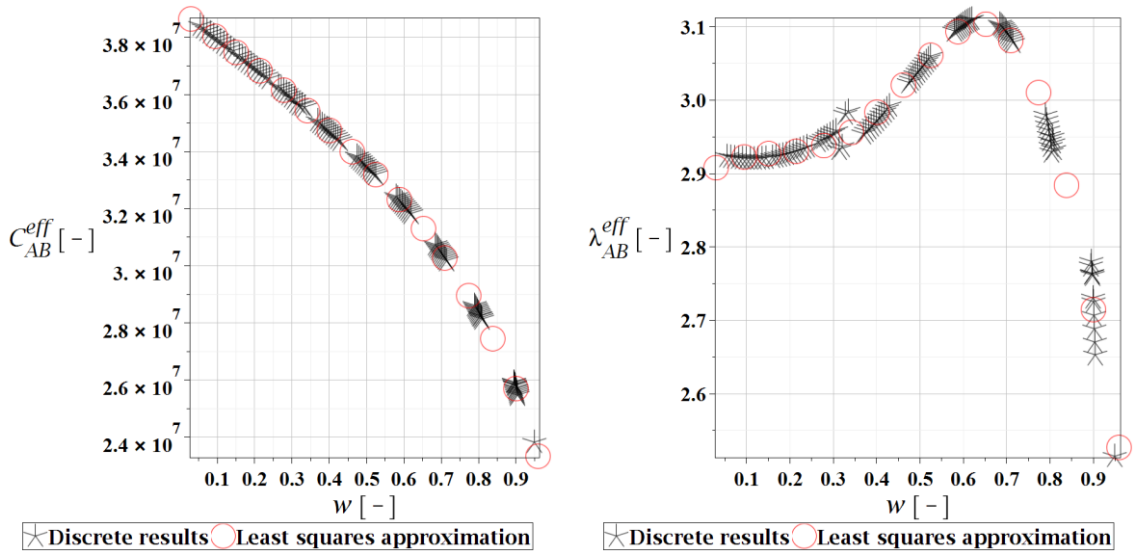

a) b)

Fig. 6.1 Approximation of effective material properties for Arruda-Boyce model a) C_{AB}^{eff}, b) λ_{AB}^{eff} w.r.t. the weakening coefficient w.

The first graph presented on Fig. 6.1 shows the two parameters included in the Arruda-Boyce potential, i.e. $C_{1,AB}^{eff}$ and λ_{AB}^{eff}. The former is depicted on the left (Fig. 6.1 a), and the latter on the right (Fig. 6.1 b). Parameters have quite different dependence on the volume fraction of interface defects; $C_{1,AB}^{eff}$ exclusively decreases together with an increase of w, while λ_{AB}^{eff} increases up to w=0.66 and then decreases. Their order of magnitude substantially differs, it is much larger for $C_{1,AB}^{eff}$, in range of 10^7 and 10^0 for λ_{AB}^{eff}. The ranks of polynomials selected are 10^{th} and formulae are following (polynomial coefficients are reduced to 3 digits from original 12):

$$C_{1,AB}^{eff}=3.88\cdot10^{7}-5.07\cdot10^{6}\cdot w-7.28\cdot10^{7}\cdot w^{2}+5.67\cdot10^{8}\cdot w^{3}-2.50\cdot10^{9}\cdot w^{4}$$
$$+6.42\cdot10^{9}\cdot w^{5}-1.00\cdot10^{10}\cdot w^{6}+9.71\cdot10^{9}\cdot w^{7}$$
$$-5.98\cdot10^{9}\cdot w^{8}+2.35\cdot10^{9}\cdot w^{9}-4.92\cdot10^{8}\cdot w^{10}, \quad (6.1)$$
$$\lambda_{AB}^{eff}=2.91+0.511\cdot w-7.29\cdot w^{2}+17.5\cdot w^{3}+283\cdot w^{4}+2.27\cdot10^{3}\cdot w^{5}+7.45\cdot10^{3}\cdot w^{6}$$
$$+1.31\cdot10^{4}\cdot w^{7}-1.27\cdot10^{4}\cdot w^{8}+6.55\cdot10^{3}\cdot w^{9}+1.37\cdot10^{3}\cdot w^{10},$$

The proposed optimization procedure allows an almost perfect approximation of the discrete results for the entire considered spectrum of volume fraction of interface defects.

Next, the second set of parameters corresponding to the Mooney-Rivlin constitutive model is presented on Fig. 6.2. This set includes two parameters of $C^{eff}_{1,MR}$, and $C^{eff}_{2,MR}$. They both exclusively decrease together with an increase of w and they have a much closer magnitude than the ones for the Arruda-Boyce constitutive model. It is in order of $10^6 - 10^7$; $C^{eff}_{1,MR}$ is approximately 5 times bigger than the $C^{eff}_{2,MR}$ and they are both reduced almost to half of their original value for a highly defective interface. Ranks of the approximating polynomials are the 9th for $C^{eff}_{1,MR}$ and the 8th for $C^{eff}_{2,MR}$

$$C^{eff}_{1,MR}=1.83\cdot10^7 - 8.24\cdot10^6\cdot w+7.11\cdot10^7\cdot w^2 - 5.73\cdot10^8\cdot w^3+2.49\cdot10^9\cdot w^4 -6.54\cdot10^9\cdot w^5+1.05\cdot10^{10}\cdot w^6 - 1.03\cdot10^{10}\cdot w^7+5.56\cdot10^9\cdot w^8 - 1.27\cdot10^9\cdot w^9, \quad (6.2)$$

$$C^{eff}_{2,MR}=3.53\cdot10^6 - 5.25\cdot10^6\cdot w+4.62\cdot10^7\cdot w^2 - 2.82\cdot10^8\cdot w^3+1.02\cdot10^9\cdot w^4 -2.16\cdot10^9\cdot w^5+2.66\cdot10^9\cdot w^6 - 1.76\cdot10^9\cdot w^7+4.08\cdot10^8\cdot w^8,$$

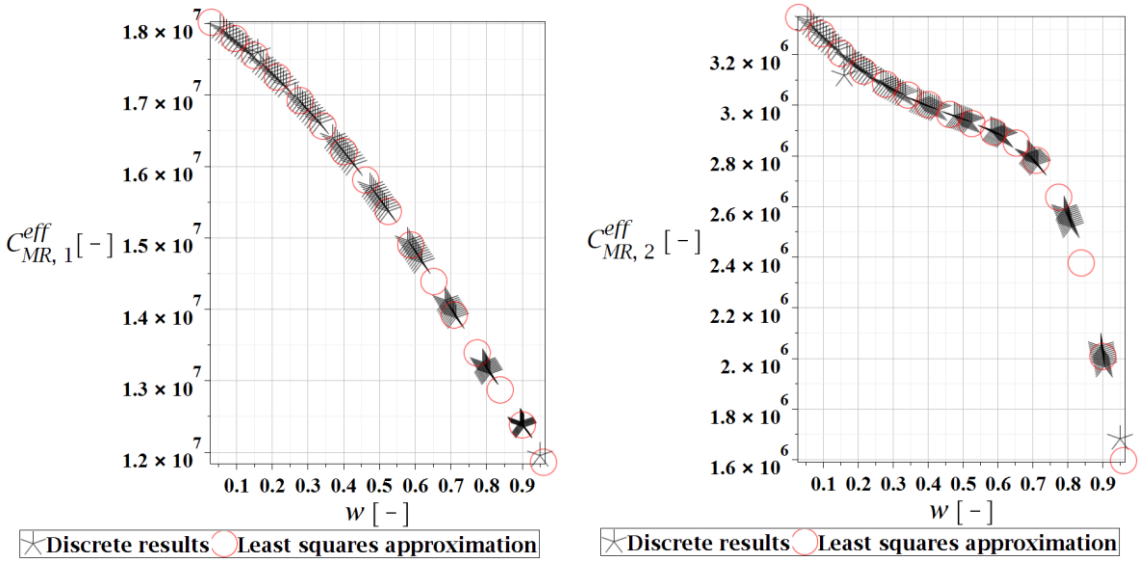

a) b)

Fig. 6.2 Approximation of effective material properties for Mooney-Rivlin model a) $C^{eff}_{1,MR}$, b) $C^{eff}_{2,MR}$ w.r.t. the weakening coefficient w.

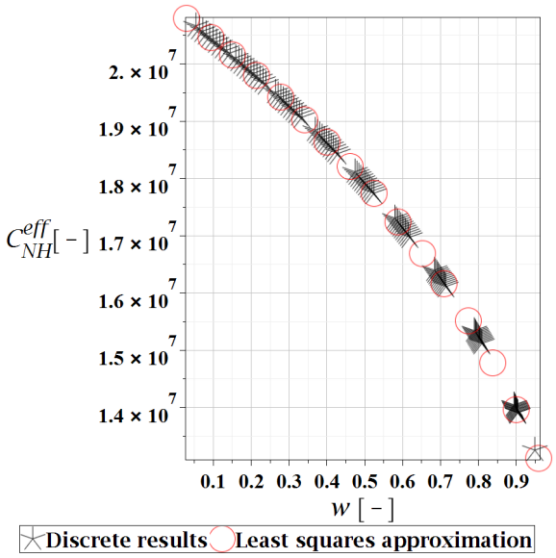

Fig. 6.3 Approximation of effective material properties for Neo-Hookean model C_{NH}^{eff}, w.r.t. the weakening coefficient w.

Again, a polynomial representation of these coefficients is coinciding very well with the discrete results.

The third graph (Fig. 6.3) presents a single parameter C_{NH}^{eff} leading its response. It is a little less affected by the volume fraction of interface defects w than the first parameters of alternative hyperelastic formulations; reduction reaches approximately 30% for the extreme values of w, but its magnitude is relatively close to the one of $C_{1,MR}^{eff}$ and $C_{1,AB}^{eff}$.

Rank of the approximating polynomial is the 10^{th} for

$$C_{NH}^{eff}=2.09\cdot10^{7}-5.74\cdot10^{6}\cdot w+1.33\cdot10^{7}\cdot w^{2}-1.43\cdot10^{8}\cdot w^{3}+8.14\cdot10^{8}\cdot w^{4}$$
$$-2.90\cdot10^{9}\cdot w^{5}+6.64\cdot10^{9}\cdot w^{6}-9.77\cdot10^{9}\cdot w^{7}+8.91\cdot10^{9}\cdot w^{8} \quad (6.3)$$
$$-4.57\cdot10^{9}\cdot w^{9}+1.01\cdot10^{9}\cdot w^{10}.$$

At this point Hypothesis 5 (a) is confirmed, because the approximating polynomials of the effective material properties do not include the strain at all. Their accuracy in approximation of the effective deformation energy is confirmed in section 6.2.2.

6.1.2. Stochastic characteristics of interface defects

Stochastic characteristics of the volume fraction of interface defects $\zeta_2(w)$ are presented next. They have been calculated with use of an algorithm presented in section 4.3

and include the two characteristics guiding the Gaussian PDF, i.e. the expected value $E_{\xi}^{opt}(w)$ and coefficient of variation $\alpha_{\xi}^{opt}(w)$. They have been determined separately for each of the augmented hyperelastic material and are all gathered in Table 6.1. A relative difference of these optimized for Arruda-Boyce constitutive model is shown in Fig. 6.4. A relatively good approximation is already available in the first iteration, where difference stays below 7%. The algorithm stops after the eight iteration and it may have been even stopped earlier if a less restrictive conditions were applied. The remaining two hyperelastic potentials require 6 (Neo-Hookean) or 7 (Mooney-Rivlin) iterations.

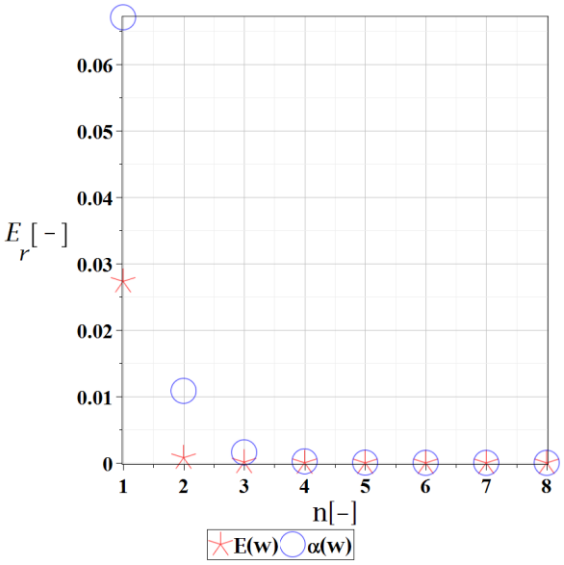

Fig. 6.4 Relative difference of optimized stochastic parameters of w for nth algorithm iteration.

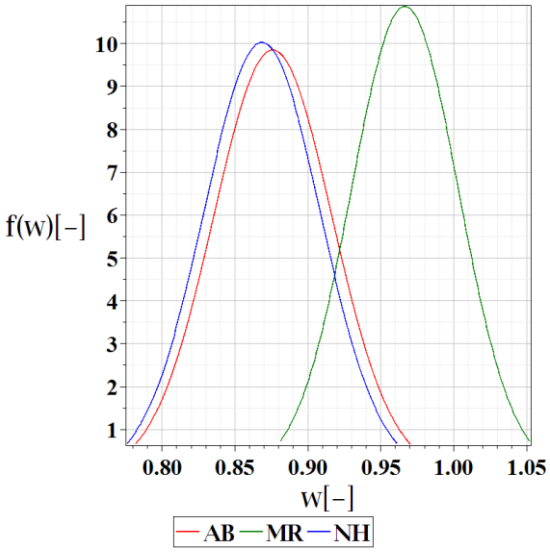

Fig. 6.5 Histogram of w for the selected hyperelastic potentials.

The levels of expectations that are required to represent the defective composite from laboratory experiments are relatively high, above $E_{\xi}^{opt}(w)>0.85$. This means that the objective composite is heavily defective (has a large number of interface defects). This is in agreement with the laboratory tests, for which the composite was softer than the virgin homogeneous material, even though at theoretical limit it allows approx. 22% stiffer response. Coefficient of variation of these volume fraction of interface defects is, on the other hand, not so high and below $\alpha_{\xi}^{opt}(w)<0.05$. This means that even a relatively low uncertainty in interface defects already causes this composite to exhibit uncertainty evidenced in the laboratory experiments (see Fig. 5.8 and Fig. 5.7). Interestingly, the level of statistical dispersion of the defects for such high expectation $E_{\xi}^{opt}(w)$ is very close to the level of dispersion in the composite. This observation proves

their high influence on the effective response. Specifically, an increase of $E(w)$ decreases the effective response of the composite. Secondly, $\alpha(w)$ increases the statistical dispersion of this response approximately to the same level for the optimized $E_{\xi}^{opt}(w)$ and $\alpha_{\xi}^{opt}(w)$. A wider discussion on this topic is provided in section 6.3.2. Characteristics recovered for the Arruda-Boyce and Neo-Hookean augmented potentials are very similar, while the ones for the Mooney-Rivlin differ from these. The Mooney-Rivlin based calculations report a higher expectation, quite close to the physical limit of 1 and lower coefficient of variation than the other two. This is majorly because the Mooney-Rivlin reports a higher expectation of the effective stress than the remaining methods, which requires a higher level of interface defects to match the laboratory results. It is accompanied by a drop of the coefficient of variation $\alpha_{MR}^{opt}(w)$ to ensure the same level of uncertainty of the effective stress, because $\alpha\left(\sigma^{eff}\right)$ always increases together with an increase of $\alpha(w)$. Uncertainty in volume fraction of interface defects is next evidenced on histogram presented in Fig. 6.5. It further exemplifies closeness of the results for the Arruda-Boyce and Neo-Hookean potentials. In these constitutive models, variation of w does not exceed the physical limit of this parameter, which is not the case of the Neo-Hookean model. A maximum of w=1 is exceeded for approx. 25% of its population. This implies that this constitutive model requires a bigger interphase then applied here (5%) to replicate the behavior of target composite and be in full accordance with theoretical limits.

Table 6.1 Optimized stochastic characteristics of the volume fraction of interface defects w.

characteristic / potential	**Arruda-Boyce**	**Neo-Hookean**	**Mooney-Rivlin**
Expectation $E_{\xi}^{opt}(w)$	$E_{AB}^{opt}(w)$=0.87619	$E_{NH}^{opt}(w)$=0.86879	$E_{MR}^{opt}(w)$=0.96681
Coefficient of variation $\alpha_{\xi}^{opt}(w)$	$\alpha_{AB}^{opt}(w)$=0.045903	$\alpha_{NH}^{opt}(w)$=0.04541	$\alpha_{MR}^{opt}(w)$=0.03801

The optimized coefficients next serve for calculation of uncertainty in the effective material coefficients of this composite due to the stochastic interface defects. It is

presented in section 6.1.4. Finally, they are used to model the response of the objective composite that is discussed in section 6.3.3.

At this point part (3) of the thesis is confirmed. Algorithm proposed in section 4 allows determination of the statistical estimators of the normally distributed volume fraction of interface defects in this composite. This estimators include expectation and coefficient of variation of the input volume fraction of interface defects.

6.1.3. Stochastic experiments

Next, the stochastic disorder of the effective composite properties is studied. It is done relative to statistical variability of the input random parameter w for fluctuating expectation of the volume fraction of interface defects in range of $E(w)\in[0.1,\ 0.5,\ 0.967]$ and for its increasing coefficient of variation $\alpha(w)\in(0,\ 0.15)$. The highest expectation differs for the three hyperelastic potentials. It is $E(w)$=0.876 for Arruda-Boyce, $E(w)$=0.869 for Neo-Hookean and $E(w)$=0.967 for Mooney-Rivlin. This choice follows the magnitude optimized for representation of the composite tested in laboratory experiments for each of these constitutive models, presented in previous section. It is preferred over constant highest expectation firstly because these effective parameters are not directly comparable in the first place and secondly to avoid repetition of these graphs for optimized set of $\{E(w),\alpha(w)\}$ that is used in section 6.3.3. Stochastic characteristics are computed for the three sets of properties driving response of the three selected hyperelastic constitutive models. They are calculated from their polynomial representations given in eqns (6.1), (6.2) and (6.3) with use of the three selected stochastic methods. They are the generalized iterative stochastic perturbation method (ISPT), Monte-Carlo simulation (MCS) with 250 000 trials and the semi-analytical approach (SAM). The MCS is calculated in 11 equidistant intervals of $\alpha(w)\in\{0,\ 0.01(6),\ \ldots,\ 0.15\}$ with one additional calculation for $\alpha_{\xi}^{opt}(w)$. Order of the ISPT applied ranges from the 8th till the 10th and it follows the rank of the polynomials so that 10th order is applied for $C_{1,NH}^{eff}$, $C_{1,AB}^{eff}$ and $C_{2,AB}^{eff}$, while the 8th order for $C_{1,MR}^{eff}$ and $C_{2,MR}^{eff}$. Please note, that for the Gaussian type of uncertainty in the input, the odd orders are explicitly zero, so that for $C_{1,MR}^{eff}$ the 8th order is applied. The below graphs always distinguish the stochastic methods by the symbol (diagonal cross for the MCS, circle for the ISPT and box for the SAM); the colors distinguish expected value of voids volume fraction $E(w)$. Characteristics considered in this study

include three sets of the expected values $E\left(C_{i,\xi}^{eff}\right)$, coefficients of variation $\alpha\left(C_{i,\xi}^{eff}\right)$, skewness $\beta\left(C_{i,\xi}^{eff}\right)$ and kurtosis $\kappa\left(C_{i,\xi}^{eff}\right)$ of the effective composite properties, where ξ denotes the three selected hyperelastic constitutive models and i differentiates the coefficients.

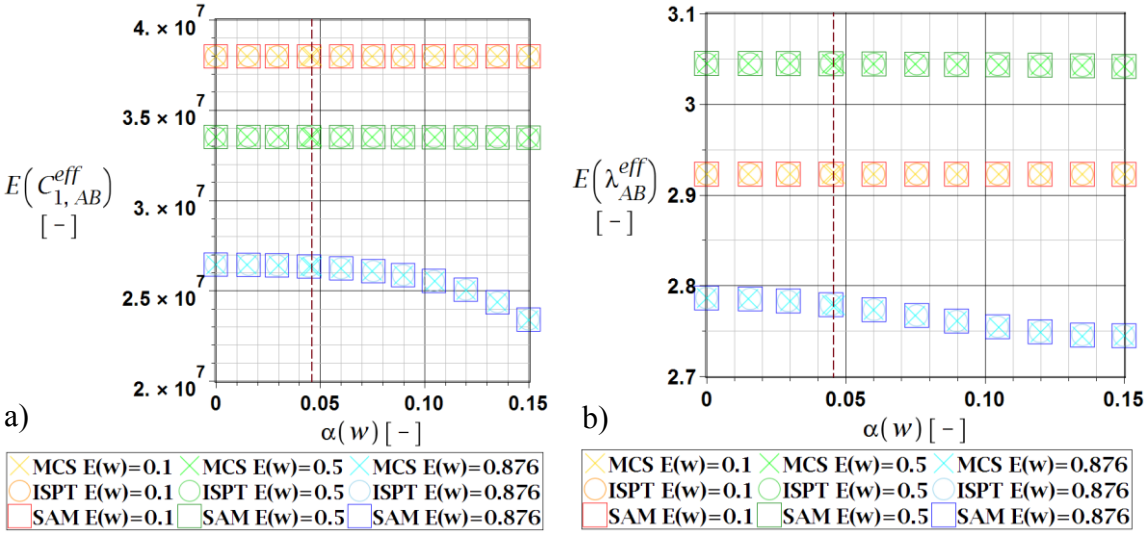

Fig. 6.6 Expected value of effective material properties for Arruda-Boyce model a) $C_{1,AB}^{eff}$, b) λ_{AB}^{eff}.

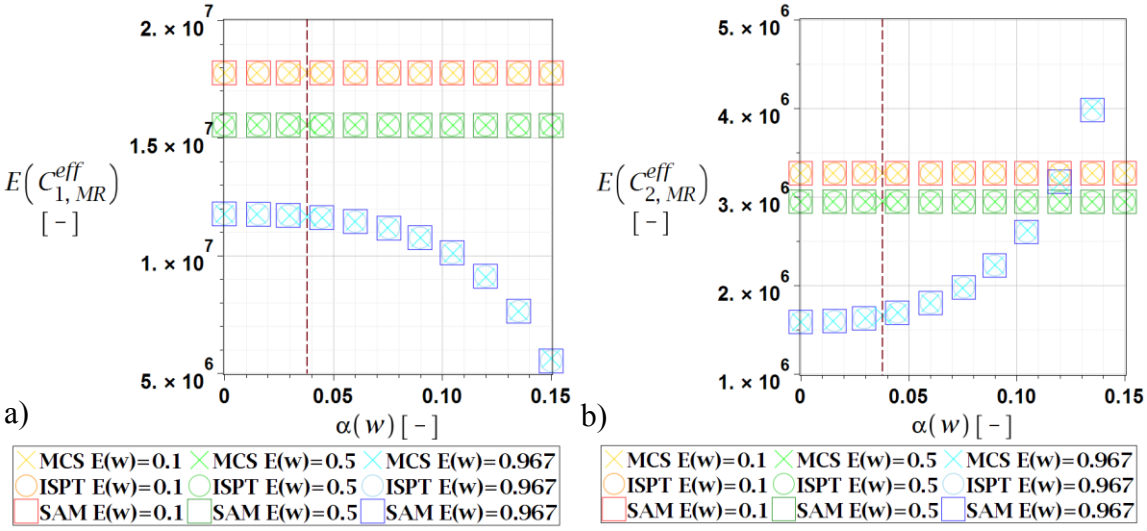

Fig. 6.7 Expected value of effective material properties for Mooney-Rivlin model a) $C_{1,MR}^{eff}$, b) $C_{2,MR}^{eff}$.

The expected values of all the properties $E\left(C_{i,\xi}^{eff}\right)$ are reported on Fig. 6.6 for the Arruda-Boyce model, Fig. 6.7 for the Mooney-Rivlin model and Fig. 6.8 a) for the Neo-Hookean model. They firstly show that the statistical disorder of the volume fraction of

interface defects is relevant only for the highest considered expectation $E(w)$=0.876. At this level its increase results in a substantial increase of $E\left(C^{eff}_{2,MR}\right)$ and $E\left(C^{eff}_{1,NH}\right)$, decrease of the $E\left(C^{eff}_{1,MR}\right)$ as well as $E\left(C^{eff}_{1,AB}\right)$ and $E\left(\lambda^{eff}_{AB}\right)$.

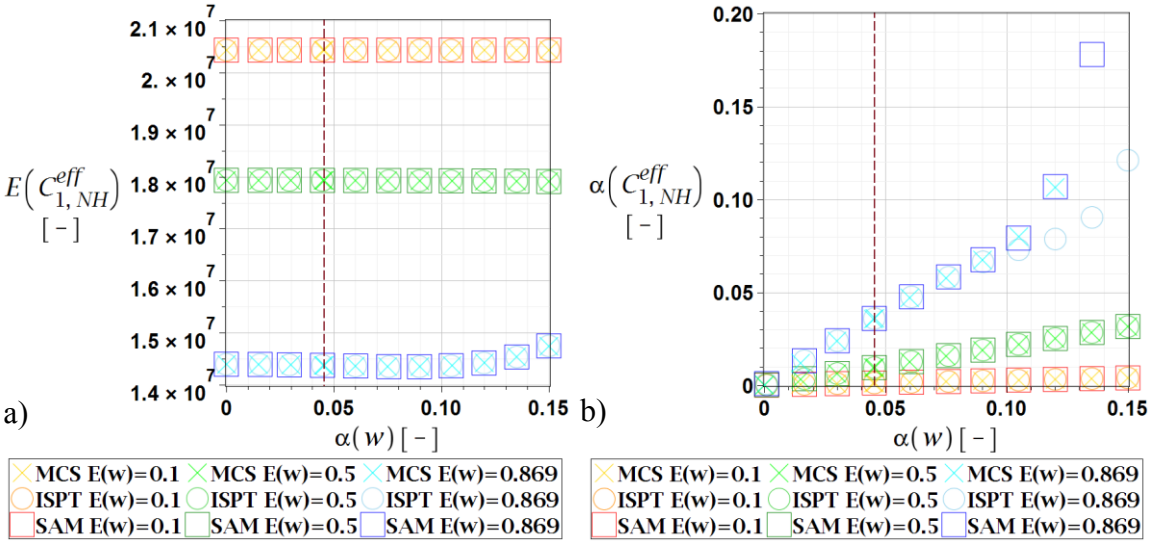

Fig. 6.8 Expected value a) and coefficient of variation b) of the effective material property for Neo-Hookean model $C^{eff}_{1,NH}$.

An increase of the expectation of volume fraction of interface defects results in a decrease of all the expectations except for the $E\left(\lambda^{eff}_{AB}\right)$, whose highest magnitude is reported for the middle $E(w)$=0.5. This observation follows the relation of these coefficients to the weakening coefficient w, which has a local maximum at w=0.66. The three stochastic methods return almost perfectly coinciding results with an exception of several simulations of the MCS for the highest $E(w)$, which return a little distant results; they always differ from the other methods less than 10%.

The coefficients of variation of the effective composite properties $\alpha\left(C^{eff}_{i,\xi}\right)$ are reported on Fig. 6.8 b), Fig. 6.9 and Fig. 6.10 w.r.t. the coefficient of variation of the volume fraction of defects $\alpha(w)$. The first of these reports results for the Neo-Hookean model, the second for the Arruda-Boyce and the third for the Mooney-Rivlin. These coefficients always increase together with an increase of $\alpha(w)$ and their magnitude depends heavily on the level of $E(w)$. For the highest $E(w)$ they are substantially higher than the coefficient of variation of the input $\alpha(w)$ and they decrease more than 10 times already for $E(w)$=0.5. They decrease further for $E(w)$=0.1, for which they became insignificant. Their magnitude greatly varies for all the effective

properties not only in-between the constitutive models, but also within the set of properties in each model. For example, magnitudes of $\alpha\left(C_{1,AB}^{eff}\right)$ is up to three times higher than the one of $\alpha\left(\lambda_{AB}^{eff}\right)$. This observation clearly indicates that they should be treated as a separate stochastic unknowns in the constitutive models even if they are considered Gaussian.

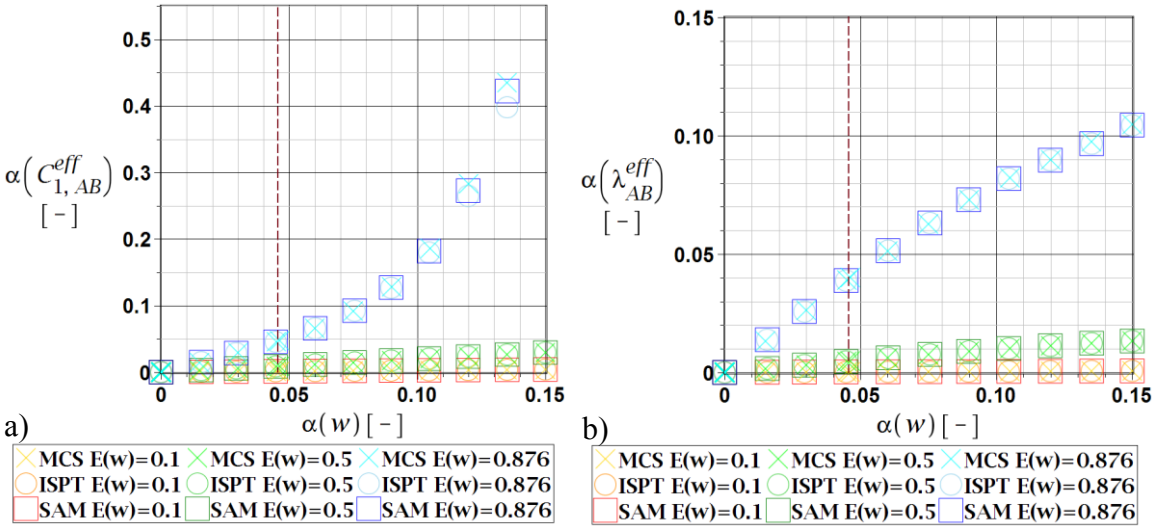

Fig. 6.9 Coefficient of variation of effective material properties for Arruda-Boyce model a) $C_{1,AB}^{eff}$, b) λ_{AB}^{eff}.

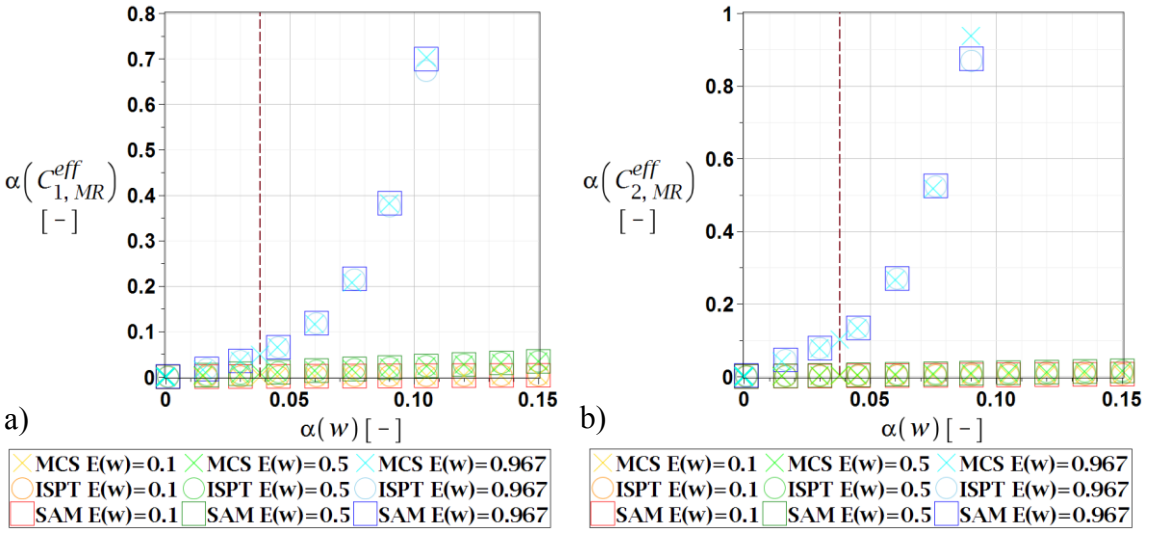

Fig. 6.10 Coefficient of variation of effective material properties for Mooney-Rivlin model a) $C_{1,MR}^{eff}$, b) $C_{2,MR}^{eff}$.

As already mentioned, coefficients of variation of the effective composite properties differ in-between the constitutive models so that the same composite approximated

by different potential will have a different level of uncertainty in its parameters. This is not obvious and totally different for the elastic isotropic case, where this composite has only two material coefficients. The stochastic methods return very similar results of $\alpha\left(C_{i,\xi}^{eff}\right)$ regardless the level of input dispersion $\alpha(w)$ and its expectation $E(w)$. This does not apply only for $\alpha\left(C_{1,NH}^{eff}\right)$ reported for the highest $E(w)$, where the three methods start to diverge at $\alpha(w)>0.11$. Despite this result, they report only minor differences.

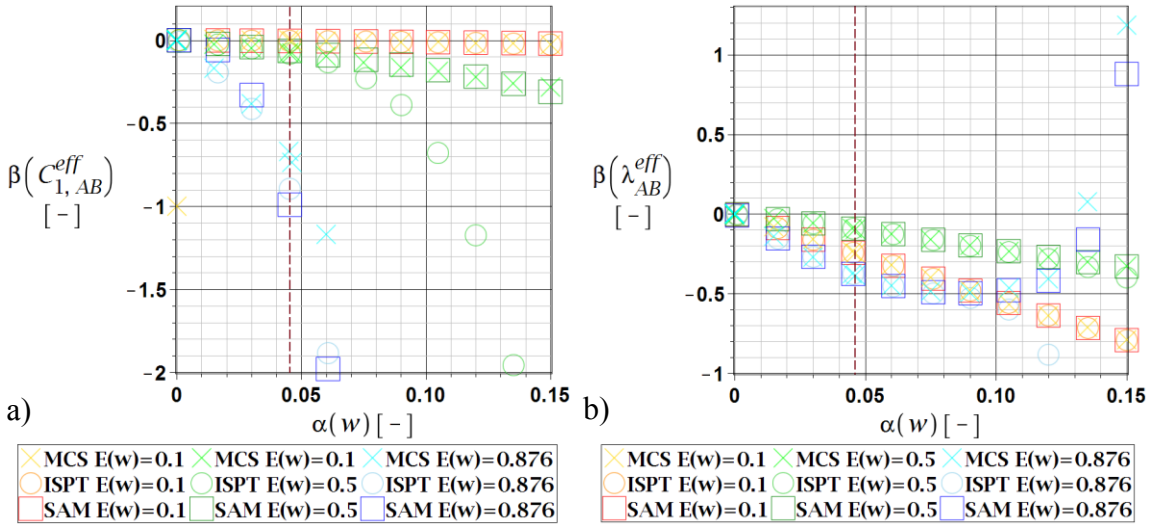

Fig. 6.11 Skewness of effective material properties for Arruda-Boyce model a) $C_{1,AB}^{eff}$, b) λ_{AB}^{eff}.

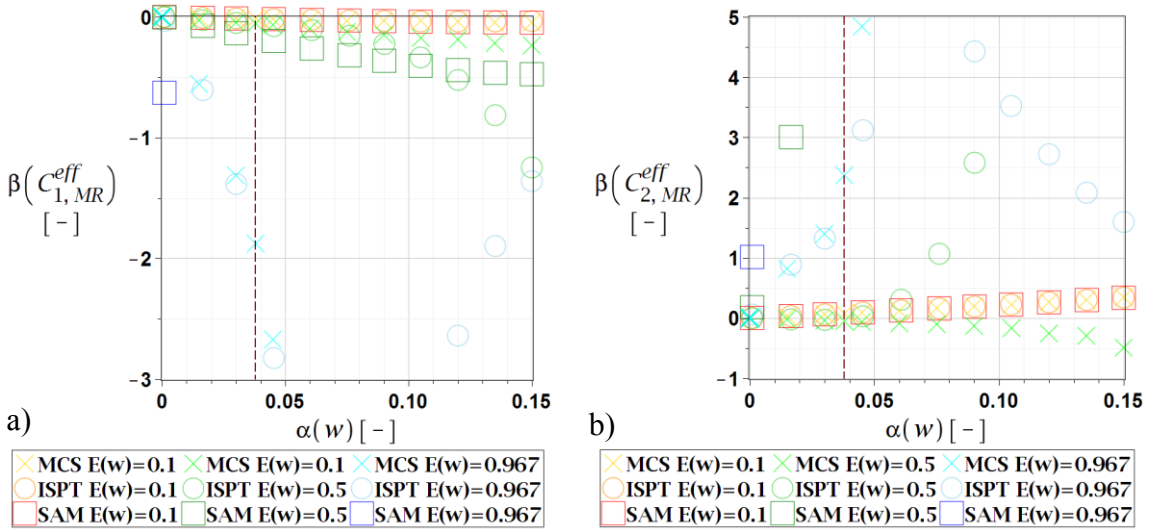

Fig. 6.12 Skewness of effective material properties for Mooney-Rivlin model a) $C_{1,MR}^{eff}$, b) $C_{2,MR}^{eff}$.

Skewness of the effective composite properties $\beta\left(C_{i,\xi}^{eff}\right)$ is reported on Fig. 6.11, Fig. 6.12 and Fig. 6.13 a) for the Arruda-Boyce, Mooneay-Rivlin and Neo-Hookean models, respectively. It is predominantly negative for all the constitutive models, input coefficients of variation and expectations. The two exceptions include the $\beta\left(C_{2,MR}^{eff}, E(w)=0.967\right)$ and $\beta\left(\lambda_{AB}^{eff}, E(w)=0.876, \alpha(w)>0.13\right)$ for which it is positive. Magnitude of this skewness almost exclusively increases together with an increase of $\alpha(w)$ and in most cases it also increases together with an increase of $E(w)$. Similarly to the $\alpha\left(C_{i,\xi}^{eff}\right)$ skewness has a unique character and magnitude for all the properties.

Results of the selected stochastic methods produce a convergent result only for a limited coefficient of variation of the input $\alpha(w)$ that decreases together with an increase of $E(w)$. In the worst case the ISPT starts to report different results for $\alpha(w)>0.05$, and the two other methods at $\alpha(w)>0.06$; they still usually remain very close for all considered levels of $\alpha(w)$ for all parameters with $E(w)=0.1$ and many with $E(w)=0.5$. In all cases the genaral course of relation of $\beta\left(C_{i,\xi}^{eff}\right)$ w.r.t. $\alpha(w)$ is the same for the three stochastic results. Because of this, this skewness can always be considered as bound in a closed interval for each level of $\alpha(w)$, for example $\beta\left(C_{1,MR}^{eff}, E(w)=0.967, \alpha(w)=0.05\right) \in (-1.45, -1.95)$. This still offers a quite precise information of this characteristic; some level of disagreement of the results does not invalidate them.

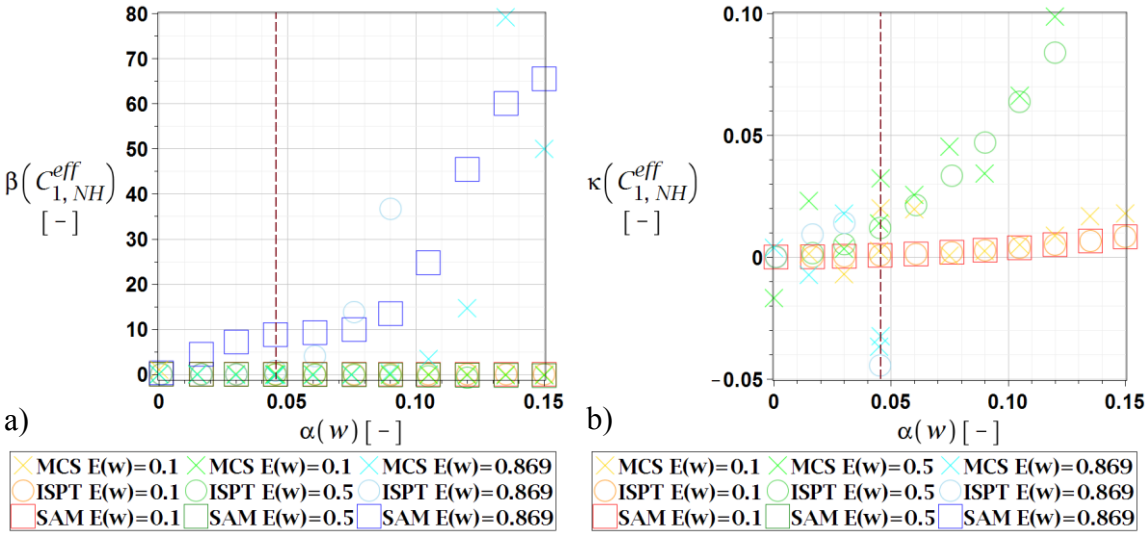

Fig. 6.13 Skewness a) and kurtosis b) of the effective material property for Neo-Hookean model $C_{1,NH}^{eff}$.

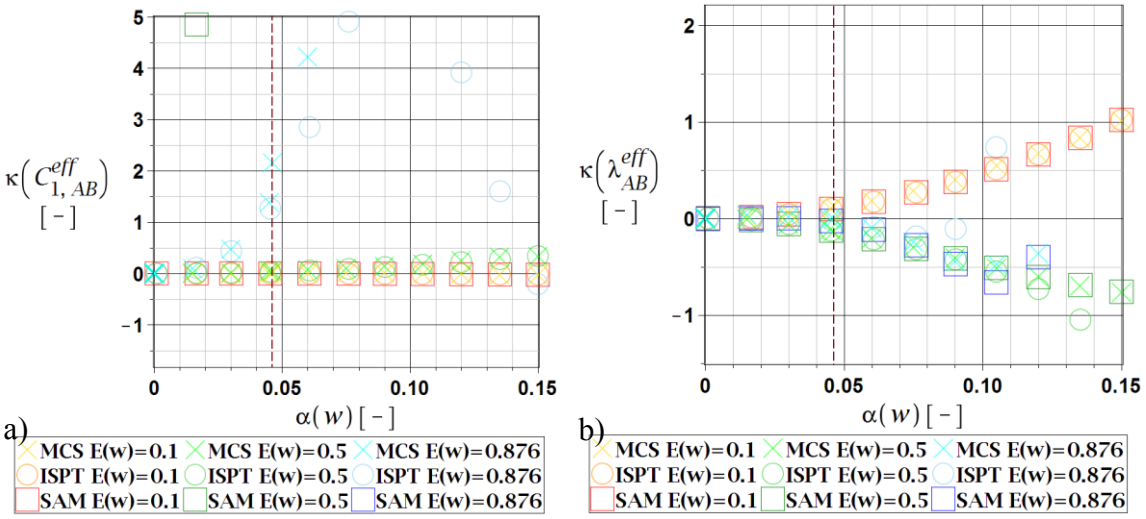

Fig. 6.14 Kurtosis of effective material properties for Arruda-Boyce model a) $C^{eff}_{1,AB}$, b) λ^{eff}_{AB}.

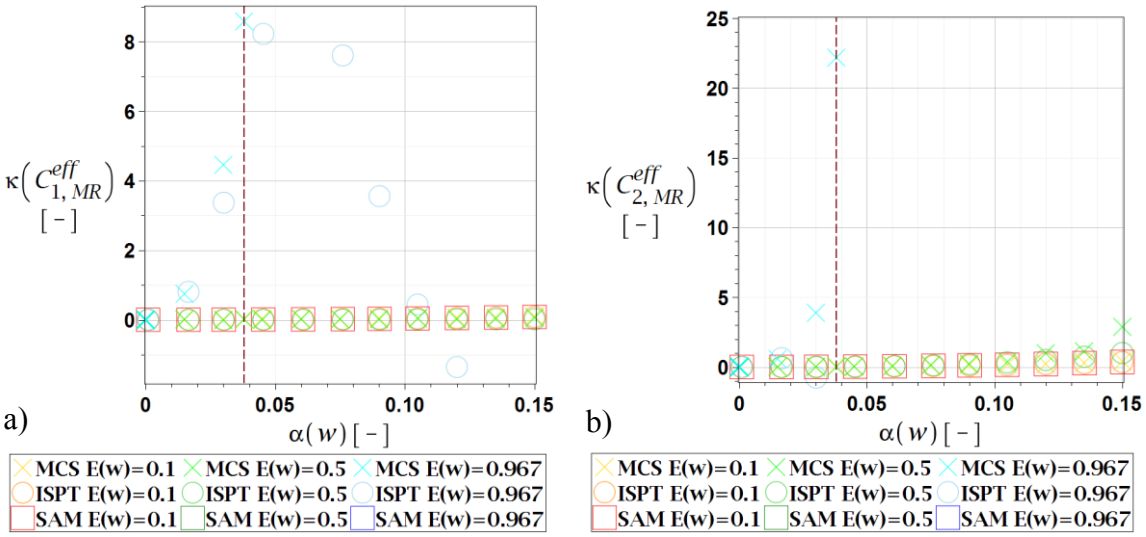

Fig. 6.15 Kurtosis of effective material properties for Mooney-Rivlin model a) $C^{eff}_{1,MR}$, b) $C^{eff}_{2,MR}$.

Kurtosis of the effective composite properties $\kappa(C^{eff}_{i,\xi})$ is reported on Fig. 6.14 b), Fig. 6.15 and Fig. 6.16 for the Neo-Hookean, Arruda-Boyce and Mooney-Rivlin models. It keeps close to 0 for the lower expectations $E(w)$ despite the $\kappa(C^{eff}_{2,MR})$ and $\kappa(\lambda^{eff}_{AB})$. Its magnitude generally increases together with an increase of $\alpha(w)$ and has different value for all the parameters. Agreement of the three stochastic methods is the worst of all the considered characteristics. They lose convergence especially for the highest $E(w)$ and $\alpha(w)$>0.05. The MCS returns highly oscillatory results that tend to be

dispersed around the results of the other two methods. The ISPT keeps close to the MCS or the SAM for majority of the results, but it starts to diverge at $\alpha(w)>0.04$ for several kurtoses that are computed for the highest $E(w)$. The best coincidence of the results is reported for $\kappa\left(\lambda_{AB}^{eff}\right)$, which is very high for all the methods, domain of $\alpha(w)$ and considered $E(w)$ and the worst for $\kappa\left(C_{1,NH}^{eff}\right)$, which also has the lowest magnitude below 0.1.

At this point Hypothesis 1 (a) is proved. The random input variable has an influence on the effective material parameters and their stochastic characteristics.

6.1.4. Stochastic characteristics for the optimized statistical estimators of *w*

Stochastic characteristics of the effective material properties $\zeta_4\left(C_{i,\xi}^{eff}\left(\zeta_2(w)\right)\right)$ are next presented for the optimized uncertainty of the input $\left(E_{\xi}^{opt}(w),\alpha_{\xi}^{opt}(w)\right)$ that was calculated in section 6.1.2.; they are intended for usage directly in definition of the composite constitutive relation and follow uncertainty of the objective composite from laboratory experiments. Their recovery comes from their continuous representations (ISPT, SAM) or dedicated simulation (MCS); it follows the algorithm proposed in Fig. D.1 Please note, that the optimized characteristics of *w* slightly differ for the alternative augmented hyperelastic potentials and thus they are not interchangeable; these characteristics consider the influence of the interface defects by only; for convenience, all the graphs presented in section 6.1.3 already account for them. They may be read-out on a cross-section of brown dotted line and the curve presenting stochastic characteristic of the selected parameter (given in blue).

These characteristics are next aggregated in Table 6.2 as single values or closed intervals, depending coincidence of stochastic methods. Expectations of these effective parameters stay in the same order of 10^7, despite the $E\left(\lambda_{AB}^{eff}\right)_{\mathrm{CB5}}$, which is very small. Coefficients of variation stay around $0.04-0.05$ despite the $\alpha\left(C_{2,MR}^{eff}\right)_{\mathrm{CB5}}$. Their magnitude is quite close to the one of the input random parameter. Coincidence of the stochastic methods for these characteristics is almost perfect. It is much lower for the skewness and kurtosis, but usually the difference is not too high. These higher order characteristics are nonzero for all the effective parameters. Their magnitude and sign differs, but all of them are rather distant from the Gaussian type of randomness.

Their accurate representation would require a more complicated probability density that also accounts for the higher stochastic characteristics. Please note, that these characteristics substantially differ for each of the effective property so that they must be represented by different PDFs. This is also true for accuracy of their estimation.

Table 6.2 Stochastic characteristics of the effective material coefficients.

characteristic / potential	**Arruda-Boyce**	**Neo-Hookean**	**Mooney-Rivlin**
Expectation $E\left(C_{i,\xi}^{eff}\right)$	$E\left(C_{1,AB}^{eff}\right)_{\mathrm{CB5}}=$ $=2.632\cdot10^{7}$, $E\left(\lambda_{AB}^{eff}\right)_{\mathrm{CB5}}=2.779$	$E\left(C_{1,NH}^{eff}\right)_{\mathrm{CB5}}=1.437\cdot10^{7}$	$E\left(C_{1,MR}^{eff}\right)_{\mathrm{CB5}}=$ $=1.174\cdot10^{7}$, $E\left(C_{2,MR}^{eff}\right)_{\mathrm{CB5}}=1.815\cdot10^{7}$
Coefficient of variation $\alpha\left(C_{i,\xi}^{eff}\right)$	$\alpha\left(C_{1,AB}^{eff}\right)_{\mathrm{CB5}}=0.0476$, $\alpha\left(\lambda_{AB}^{eff}\right)_{\mathrm{CB5}}=0.0403$	$\alpha\left(C_{1,NH}^{eff}\right)_{\mathrm{CB5}}=0.0359$	$\alpha\left(C_{1,MR}^{eff}\right)_{\mathrm{CB5}}=$ $=\langle 0.0579,0.0598\rangle$, $\alpha\left(C_{2,MR}^{eff}\right)_{\mathrm{CB5}}=$ $=\langle 0.113,0.117\rangle$
Skewness $\beta\left(C_{i,\xi}^{eff}\right)$	$\beta\left(C_{1,AB}^{eff}\right)_{\mathrm{CB5}}\in$ $\in\langle -0.0714,$ $-0.0988\rangle$, $\beta\left(\lambda_{AB}^{eff}\right)_{\mathrm{CB5}}=-0.371$	$\beta\left(C_{1,NH}^{eff}\right)_{\mathrm{CB5}}\in$ $\in\langle 1.14, 9.287\rangle$	$\beta\left(C_{1,MR}^{eff}\right)_{\mathrm{CB5}}\in$ $\in\langle -1.80, -1.86\rangle$, $\beta\left(C_{2,MR}^{eff}\right)_{\mathrm{CB5}}$ $\in\langle 2.32,2.44\rangle$
Kurtosis $\kappa\left(C_{i,\xi}^{eff}\right)$	$\kappa\left(C_{1,AB}^{eff}\right)_{\mathrm{CB5}}\in$ $\in\langle 1.554, 2.243\rangle$, $\kappa\left(\lambda_{AB}^{eff}\right)_{\mathrm{CB5}}\in$ $\in\langle -0.0190, 0.00668\rangle$	$\kappa\left(C_{1,NH}^{eff}\right)_{\mathrm{CB5}}\in$ $\in\langle -0.0385,$ $-0.0442\rangle$	$\kappa\left(C_{1,MR}^{eff}\right)_{\mathrm{CB5}}\in$ $\in\langle 6.64, 8.27\rangle$, $\kappa\left(C_{2,MR}^{eff}\right)_{\mathrm{CB5}}$ $\in\langle 0.065, 1.24\rangle$

At this point part (4) of the thesis is confirmed. It is possible to determine the effective material properties of the composite with stochastic interface defects together with their stochastic characteristics for the selected hyperelastic constitutive models, as exemplified in section 6.1.1, 6.1.3 and 6.1.4. They may be used for a wide range of defects volume fraction in the range of $[0.09-0.95]$. This is true at least for the

selected underlying hyperelastic formulations and the objective composite. Moreover, magnitude of these characteristics reported by different stochastic methods is very close to each other.

6.2. Effective deformation energy in composite with interface defects

In this section, deformation energy of the objective composite is taken into consideration. It consists of three parts. In the first one deterministic results are presented. In the second, approximation error coming from the techniques applied is rigorously studied. In the third, stochastic analysis is performed with an input variable of defects volume fraction. Results of this section have been partially included in publications [265] and [264].

Deformation energy is calculated in a discrete manner according to procedure described in section 4.3. It is retrieved from a set of unitary uniaxial elongations of the composite RVE solved in the FEM system ABAQUS. Details of this analysis are included in sections 4.1 and 4.2.

6.2.1. Deterministic analysis

Deterministic analysis of deformation energy U^{eff} is performed with respect to the given strain level ε_{11} for an increasing volume fraction of interface defects w. It represents only the uniaxial stretch, which follows the underlying constitutive models selected for description of the effective material response; they are all isotropic. Results of the discrete FEM simulations are approximated here with use of two alternative methods. The first one uses a bivariate polynomial and the second one is adjacent to the three selected potentials, where material coefficients are dependent on w. Effective material coefficients have already been determined in section 6.1; this method is denoted as the augmented material model. Bivariate polynomial has a following form:

$$U_{\xi}^{eff,BPO} = \mathrm{P}_{\xi}(\varepsilon_{11},w)=\sum_{i=0}^{n}\sum_{j=0}^{n} a_{\xi n,ij}\, w^{i}\cdot\varepsilon_{11}{}^{j}, \tag{6.4}$$

where n denotes a rank of approximating polynomial, ξ stands for the three potentials selected for the deterministic part (see Appendix A) and $a_{\xi,ij}$ represent polynomial coefficients. Both rank and coefficients of this polynomial are optimized with use of a procedure explained in Appendix C. This rank is 10 for Arruda-Boice and Neo-Hokean

models and 9 for Mooney-Rivlin. Full expansion of the optimized polynomial for the Arruda-Boyce model is given below

$$\begin{aligned}
U_{AB}^{eff,BPO} = & -9.97\cdot10^{6}\cdot w + 3.58\cdot10^{6}\cdot w^{4} - 9.22\cdot10^{5}\cdot w^{3} - 9.56\cdot10^{5}\cdot w^{10} + 2.45\cdot10^{6}\cdot w^{9} \\
& + 1.35\cdot10^{5}\cdot w^{2} - 6.87\cdot10^{6}\cdot w^{7} - 4.21\cdot10^{2}\cdot\varepsilon_{11} + 6.28\cdot10^{7}\cdot\varepsilon_{11}^{2} - 4.22\cdot10^{7}\cdot\varepsilon_{11}^{3} \\
& + 4.13\cdot10^{7}\cdot\varepsilon_{11}^{4} - 3.24\cdot10^{7}\cdot\varepsilon_{11}^{5} + 1.42\cdot10^{7}\cdot\varepsilon_{11}^{6} + 1.08\cdot10^{6}\cdot w^{6} - 8.19\cdot10^{6}\cdot w^{5} \\
& - 6.69\cdot10^{6}\cdot\varepsilon_{11}\cdot w^{7} - 8.00\cdot10^{6}\cdot\varepsilon_{11}^{2}\cdot w^{7} + 3.19\cdot10^{6}\cdot\varepsilon_{11}^{3}\cdot w^{7} - 1.65\cdot10^{6}\cdot\varepsilon_{11}^{5}\cdot w^{7} \\
& + 7.14\cdot10^{6}\cdot\varepsilon_{11}\cdot w^{9} + 1.63\cdot10^{7}\cdot\varepsilon_{11}^{2}\cdot w^{9} - 3.69\cdot10^{6}\cdot\varepsilon_{11}\cdot w^{10} - 1.27\cdot10^{7}\cdot\varepsilon_{11}^{2}\cdot w^{10} \\
& + 1.64\cdot10^{6}\cdot\varepsilon_{11}^{3}\cdot w^{10} + 1.74\cdot10^{5}\cdot\varepsilon_{11}^{4}\cdot w^{10} + 4.39\cdot10^{5}\cdot\varepsilon_{11}\cdot w - 1.48\cdot10^{7}\cdot\varepsilon_{11}^{2}\cdot w \\
& + 9.92\cdot10^{6}\cdot\varepsilon_{11}^{3}\cdot w - 6.95\cdot10^{6}\cdot\varepsilon_{11}^{4}\cdot w - 5.30\cdot10^{5}\cdot\varepsilon_{11}\cdot w^{2} - 4.63\cdot10^{6}\cdot\varepsilon_{11}^{2}\cdot w^{2} \\
& + 4.34\cdot10^{6}\cdot\varepsilon_{11}^{3}\cdot w^{2} - 1.23\cdot10^{7}\cdot\varepsilon_{11}^{4}\cdot w^{2} + 1.48\cdot10^{7}\cdot\varepsilon_{11}^{5}\cdot w^{2} + 2.76\cdot10^{6}\cdot\varepsilon_{11}\cdot w^{3} \\
& - 3.72\cdot10^{6}\cdot\varepsilon_{11}^{2}\cdot w^{3} - 7.09\cdot10^{6}\cdot\varepsilon_{11}\cdot w^{4} + 9.73\cdot10^{5}\cdot\varepsilon_{11}^{2}\cdot w^{4} + 2.29\cdot10^{6}\cdot\varepsilon_{11}^{3}\cdot w^{4} \\
& + 8.06\cdot10^{6}\cdot\varepsilon_{11}\cdot w^{5} - 3.13\cdot10^{6}\cdot\varepsilon_{11}^{4}\cdot w^{6} + 2.74\cdot10^{2}
\end{aligned} \tag{6.5}$$

Other full expansions are not provided, because the stochastic results are based solely on the Arruda-Boyce augmented model. Please note, that this response surface is not a full 10^{th} order bivariate polynomial, which follows the implementation of selected optimization solver. Optimal solution is searched among all possible values of polynomial coefficients and some of them are null.

Formulas applied for the augmented material model are following

$$U_{MR}^{eff,AMM} = C_{1,MR}^{eff}(w)\cdot(\mathrm{I}_1 - 3) + C_{1,MR}^{eff}(w)\cdot(\mathrm{I}_2 - 3) \tag{6.6}$$

for Mooney-Rivlin materials,

$$U_{NH}^{eff,AMM} = C_{1,NH}^{eff}(w)\cdot(\mathrm{I}_1 - 3) \tag{6.7}$$

for the Neo-Hookean potential and

$$U_{AB}^{eff,AMM}=C_{1,AB}^{eff}(w)\cdot\left(\begin{array}{c}\left(\frac{1}{2}\mathrm{I}_1-3\right)+\frac{1}{20\left(\lambda_{AB}^{eff}(w)\right)^2}+\frac{1}{1050\left(\lambda_{AB}^{eff}(w)\right)^4}\left(\mathrm{I}_1^3-27\right)\\ +\frac{19}{7000\left(\lambda_{AB}^{eff}(w)\right)^6(w)}\left(\mathrm{I}_1^4-81\right)\\ +\frac{519}{673750\left(\lambda_{AB}^{eff}(w)\right)^8}\left(\mathrm{I}_1^5-243\right)\end{array}\right) \tag{6.8}$$

for the case of Arruda-Boyce model. Augmentation of all three constitutive models works in the same way. All material parameters are considered relative to the interface defects volume fraction. This relation is recovered by optimization process described in Appendix B. They are next included in formulae of the effective deformation energy and the effective stress. In such an approach a priori selection of the underlying hyperelastic constitutive model is totally transparent to the algorithm. The only difference is the number of effective material parameters whose dependence must be determined.

These three sets of results for U^{eff} are presented on Fig. 6.16. The strain energy starts at zero for a zero strain ε_{11} and it increases exponentially together with an increase of ε_{11}. It also strictly depends upon the defects volume fraction w and is monotonic; a decrease of the parameter w always results in a decrease of strain energy U^{eff}. The strain energy equals to $U^{eff}=3.930\cdot10^6$ Pa for the smallest considered $w=0.1$ and at the maximum strain of $\varepsilon_{11}=0.275$; it decreases until approximately $U^{eff}=2.730\cdot10^6$ Pa for the largest considered value $w=0.9$. The three selected potentials return a very similar deformation energy amount recovered from the FEM experiments with a difference less than 4%. This validates the computations, because each potential separately fits the laboratory tests and has been computed independently from the others.

Both, the functional and polynomial approximations of the effective deformation energy prove to be suitable and enough accurate. Their difference from the discrete FEM results is not noticeable on Fig. 6.16 and is further verified with error analysis in the next section.

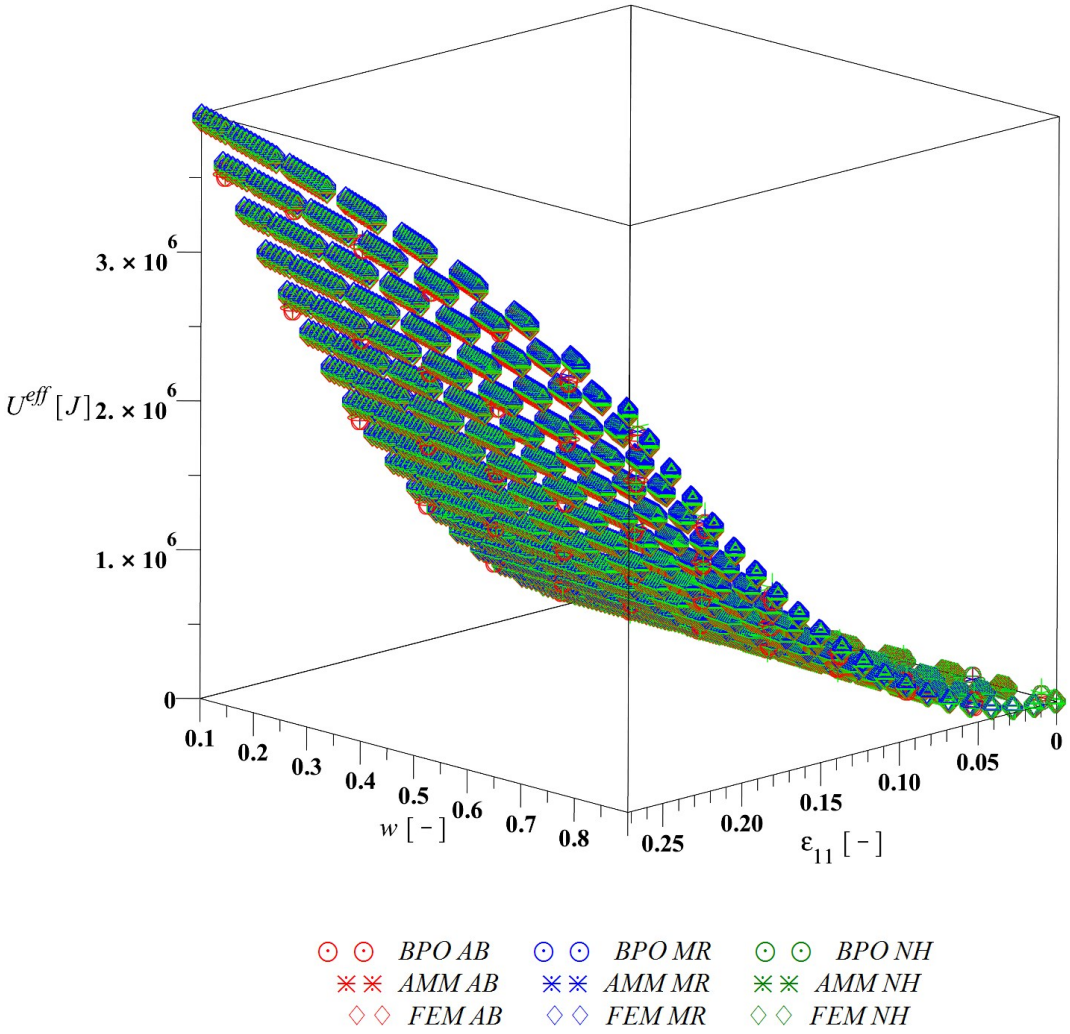

Fig. 6.16 Effective deformation energy U^{eff} w.r.t. the volume fraction of defects w for an increasing uniaxial strain ε_{11}.

6.2.2. Error of approximations

In this section, a detailed and quantitative result of approximations via the AMM and BPO is presented. It reports their relative error denoted as E_r for an increasing uniaxial strain ε_{11} and an increasing volume fraction of interface defects w. It has been calculated according to the following formula

$$E_{r,i}\left(U_{\xi}^{eff,x}\right)=\sum_{i=1}^{m}\left(\frac{U_{s,i}^{\xi,exact}(\varepsilon_{11,i},w_i)-U_{\xi}^{eff,x}(\varepsilon_{11}=\varepsilon_{11,i},w=w_i)}{U_{s,i}^{\xi,exact}(\varepsilon_{11,i},w_i)}\right), \tag{6.9}$$

where the approximations are denoted by index x and m stands for the number of FEM simulations throughout the entire domain of (w, ε_{11}).

This error for the bivariate polynomial is calculated as

$$E_{r,BPO,\xi}=\frac{\left|\sum_{i=1}^{m}\left(U_{s,i}^{\xi,exact}(\varepsilon_{11,i},w_i)-P_{\xi n}(\varepsilon_{11}=\varepsilon_{11,i},w=w_i)\right)\right|}{\sum_{j=1}^{\xi}U_{s,i}^{\xi,exact}(\varepsilon_{11,i},w_i)}. \tag{6.10}$$

and the one of the augmented material model as

$$E_{r,AMM,\xi}=\frac{\left|\sum_{i=1}^{m}\left(U_{s,i}^{\xi,exact}(\varepsilon_{11,i},w_i)-U_{s,i}^{\xi,AMM}(\varepsilon_{11,i},w_i)\right)\right|}{\sum_{j=1}^{\xi}U_{s,i}^{\xi,exact}(\varepsilon_{11,i},w_i)}. \tag{6.11}$$

This errors are set together with a mean relative error of the effective deformation energies resulting from three selected matrix and interphase formulations that it is calculated in a following way

$$E_{r,FEM,i}\left(U^{eff,FEM}\right)=\sum_{i=1}^{\xi}\left(\frac{U_{s,i}^{\xi,exact}(\varepsilon_{11,i},w_i)}{\sum_{j=1}^{\xi}U_{s,i}^{\xi,exact}(\varepsilon_{11,i},w_i)}\right), \tag{6.12}$$

and denoted as ‘FEM’ on Fig. 6.17 till Fig. 6.20. They all present results for all three potentials marked by different symbols.

The first two of them, i.e. Fig. 6.17 and Fig. 6.18 are plotted w.r.t. the uniaxial strain ε_{11} and differentiate with colors the results for different volume fractions of interface defects w. They firstly show, that the relative error of approximations E_r is always below 4% and it decreases almost linearly together with ε_{11}. This means that the more relevant the composite influence on the overall deformation of the body in macro (engineering) scale, the more accurate it is. At ε_{11}=0.275 the relative error is below a 1.5%. where ξ denotes the different potentials. The error of approximations is close to the relative error between potentials but never exceeds it. Approximations of the other potentials almost perfectly coincide with the discrete FEM results and their error is always below 1%. All the errors E_r increase a little together with an increase of w with a considerable fluctuation, but this increase is always below 0.5% for all levels of ε_{11} and thus a variation of w practically does not impose an additional difference between the potentials and an error of approximations.

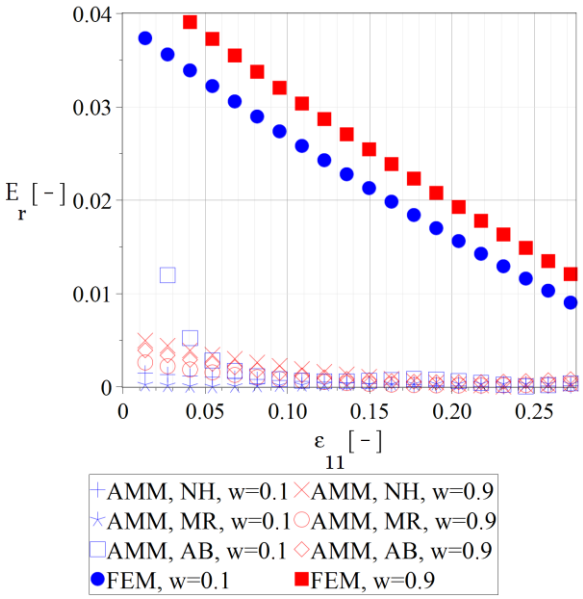

Fig. 6.17 Relative error of functional deformation energy approximations E_r w.r.t. uniaxial strain ε_{11}.

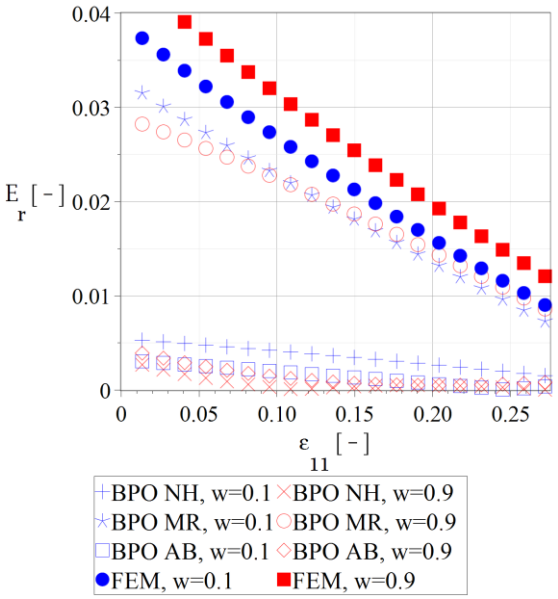

Fig. 6.18 Relative error of bivariate polynomial deformation energy approximations E_r w.r.t. uniaxial strain ε_{11}.

The two remaining graphs, i.e. Fig. 6.19 and Fig. 6.20 show the error E_r w.r.t. volume fractions of interface defects *w* and differentiate with colors the results for different uniaxial strains ε_{11}. They further depict that virtually all inaccuracies introduced by approximations are much lower than the relative error between the FEM formulations. This is especially visible for the augmented material model, shown on Fig. 6.19, for which this difference is typically an order of magnitude lower; it is typically below 0.005. For the bivariate polynomial approximation this error is still lower than the relative error of potentials, but for high strains, it is of the same order as FEM. Interestingly, while the relative error of potentials always increases together with an increase of *w*, the error introduced by approximations highly oscillate for different magnitudes of *w*.

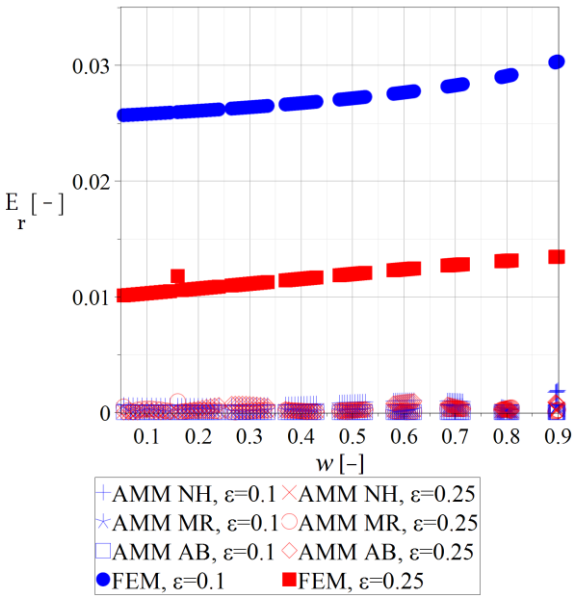

Fig. 6.19 Relative error of deformation energy coming from the augmented material model E_r w.r.t. the volume fraction of defects *w*.

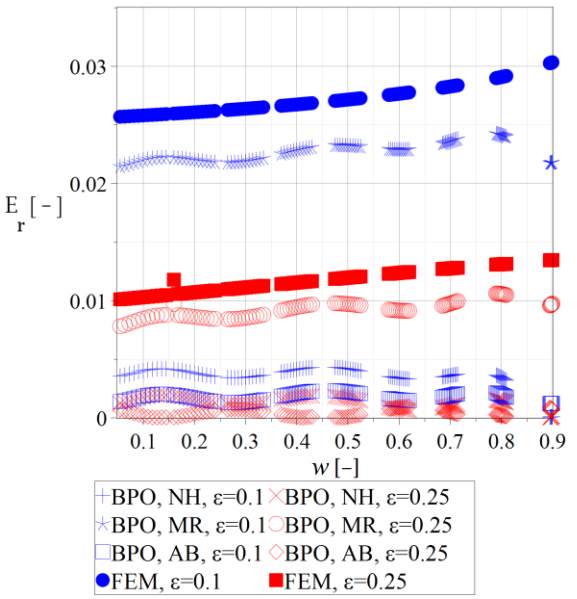

Fig. 6.20 Relative error of E_r coming from bivariate polynomial deformation energy approximations w.r.t. the volume fraction of defects *w*.

Since the relative error is always higher than the error of the augmented material model and polynomial approximation and thus the highest importance in determination of the composite strain energy lays in fitting of the matrix response to hyperelastic laws and their proper choice for the considered composite and deformation type. As already mentioned, it is not expected for the different potentials to return exactly the same strain energies even for w=0 simply because their formulation is different, but the closer results they return, the bigger the confidence that the computations are accurate. This is especially because they are fitted and run separately. The highest error of approximation has Mooney-Rivlin potential for both, the augmented material model and the polynomial approximation.

As it has been documented above, both approximations introduce a much smaller error of deformation energy than the mean difference between the potentials. Because of this only one approximation is used for stochastic experiments performed in in section 6.2.3. For these, the bivariate polynomial representation is selected principally because the polynomials are much more widely utilized and better verified for the three selected stochastic methods (see section 2.2). This is also the reason for dropping abbreviations ‘FEM’, ‘AMM’, ‘BPO’ in Figures connected to stochastic experiments.

At this point Hypothesis 6 (a) is confirmed together with Hypothesis 7 (a), because both the 'AMM' and 'BPO' have a very low approximation error that is lower than the relative difference between the hyperelastic formulations.

6.2.3. Stochastic experiments

The final part of effective deformation energy U^{eff} study is computation of its stochastic characteristics. It is done relative to statistical variability of the input random parameter w for fluctuating expectation of the volume fraction of interface defects in range of $E(w)\in[0.1,\ 0.3,\ 0.876]$, for its increasing coefficient of variation $\alpha(w)\in(0,\ 0.25)$ and for different levels of the uniaxial strain within $\varepsilon_{11}\in(0,\ 0.275)$. The highest expectation $E(w)$ follows the magnitude optimized for the objective composite to minimize the repetitions and specify its full characteristics of deformation. This calculation follows the classical integral definition of the kth central probabilistic moment, as follows

$$m_k\left(U^{eff}\left(w;\varepsilon_{11}\right)\right)=\int_{-\infty}^{+\infty}\left(U^{eff}\left(w;\varepsilon_{11}\right)-E\left(U^{eff}\left(w;\varepsilon_{11}\right)\right)\right)^k p(w)\,dx \tag{6.13}$$

Effective strain energy is further expanded with use of random Taylor series so that

$$U^{eff}\left(w;\varepsilon_{11}\right)=U^{0,eff}\left(w;\varepsilon_{11}\right)+\sum_{i=1}^{n}\frac{1}{i!}\frac{\partial^i U^{eff}\left(w;\varepsilon_{11}\right)}{\partial w^i}\left(w-w^0\right)^i \tag{6.14}$$

where $U^{0,eff}\left(w;\varepsilon_{11}\right)$ represents mean value of effective energy under consideration that is calculated for the mean value of the parameter w; odd order terms in this expansion simply vanish. Basis of the stochastic calculus is a bivariate polynomial shown in eqn (6.5). This function is up to 10 times differentiable with respect to w, where the 10th derivative is simply a polynomial with respect to ε_{11} and constant for w. The ISPT of up to the 10th order could be applied for it. Expected values, coefficient of variations, skewness and kurtosis of U^{eff} are computed independently by two stochastic methods, i.e. the 10th order iterative stochastic perturbation technique (ISPT) and Monte-Carlo simulation (MCS) computed for 350 000 trials for any discrete point given in the below figures. The order of the ISPT was dictated by the rank of optimized bivariate polynomial, which is 10 (see eqn (6.5)). A selection of the number of trials in the MCS was dictated by a high convergence of results with this coming from the highest number

of trials allowed by available hardware, i.e. 450 000 trials. The semi-analytical method was not applied here because of a poor convergence of its results with the other methods reported for the effective stress. For these analyses Arruda-Boyce potential is selected. The two other potentials are not taken into consideration because coincidence of their deterministic results reported in previous section is very high. Dependence of results of stochastic experiments on the choice of potential is verified in further section (6.3.2) dedicated for effective stress; their results differ already in the deterministic case. As stated before, in this part of research abbreviations 'FEM', 'AMM', 'BPO' are dropped on the graphs. This is because only one of approximation approaches is selected for further stochastic experiments (it is the BPO). Its rank is applied after optimization done for the deterministic analysis.

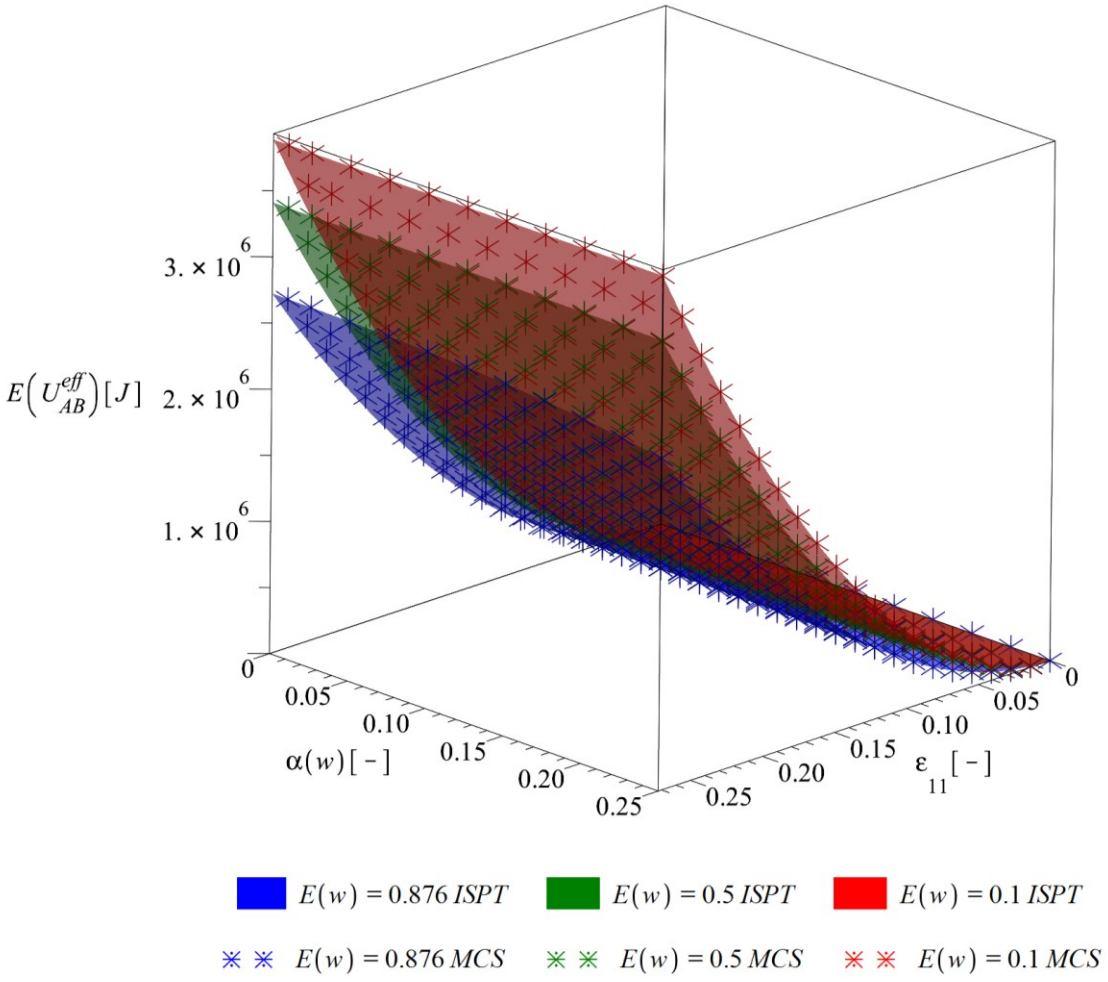

Fig. 6.21. Expected value of the effective deformation energy $E\left(U^{eff}\right)$.

Expected values of the effective deformation energy $E\left(U^{eff}\right)$ are shown in Fig. 6.21. They always increase together with an increase of ε_{11} and together with a decrease of

expected value of defects volume fraction $E(w)$. Their dependency on the input random dispersion $\alpha(w)$ is very small, which is typical for the Gaussian input parameters especially in the elastic case [82]. Extent of decrease of expectations for extreme $E(w)$ is comparable to the one in the deterministic case presented on Fig. 6.16. The alternative stochastic methods coincide perfectly.

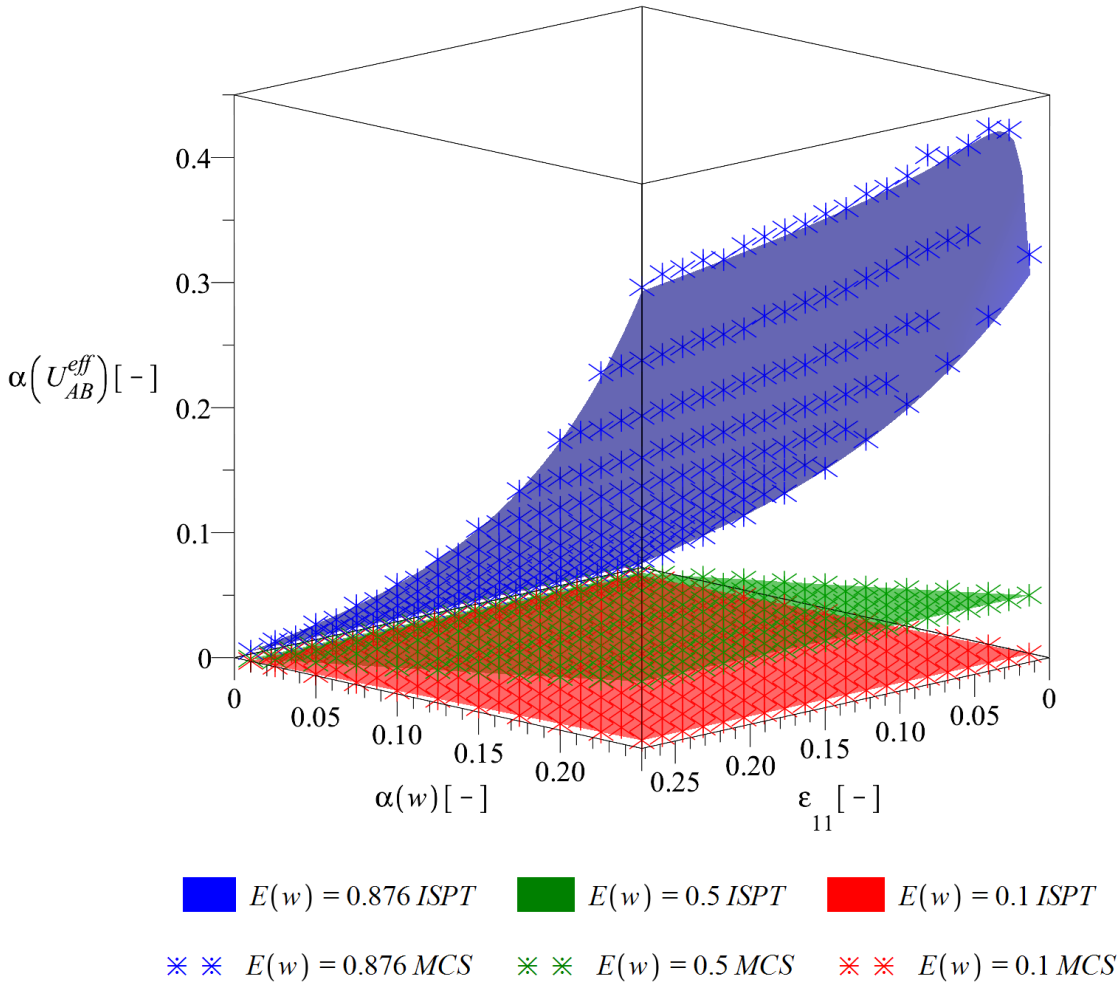

Fig. 6.22 Coefficient of variation of the effective deformation energy $\alpha\left(U^{eff}\right)$.

Coefficients of variation $\alpha\left(U^{eff}\right)$ are presented in Fig. 6.22. They are practically independent of ε_{11}, but are quite sensitive to changes of expectation and coefficient of variation of an input random variable $E(w)$, $\alpha(w)$. They increase together with an increase of $\alpha(w)$ and $E(w)$. This coefficient is nearly 10 times lower for $E(w)$=0.1 than for $E(w)$=0.5 and another 10 times higher for $E(w)$=0.876. This means that the volume fraction of defects in the composite plays a crucial role for the mean and expected values of this energy and also for its dispersion; this dispersion can even be much higher than the one of w. This is even more astonishing knowing the volume fraction of defects

(w=0.1 means that V^d corresponds to approx. 0.005 V by only). Correspondence of the two probabilistic methods for the first two probabilistic characteristics ($E\left(U^{eff}\right)$, $\alpha\left(U^{eff}\right)$) is perfect for the entire analyzed statistical scattering. The ISPT together with MCS even perfectly coincide for a local strong decrease of $\alpha\left(U^{eff}\right)$ returned for very low levels of strain and $E(w)$=0.876 by only.

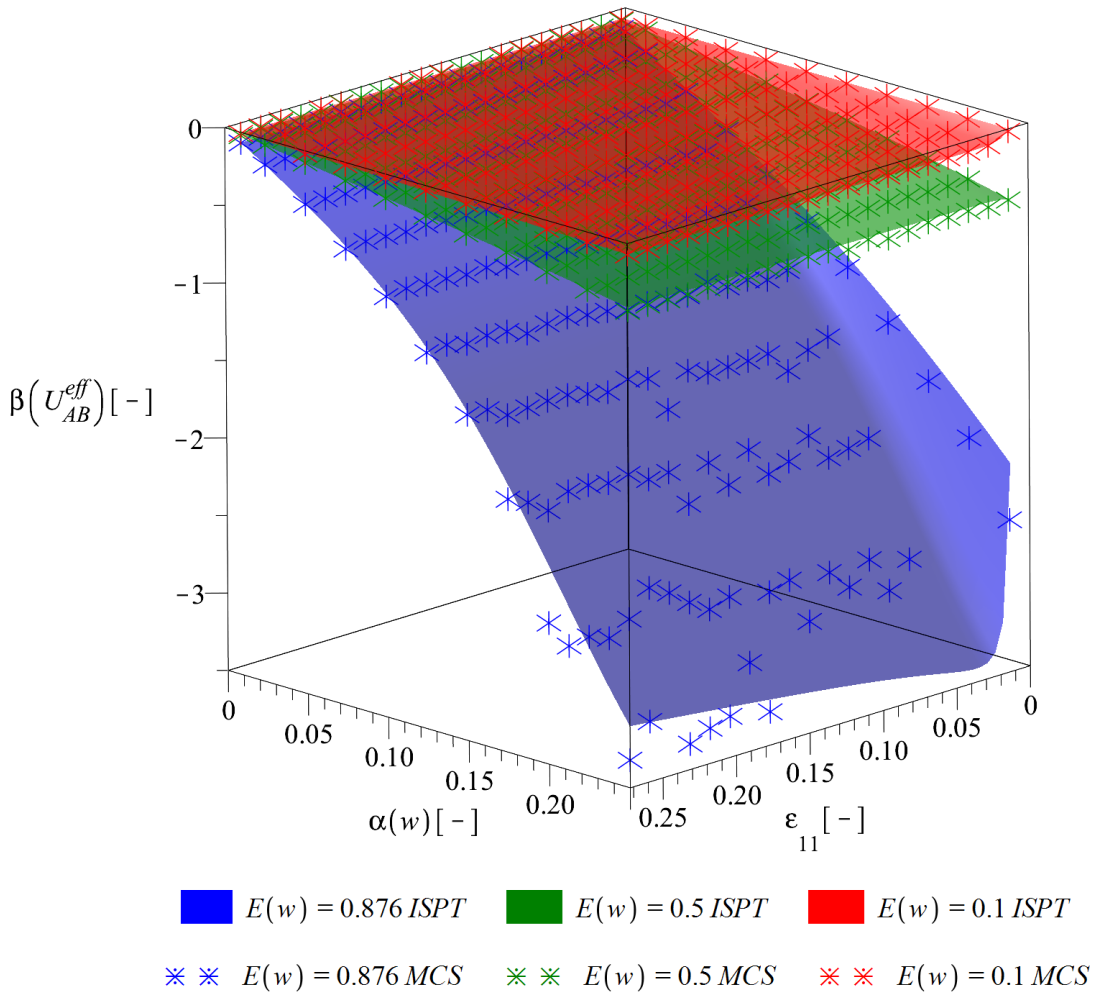

Fig. 6.23. Skewness of the effective deformation energy $\beta\left(U^{eff}\right)$.

Higher order probabilistic characteristics, i.e. skewness $\beta\left(U^{eff}\right)$ (Fig. 6.23) and kurtosis $\kappa\left(U^{eff}\right)$ (Fig. 6.24) are both increasing their magnitude together with an increase of $\alpha(w)$ as well as $E(w)$ and generally decreasing in magnitude together with an increase of ε_{11}. Skewness remains always negative, whereas kurtosis - almost always positive. The level of the strain is important especially for low strains, for which the magnitudes of characteristics and their rate of change are the highest. Results of alternative probabilistic methods are still very good for skewness and conditional for kurtosis. Some differences are visible only for the highest expectation $E(w)$=0.876. Skewness

starts to disagree for a high coefficient of dispersion of the input $\alpha(w)>0.18$ as well as for kurtosis with $\alpha(w)>0.12$. For these domains the MCS already returns a highly fluctuating result. This may possibly be improved by a substantial increase in the trials number (at least 2−3 times), but this is not possible on the available hardware. Either way, a standard deviation of more than 0.15 is rather not observed for polymeric composites. This is proved for the objective composite by laboratory experiments, where this dispersion stays around 5−8% despite some initial fluctuation.

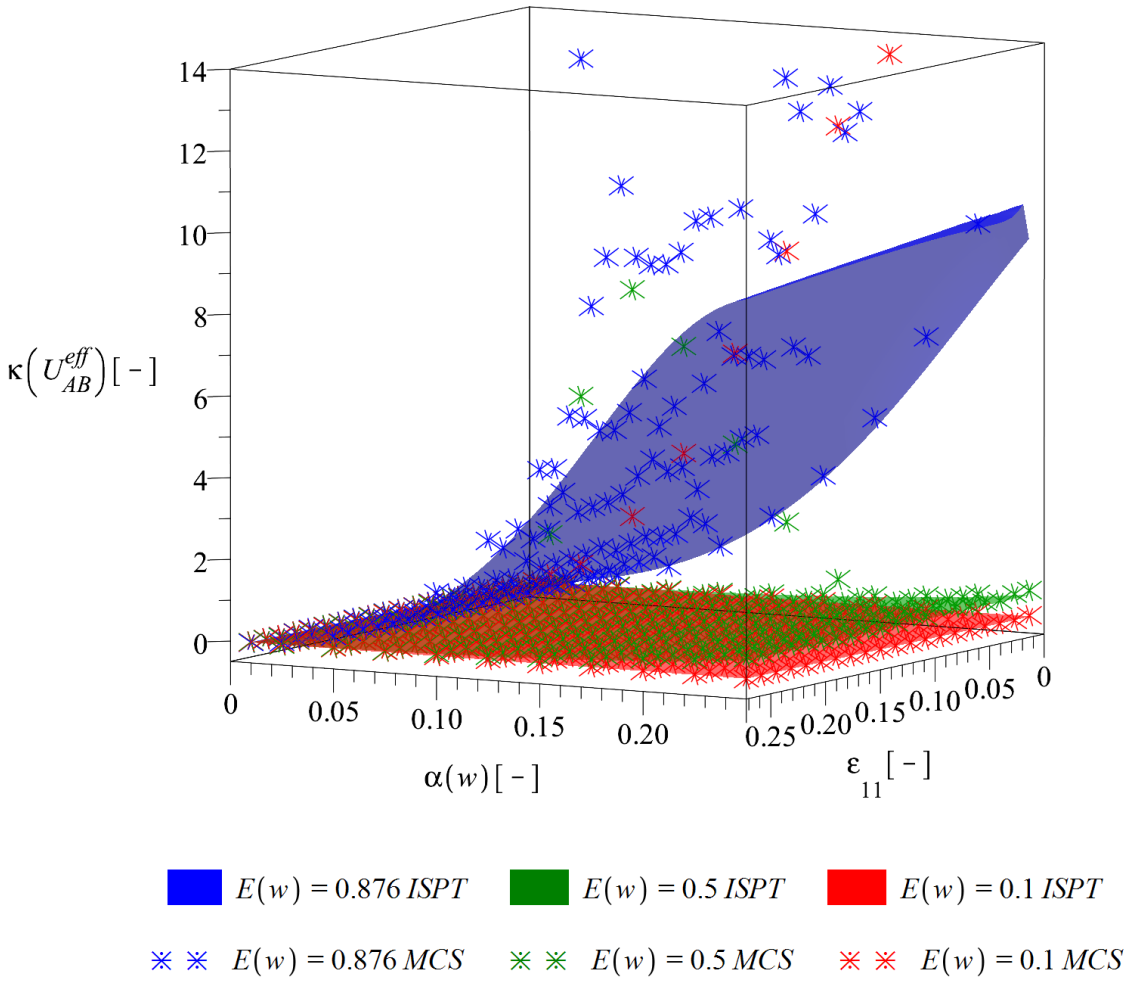

Fig. 6.24. Kurtosis of the effective deformation energy $\kappa\left(U^{eff}\right)$.

The resulting homogenized deformation energy is definitely not Gaussian because of a non-zero skewness and kurtosis. Its probability density function (PDF) changes character together with a variation of the strain level. Characteristics are most sensitive to strain changes close to zero and are also not unique for $E(w)$. An increase of $E(w)$ always decreases expectation and increases dispersion as well as magnitudes of higher order characteristics. In view of the above, stochastic interface defects are not only

decreasing overall deformation energy of the composite but also increase a band of possible deformation curves. Moreover, higher order probabilistic characteristics computed stochastic perturbation technique, even in the iterative mode [132,325], do not coincide perfectly with the statistical estimators of skewness and kurtosis computed via the Monte-Carlo scheme. They diverge from each other while increasing input coefficient of variation of the interphase parameter w especially for kurtosis computed for $E(w)=0.876$ and $\alpha(w)>0.12$; this may be improved by an increase of trials number in the MCS and order of the ISPT. Beware that the latter also requires an increase of the rank of the response function. However, sign and character of this characteristics is still the same, affected are mostly their magnitudes. Regardless of some discrepancy of the higher order characteristics, the ISPT may be well used especially for the expectations and coefficients of variation, which match perfectly with the MCS. It is preferred because of remarkable time savings in computational analysis; time effort of the ISPT is very close to several solutions of the FEM problem than hundreds of thousands required for the MCS to become convergent.

It has been documented in this section by numerical experiments that deformation process of the objective composite is remarkably affected by stochastic interface defects w. Its effective deformation energy U^{eff} is considerably decreased together with an increase of volume fraction of interface defects for an entire spectrum of strains verified in this study. Extent of this decrease is up to 40%. Stochastic interface defects also cause a noticeable dispersion of U^{eff} up to 40%, increasing together with an increase of expectation of this defects volume fraction and its statistical dispersion $E(w)$, $\alpha(w)$. This proves Hypothesis 1 part (b).

6.3. Effective stress in composite with interface defects

This section is dedicated to analysis of an effective stress in particulate composite with stochastic interface defects. Firstly, it presents the deterministic (section 6.3.1) and stochastic numerical experiments (section 6.3.2) for an increasing strain level and an increasing volume fraction of interface defects. Finally, it presents the stochastic characteristics of the effective stress for the objective composite and confronts it with the laboratory results (section 6.3.3). These characteristics are returned for the optimized values of the input uncertain variable of volume fraction of interface defects that have been determined in section 6.1.2.

6.3.1. Deterministic results

Effective stress is obtained according to three analytical formulas, separate for each hyperelastic formulation. They are following:

$$\sigma_{MR}^{eff}=\left(2C_{1,MR}^{eff}(w)+\frac{2C_{2,MR}^{eff}(w)}{\lambda}\right)\left(\lambda^2-\frac{1}{\lambda}\right) \tag{6.15}$$

for Mooney-Rivlin theory

$$\sigma_{AB}^{eff}=2C_{1,\mathrm{AB}}^{\mathrm{eff}}(w)\left(\lambda-\frac{1}{\lambda^2}\right) \cdot\left(\begin{array}{c}\frac{1}{2}+\frac{2}{20\left(\lambda_{AB}^{eff}\right)^2(w)}\left(\mathrm{I}_1-9\right)+\frac{3}{1050\left(\lambda_{AB}^{eff}\right)^4(w)}\left(\mathrm{I}_1^2-27\right) \\ +\frac{4\cdot 19}{7000\left(\lambda_{AB}^{eff}\right)^6(w)}\left(\mathrm{I}_1^3-81\right) \\ +\frac{5\cdot 519}{673750\left(\lambda_{AB}^{eff}\right)^8(w)}\left(\mathrm{I}_1^4-243\right)\end{array}\right) \tag{6.16}$$

for Arruda-Boyce model and

$$\sigma_{NH}^{eff}=2C_{1,NH}^{eff}(w)\left(\lambda-\tfrac{1}{\lambda^2}\right). \tag{6.17}$$

in case of the Neo-Hookean potential.

Effective material coefficients $C_{1,MR}^{eff}$, $C_{2,MR}^{eff}$, $C_{1,AB}^{eff}$, λ_{AB}^{eff} and $C_{1,NH}^{eff}$ used here are exactly the same as the ones in functional formulation of the effective deformation energy U^{eff}. They were determined in section 6.1.

Similarly to the U^{eff}, effective stress is also approximated with use of a bivariate polynomial so that

$$\sigma_{\xi}^{eff,Approx}=\mathrm{P}_{\xi}(\varepsilon_{11},w)=\sum_{\mathrm{i}=0}^{\mathrm{m}}\sum_{\mathrm{j}=0}^{\mathrm{m}}\mathrm{v}_{\xi\mathrm{m,ij}}\,w\cdot\varepsilon_{11} \tag{6.18}$$

where $\mathrm{v}_{\xi,\mathrm{ij}}$ represent polynomial coefficients and m an order of polynomial. They are both optimized independent from the ones recovered for U^{eff} but using the same procedure as the effective deformation energy presented in Appendix C. The difference

here is that the augmented material model presented in eqns (6.15) till (6.17) strictly results from analytical calculus (with an addition of parameter dependency on w) and is not anymore an approximation of discrete FEM results. Because of this fact, the below graphs only contain 'BPO' and 'AMM' results and not the 'FEM'. The rank of this polynomials is optimized independently for all three potentials. They are of the 8th order for Arruda-Boice and Mooney-Rivlin and the 6th order for the Neo-Hokean potential. A full expansion for the Mooney-Rivlin model is following (for brevity approximated here to three digits precision from original 12)

$$\begin{aligned}\sigma_{MR}^{eff,BPO}[\mathrm{Pa}]=&2.59\cdot10^{6}\cdot w-6.92\cdot10^{8}\cdot w^{4}+1.99\cdot10^{8}\cdot w^{3}\\&-3.22\cdot10^{7}\cdot w^{2}-2.71\cdot10^{8}\cdot w^{8}+1.04\cdot10^{9}\cdot w^{7}+1.12\cdot10^{9}\cdot\varepsilon_{11}\cdot w^{6}-1.12\cdot10^{7}\cdot\varepsilon_{11}{}^{5}\cdot w^{6}\\&+1.49\cdot10^{7}\cdot\varepsilon_{11}{}^{4}\cdot w^{7}+5.25\cdot10^{8}\cdot\varepsilon_{11}\cdot w^{8}-5.31\cdot10^{7}\cdot\varepsilon_{11}{}^{2}\cdot w^{8}-4.96\cdot10^{6}\cdot\varepsilon_{11}{}^{3}\cdot w^{8}\\&+4.01\cdot10^{6}\cdot\varepsilon_{11}{}^{4}\cdot w^{4}+1.29\cdot10^{8}\cdot\varepsilon_{11}-2.07\cdot10^{7}\cdot\varepsilon_{11}{}^{2}+6.28\cdot10^{7}\cdot\varepsilon_{11}{}^{3}-6.49\cdot10^{7}\cdot\varepsilon_{11}{}^{4}\\&+5.49\cdot10^{7}\cdot\varepsilon_{11}{}^{5}-2.76\cdot10^{7}\cdot\varepsilon_{11}{}^{6}-1.65\cdot10^{9}\cdot w^{6}+1.41\cdot10^{9}\cdot w^{5}-1.39\cdot10^{9}\cdot\varepsilon_{11}\cdot w^{7}\\&+9.33\cdot10^{7}\cdot\varepsilon_{11}{}^{2}\cdot w^{7}-9.41\cdot10^{7}\cdot\varepsilon_{11}{}^{3}\cdot w^{7}-2.38\cdot10^{7}\cdot\varepsilon_{11}\cdot w+1.41\cdot10^{7}\cdot\varepsilon_{11}{}^{2}\cdot w\\&-1.73\cdot10^{7}\cdot\varepsilon_{11}{}^{3}\cdot w+1.16\cdot10^{7}\cdot\varepsilon_{11}{}^{4}\cdot w-7.48\cdot10^{7}\cdot\varepsilon_{11}\cdot w^{2}-0.09\cdot10^{7}\cdot\varepsilon_{11}{}^{2}\cdot w^{2}\\&+2.63\cdot10^{6}\cdot\varepsilon_{11}{}^{3}\cdot w^{2}+2.98\cdot10^{5}\cdot\varepsilon_{11}{}^{4}\cdot w^{2}-6.31\cdot10^{8}\cdot\varepsilon_{11}{}^{5}\cdot w^{2}+2.71\cdot10^{8}\cdot\varepsilon_{11}\cdot w^{3}\\&+8.89\cdot10^{7}\cdot\varepsilon_{11}{}^{2}\cdot w^{3}-4.83\cdot10^{8}\cdot\varepsilon_{11}\cdot w^{4}-8.78\cdot10^{7}\cdot\varepsilon_{11}{}^{2}\cdot w^{4}-2.94\cdot10^{6}\cdot\varepsilon_{11}{}^{3}\cdot w^{4}\\&-7.74\cdot10^{4}\end{aligned}\tag{6.19}$$

Similarly to the effective strain energy, this optimized polynomial is not a full bivariate polynomial of the 8th order, but it is 8 times differentiable with respect to w. The remaining expansions were skipped for the brevity of the results.

The effective stress σ^{eff} is presented in Fig. 6.25. It is plotted in addition to the uniaxial strain ε_{11} and relative to the volume fraction of interface defects w for three selected hyperelastic potentials. This figure firstly shows that the stress at $\sigma^{eff}(\varepsilon_{11}=0)=0$ and it increases up to values close to expectations coming from laboratory tests reported in Fig. 5.6 for the virgin homogeneous material and the objective composite. Two potentials, i.e. the Arruda-Boyce and Neo-Hookean produce a very similar result with a relative difference less than 1.6% that decreases for decreasing w. The Mooney-

Rivlin potential reports considerably higher magnitude of stresses especially for high levels of strain (up to +30% for $\varepsilon_{11}\rightarrow 0.275$). This relative difference decreases together with a decrease of ε_{11} and also deceases together with an increase of w; it originates from different formulation of potentials and approximations used to retrieve the stress in alternative constitutive models and thus it is not entirely surprising. Mooney-Rivlin is based on the first two invariants, while the remaining constitutive models only on the first one. Interestingly, interface defects have so high influence on the stresses of the composite that its strengthening with respect to the virgin homogeneous material vanishes already for medium volume fraction of defects.

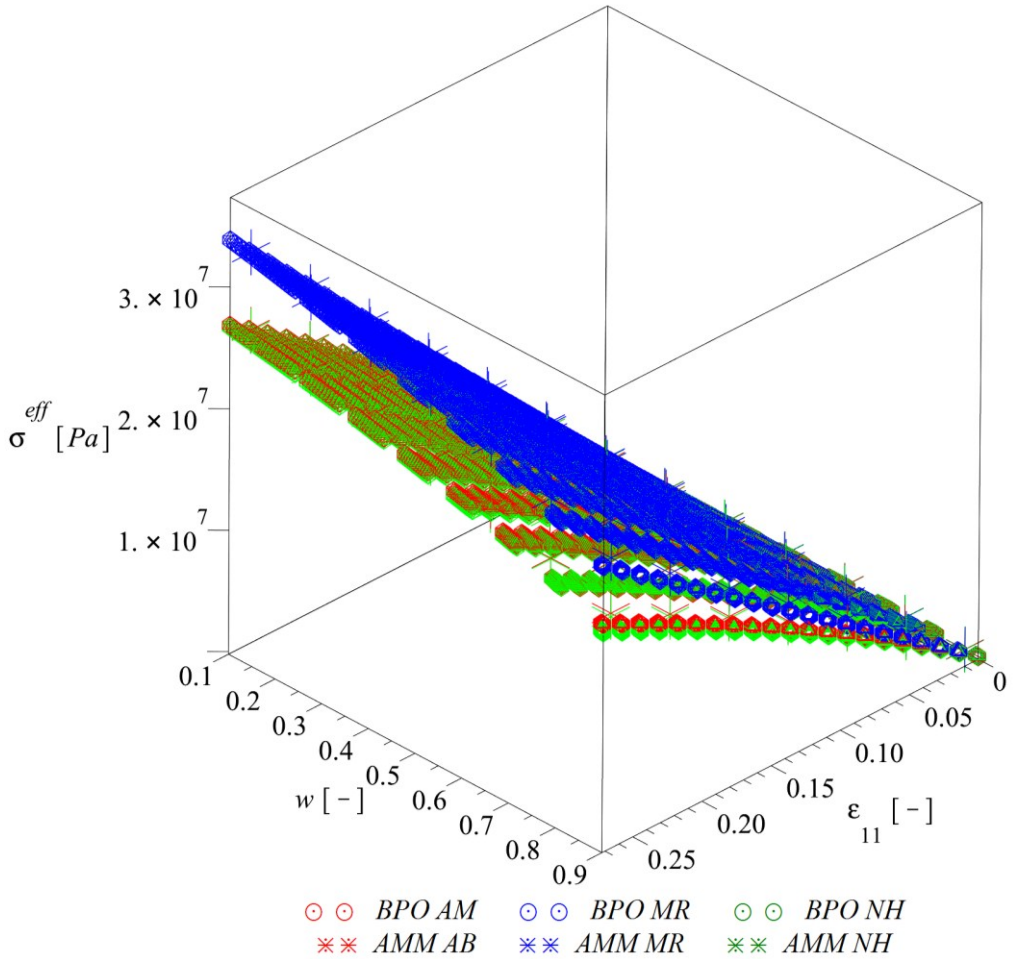

Fig. 6.25 Effective stress of the RVE σ^{eff} w.r.t. the volume fraction of defects w for an increasing uniaxial strain ε_{11}.

At ε_{11}=0.275 for the smallest volume fraction of defects considered w=0.05 it reaches ($\sigma^{eff}_{AB}/\sigma^{m}_{AB}$=1.192, $\sigma^{eff}_{NH}/\sigma^{m}_{NH}$=1.172, $\sigma^{eff}_{MR}/\sigma^{m}_{MR}$=1.483); for w>0.27 the composite is already softer than the virgin homogeneous material approximation σ^{m}_{ξ} (apart from the Mooney-

Rivlin for which it is softer than σ_{ξ}^{m} for w>0.67). Reduction of the stresses at ε_{11}=0.275 for the highest considered w=0.9 reaches following values $\sigma_{AB}^{eff}(\varepsilon_{11}=0.275)$=18.52 MPa, $\sigma_{NH}^{eff}(\varepsilon_{11}=0.275)$=17.51 MPa and $\sigma_{MR}^{eff}(\varepsilon_{11}=0.275)$=23.25 MPa. This weakening is also observed in laboratory experiments; it is plotted on Fig. 5.6.

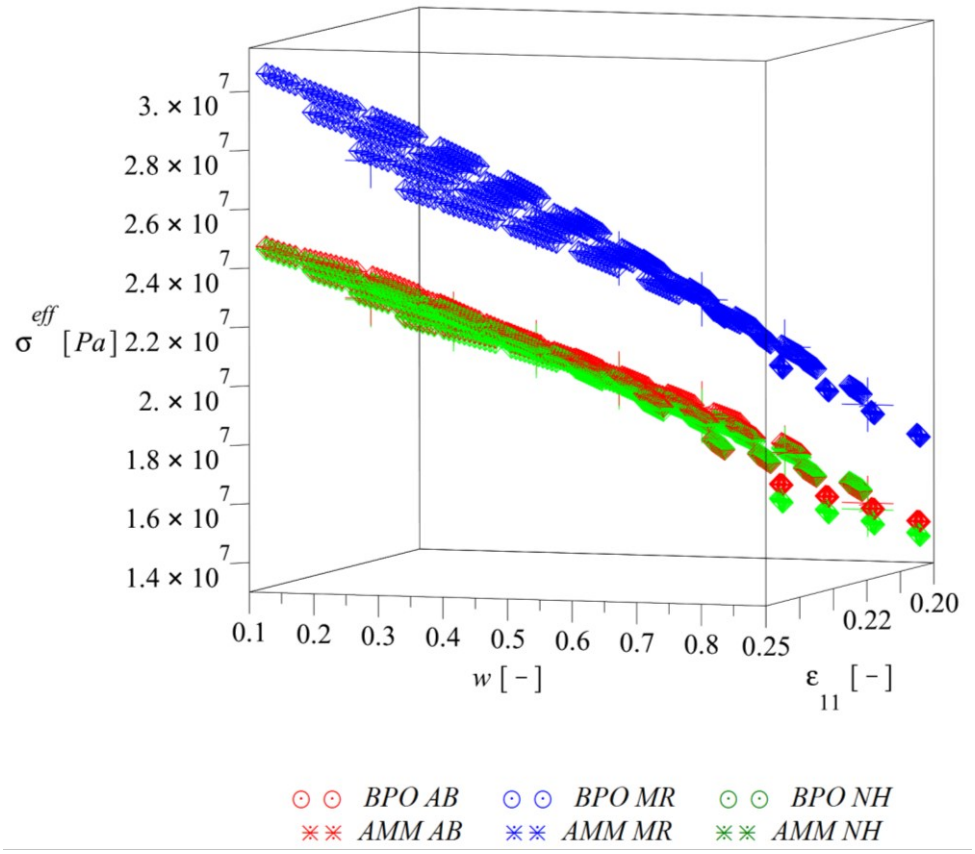

Fig. 6.26 Close-up of the effective stress of the RVE σ^{eff} w.r.t. the volume fraction of defects w for an increasing uniaxial strain ε_{11}.

A closer look of the stresses recovered from numerical experiments at high strain rates in the range of $\varepsilon_{11}\in(0.23, 0.27)$ is provided in Fig. 6.26. It firstly shows that the bivariate polynomial approximations of stresses (BPO) perfectly coincides with the augmented material model (AMM) for entire considered spectrum of w and ε_{11}. It is important because the BPO is used in further considerations including stochastic experiments. A detailed approximation error consideration is skipped for brevity of the results. It is not higher than the one of the effective deformation energy, whose error was considered in detail in section 6.2.2.

This figure is included here also to better visualize a quite substantial difference of the results recovered by the Mooney-Rivlin approach with respect to the other ones, whose

origin has been previously underlined. Results coming from this approach are preserved in stochastic experiments specifically to exemplify that they will depend on the selected underlying potential even when their fits to the lab tests and strain energy is practically the same and with maximally 4% mean difference for entire considered region of (w, ε_{11}). Because of this, one shall not limit himself to just one formulation but instead compare several of them and formulate conclusions on the basis of their contrast.

A further discussion of coincidence of the results coming from laboratory tests and numerical experiments is included in section 6.3.3. The stress coming from laboratory experiments of the objective composite lays within the application region of the augmented material model. The recovered volume fraction of interface defects is presented in section 6.1.2. This proves Hypothesis 7 (b).

6.3.2. Stochastic analysis

A statistical disorder of the composite effective stress σ^{eff} is next determined relative to random variability in the volume fraction of interface defects w. It is done on the basis of optimized bivariate polynomial representation of these stress (presented in eqn (6.19)) with use of three independent stochastic methods, i.e. the generalized iterative stochastic perturbation of order 6 or 8, the Monte-Carlo simulation with 150.000 trials and the semi-analytical method; the 8^{th} order ISPT was used for Arruda-Boice and Mooney-Rivlin, while the 6^{th} order for the Neo-Hokean potential. This was dictated by rank of the optimized bivariate response function. Stochastic characteristics are recovered in a joint domain of strain $\varepsilon_{11} \in (0.23, 0.27)$ and coefficient of variation of this random parameter $\alpha(w) \in (0, 0.25)$ for its three expected values $E(w) \in [0.1,\ 0.3, 0.5]$. They could not be simply reduced to a single variable functions, because the statistics of the σ^{eff} are not unique in the entire strain region (see Fig. 5.7) as it is for the linear reversible composites and materials, which are simply governed by the stiffness tensor having constant components [65].

Probabilistic considerations are mainly focused on four following aspects:

1. importance of variation and expectation of volume fraction of interface defects $\alpha(w)$, $E(w)$ is analyzed for the resulting stochastic characteristics of the effective stress σ^{eff}
2. influence of strain on these characteristics is determined; it is verified if it could be omitted from stochastic calculations

3. coincidence of the three selected probabilistic methods on these characteristics is checked (ISPT, MCS, SAM); this is done to validate the stochastic calculations
4. importance of a choice of hyperelastic potential is studied on the basis of the three selected potentials (best representing the matrix and interphase response, see Appendix A).

This section includes results of the first four stochastic characteristics of the effective stress of the defective composite, i.e. its expected value $E(\sigma^{eff})$, coefficient of variation $\alpha(\sigma^{eff})$, skewness $\beta(\sigma^{eff})$ and kurtosis $\kappa(\sigma^{eff})$. Each of these coefficients are visualized on two three-dimensional graphs. The first one three different expected values of input volume fraction of defects $E(w)\in(0.1, 0.3, 0.5)$ are set together, while in the second one results coming from three selected probabilistic results are presented. Such a choice proved to be much more readable than rendering all the above information on a single graph. Legends in these graphs are always plotted with three sets of colors, i.e. reds represent the results for Mooney-Rivlin potential (MR), greens represent the results for Neo-Hookean potential (NH) and blues represent the results coming from Arruda-Boyce potential (AB). The color intensity indicates two alternative things. In the first set of graphs for each stochastic characteristic, i.e. Fig. 6.27, Fig. 6.29, Fig. 6.31 and Fig. 6.33 it differentiates the expected values of input volume fraction of voids $E(w)$=0.1, $E(w)$=0.3 and $E(w)$=0.5. In these graphs the results were limited to the Mooney-Rivlin and Arruda-Boyce potentials and computed solely for the ISFEM. This was done because the Arruda-Boyce and Neo-Hookean returned very close results to each other and the ISPT is solution method preferred in this thesis. This is because the computational effort in semi-analytical considerations and perturbation-based approaches (2^{nd} and 4^{th} order) are negligible when compared with this corresponding to the Monte-Carlo simulation (MCS) and the SFEM does not have a limitation of differentiability of the response function. In the second set of graphs, i.e. Fig. 6.28, Fig. 6.30, Fig. 6.32, Fig. 6.34 color intensity differentiates three stochastic methods used i.e. the stochastic finite element method (SFEM), the Monte-Carlo simulation (MCS) and the semi-analytical method (SAM); these graphs are plotted for $E(w)$=0.5. The ISPT and SAM produce continuous results in the entire domain of $\alpha(w)$ and ε_{ij}, while the MCS – discrete points evenly distributed through this domain; this is a trait of the MCS; therefore the MCS is plotted as points and the ISPT and SAM with a surface. Description of these graphs is provided in a following way: first each characteristic is

described separately, focusing on its dependency on $\alpha(w)$, $E(w)$ and ε_{11}, coincidence of probabilistic methods and of hyperelastic potentials and then a holistic discussion of all the characteristics is provided; it is especially focused on the coincidence of the results coming from different hyperelastic potentials, variation of strain and influence of the stochastic variation of defects.

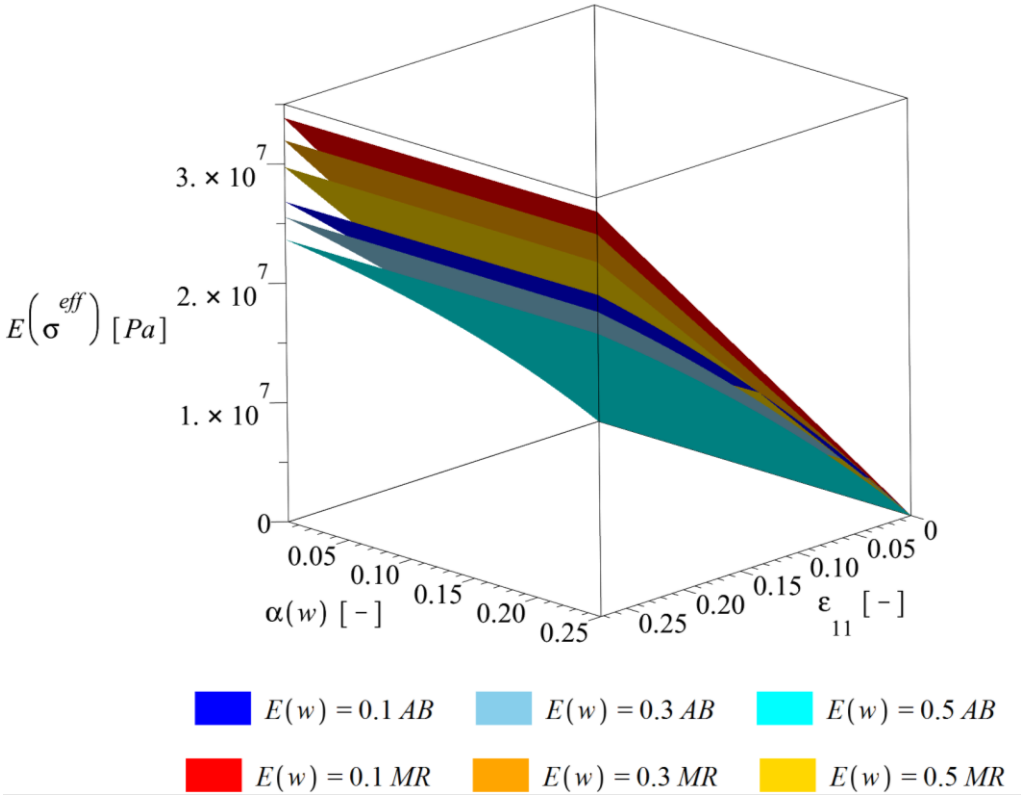

Fig. 6.27 Expected value of the effective stress of the RVE $E(\sigma^{eff})$ w.r.t. the coefficient of variation of the volume fraction of defects $\alpha(w)$ for an increasing uniaxial strain ε_{11} and expected value of the interface defects $E(w)$.

Expected values of the effective stress $E(\sigma^{eff})$ are included on Fig. 6.27 and Fig. 6.28. They always start from zero and increase together with an increase of strain for all the levels of input dispersion $\alpha(w)$, irrespective of the expected values of interface defects volume fraction, for all probabilistic methods and hyperelastic potentials. Their level of increase in magnitude reaches $E(\sigma^{eff},\varepsilon_{11}=0.275) \in (24.2, 34.8)$ MPa and depends mostly on the potential applied and on $E(w)$. It is not too much dependent on $\alpha(w)$.

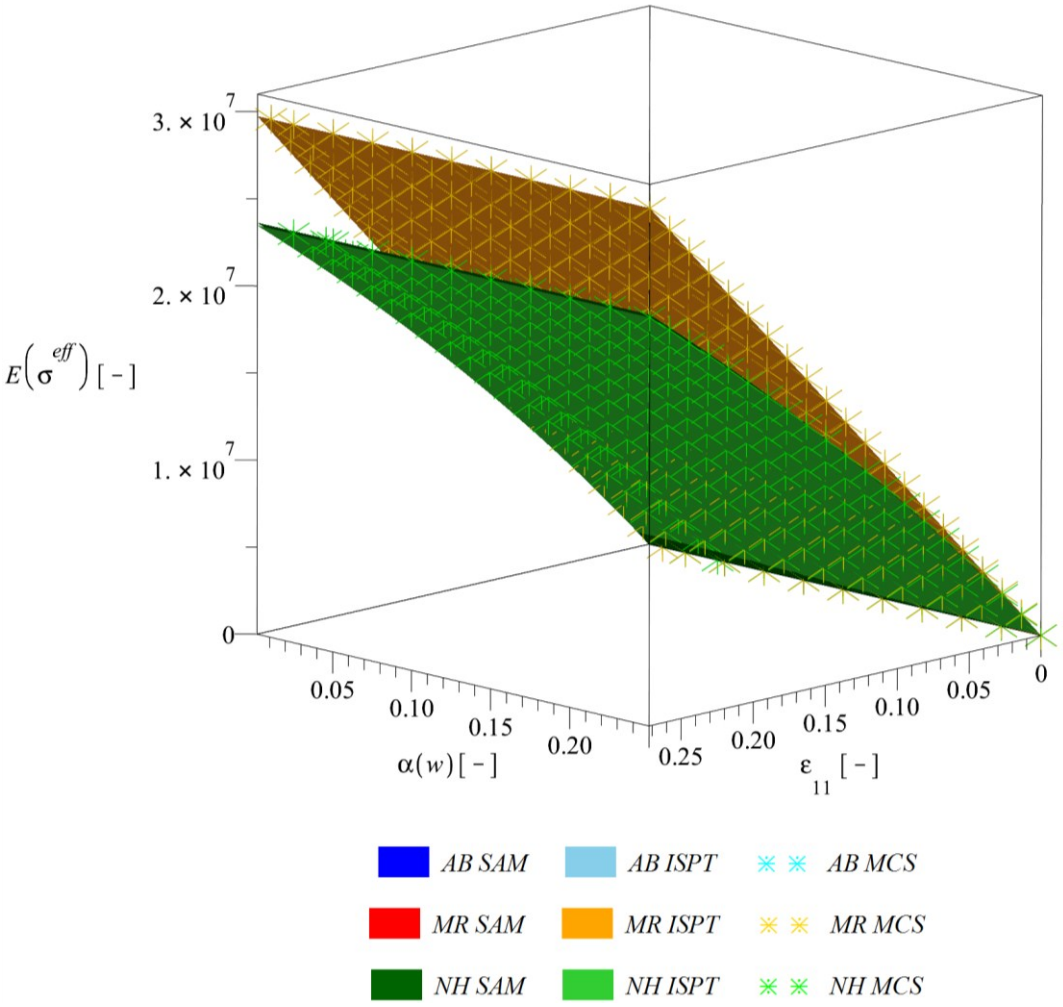

Fig. 6.28 Expected value of the effective stress of the RVE $E(\sigma^{eff})$ w.r.t. the coefficient of variation of the volume fraction of defects $\alpha(w)$ for an increasing uniaxial strain ε_{11} and different hyperelastic potentials.

An increase of expectation of volume fraction of interface defects (defects intensity) obviously always decreases the magnitude of $E(\sigma^{eff})$ (see color intensities on Fig. 6.27); this observation is also consistent with a dependency of σ^{eff} on w reported on Fig. 6.25 included in deterministic considerations of σ^{eff}. This decrease is higher for the Mooney-Rivlin potential than for the Arruda-Boyce (8.7 MPa vs 5.4 MPa) and it is higher from $E(w)$=0.3 to $E(w)$=0.5 than from $E(w)$=0.1 to $E(w)$=0.3. Similarly to the deterministic case, coincidence of the results coming from Arruda-Boyce and Neo-Hookean potentials is very high; they are within 1% of each other even for ε_{11}=0.275. The Mooney-Rivlin returns results always higher than the remaining potentials. This difference goes up to 26%, it decreases together with a decrease of ε_{11} and an increase of $E(w)$.

Next, correspondence of results coming from three selected stochastic methods is considered; it is distinguished with color intensities on Fig. 6.28. The methods agree very well independently from the level of $\alpha(w)$. The expected values of effective stress are not too much dependent on the input dispersion of interface defects $\alpha(w)$, variation of $E(\sigma^{eff})$ does not exceed 2% for its selected variation. Expectations coming from Arruda-Boyce potential agrees with the Arruda-Boyce so well, that their curves match perfectly on the graph and a blue plane is covered by green.

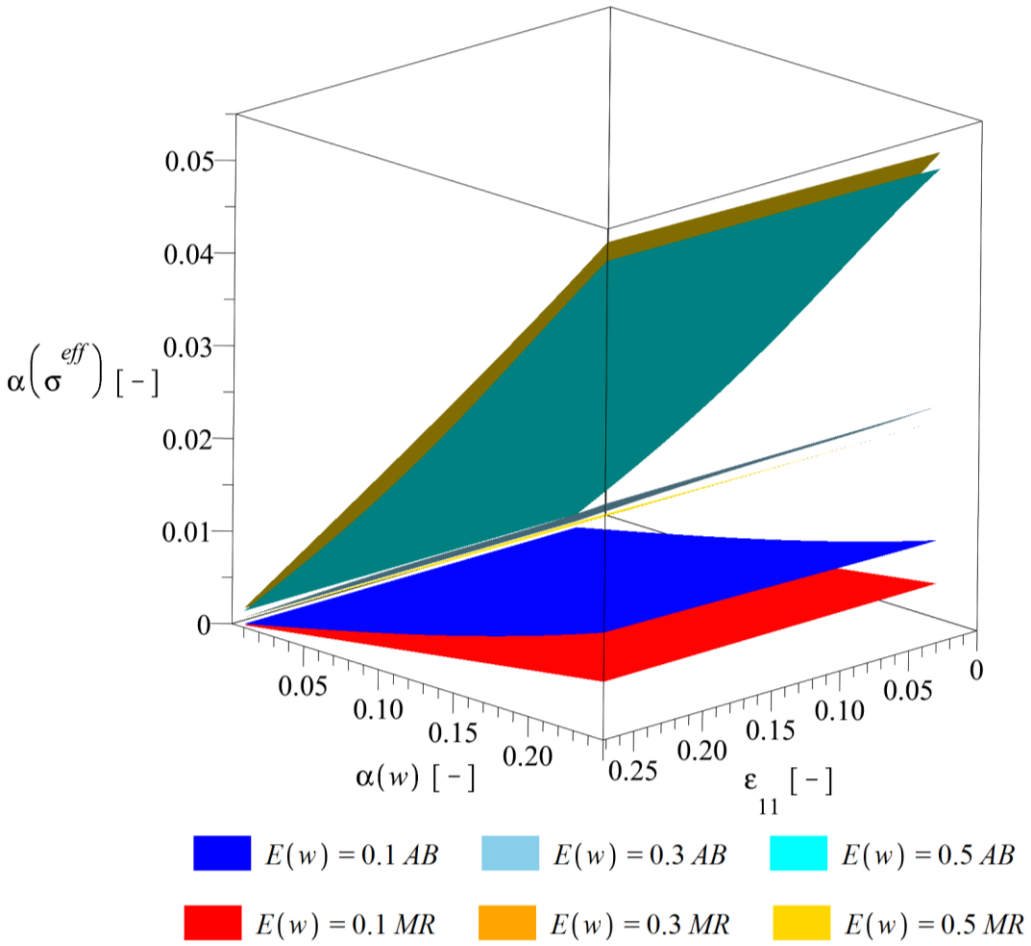

Fig. 6.29 Coefficient of variation of the effective stress of the RVE $\alpha(\sigma^{eff})$ w.r.t. the coefficient of variation of the volume fraction of defects $\alpha(w)$ for an increasing uniaxial strain ε_{11} and expected value of the interface defects $E(w)$.

The coefficient of variation of the effective stress $\alpha(\sigma^{eff})$ is reported on Fig. 6.29 and Fig. 6.30 with relation to ε_{11} and $\alpha(w)$. Following the probability theory, it always starts from zero for $\alpha(w)=0$; it increases almost linearly together with its increase but is always smaller than $\alpha(w)$. Its magnitude strictly depends on the expected value of

volume fraction of interface defects $E(w)$ - it always increases together with an increase of $E(w)$, up to seven times for the extreme cases. A variation of strain have only a marginal influence on the magnitude of $\alpha(\sigma^{eff})$ – much below 1%. A correspondence of the selected hyperelastic potentials is almost perfect for $E(w)\geq 0.3$, for which they return results differing less than 1%. This is entirely different for $E(w)=0.1$, where the MR returns up to 30% lower results (see Fig. 6.30), but the two other methods still remain convergent.

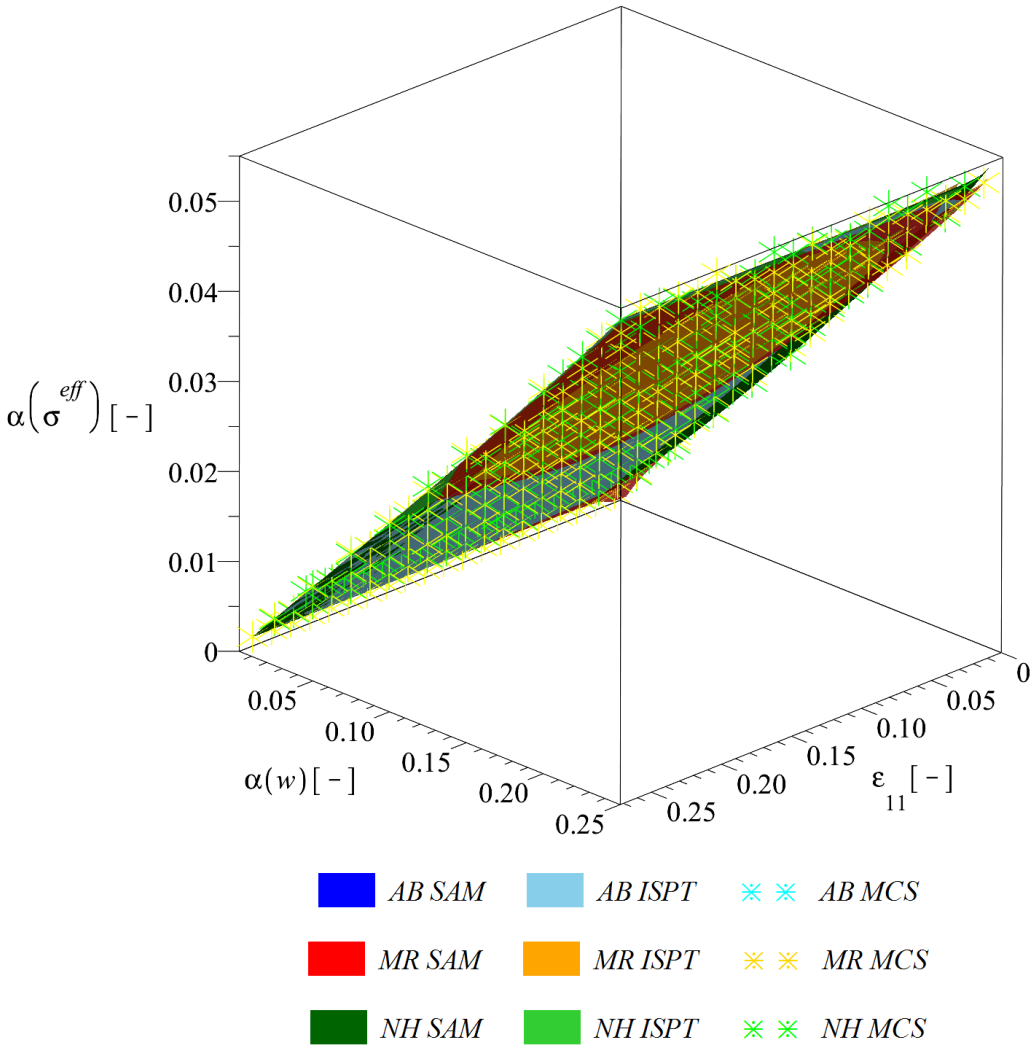

Fig. 6.30 Coefficient of variation of the effective stress of the RVE $\alpha(\sigma^{eff})$ w.r.t. the coefficient of variation of the volume fraction of defects $\alpha(w)$ for an increasing uniaxial strain ε_{11} and different hyperelastic potentials.

The results of $\alpha(\sigma^{eff})$ for the three selected stochastic methods are reported on Fig. 6.30. Similarly to the expected values, their correspondence is very high. Difference does not exceed 3% but it increases together with an increase of $\alpha(w)$ and persists for all $E(w)$.

This holds also for all other expected values of $E(w)$, which are not presented on this graph. Coefficient of variation of the effective stress increases together with an increase of $E(w)$, its maximum values reported by the ISFEM are following: for $E(w)$=0.1 $\alpha(\sigma^{eff})$=0.0096, for $E(w)$=0.3 $\alpha(\sigma^{eff})$=0.0205 and for $E(w)$=0.05 – $\alpha(\sigma^{eff})$=0.54 (see Fig. 6.30). The difference between the hyperelastic potentials is a little bigger. It is especially high for small expectations of the input $E(w)$ and decreases together with their increase. Relation of $\alpha(\sigma^{eff})$ to $\alpha(w)$ is close to linear irrespective of the expectation of $E(w)$.

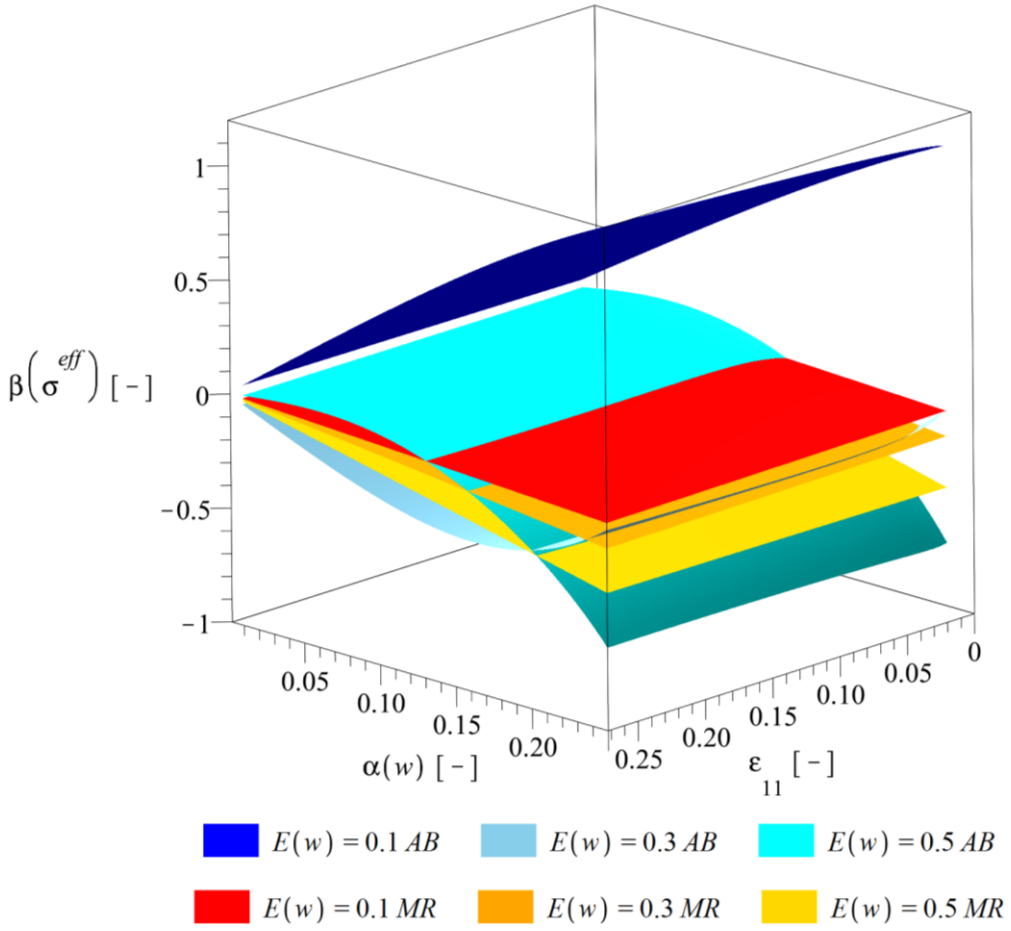

Fig. 6.31 Skewness of the effective stress of the RVE $\beta(\sigma^{eff})$ w.r.t. the coefficient of variation of the volume fraction of defects $\alpha(w)$ for an increasing uniaxial strain ε_{11} and expected value of the interface defects $E(w)$.

The skewness of the effective stress $\beta(\sigma^{eff})$ is presented on Fig. 6.31 and Fig. 6.32 with relation to ε_{11} and $\alpha(w)$. It generally increases in magnitude together with an increase of $\alpha(w)$ and it decreases together with an increase of $E(w)$. It is contained in the range of $\beta(\sigma^{eff}) \in (-2.4, 1.1)$ and is practically independent from ε_{11}. Magnitude of skewness

$\beta(\sigma^{eff})$ is always 0 for $\alpha(w)=0$ and its monotonicity strictly depends on $E(w)$. It is predominantly negative for expected values above $E(w)=0.1$ and positive otherwise. The three potentials return quite convergent results with an exception to $E(w)=0.1$ shown on Fig. 6.31, where the difference between Mooney-Rivlin (MR) and Arruda-Boyce is substantial. They even report an opposite sign for a limited range of $\alpha(w)$.

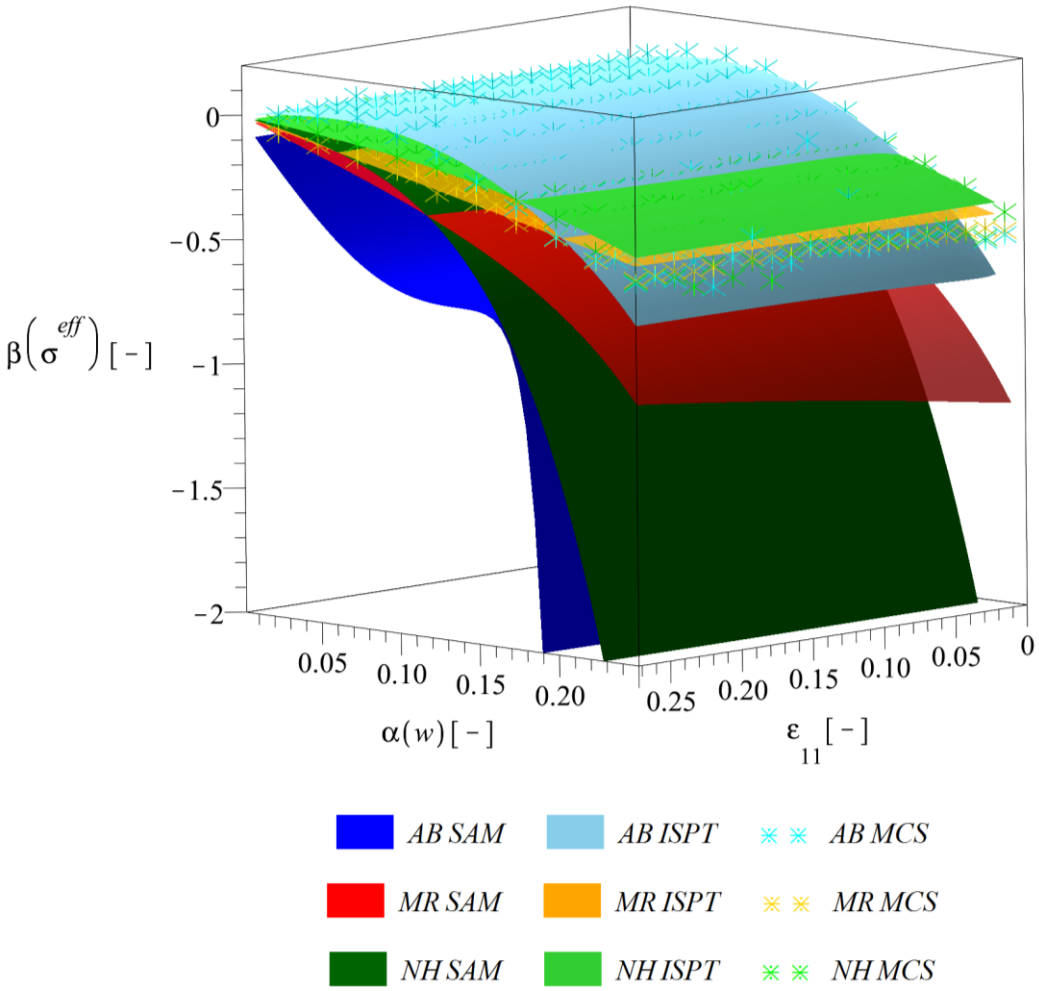

Fig. 6.32 Skewness of the effective stress of the RVE $\beta(\sigma^{eff})$ w.r.t. the coefficient of variation of the volume fraction of defects $\alpha(w)$ for an increasing uniaxial strain ε_{11} and different hyperelastic potentials.

Coincidence of the results of $\beta(\sigma^{eff})$ coming from different stochastic methods is not perfect (see Fig. 6.32). The semi-analytical method especially diverges and returns higher magnitudes than the ISPT and the MCS. The ISPT and the MCS are much closer to each other but still their results differ up to 28%.

Kurtosis of the effective stress $\kappa(\sigma^{eff})$ is presented on Fig. 6.33 and Fig. 6.34. It is predominantly positive and increases magnitude together with an increase of $\alpha(w)$. It is

negative only for $E(w)$=0.3 returned by the SAM and is practically independent from ε_{11}. The highest magnitude is observed for $E(w)$=0.5 and it decreases together with a decrease of $E(w)$. The generalized iterative stochastic perturbation method and the Monte-Carlo simulation produce a similar $\kappa(\sigma^{eff})$ in entire spectrum of $\alpha(w)$ and ε_{11}; the semi-analytical method return much higher results, which start to diverge from the other ones for $\alpha(w)$>0.07 (see Fig. 6.33).

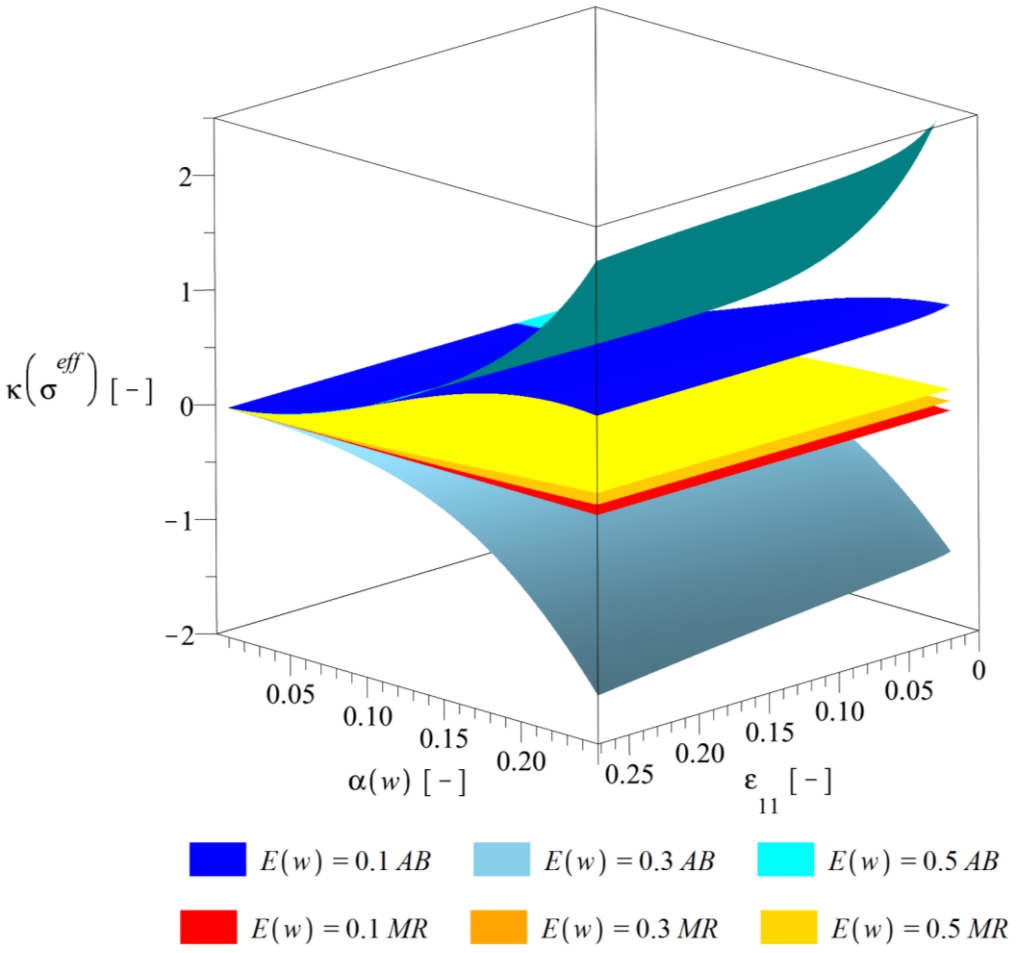

Fig. 6.33 Kurtosis of the effective stress of the RVE $\kappa(\sigma^{eff})$ w.r.t. the coefficient of variation of the volume fraction of defects $\alpha(w)$ for an increasing uniaxial strain ε_{11} and expected value of the interface defects $E(w)$.

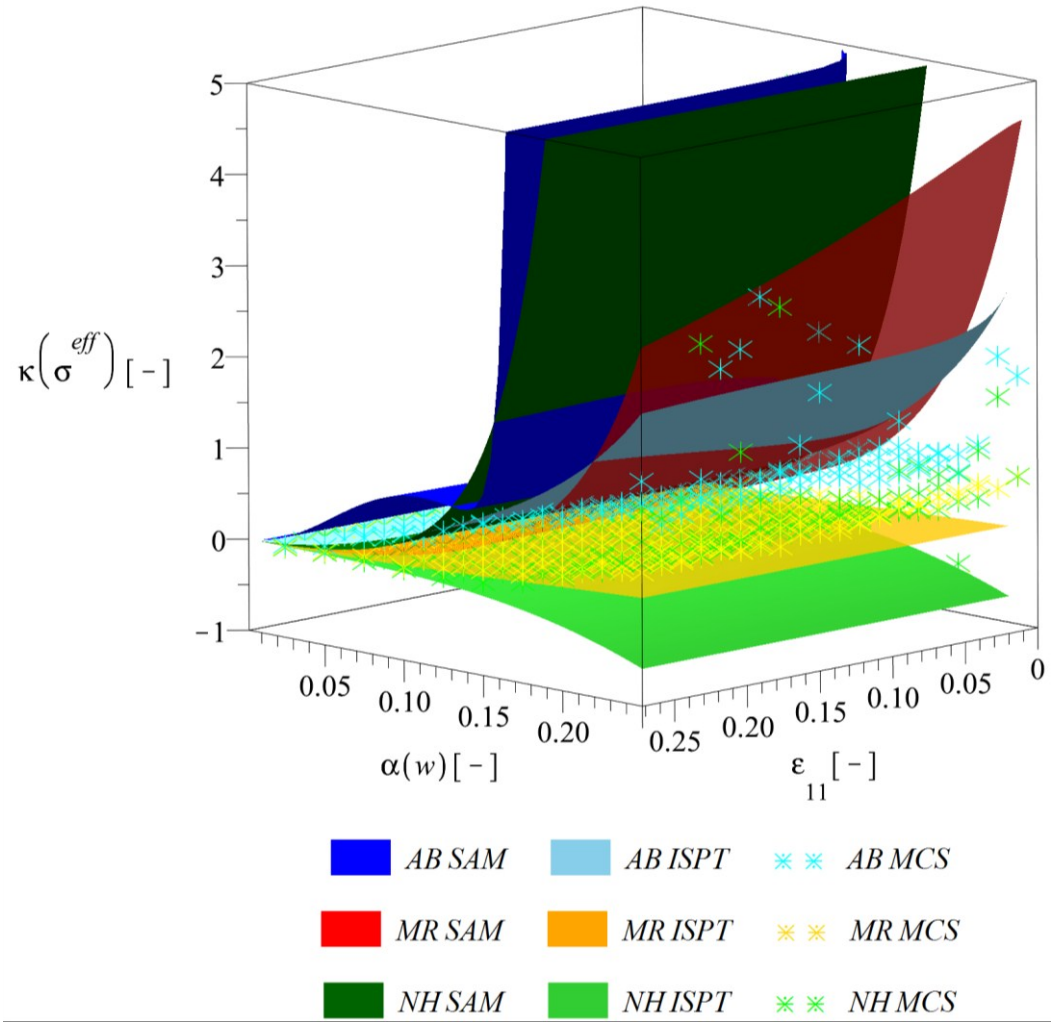

Fig. 6.34 Kurtosis of the effective stress of the RVE $\kappa(\sigma^{eff})$ w.r.t. the coefficient of variation of the volume fraction of defects $\alpha(w)$ for an increasing uniaxial strain ε_{11} and different hyperelastic potentials.

Summarizing, expected value of volume fraction of interface defects $E(w)$ has a very similar influence on stochastic characteristics of σ^{eff} for all three hyperelastic potentials. Its increase always decreases the expectations of σ^{eff}, increases the coefficient of variation, and increases magnitude of both, the skewness and kurtosis (the only exception for this rule is Arruda-Boyce potential and $E(w)$=0.1). According to the above observation, the interface defects not only decrease the effective stress but also increase its dispersion and higher stochastic characteristics. This also means that a PDF of the effective stress under uncertain volume fraction of interface defects is distant from Gaussian. At this point Hypothesis 1 part (c) is proved. Finally, the stochastic characteristics of both, the effective deformation energy and also the effective stress depend on the strain level, which confirms Hypothesis 5 (b).

6.3.3. Stochastic characteristics for optimum statistical estimators of *w* and its verification with laboratory results

The main goal of this section is (1) verification of performance of the proposed algorithm for numerical determination of stochastic interface defects characteristics and also (2) a check if the proposed augmentation of selected hyperelastic potentials is able to adequately represent a response of the composite with stochastic interface defects. For this purpose two sets of graphs are introduced. They both include the first four stochastic characteristics of the effective stress calculated for optimized values of $E(w)$ and $\alpha(w)$; they have been determined in section 6.1.2. These relations are presented w.r.t. the level of the strain in the same range as the other experiments $\varepsilon_{11} \in (0.0, 0.275)$. These relations are accompanied by the expected value and coefficient of random dispersion of this stress coming from laboratory experiments for a virgin homogeneous material and for a defective composite (objective composite); such collation allows a visual verification of the proposed constitutive models. Calculations are based on the same response functions as the preceding section (6.3.2). Order of the ISPT and integration used in the SAM are also follows it. The difference comes in the MCS, which has 450 000 trials. This is allowed because of a much smaller number of data points required to recover from this discrete method than in the previous section, where it was probed also for variable $\alpha(w)$; it is calculated only for the optimized $E_{\xi}^{opt}(w)$ and $\alpha_{\xi}^{opt}(w)$. Two dimensional graphs are preferred, because they visualize much better magnitudes of the effective stress; a secondary axis for $\alpha(w)$ is not required anymore. The first set of graphs, i.e. Fig. 6.35, Fig. 6.37, Fig. 6.39 and Fig. 6.41 provides results for three different stochastic methods calculated for the Arruda-Boyce hyperelastic constitutive model. The second set of graphs i.e. Fig. 6.36, Fig. 6.38, Fig. 6.40 and Fig. 6.42 is aimed to confront the results of two hyperelastic potentials, Arruda-Boyce and Neo-Hookean. The Mooney-Rivlin model was not included here, because the optimized expectation of the input variable is very close to its physical limit and this constitutive model returned much different results of the effective stress than the remaining two constitutive models. The above mentioned graphs present the laboratory results always with green diagonals that are labeled with ‘EXP’. The first set of graphs distinguish different stochastic models with symbols and the second one uses them for differentiation of the hyperelastic constitutive models; results for optimized characteristics of the input random variable are labeled with ‘OPT’.

Expectation of the effective stress for different stochastic methods is presented in Fig. 6.35. They all perfectly agree with each other and provide quite an accurate representation of stress expectation returned by the laboratory experiments (labeled as EXP CB5%). Additional curves are also presented for the extreme expectations of input random parameter, i.e. $E(w)$=0.95 and $E(w)$=0 to provide an envelope of responses possible to represent by the proposed augmentation of constitutive models. Not surprisingly, the expectation of stress for the composite without interface defects (returned for $E(w)$=0) allows a high strengthening of the virgin homogenous material. This theoretical limit is not reproduced by the experiment due to the interface defects. In fact, the composite with the CB filler is softer than the virgin homogeneous material; the proposed augmentation works for both cases. The lower limit of $E(w)$=0.95 that is considered here (physical limit of w is 1) given in brown allows even a higher than softening of this composite response than observed in reality for the objective composite. Please note, that this selected limit better approximates the laboratory result for the highest strain level, but overall it is more distant from this result than the 'OPT' solution.

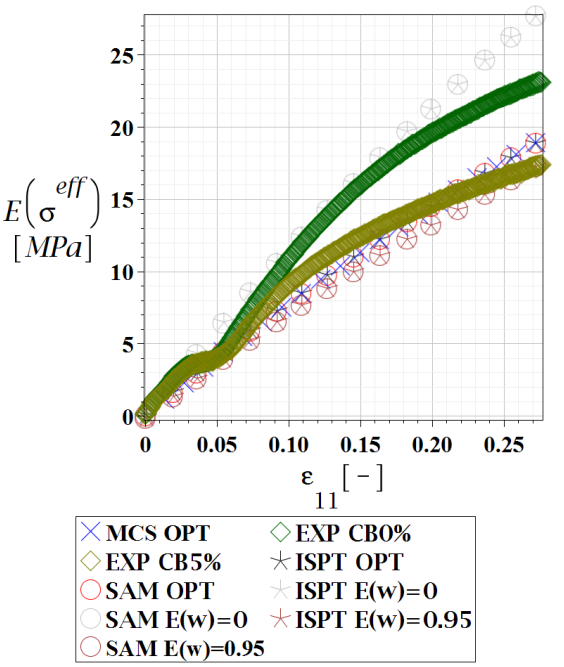

Fig. 6.35 Expected value of the effective stress $E(\sigma^{eff})$ w.r.t. uniaxial strain ε_{11}, optimized values of $E(w)$ and $\alpha(w)$ and three stochastic techniques.

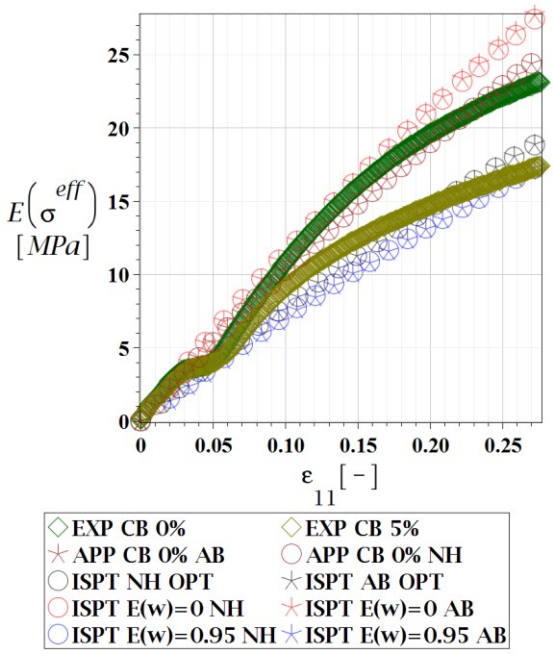

Fig. 6.36 Expected value of the effective stress $E(\sigma^{eff})$ w.r.t. uniaxial strain ε_{11}, optimized values of $E(w)$ and $\alpha(w)$ and two material formulations.

An effect of the underlying hyperelastic potential on expectations of the effective stress $E(\sigma^{eff})$ is presented on Fig. 6.36; it is also considered w.r.t. an increasing level of strain ε_{11}. Selected potentials return exactly the same expectation for the optimized solution of $E_{\xi}^{opt}(w)$ and $\alpha_{\xi}^{opt}(w)$ (given in black on the graph) irrespective to the given level of strain. This is also well justified by the closeness of the optimized values of $E_{\xi}^{opt}(w)$ and $\alpha_{\xi}^{opt}(w)$ for these two constitutive models reported in section 6.1.2. A slight difference of results between these constitutive models exists for $E(w)$=0.95 and $E(w)$=0 but it is only marginal. It means that these two potentials return slightly different result for a very high expectation of interface defects volume fraction.

This graph (Fig. 6.36) also presents an approximation of the virgin homogeneous material response with the two hyperelastic potentials with no defects given in brown and labeled with 'APP'. Similarly to the experimental part, it is always higher than the one for the defective composite, but still lower than the theoretical limit of polymer strengthening with CB particles. The coefficient of random dispersion of the input random variable $\alpha(w)$ has a very small impact on expectations of the effective stress and thus it is omitted here.

A perfect match of the proposed hyperelastic constitutive models and the experiments is not fully assured. They would require an additional factor accounting for the local softening that exponentially comes to zero outside the softening region. Such an approach would reduce its influence on response of this composite for strain levels unaffected by the softening. It is not proposed here because it has nothing in common with hyperelasticity and has a very limited effect on the response of this polymer for higher strain rates (see Fig. A.1). Its addition is intended in future research. Please note that the initial softening was not perfectly represented already for the virgin homogeneous material (dark green diamond on Fig. 6.36) and it is not possible to be replicated by any hyperelastic constitutive model known to the author.

At this point part (2) of the thesis is confirmed. The proposed augmented material model could be applied with success to the real case scenario basing on the selected hyperelastic formulations. It is applied with success to the objective HDPU based composite. This also confirms Hypothesis 2.

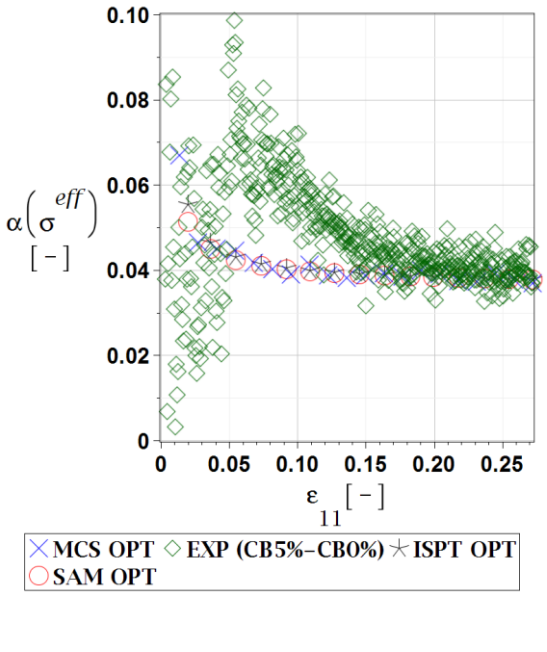

Fig. 6.37 Coefficient of variation of the effective stress $\alpha(\sigma^{eff})$ w.r.t. uniaxial strain ε_{11}, optimized values of $E(w)$ and $\alpha(w)$ and three stochastic techniques.

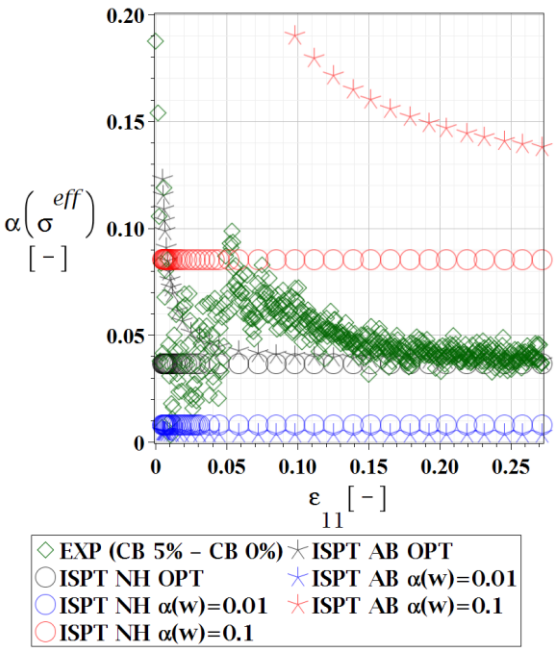

Fig. 6.38 Coefficient of variation of the effective stress $\alpha(\sigma^{eff})$ w.r.t. uniaxial strain ε_{11}, optimized values of $E(w)$ and $\alpha(w)$ and two material formulations.

The coefficients of random dispersion of the effective stress $\alpha(\sigma^{eff})$ are presented on Fig. 6.37 and Fig. 6.38. They firstly show that the difference in the coefficients of random dispersion considered in laboratory experiments $\left(\alpha\left(\sigma^{lab}_{CB\,5\%}\right)(\varepsilon_{11}) - \alpha\left(\sigma^{lab}_{CB\,0\%}\right)(\varepsilon_{11})\right)$ labeled as (EXP CB5%−CB0%) is very well captured by the proposed augmented constitutive model. This is especially true for the higher levels of the applied strain, where this difference stabilizes. Some fluctuation for low strains is not captured by this constitutive model, but it is most likely caused by the local softening mentioned above. The three stochastic methods return almost perfectly coinciding results. Only the SAM overestimates this coefficient a little for small strain levels; difference does not exceed 5% and vanishes with an increase of ε_{11}.

The two alternative hyperelastic constitutive models both return a very close estimation of $\alpha^{opt}_{\xi}(w)$, which are $\alpha^{opt}_{AB}(w)$=0.045903 and $\alpha^{opt}_{NH}(w)$=0.04541. Coefficient of random dispersion of the effective stress $\alpha(\sigma^{eff})$ returned by them for these optimized values is very close. It only differs for small levels of strain; above ε_{11}=0.07 this difference is less than 5% and above ε_{11}=0.13 it is already marginal. Coincidence of the results returned

by the two augmented constitutive models is even better for smaller $\alpha(w)$=0.01, for which they perfectly coincide. It gets much worse for $\alpha(w)$=0.1, where it is already more than twofold. Generally, the higher is the input coefficient of variation the higher is the difference between the results coming from different potentials.

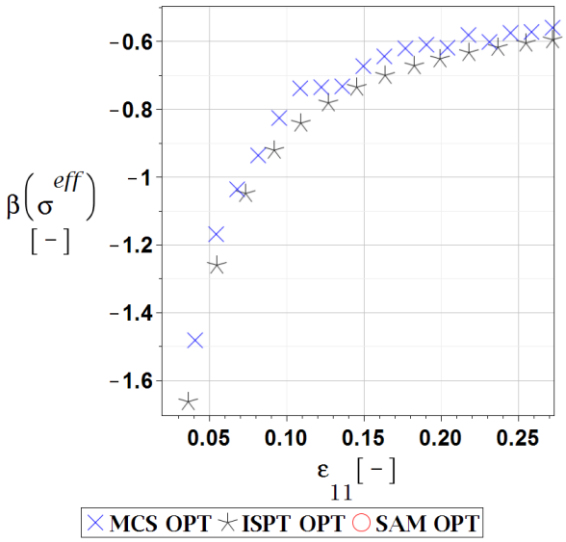

Fig. 6.39 Skewness of the effective stress $\beta(\sigma^{eff})$ w.r.t. uniaxial strain ε_{11}, optimized values of $E(w)$ and $\alpha(w)$ and two material formulations.

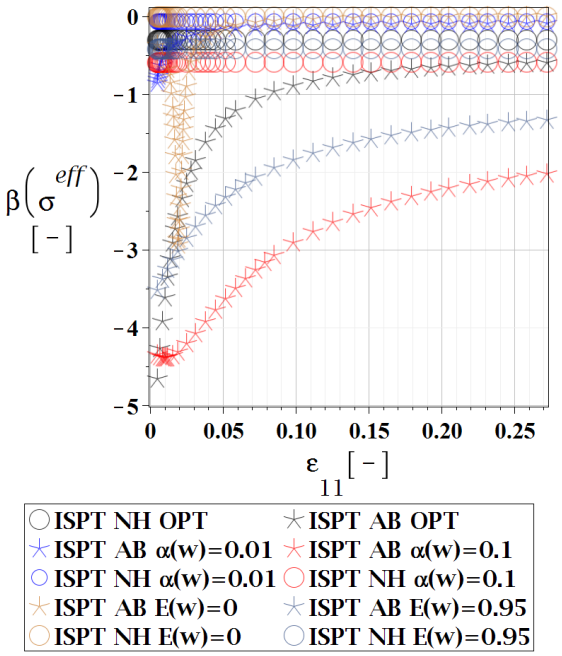

Fig. 6.40 Skewness of the effective stress $\beta(\sigma^{eff})$ w.r.t. uniaxial strain ε_{11}, optimized values of $E(w)$ and $\alpha(w)$ and two material formulations.

Skewness of the effective stress $\beta(\sigma^{eff})$ for the optimized characteristics of w is presented on Fig. 6.39 and Fig. 6.40. It is negative and always increases with an increase of strain ε_{11} to an apparent maximum of approx. −0.6. Again, coincidence of the ISPT and the MCS is good and the SAM returns different results; the MCS returns a little lower magnitude than the ISPT and shows a little bit of fluctuation. This may suggest that number of trials required by this method to obtain a full convergence may still be higher than the one proposed. This skewness returned by the Neo-Hookean augmented constitutive model is always smaller than the one for the Arruda-Boyce (see Fig. 6.40) and independent from the level of the strain ε_{11}. It is not the case of the Arruda-Boyce, which increases in magnitude together with a decrease of ε_{11}. Both, an increase of input expectation $E(w)$ and coefficient of random dispersion $\alpha(w)$ always cause an increase of skewness of the effective stress $\beta(\sigma^{eff})$;

the expectation seem to be more relevant, because it causes a bigger variation of this characteristic.

Kurtosis of the effective stress $\kappa(\sigma^{eff})$ is presented on Fig. 6.41 and Fig. 6.42 for the optimized statistical estimators of w. It is always positive and decreasing together with an increase of strain. This decrease is evident for the Arruda-Boyce and very limited for the Neo-Hookean augmented constitutive model. The Monte-Carlo simulation returns a little higher result than the generalized iterative stochastic perturbation method and the semi-analytical method returns a totally different result than the other methods. The MCS has still a little noise (not a full convergence) despite a very high number of trials used. This may be caused by a very extended representative function that is sensitive to changes in strain levels. Similarly to the skewness, the Arruda-Boyce has a higher magnitude of kurtosis than the Neo-Hookean augmented constitutive model that is much more sensitive to variations of strain close to 0.

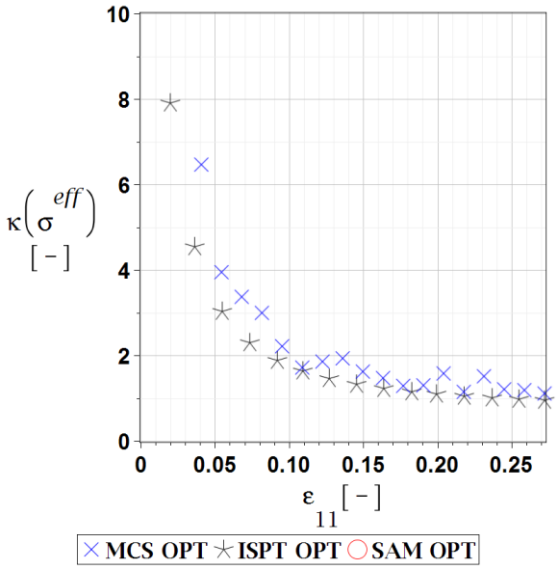

Fig. 6.41 Kurtosis of the effective stress $\kappa(\sigma^{eff})$ w.r.t. uniaxial strain ε_{11}, optimized values of $E(w)$ and $\alpha(w)$ and two material formulations.

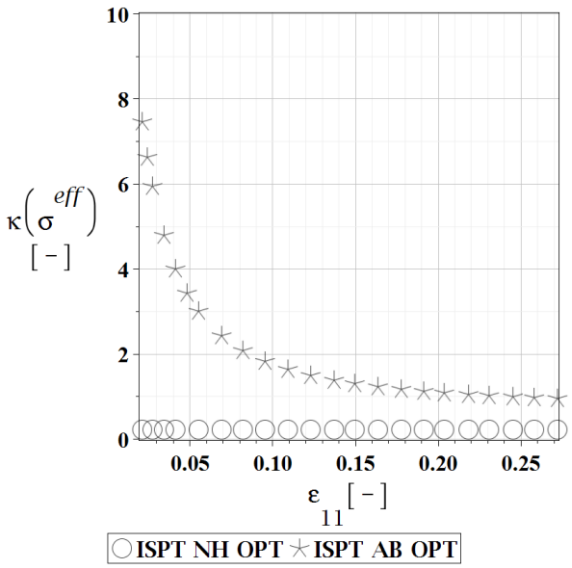

Fig. 6.42 Kurtosis of the effective stress $\kappa(\sigma^{eff})$ w.r.t. uniaxial strain ε_{11}, optimized values of $E(w)$ and $\alpha(w)$ and three stochastic techniques.

7. Concluding remarks and future prospects

7.1. Concluding remarks

[1] This dissertation reports a successful implementation of the interphase constitutive model in determination of the effective material properties, effective deformation energy and effective stress in hyperelastic particulate composites with stochastic interface defects. It also provides a theoretical formulation of the probabilistic homogenization for these materials (completion of Obj. 2) and implements it with use of computational algorithms. Applicability of the proposed approach is confirmed for the objective composite manufactured with Laripur 5020 high density polyurethane (HDPU) and F60 fullerene reinforcement. This is done with a joint usage of laboratory experiments performed by the author and a computational framework proposed in this dissertation. This work also provides an extensive analysis of dependence of these state functions on the volume fraction of interface defects, level of the applied strain and an underlying hyperelastic potential. It is additionally proved here that a joint usage of the generalized iterative stochastic perturbation technique (ISPT) and the finite element method allows reliable determination of the first four probabilistic characteristics of the above three state functions in the hyperelastic particle-reinforced composites with uncertain interface defects.

[2] In this dissertation a concept of the augmented hyperelastic constitutive model is introduced. This augmentation applies directly to all the material parameters of the arbitrary isotropic hyperelastic constitutive model. It introduces a single variable of the volume fraction of interface defects. This Gaussian variable describes an influence of the stochastic interface defects on the objective composite. Specifically, all the material parameters are considered as certain univariate polynomial functions of this input variable; other functions could be applied also. The proposed augmentation allows for prediction of the effective properties, effective deformations and effective stress in this defective composite that have an arbitrary volume of the interface defects (or, upon additional computations, their number and radius). Upon additional laboratory experiments, this concept also allows for determination of statistical estimators of this variable for a real composite and determination of its effective material properties together with their statistical estimators (expected value, coefficient of variation, skewness, kurtosis). This reverse approach is validated with success for the objective

composite under uniaxial stretch. The augmented material model is applicable for a wide range of composites ranging from these, whose stiffness is still higher than the one of the virgin homogeneous material (weakly defective composites) till composites, for which defects weaken the material more than the filler stiffens the matrix (highly defective composites). It also allows to verify the theoretical upper bound of stiffening when the bond between the matrix and the filler is perfect for $E(w)$=0.0 and the lower bound, when the filler is not bond at all to the matrix (friction is not accounted for). In this case $E(w)$=1. Importantly, the augmented material model may be applied for an arbitrary underlying hyperelastic constitutive model with variable number of material parameters and invariants incorporated in it. The only difference in the underlying algorithm is the number of the effective material parameters to use and complexity of computations (the more invariants and material properties, the more involving are computations). Such parameters are not possible to retrieve with purely analytical, numerical or experimental way. The available research in this area is purely theoretical / numerical and this dissertation is a first known to the author application of such theoretical considerations in practice. Even more importantly, it is done with a success (completion of Obj. 17).

The augmented material model works very well for the effective deformation energy of the objective composite under uncertain stretch, for which relative error is at most 5% (usually below a single percent); it is much smaller than the difference of this energy received for the three selected hyperelastic constitutive models. This augmentation works well also for prediction of the effective stress in this composite. Recovered state functions lay inside the applicability region of the proposed probabilistic homogenization. Statistical estimators of the input uncertain variable are close for the three selected hyperelastic constitutive models (completion of Obj. 18). The augmented material concept should be applied to a specific constitutive model, because it seems a little sensitive to the number of invariants included therein. This effect should be reduced upon application of more types of stretches in laboratory experiments. These would allow a better approximation of the initial material parameters in these constitutive models to the virgin homogeneous material that results in closer magnitudes of the effective stress.

[3] Proposed probabilistic homogenization algorithm enables determination of the above mentioned three state functions together with their first four stochastic

characteristics under uncertain volume fraction of Gaussian interface defects and for a variable level of the applied strain. It also allows determination of statistical estimators of the random input variable, which are the expected value and the coefficient of random dispersion; their resulting magnitudes reported for the objective composite lay inside the applicability region of the proposed probabilistic homogenization theory; this is valid for all the three selected underlying hyperelastic constitutive models. The proposed algorithm could also be used for other isotropic hyperelastic constitutive models independently of their initial assumptions and number of the effective material parameters (completion of Obj. 3). Magnitudes and stochastic characteristics of the effective material parameters vary for each of the constitutive models. Therefore, the computed results are valid only for the underlying constitutive model. This applies also for the effective stress. The results tend to be dependent on the invariants included in the underlying constitutive model and not so much on the number of material parameters. Proposed algorithm may be extended for the most general anisotropic case with an arbitrary predefined random dispersion of input uncertain variable. This would require higher amount of independent laboratory tests with ample number of trials. Additional laboratory experiments are, for example, pure shear, simple shear or biaxial stretch tests.

[4] The secondary algorithm proposed here allows determination of stochastic characteristics of the interface defect volume fraction in composites with stochastic interface defects. It could be applied for an arbitrary underlying hyperelastic isotropic material (completion of Obj. 4). Its efficiency was proved on the basis of the three selected underlying hyperelastic constitutive models. This algorithm is quite accurate already in its first iteration (7% relative error) and the stop criteria are met usually on the 6^{th} till 8^{th} iteration, depending on the underlying hyperelastic constitutive model; this observation is based on analyses done for the objective composite. Application of this algorithm is currently limited for the Gaussian input uncertain variable, but its extension to other probability distributions is also possible. This would require inclusion of additional steps that optimize higher stochastic characteristics of the effective stress and also a larger number of specimens in laboratory experiments. This is because the higher stochastic characteristics are much more sensitive to the number of specimens than the lower ones.

[5] Statistical estimators of the input uncertain variable (volume fraction of interface defects) computed for the objective composite are very close for the two selected underlying constitutive models, i.e. Arruda-Boyce and Neo-Hookean and differ slightly for the Mooney-Rivlin; for this model expectation is higher and the coefficient of variation – lower. The major reason for this is the fact that determination of estimators is based on the stochastic characteristics of the effective stress, which is higher for the Mooney-Rivlin (completion of objective Obj. 10). The expected values are relatively close to the theoretical limits. They vary from 0.87 till 0.97 of the interface volume. This is mainly because of the high reduction of stiffness in the objective composite in relation to the virgin homogeneous material. The coefficients of random dispersion are relatively low. They are smaller than 0.05 and very close to the ones of the effective stress in the objective composite; this is especially true for strains above 0.1. Variation of the input random variable for the Mooney-Rivlin exceeds a little the physical limit; for this underlying constitutive model a slightly bigger interphase volume should be proposed.

[6] Laboratory experiments included single and cyclic uniaxial stretch of the virgin homogeneous material (Laripur 5020) and the objective composite (completion of Obj. 5). They have been performed because of lack of laboratory data for this specific material and strain range; this is true especially when any variation or stochastic characteristics of its response is required for a realistic selection of computational input parameters. They were initially thought for the purpose of calibration and verification of the proposed algorithms, but brought valuable insights even without the numerical application. They firstly proved that the objective composite sustains smaller stress and is softer than the virgin homogeneous material. This is true for the first loading curve and the subsequent loadings also. The extent of relaxation after the first loading is much closer for both materials, but it is also smaller for the objective composite. The expected values of stress under uniaxial stretch are from 1.1 till 1.4 times higher for the virgin homogeneous material. This ratio increases slowly together with an increase of strain and it shows a small fluctuation for strains under 0.05. The standard deviation in the cyclic stretch is a little increasing together with an increase of strain level and it goes up to 1.4 MPa; it is higher for the objective composite. Coefficients of variation of stress in single stretch decrease together with an increase of strains; they stabilize for strains higher than 0.175. The ones computed for the virgin homogeneous material are

definitely smaller than the ones of the objective composite. Difference of these coefficients (of the virgin homogeneous material and the objective composite) is fluctuating at small strains and stabilizes for strains above 0.06 at a level of approximately 0.05 (completion of Obj. 6 and Obj. 7). Such behavior indicates that an addition of the filler and subsequent generation of the interface defects introduces additional dispersion of stress that has rather a constant character for higher strains. This observation is used in algorithms for determination of statistical estimators of the volume fraction of interface defects.

The sustained stress in the objective composite is always lower than the one in the virgin homogeneous material, which indicates that interface defects can not only affect the theoretical reinforcing limit but also can actually make the composite softer than this matrix. This proves their importance already during laboratory experiments; this observation is further supported by numerical experiments. Quite importantly, coefficient of variation of stress in the matrix recovered in laboratory study $\alpha(\sigma^m_{lab})$ clearly depends upon the strain level; its difference for small strain levels (linear elastic region) and high strain rates (hyperelastic region) is almost tenfold; this coefficient $\alpha(\sigma^m_{lab})$ is remarkably larger for low strain levels. This is fundamental information for any uncertainty study in composites and also in the virgin homogeneous material. This is because it strongly undermines a selection of a constant level of randomness in material for all the strain levels. One should instead provide some functional representation of the material randomness w.r.t. the strain, which complicates the stochastic computations. This affects especially the Monte-Carlo simulations, which must be repeated for different strain levels.

[7] The stress-strain curve of the virgin homogeneous material in uniaxial stretch is best approximated by the Arruda-Boyce model among eight verified constitutive models. It is also fitted very well by the Neo-Hookean and Mooney-Rivlin models (completion of Obj. 8). They all are very close to the experimental result and also presented plausible relations of the pure shear and simple shear tests. As expected, neither constitutive model was able to predict the local softening observed during laboratory experiments. Its existence affected the fitting accuracy, but additional parameters were not included for better fitting. This is because the objective composite remains hyperelastic for higher strains and also because the algorithms were aimed

at hyperelastic constitutive models by only. A dedicated constitutive model for the objective composite is planned for future research.

[8] The response surface method was introduced, implemented computationally and applied for the state functions of the objective composite. It approximates very well the effective deformation energy and the effective stress. Total relative error of this approximation does not exceed 3% for both state functions. A three-step procedure proposed for its optimization proves to be suitable and ensures a very high correlation (above 0.9999) and low sum of square errors of this approximation even for low rank polynomials; this is achieved already for rank 3 full bivariate polynomials and exemplified in this dissertation for the effective deformation energy. An additional visual verification prevents overfitting and allows identification of any local effects invisible in the numerical criteria. This is especially relevant for deformation energies, whose differences in magnitudes for low and high strains are very high (completion of Obj. 13). The proposed approach could be further extended to multivariate polynomials and used directly for problems with multiple input random variables (completion of Obj. 1). It is introduced as a first step for consideration of more than one uncertain parameter or/and variable.

[9] The effective material parameters of the defective composite are recovered according to a four-step process described in Appendix B. They are all positive and have a smooth relation with the volume fraction of interface defects. The defects decrease all the effective material properties for the selected underlying constitutive models. The only exception is a measure of the limiting network stretch for Arruda-Boyce model; it initially increases and reaches a maximum at w=0.65 and then decreases slightly for higher volume fraction of defects. The other parameters are reduced by up to 35% of their initial value for a perfectly bond composite (at w=0.95). This reduction is reached for only 5% of an interphase and corresponds to a significant reduction of sustained (effective) stress also (completion of Obj. 9). Magnitudes and number of material parameters differ among the selected underlying constitutive models and so does their relation to the input random variable. Thus, they must be considered separately for stochastic calculations and their fluctuation is not interchangeable. This is also the main reason why the probabilistic homogenization algorithm and the augmented material model concept was designed to be applicable for an arbitrary underlying hyperelastic constitutive model.

[10] Stochastic characteristics of the effective composite parameters are inherent for each of these parameters. They have an independent relation with the level of dispersion of the input uncertain parameter and a non-unique dependence on the expectation of interface defects volume fraction. According to the results, each parameter should be treated as a separate random variable in constitutive model of the defective composite (completion of Obj. 11). Expectations of these parameters decrease together with an increase of defects volume and are rather indifferent to the random dispersion of the input; it affects expectations of the highly defective interface by only. Random dispersion of these parameters tends to be higher than the dispersion of the volume fraction of interface defects for high expected values and it is much lower for expected values below 0.5. Skewness is generally negative, increases in magnitude together with coefficient of variation of the input random variable and also increases together with an increase of its expectation. Kurtosis has no common trend among different effective material properties.

[11] In this dissertation stochastic characteristics of the effective material parameters are recovered for the objective composite (completion of Obj. 12). Magnitudes of these characteristics are reported here as closed intervals determined upon application of three independent stochastic methods. These intervals are bigger for the higher characteristics and coincide to a single point with precision of four digits for the expectations and also coefficients of variation (with an exception to Arruda-Boyce). They may be used directly in fitting of a selected distribution function defining each of them. Upon this step, the effective material parameters may be directly applied in probabilistic analysis of structural elements. This was not possible prior to application of the proposed algorithm simply because the interface defects are practically impossible to quantify by separated laboratory (or numerical) experiments, especially when their statistical estimators are sought. Application of these uncertain parameters in composite constitutive model results in statistical estimators of its deformation and stress being dependent on the strain level, which also answers the problem indicated in [6].

[12] Effective deformation energy of composite with the stochastic interface defects is considerably decreased together with an increase of the volume fraction of interface defects for an entire spectrum of strains verified in this dissertation. Extent of this decrease is up to 40%. This also applies for the expectations of this strain energy, which is decreased in similar manner; these expectations are indifferent to the level

of statistical dispersion of defects volume fraction. An increase of expectation of the input random variable also affects the higher stochastic characteristics of the effective deformation energy. Coefficient of variation and kurtosis is increased, while the skewness decreased together with its decrease. These characteristics also increase considerably together with an increase of dispersion of the input random variable. The proposed defective interface constitutive model catches degradation of the composite deformation energy independently from the applied hyperelastic potential. This is verified here by a relative error study of the FEM approximations, which are always kept below a single percent. The above observation also proves that the effective deformation energy can be approximated w.r.t. the volume fraction of interface defects. This is valid with an assumption that for the defective composite its material coefficients depend only on this variable and that they are constant for all the levels of the strain in range of $\varepsilon_{11} \in (0, 0.275)$ (completion of Obj. 14, part 1 and Obj. 15, part 1).

[13] Effective stress of the composite with stochastic interface defects could be higher or considerably lower (up to 35%) than stress in the virgin homogeneous material under the same level of the strain. This mainly depends on the extent of stochastic interface defects. They decrease the effective stress of the composite to such an extent that a highly defective interphase cancels all the positive effect of a stiff filler. A theoretical limit for strengthening of the composite with 5% CB that is considered here is approx. 1.2. A magnitude of the effective stress reported from the proposed algorithm is not unique for the three selected hyperelastic potentials. They are within 0.5% difference for the Arruda-Boyce and Neo-Hookean formulations, but up to 30% higher for the Mooney-Rivlin. This may be affected by their formulation, where the first two of them depend on the first invariant, while the Mooney-Rivlin underlying model – on the first two invariants (completion of Obj. 14, part 2).

[14] Stochastic characteristics of the effective stress have been recovered for the three hyperelastic potentials selected in the fitting process of the matrix and with use of the three independent stochastic methods (ISPT, SAM, MCS). They have been computed for strains below 0.275 and coefficient of random dispersion of the input of up to 0.25. Results produced for the three hyperelastic potentials were not exactly unique. The ones for the Mooney-Rivlin have much higher expectations and for the Arruda-Boyce - higher magnitude of skewness and kurtosis than these reported for

the alternative potentials. The only characteristic that have a very coinciding results for all of them is the coefficient of variation. The general influence of the input coefficient of variation $\alpha(w)$ and the level of strain ε_{11} is, however, very similar for all the potentials (completion of Obj. 15, part 2). Expected value of volume fraction of interface defects has a very similar influence on stochastic characteristics of the effective stress for all the three hyperelastic potentials. Its increase always decreases the expectations of this stress, increases the coefficient of variation, and increases magnitude of both, the skewness and kurtosis (the only exception for this rule is Arruda-Boyce potential and $E(w)=0.1$). According to the above observation, the interface defects not only decrease the effective stress but also increase its dispersion and higher stochastic characteristics. This also means that a PDF of the effective stress under uncertain volume fraction of interface defects is distant from Gaussian.

Stress curve of the objective composite under uniaxial stretch is approximated quite well by the recovered effective stress curve. Accuracy of this approximation is not worse than an initial approximation of this curve for the virgin homogeneous material by the underlying hyperelastic constitutive models. Approximation of coefficient of random dispersion of this stress is also quite accurate, especially for higher levels of the strain above 0.13. The above observations are valid for all the three underlying hyperelastic constitutive models. Corresponding statistical estimators of the input random variable lay inside the applicability region of the proposed probabilistic homogenization theory. These results are expected to be even better for composites not having the initial softening region. Without any doubts, the proposed algorithm allowed for computation of the effective stress and also effective material properties of composite with stochastic interface defects together with their stochastic characteristics, in particular these of the objective composite (completion of Obj. 20).

[15] Stochastic characteristics of the effective deformation energy and the effective stress are both dependent on the level of the strain. This dependence is higher for the deformation energy and especially visible for strains close to zero and on transition from linear elasticity to hyperelasticity. This fact should not be disregarded in probabilistic calculations on structural level that use such kind of composites. The proposed augmented material model already accounts for it and given algorithms allow for determination of the corresponding effective material parameters (completion of Obj. 16).

[16] All the stochastic computations have been performed here with use of three independent stochastic methods. They are the generalized iterative stochastic perturbation, semi-analytical and crude Monte-Carlo simulation methods. This is done to verify correctness of their results that are analyzed here and also to verify, which one is most suitable in context of accuracy and computation time. This approach additionally enables providing an interval of values in which certain characteristics lay even when the methods are not perfectly coinciding. This agreement of the results is very high for the effective material properties and not perfect for the effective deformation energy and the effective stress under uniaxial stretch. Expectedly, the lower stochastic characteristics (expected value and coefficient of variation) are almost always approximated very well by all the methods and the higher ones (coefficient of skewness and kurtosis) have much lower coincidence among the selected methods. This coincidence is also progressively worse together with an increase of coefficient of random dispersion of the input and also an increase of its expected value. This is especially visible for the effective stress independently of the underlying constitutive model, but reported also for the other state functions. A high divergence is noted for the semi-analytical method in higher stochastic characteristics of the effective deformation and the effective stress. This is especially visible for higher coefficients of random dispersion of the input. This indicates that this method is not perfectly suited for hyperelastic composites; it still can be used for the effective material properties (completion of Obj. 19).

The level of uncertainty in the objective composite is not very high - coefficient of variation of the effective stress is approx. 0.05. In this region the generalized iterative stochastic perturbation coincides very well with the Monte-Carlo simulation and, conditionally, also the semi-analytical method does. This perfectly justifies calculation of statistical estimators of the input by the stochastic perturbation method by only. A good coincidence of this methods also justifies correctness of computed stochastic characteristics of the effective material parameters. The effective state functions in the composite with stochastic interface defects all have a non-Gaussian distribution, because they demonstrate a non-zero skewness and kurtosis. They became more distant from it together with an increase of expectations of the volume fraction of interface defects. Stochastic characteristics of the state functions and the effective material parameters are not unique for all the hyperelastic potentials even though they are based

on exactly the same experimental results. This means that a choice of potential not only has an impact on the magnitude of the effective stress, but also on its dispersion and probability density; as already mentioned above, level of the strain also has an impact on the effective deformation energies and the effective stress, but not on the effective material properties. According to the above, the PDF of each effective material parameter and effective state variable depends on the choice of the hyperelastic constitutive model and, obviously, on the extent of stochastic interface defects.

[17] The ISPT solution ensures almost perfect coincidence of results with a classical Monte-Carlo simulation; it is perfect for expectations and coefficients of variations and very high for skewness and kurtosis. This has been verified for expected values of volume fraction of interface defects $E(w)$ from 0.1 till 0.96, for its coefficient of variation $\alpha(w)$ up to 0.25 (0.15 for effective material properties) and for the strain level below 0.275. Small inaccuracy is reported only for skewness and kurtosis for the highest considered expected values of the input uncertain variable and its coefficient of random dispersion larger than 0.11; this level of input dispersion is more than twice higher than the one observed in the objective composite. This proves that the ISPT method is applicable for the considered stochastic process. It is much less computationally intensive than the Monte-Carlo simulation technique and provides a better coinciding result than the semi-analytical method (confirmation of Hypothesis 3).

7.2. Future prospects

Future research attentions will be focused on four particular efforts

1. extension of the proposed probabilistic homogenization framework to incorporate hysteresis in this material,
2. extension of the applicability region to higher strains above 100%, as in the preliminary laboratory experiment (see Fig. A.1),
3. extension of the proposed probabilistic homogenization algorithm to cover fully anisotropic composites and
4. introduction of single or multiple non-Gaussian variables in the current ISFEM analysis of the state functions.

A preliminary study for stochastic hyperelastic response with hysteresis has been already performed for the virgin homogeneous material and published in [70].

Numerical approximation of an initial stress-strain relation including hysteresis is shown on the below Fig. 7.1.

Applicability region of the proposed methodology to determine the effective state functions in composites with stochastic interface defects is currently verified for strains until 0.275. Its extension is possible, but would require an additional remeshing in the FEM during deformation process and also additional sets of laboratory tests.

Anisotropy is quite well known for single-phase materials [326,327]. In composites it is a relatively new topic that occurs not only in the reversible elastic region of their deformation. Consideration of some anisotropic models of hyperelasticity and theoretical introduction of anisotropic nonlinear probabilistic homogenization would be highly valuable. This would require consideration of additional types of deformation of the objective composite in the numerical and also experimental context.

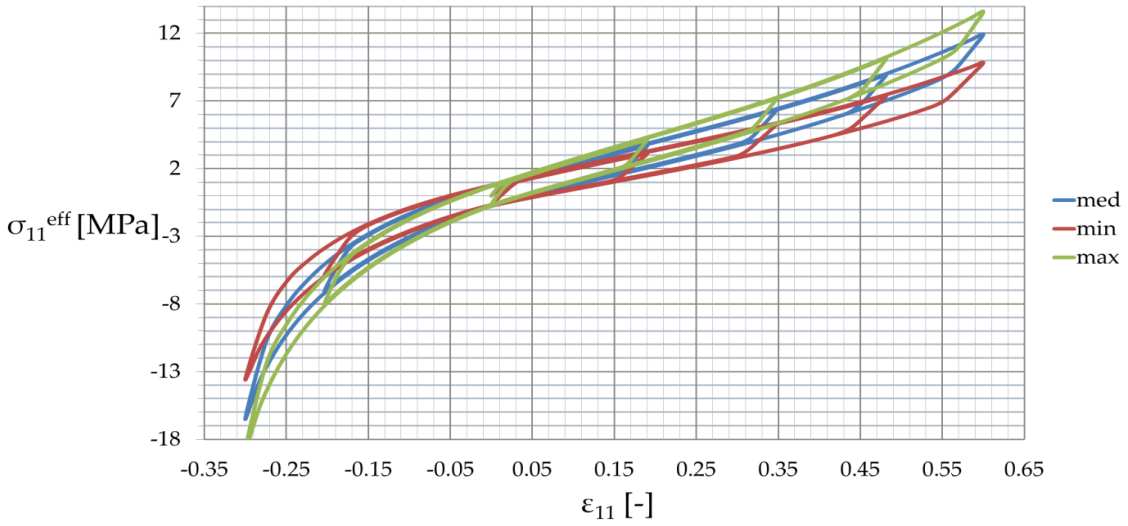

Fig. 7.1 Stress-strain relation of hyperelastic medium under cyclic loading. Study for the virgin homogeneous material [70].

It is assumed here that the volume fraction of interface defects is Gaussian. This assumption is well justified, but waiving it would also be profitable in case when some information on the interface defects is available. Some commonly used distribution to consider are log-normal [277], Gumbell [328,329], Weibull [330] and other distributions [331,332,333]. A secondary direction for extension of the stochastic calculus is theoretical formulation and numerical implementation of probabilistic homogenization for multiple correlated input uncertain variables

or parameters. This is important, because commonly a wider set of uncertain parameters affects a single state function. Summation of their separated influence is not sufficient simply because of their cross-effect and possible covariance. The first additional random variable enriching the proposed constitutive model may be the strain, whose measurement is subjected to inaccuracy resulting in its statistical dispersion. A relevant bivariate response surface is already determined in this dissertation.

Acknowledgements and funding

The author would like to acknowledge financial support of

- the grant 2016/21/N/ST8/01224 from the National Science Center in Cracow, Poland,
- the scholarship form the Minister of Higher Education for the outstanding young scientists SMN/16/0563/2020,
- the IACM scholarship for participation in WCCM & ECCOMAS Congress 2020,
- the IASSAR scholarship for participation in ICOSSAR Conference 2017,
- the ECCOMAS scholarship for participation in ECCOMAS Congress 2016,
- the scholarship from Rector's Fund of Lodz University of Technology RNN/WFS/27/2018,
- the scholarships from Dean's Fund for Young Investigators WBAS/17/2021, WBAS/MN/11/2019, WBAS/MN/30/2018,
- the Erasmus+ scholarship at Politecnico di Milano, Milan, 2014,
- the Erasmus scholarship at Technische Universität Wien, Vienna, 2013.

The author further acknowledges that *this research was supported in part by PLGrid Infrastructure*. This especially concerns deterministic part of numerical experiments.

Literature

[1] J E Mark, *Physical properties of polymers handbook*, 2nd ed. New York, USA: Springer, 2007.

[2] G Heinrich, M Klűppel, and T A Vilgis, "Reinforcement of elastomers," *Curr. Opin. Solid State Mater. Sci.*, vol. 6, pp. 195-203, 2002.

[3] T A Vilgis, G Heinrich, and M Klüppel, *Reinforcement of polymer nanocomposites: Theory, experiment and applications*. Cambridge, USA: University Press, 2009.

[4] M Khalifa, S Anandhan, G Wuzella, H Lammer, and A R Mahendran, "Thermoplastic polyurethane composites reinforced with renewable and sustainable fillers – a review," *Polym-Plast Tech. Mat.*, vol. 59, no. 16, pp. 1751-1769, 2020.

[5] B Masa, L Nahlik, and P Hutar, "Particulate composite materials: Numerical modeling of a cross-linked polymer reinforced with alumina-based particles," *Mech. Compos. Mater.*, vol. 49, pp. 421-428, 2013.

[6] M R Delfani and V Bagherpour, "Overall properties of particulate composites with periodic microstructure in second strain gradient theory of elasticity," *Mech. Mater.*, vol. 113, pp. 89-101, 2017.

[7] Y Fukahori, "The mechanics and mechanism of the carbon black reinforcement of elastomers," *Rubber Chem. Techn.*, vol. 76, pp. 548-566, 2003.

[8] M Kamiński and D Sokołowski, "Dual probabilistic homogenization of the rubber-based composite with random carbon black particle reinforcement," *Comp. Struct.* , vol. 140, pp. 783-797, 2016.

[9] D Sokołowski and M Kamiński, "Probabilistic homogenization of random composite with ellipsoidal particle reinforcement by the iterative stochastic finite element method," in *Computer methods in mechanics (CMM2017): Proceedings of the 22nd International Conference on Computer Methods in Mechanics*, J Podgorski et al., Eds. Gdańsk: AIP Conference Proceedings, 2018, vol. 1922, ch. 020003, pp. 1-10.

[10] M Kamiński and D Sokołowski, "Stochastic interphase effect in rubber-carbon black composites in homogenization method," in *ICCS19 19th International Conference on Composite Structures*, Porto, 2016, p. 33.

[11] D Sokołowski and M Kamiński, "Computational homogenization of anisotropic carbon/rubber composites with stochastic interface defects," in *Carbon-based nanofillers and their rubber nanocomposites*, Y Srinivasarao et al., Eds.: Elsevier, 2019, ch. 11.

[12] J Wawrzynek, *Methods of statistical reasoning and description (in Polish)*. Wrocław, Poland: Economics Academy Publisher, 2007.

[13] I N Bronsztejn, K A Siemiendiajew, G Musiol, and H Muhling, *Modern compedium of mathematics (in Polish)*, 5th ed. Warsaw, Poland: Polish Scientific

Publisher, 2009.

[14] R E Melchers, *Structural reliability analysis and prediction*, 3rd ed. Chichester, England: Wiley, 2002.

[15] X Wang, X Xu, and S U Choi, "Thermal conductivity of nanoparticle-fluid mixture," *J. Thermophys. Heat Trans.*, vol. 13, pp. 474-480, 1999.

[16] C Lopes-Pernia et al., "Optimizing the homogenization technique for graphene nanoplatelet/yttria tetragonal zirconia composites: Influence on the microstructure and the electrical conductivity," *J. Alloy. Comp.*, vol. 767, pp. 994-1002, 2018.

[17] C Miehe, J Diez, S Goktepe, and L Schanzel, "Coupled thermovisco-elastoplasticity of glassy polymers in the logarithmic strain space based on the free volume theory," *Int. J. Sol. Struct.*, vol. 48, no. 13, pp. 1799-1817, 2011.

[18] R M Christensen, *Mechanics of composite materials*. New York, USA: Wiley, 1979.

[19] S Timoshenko and J N Goodier, *Elasticity theory*. New York, USA: McGraw-Hill, 1951.

[20] C Zener, *Elasticity and anelasticity of metals*. Chicago, USA: University of Chicago, 1948.

[21] J D Humphrey, *Cardiovascular solid mechanics: cells, tissues and organs*. New York, USA: Springer, 2002.

[22] S Glotzer and W Paul, "Molecular and mesoscale simulation methods for polymer materials," *Annual Rev. Mater. Res.*, vol. 32, pp. 401-436, 2002.

[23] A Bhowmick, *Current topics in elastomers research*. Boca Raton, USA: CRC Press, 2008.

[24] R M Christensen, *Theory of viscoelasticity*. Dover, England: Dover Publishing, 2010.

[25] J L Chaboche, "A review of some plasticity and viscoplasticity constitutive theories," *Int. J. Plast.* , vol. 24, pp. 1642-1693, 2008.

[26] B Yang, B Kim, and H Lee, "Predictions of viscoelastic strain rate dependent behavior of fiber-reinforced polymeric composites," *Compos. Struct.* , vol. 94, no. 4, pp. 1420-1429, 2012.

[27] M Ostoja-Starzewski and J Zhang, "Mesoscale bounds in viscoelasticity of random composites," *Mech. Res. Comm.* , vol. 68, pp. 98-104, 2015.

[28] G Heinrich, J Struve, and G Gerber, "Mesoscopic simulation of dynamic crack propagation in rubber materials," *Polymer*, vol. 43, pp. 395-401, 2002.

[29] T Harth, S Schwan, J Lehn, and F Kollmann, "Identification of material parameters for inelastic constitutive models: statistical analysis and design of experiments," *Int. J. Plast.*, vol. 20, pp. 1403-1440, 2004.

[30] J Mandel, F L Roth, M N Steel, and R D Stiehler, "Measurement of the aging of rubber vulcanizates," *J. Res. Nat. Bureau Stand. – C: Engrg. & Instr.*, vol. 63C, no. 2, pp. 141-145, 1959.

[31] P H Mott and C M Roland, "Aging of natural rubber in air and seawater," *Rubber Chem. Technol.* , vol. 74, pp. 79-88, 2001.

[32] L Mullins, "Softening of rubber by deformation," *Rubber Chem. Technol.*, vol. 42, pp. 339-362, 1969.

[33] R Ogden and D Roxburgh, "A pseudo-elastic model for the Mullins effect in filled rubber," *Proc. Roy. Soc.*, vol. 455, pp. 2861-2877, 1999.

[34] A Dorfmann and R Ogden, "A constitutive model for the Mullins effect with permanent set in particle reinforced rubber," *Int. J. Sol. Struct.*, vol. 41, pp. 1855-1878, 2004.

[35] H Lorenz, M Klüppel, and G Heinrich, "Microstructure-based modeling and FE implementation of filler induced stress softening and hysteresis of reinforced rubbers," *J. Appl. Math. Mech. Z. Angew. Math. Mech.*, vol. 92, no. 8, pp. 608-631, 2012.

[36] K Y Volokh, "On modeling failure of rubber-like materials," *Mech. Res. Comm.*, vol. 37, pp. 684-689, 2010.

[37] K Y Volokh, "Review of the energy limiters approach to modeling failure of rubber," *Rubber Chem. Technol.*, vol. 86, no. 3, pp. 470-487, 2013.

[38] L R Treloar, *The physics of rubber elasticity*. Oxford, England: Clarendon Press, 1975.

[39] G Heinrich, E Straube, and G Helmis, "Rubber elasticity of polymer networks: theories," *Adv. Polymer Sci.*, vol. 85, pp. 33-87, 1988.

[40] G A Holzapfel, *Nonlinear solid mechanics: A continuum approach for engineering*. Chichester, England: Wiley, 2000.

[41] C Truesdell and W Noll, *The non-linear field theories of mechanics*, 3rd ed. Berlin-Heidelberg, Germany: Springer, 2004.

[42] T Sussman and K J Bathe, "A finite element formulation for nonlinear incompressible elastic and inelastic analysis," *Comput. Struct.*, vol. 26, pp. 357-409, 1987.

[43] G Heinrich and M Kaliske, "Theoretical and numerical formulation of a molecular based constitutive tube-model of rubber elasticity," *Comput. Theor. Polym. Sci.*, vol. 7, pp. 227–241, 1997.

[44] M Kaliske and H Rothert, "On the finite element implementation of rubber-like materials at finite strains," *Engrg. Comput.* , vol. 14, no. 2, pp. 216–232, 1997.

[45] T Jin, L Yu, Z Yin, and H Xiao, "Bounded elastic potentials for rubberlike materials with strain-stiffening effects," *Z. Angew. Math. Mech.*, vol. 94, pp. 1-12, 2014.

[46] M Mooney, "A theory of large elastic deformation," *J. Appl. Phys.*, vol. 11, no. 9, pp. 582–592, 1940.

[47] R S Rivlin, "Large elastic deformations of isotropic materials. IV. Further developments of the general theory," *Phil. Trans. R. Soc. Lond. Ser. A: Math.*

Phys. Sci., vol. 241, no. 835, pp. 379–397, 1948.

[48] R W Ogden, "On the overall moduli of non-linear elastic composite materials," *J. Mech. Phys. Solids*, vol. 22, no. 6, pp. 541-553, 1974.

[49] R W Ogden, *Non-linear elastic deformations*, 1st ed. Dover, England: Dover Publ., 1984.

[50] O H Yeoh, "Some forms of the strain energy function for rubber," *Rubber Chem. Technol.*, vol. 66, no. 5, pp. 754-771, 1993.

[51] E Arruda and M C Boyce, "A three-dimensional model for the large stretch behavior of rubber elastic materials," *J. Mech. Phys. Solids*, vol. 41, no. 2, pp. 389-412, 1993.

[52] A N Gent, "A new constitutive relation for rubber," *Rubber Chem. Technol.*, vol. 69, pp. 59–61, 1996.

[53] M Kaliske and G Heinrich, "An extended tube-model for rubber elasticity: statistical-mechanical theory and finite element implementation," *Rubber Chem. Technol.*, vol. 72, pp. 602-632, 2010.

[54] P Dłużewski, "Anisotropic hyperelasticity based upon general strain measures," *J. Elasticity*, vol. 60, pp. 119-129, 2000.

[55] M Hossain and P Steinmann, "More hyperelastic models for rubber-like materials: consistent tangent operators and comparative study," *J. Mech. Behav. Mater.*, vol. 22, no. 1-2, pp. 27–50, 2013.

[56] H M James and E J Guth, "Theory of the elastic properties of rubber," *J. Chem. Phys.*, vol. 11, no. 455–481, 1943.

[57] E M Arruda and M C Boyce, "Anisotropy and localization of plastic deformation," *J. Mech. Phys. Solids.*, vol. 41, no. 389–412, 1993.

[58] P D Wu and E van der Giessen, "On improved 3-D non-Gaussian network models for rubber elasticity," *Mech. Res. Commun.*, vol. 19, pp. 427-433, 1992.

[59] P J Flory, "Thermodynamic relations for high elastic materials," *Trans. Farad. Soc.*, vol. 57, pp. 829-838, 1961.

[60] C Miehe, S Göktepe, and F Lulei, "A micro-macro approach to rubber-like materials—part I: The non-affine micro-sphere model of rubber elasticity," *J. Mech. Phys. Solids*, vol. 53, pp. 2231–2258, 2005.

[61] E Pucci and G Saccomandi, "A note on the Gent model for rubber-like materials," *Rubber Chem. Technol.*, vol. 75, pp. 839-851, 2002.

[62] O Lopez-Pamies, "A new I1-based hyperelastic model for rubber elastic materials," *C. R. Mec.*, vol. 338, no. 1, pp. 3-11, 2010.

[63] G Marckmann and E Verron, "Comparison of hyperelastic models for rubber-like materials," *Rubber Chem. Technol.*, vol. 79, pp. 835-857, 2006.

[64] Y Shen, K Chandrashekhara, W F Breig, and L R Oliver, "Neural network based constitutive model for rubber material," *Rubber Chem. Technol.*, vol. 77, no. 2, pp. 257-277, 2004.

[65] F Elhaouzi et al., "Hyperelastic behavior and dynamic mechanical relaxation in carbon black-polymer composites," *Polymer Comp.*, vol. 40, no. 8, pp. 3005-3011, 2019.

[66] F Fritzen and O Kunc, "Two-stage data-driven homogenization for nonlinear solids using a reduced order model," *Eur. J. Mech. A/Sol.*, vol. 69, pp. 201-220, 2018.

[67] X Li, Z Li, and Y Xia, "Three-dimensional numerical simulations on the hyperelastic behavior of carbon-black particle filled rubbers under moderate finite deformation," *Comp. Mater. Sci.* , vol. 55, pp. 157-165, 2012.

[68] A Shahabodini, R Ansari, and M Darvizeh, "Multiscale modeling of embedded graphene sheets based on the higher-order Cauchy-Born rule: Nonlinear static analysis," *Compos. Struct.*, vol. 165, pp. 25-43, 2017.

[69] I Temizer and T I Zohdi, "A numerical method for homogenization in non-linear elasticity," *Comput. Mech.*, vol. 40, no. 2, pp. 281-298, 2007.

[70] D Sokołowski and M Kamiński, "Hysteretic behavior of random particulate composites by the stochastic finite element method," *Materials*, vol. 12, p. 2909, 2019.

[71] M Leonard, M Wang, O Lopez-Pamies, and T Toshio Nakamura, "The nonlinear elastic response of filled elastomers: Experiments vs. theory for the basic case of particulate fillers of micrometer size," *J. Mech. Phys. Solids*, vol. 135, p. 103781, 2019.

[72] F López Jiménez, "Variations in the distribution of local strain energy within different realizations of a representative volume element," *Compos. Part B-Eng.*, vol. 176, p. 107111, 2019.

[73] Y Ban and Mi C, "On spherical nanoinhomogeneity embedded in a half-space analyzed with Steigmann–Ogden surface and interface models," *Int. J. Solids Struct.*, vol. 216, pp. 123-135, 2021.

[74] A Franus and S Jemioło, "Consistent polynomial expansions of stored energy function for incompressible hyperelastic materials," arXiv:2101.06169, 2021.

[75] T D Pallicity and T Böhlke, "Effective viscoelastic behavior of polymer composites with regular periodic microstructures," *Int. J. Solids Struct.*, vol. 216, pp. 167-181, 2021.

[76] S Avril, P Badel, and A Duprey, "Anisotropic and hyperelastic identification of in vitro human arteries from full-field optical measurements," *J. Biomech.*, vol. 43, no. 15, pp. 2978-2985, 2010.

[77] S Sakata, F Ashida, T Kojima, and M Zako, "Three-dimensional stochastic analysis using a perturbation based homogenization metod for elastic properties of composite material considering microscopic uncertainty," *Int. J. Sol. & Struct*, vol. 45, pp. 894-907, 2007.

[78] A L Kalamkarov and A G Kolpakov, *Analysis, design and optimization of composite structures*. New York, USA: Wiley, 1997.

[79] M Guedri, A M Lima, N Bouhaddi, and D Rade, "Robust design of viscoelastic structures based on stochastic finite element models," *Mech. Sys. Signal Proc.*, vol. 24, no. 1, pp. 59-77, 2010.

[80] A Clément, C Soize, and J Yvonnet, "Computational nonlinear stochastic homogenization using a nonconcurrent multiscale approach for hyperelastic heterogeneous microstructures analysis," *Int. J. Numer. Meth. Eng.*, vol. 91, pp. 799-824, 2012.

[81] S Nezamabadi, H Zahrouni, and J Yvonnet, "Solving hyperelastic material problems by asymptotic numerical method," *Comput. Mech.*, vol. 47, pp. 77-92, 2011.

[82] M Kamiński and D Sokołowski, "An introduction to stochastic finite element method analysis of hyper-elastic structures," *ECCOMAS Congress 2016 - Proceedings of the 7th European Congress on Computational Methods in Applied Sciences and Engineering*, vol. 3, pp. 6078-6090, 2016, ISSN: 00002016.

[83] Z Liu, M A Bessa, and W K Liu, "Self-consistent clustering analysis: An efficient multi-scale scheme for inelastic heterogeneous materials," *Comput. Method. Appl. Mech. Eng.* , vol. 206, pp. 319–341, 2016.

[84] B Staber and J Guilleminot, "Stochastic hyperelastic constitutive laws and identification procedure for soft biological tissues with intrinsic variability," *J. Mech. Behav. Biomed.*, vol. 65, pp. 743-752, 2017.

[85] B Staber and J Guilleminot, "Stochastic modeling of the Ogden class of stored energy functions for hyperelastic materials: the compressible case," *J. Appl. Math. Mech. Z. Angew. Math. Mech.*, vol. 97, no. 3, pp. 273-295, 2017.

[86] O Lopez-Pamies and M I Idiart, "Fiber-reinforced hyperelastic solids: a realizable homogenization constitutive theory," *J. Eng. Math.*, vol. 68, pp. 57-83, 2010.

[87] F López Jiménez, "Modeling of soft composites under three-dimensional loading," *Compos. Part B-Eng.*, vol. 59, pp. 173-180, 2014.

[88] B Staber and J Guilleminot, "Functional approximation and projection of stored energy functions in computational homogenization of hyperelastic materials: A probabilistic perspective," *Comput. Method. Appl. Mech.*, vol. 313, pp. 1-27, 2017.

[89] T Hien and M Kleiber, "On solving nonlinear transient heat transfer problems with random parameters," *Comput. Meth. Appl. Mech. Engrg*, vol. 151, pp. 287-299, 1998.

[90] D Xiu and G E Karniadakis, "A new stochastic approach to transient heat conduction modeling with uncertainty," *Int. J.Heat Mass Tran.*, vol. 46, pp. 4681-4693, 2003.

[91] Ł Figiel and M Kamiński, "Numerical probabilistic approach to sensitivity analysis in a fatigue delamination problem of a two layer composite," *Appl. Math. Comput.* , vol. 209, pp. 75-90, 2009.

[92] M Kamiński, "On probabilistic fatigue models for composite materials," *Int. J.*

Fatigue, vol. 24, no. 2-4, pp. 477-495, 2002.

[93] G Mustafa, A Suleman, and C Crawford, "Probabilistic micromechanical analysis of composite material stiffness properties for a wind turbine blade," *Compos. Struct.*, vol. 131, pp. 905-916, 2015.

[94] M Vořehovský, "Incorporation of statistical length scale into Weibull strength theory for composites," *Compos. Struct.*, vol. 92, no. 9, pp. 2027-2034, 2010.

[95] A Karakoç and J Freud, "A statistical failure initiation model for honeycomb materials," *Compos. Struct.* , vol. 95, pp. 154-162, 2013.

[96] M Kamiński, *The stochastic perturbation method for computational mechanics*, 1st ed. Chichester, England: Wiley, 2013, ISBN:9780470770825.

[97] M Kamiński, "On semi-analytical probabilistic finite element method for homogenization of the periodic fiber-reinforced composites," *Int. J. Numer. Met. Eng.*, vol. 86, no. 9, pp. 1144–1162, 2011.

[98] M E Cruz and A T Patera, "A parallel Monte-Carlo finite element procedure for the analysis of multicomponent media," *Int. J. Num. Meth. Engrg* , vol. 38, pp. 1087-1121, 1995.

[99] J E Hurtado, "Reanalysis of linear and nonlinear structures using iterated shanks transformation," *Comput. Method. Appl. M.*, vol. 191, no. 37-38, pp. 4215–4229, 2002.

[100] J E Hurtado and A H Barbat, "Monte-Carlo techniques in computational stochastic mechanics," *Arch. Comput. Meth. Engrg.*, vol. 5, no. 1, pp. 3-30, 1998.

[101] M Hamada, A Wilson, C Reese, and H Martz, *Bayesian reliability*. Berlin-Heildelberg, Germany: Springer, 2008.

[102] D J Lunn, A Thomas, N Best, and D Spiegelhalter, "WinBUGS - A Bayesian modelling framework: Concepts, structure, and extensibility," *Stat. Comput.*, vol. 10, no. 4, pp. 325-337, 2000.

[103] H Zimmermann, "Fuzzy set theory," *Wiley Interdisciplinary Review: Comput. Stat.*, vol. 2, no. 3, pp. 317-332, 2010.

[104] Z Li and H Pasternak, "Experimental and numerical investigations of statistical size effect in S235JR steel structural elements," *Constr. Build. Mater.*, vol. 206, pp. 665-673, 2019.

[105] Q Guo and A E Jeffers, "Finite-element reliability analysis of structures subjected to fire," *J. Struct. Eng.*, vol. 141, no. 4, p. 04014129, 2015.

[106] A Athmani, A Khemis, and A H Chaouche, "Buckling uncertainty analysis for steel pipelines buried in elastic soil Using FOSM and MCS methods," *Int. J. Steel Struct.*, vol. 19, pp. 381–397, 2019.

[107] N Metropolis and S Ulam, "The Monte Carlo method," *J. Ame. Stat. Assoc.*, vol. 44, pp. 335-341, 1949.

[108] A A Chojaczyk, A P Teixeira, L C Neves, J B Cardoso, and C Guedes Soares, "Review and application of artificial neural networks models in reliability analysis

of steel structures," *Struct. Saf.*, no. 52, pp. 78-89, 2015.

[109] W K Hastings, "Monte carlo sampling methods using Markov chains and their applications," *Biometrika*, vol. 57, no. 1, pp. 97-109, 1970.

[110] J S Bendat and A G Piersol, *Random data: Analysis and measurement procedures*. New York, USA: Wiley, 1971.

[111] A Doucet, S Godsill, and C Andrieu, "On sequential Monte Carlo sampling methods for Bayesian filtering," *Stat. Comput.*, vol. 10, no. 3, pp. 197-208, 2000.

[112] S N Wilkinson, J M Olley, T Furuichi, J Burton, and A E Kinsey-Henderson, "Sediment source tracing with stratified sampling and weightings based on spatial gradients in soil erosion," *J. Soil. Sed.*, vol. 15, no. 10, pp. 2038-2051, 2015.

[113] K Winkelmann, *Computation of reliability of civil engineering structures with simulation methods and with response surface method (in Polish)*. Gdańsk, Poland: Gdansk University of Technology, 2013.

[114] J C Helton and F J Davis, "Latin hypercube sampling and the propagation of uncertainty in analyses of complex systems," *Reliab. Eng. Syst. Safe.*, vol. 81, no. 1, pp. 23-69, 2003.

[115] D B Chung, M A Gutierrez, and L L Graham-Brady, "Efficient numerical strategies for spectral stochastic finite element models," *Int. J. Numer. Meth. Eng.*, vol. 64, no. 10, pp. 1334-1349, 2005.

[116] R G Ghanem and P D Spanos, *Stochastic finite elements: A spectral approach*. Berlin, Germany: Springer, 1991.

[117] R G Ghanem and P D Spanos, "Spectral techniques for stochastic finite elements," *Arch. Comput. Methods Eng.*, vol. 4, no. 1, pp. 63-100, 1997.

[118] P Sasikumar, A Venketeswaran, R Suresh, and S Gupta, "A data driven polynomial chaos based approach for stochastic analysis of CFRP laminated composite plates," *Compos. Struct.*, vol. 125, pp. 212-227, 2015.

[119] G Blatman and B Sudret, "An adaptive algorithm to build up sparse polynomial chaos expansions for stochastic finite element analysis," *Probabilistic Eng. Mech.*, vol. 25, no. 2, pp. 183-197, 2010.

[120] M Tootkaboni and L Graham-Brady, "A multiscale spectral stochastic method for homogenization of multiphase periodic composites with random material properties," *Int. J. Num. Meth. Engrg* , vol. 83, pp. 59-90, 2010.

[121] X F Xu and L Graham-Brady, "A stochastic computational method for evaluation of global and local behavior of random elastic media," *Comput. Method. Appl. M.*, vol. 194, no. 42-44, pp. 4362-4385, 2005.

[122] M Kleiber and T D Hien, *The stochastic finite element method*. Chichester, England: Wiley, 1992.

[123] W K Liu, T Belytschko, and A Mani, "Random field finite elements," *Int. J. Numer. Meth. Eng.*, vol. 23, pp. 1831-1845, 1986.

[124] B Pokusiński, "Reliability of selected diagrid steel bar constructions (in Polish),"

Lodz University of Technology, Lodz, Master Thesis 2020.

[125] M Kamiński, "Generalized perturbation-based stochastic finite element method in elastostatics," *Comput. Struct.*, vol. 85, no. 10, pp. 586-594, 2007.

[126] H G Matthies, C E Brenner, C G Bucher, and G C Soares, "Uncertainties in probabilistic numerical analysis of structures and solids," *Struct. Saf.*, vol. 19, no. 3, pp. 283-336, 1997.

[127] G Stefanou and M Papadrakakis, "Stochastic finite element analysis of shells with combined random material and geometrical properties," *Comput. Meth. Appl. M.*, vol. 193, no. 1-2, pp. 139-160, 2004.

[128] G Stefanou, D Savvas, and M Papadrakakis, "Stochastic finite element analysis of composite structures based on material microstructure," *Compos. Struct.*, vol. 132, pp. 384-392, 2015.

[129] P Sasikumar, R Suresh, and S Gupta, "Analysis of CFRP laminated plates with spatially varying non-Gaussian inhomogeneities using SFEM. ," *Compos. Struct.* , vol. 112, pp. 308-326, 2014.

[130] M Kamiński and P Świta, "Generalized stochastic finite element method in elastic stability problems," *Comput. Struct.*, vol. 89, pp. 1241-1242, 2011.

[131] R Honda, "Stochastic BEM with spectral approach in elastostatic and elastodynamic problems with geometrical uncertainty," *Eng. Anal. Bound. Elem.*, vol. 29, no. 5, pp. 415-427, 2005.

[132] M Kamiński, "Iterative scheme in determination of the probabilistic moments of the structural response in the stochastic perturbation-based boundary element method," *Comput. Struct.*, vol. 15, pp. 86-95, 2015.

[133] C Wang, Z Qiu, and D Wu, "Numerical analysis of uncertain temperature field by stochastic finite difference method," *Sci. China Ser. G.*, vol. 57, pp. 698-707, 2014.

[134] O Zienkiewicz, R Taylor, and J Zhu, *The Finite Element Method Set. Its Basis and Fundamentals*, 6th ed. Amsterdam: Elsevier, 2005.

[135] A H Ang and W H Tang, *Probability concepts in engineering. Emphasis on applications in civil and environmental engineering*. London, England: Wiley, 2007.

[136] O Ditlevsen and H O Madsen, *Structural reliability methods*. New York, USA: Wiley, 1996.

[137] P Thoft-Christensen and M J Baker, *Structural reliability theory and its applications*. Berlin, Germany: Springer, 1982.

[138] J Murzewski, *Safety of civil engineering structures (in Polish)*. Warsaw, Poland: Arkady, 1970.

[139] P Marek, M Gustar, and T Anagnos, *Simulation-based reliability assessment for structural engineers*. Boca Raton, USA: CRC Press, 1996.

[140] T A Cruse, *Reliability-based mechanical design*. New York, USA: Marcel

Dekker, 1997.

[141] A Haldar and S Mahadevan, *Reliability assessment using stochastic finite element analysis*. New York, USA: Wiley, 2000.

[142] M Kamiński and J Szafran, "Stochastic finite element analysis and reliability of steel telecommunication towers," *CMES: Comput. Model. Eng. Sci.*, vol. 97, pp. 269-276, 2012.

[143] S Woliński and K Wróbel, *Reliability of civil engineering structures (in Polish)*. Rzeszów, Poland: Rzeszow University of Technology Publisher, 2001.

[144] D Sokołowski and M Kamiński, "Some reliability issues of the corrugated I-beam girder," *Engrg. Trans.*, vol. 63, no. 3, pp. 297-315, 2015.

[145] D Sokołowski and M Kamiński, "Reliability analysis of the corrugated I-beam girder with ribs," *ICE Proc. Engrg. Comput. Mech.*, vol. 168, pp. 49-58, 2015.

[146] D Sokołowski and M Kamiński, *SFEM reliability analysis of the corrugated steel I-beam girder with vertical ribs*. Warsaw, Poland: Proc. XX International Seminar of IASS Polish Chapter, 2014.

[147] D Sokołowski and M Kamiński, *An introduction to the SFEM reliability analysis of the corrugated steel I-beam girder*. Olsztyn, Poland: Proc. XIX International Seminar of IASS Polish Chapter, 2013.

[148] D Sokołowski, "Comparative analyisis of reliability of sinusoidal web girder using first order methods (FORM) and second order methods (SORM)," in *Budmika 2014 National student civil engineering conference: full papers (in Polish)*, T Garbowski and D Siniacki, Eds. Poznań, Poland, 2014, pp. 215-225.

[149] D Sokołowski and M Kamiński, "Reliability analysis of the corrugated web I girder under corrosion or fire by the stochastic finite element method and SORM," in *Safety, reliability, risk, resilience and sustainability of structures and infrastructure 12th Int. Conf. on Structural Safety and Reliability*, C Bucher, B R Ellingwood, and D M Frangopol, Eds. Vienna, Austria: TU-Verlag, 2017, pp. 2779 – 2788.

[150] D Sokołowski, M Kamiński, and M Strąkowski, "Stochastic finite element method reliability analysis of the corrugated I-beam girder," *CMES: Comput. Model. Eng. Sci.*, vol. 9, no. 3, pp. 209-231, 2014.

[151] D Sokołowski, "Stochastic finite element method reliability analysis of the corrugated I-beam girder under corrosion or fire," Lodz University of Technology, Lodz, Master Thesis 2015.

[152] H Ho and L T Drzal, "Evaluation of interfacial mechanical properties of fiber reinforced composites using the micro-indentation method," *Compos. Part A Appl-S.*, vol. 27, pp. 961-971, 1996.

[153] G Zavarise, P Wriggers, E Stein, and B A Schrefler, "A numerical model for thermomechanical contact based on microscopic interface laws," *Mech. Res. Comm.*, vol. 19, pp. 173-182, 1992.

[154] A Z Khurshudyan, "The meso-scale behavior of anisotropic particle-reinforced

thermo-elastic composites," *Continuum Mech. Thermodyn.*, vol. 33, no. 1, pp. 1-12, 2021.

[155] S Chang, S J Chao, and Y Chang, "Estimates of elastic moduli for granular material with anisotropic random packing structure," *Int. J. Sol. Struct.*, vol. 32, pp. 1989-2008, 1995.

[156] Y Benveniste, "The effective mechanical behavior of composite material with imperfect contact between the constituents," *Mech. Mater.*, vol. 4, pp. 197-208, 1985.

[157] S Firooz and A Javili, "Understanding the role of general interfaces in the overall behavior of composites and size effects," *Comp. Mater. Sci.* , vol. 162, pp. 245-254, 2019.

[158] J Lamon, "Interfaces and interphases," in *Ceramic matrix composites: Fiber reinforced ceramics and their applications*, W Krenkel, Ed. Weinheim, Germany: Wiley, 2008, pp. 169-179.

[159] D Sokołowski and M Kamiński, "Homogenization of carbon/polymer composites with anisotropic distribution of particles and stochastic interface defects," *Acta Mech.* , vol. 229, pp. 3727–3765, 2018.

[160] C Soize, "Tensor-valued random fields for meso-scale stochastic model of anisotropic elastic microstructure and probabilistic analysis of representative volume element size," *Prob. Engrg Mech.*, vol. 23, pp. 307-323, 2018.

[161] B Yang, Y Hwang, and H Lee, "Elastoplastic modeling of polymeric composites containing randomly located nanoparticles with an interface effect," *Compos. Struct.* , vol. 99, pp. 123-130, 2013.

[162] H S Choi and J D Achenbach, "Stress states at neighboring fibers induced by single-fiber interphase defects," *Int. J. Sol. Struct.*, vol. 32, pp. 1555-1570, 1995.

[163] T Goudarzi, D W Spring, G H Paulino, and O Lopez-Pamies, "Filled elastomers: A theory of filler reinforcement based on hydrodynamic and interphasial effects," *J. Mech. Phys. Solids*, vol. 80, pp. 37-67, 2015.

[164] A B Meddeb, T Tighe, Z Ounaies, and O Lopez-Pamies, "Extreme enhancement of the nonlinear elastic response of elastomer nanoparticulate composites via interphases," *Compos. Part B-Eng.*, vol. 159, pp. 166-173, 2019.

[165] S M Paran et al., "To what extent can hyperelastic models make sense the effect of clay surface treatment on the mechanical properties of elastomeric nanocomposites?," *Macromol. Mater. Eng.*, vol. 302, no. 7, p. 1700036, 2017.

[166] M Qu et al., "Nanoscale visualisation and multiscale mechanical implications of bound rubber interphases in rubber-carbon black nanocomposites," *Soft Matter* , vol. 7, pp. 1066-1077, 2011.

[167] A Bismarck et al., "Development of novel composites through fibre and interface/interphase modification," *IOP Conference Series: Materials Science and Engineering*, p. 139, 2016.

[168] K Livanov, L Yang, A Nissenbaum, and D Wagner, "Interphase tuning for

stronger and tougher composites," *Sci. Rep.*, vol. 6, p. 26305, 2016.

[169] G Shang-Lin and E Mäder, "Characterization of interphase nanoscale property variation in glass fiber reinforced polypropylene and epoxy resin composites," *Compos. Part A Appl-S.*, vol. 33, no. 4, pp. 559-576, 2002.

[170] M Kamiński and M Kleiber, "Stochastic structural interface defects in fiber composites," *Int. J. Sol. Struct.*, vol. 33, pp. 3035-3056, 1996.

[171] A L Duigou, P Davies, and C Baley, "Exploring durability of interfaces in flax fibre/epoxy micro-composites," *Compos. Part A Appl-S.*, vol. 48, pp. 121-128, 2014.

[172] C Beckmann and J Hohe, "Effects of material uncertainty in the structural response of metal foam core sandwich beams," *Compos. Struct*, vol. 113, pp. 382-395, 2014.

[173] Y Koutsawa, A Karatrantos, W Yu, and D Ruch, "A micromechanics approach for the effective thermal conductivity of composite materials with general linear imperfect interfaces," *Compos. Struct.*, vol. 200, pp. 747-756, 2018.

[174] A F Whitehouse and T W Clyne, "Effects of reinforcement contact and shape on cavitation and failure in metal-matrix composites," *Compos.*, vol. 24, pp. 256-261, 1993.

[175] L Nazarenko, H Stolarski, and H Altenbach, "A statistical interphase damage model of random particulate composites," *Int. J. Plasticity*, vol. 116, pp. 118-142, 2019.

[176] K Reincke, W Grellmann, and G Heinrich, "Investigation of mechanical and fracture mechanical properties of elastomers filled with precipitated silica and nanofillers based upon layered silicates," *Rubber Chem. Techn.*, vol. 77, pp. 662-677, 2004.

[177] D Golansky, K Terada, and N Kikuchi, "Macro and micro scale modeling of thermal residual stresses in metal matrix composite surface layers by the homogenization method," *Comput. Mech.*, vol. 19, pp. 188-202, 1997.

[178] T Mura, *Micromechanics of defects in solids*. Dordrecht, Netherlands: Springer, 1987, ISBN 978-90-247-3256-2.

[179] Z Hashin, "Thermoelastic properties of fiber composites with imperfect interface," *Mech. Mat.*, vol. 8, no. 4, pp. 333-348, 1990.

[180] P S Theocaris, "Definition of interphase in composites.," in *The role of the polymeric matrix in the processing and structural properties of composite materials*, J C Seferis and L Nicolais, Eds. New York, USA, 1983.

[181] K Yanase and J Ju, "Effective elastic moduli of spherical particle reinforced composites containing imperfect interfaces," *Int. J. Damage Mech.* , vol. 21, pp. 97-127, 2012.

[182] J Wu-Gui, Z Ren-Zhi, H Quing, and T Yong-Gang, "Homogenized finite element analysis on effective elastoplastic mechanical behaviors of composite with imperfect interfaces," *Int. J. Mol. Sci.*, vol. 15, pp. 23389-23407, 2014.

[183] K Yanase and J Ju, "Overall elastoplastic damage responses of spherical particle-reinforced composites containing imperfect interfaces," *Int. J. Damage Mech.*, vol. 23, no. 3, pp. 411-429, 2014.

[184] Z Hashin, "The spherical inclusion with imperfect interface conditions," *J. Appl. Mech.*, vol. 58, pp. 444-449, 1991.

[185] Z Hashin, "Thin interphase/imperfect interface in elasticity with application to coated fiber composites," *J. Mech. Phys. Solids*, vol. 50, no. 12, pp. 2509-2537, 2002.

[186] A D Jesson and J F Watts, "The interface and interphase in polymer matrix composites: effect on mechanical properties and methods for identification," *Polymer Rev.*, vol. 52, pp. 321-354, 2012.

[187] S Ruchevskis and J Reichhold, "Effective elastic constants of fiber-reinforced polymer-matrix composites with the concept of interphase," *Scientific Proceedings of RTU, section Architecture and Construction Science*, pp. 148-161, 2002.

[188] D Sokołowski and M Kamiński, "Computational homogenization of carbon/polymer composites with stochastic interface defects," *Compos. Struct.*, vol. 183, pp. 434-449, 2018.

[189] N D Barulich, L A Godoy, and P M Dardati, "A computational micromechanics approach to evaluate elastic properties of composites with fiber-matrix interface damage," *Compos. Struct.*, vol. 154, pp. 309-318, 2016.

[190] J C Schellekens and R De Borst, "The application of interface elements and enriched or rate-dependent continua to micro-mechanical analyses of fracture in composites," *Comput. Mech.* , vol. 14, pp. 68-83, 1994.

[191] M A Gutierrez and R de Borst, "Numerical analysis of localization using a viscoplastic regularization: influence of stochastic material defects," *Int. J. Num. Meth. Engrg.*, vol. 44, pp. 1823-1841, 1999.

[192] S Gehant, C Fond, and R Schirrer, "Criteria for cavitation of rubber particles: Influence of plastic yielding in the matrix," *Int. J. Fract.*, vol. 122, pp. 161-175, 2003.

[193] M E Gurtin, *An introduction to continuum mechanics*. Pittsburhg, Pennsylvania: Academic press, 1982.

[194] I G Kevrekidis et al., "Equation-free, coarse-grained multiscale computation: Enabling microscopic simulators to perform system-level analysis," *Commun. Math. Sci.*, vol. 1, pp. 715-762, 2003.

[195] D Jeulin and M Ostoja-Starzewski, Eds., *Mechanics of random and multiscale structures*. Wien, Austria: Springer, 2001.

[196] E Saavedra Flores, F Diaz Delao, M Friswell, and J Sienz, "A computational multi-scale approach for the stochastic mechanical response of foam-filled honeycomb cores," *Compos. Struct.* , vol. 94, no. 5, pp. 1861-1870, 2012.

[197] H J Bungartz and M Griebel, "Sparse grids," *Acta Numer.*, vol. 13, pp. 147-269,

2004.

[198] C Garcia-Cervera, W Ren, and J Lu, "Sequential multiscale modeling using sparse representation," *Commun. Comput. Phys.*, vol. 4, pp. 1025-1033, 2008.

[199] C C Tasan et al., "Strain localization and damage in dual phase steels investigated by coupled in-situ deformation experiments and crystalplasticity simulations," *Int. J. Plasticity*, vol. 63, pp. 198–221, 2014.

[200] F Roters et al., "Overview of constitutive laws, kinematics, homogenization and multiscale methods in crystal plasticity finite-element modeling: Theory, experiments, applications," *Acta Materialia*, vol. 58, pp. 1152–1211, 2010.

[201] G Cusatis, R Rezakhani, M Alnaggar, Z Zhou, and D Pelessone, "Multiscale computational models for the simulation of concrete materials and structures," in *Proceedings of EURO-C 2014, Computational Modelling of Concrete and Concrete Structures*, N Bicanic et al., Eds.: CRC Press/Taylor & Francis Group, 2014, pp. 23-38.

[202] P Kanouté, D P Boso, J L Chaboche, and B A Schrefler, "Multiscale methods for composites: A review," *Comput. Method Eng.*, vol. 16, no. 1, pp. 31-75, 2009.

[203] A Brandt, "Scientific computation: Review," in *Multiscale and multiresolution methods: Theory and applications, Yosemite Educational Symposium Conf. Proc.*, T J Barth, Ed.: Springer, 2001, ch. 20, pp. 3-96.

[204] E Weinan and B Engquist, "The heterogeneous multi-scale methods," *Commun. Math. Sci.*, vol. 1, pp. 87-133, 2003.

[205] A I Ruban, *Fluid dynamics part 2: Asymptotic problems of fluid dynamics*. Oxford, England: Oxford U Press, 2015.

[206] J Kevorkian and J D Cole, *Perturbation methods in applied mathematics*. New York, USA: Springer, 1981.

[207] J Zhao, H Li, G Cheng, and Y Cai, "On predicting the effective elastic properties of polymer nanocomposites by novel numerical implementation of asymptotic homogenization method," *Compos. Struct.*, vol. 135, pp. 297-305, 2015.

[208] V I Arnold, *Geometrical methods in the theory of ordinary differential equations*. New York, USA: Springer, 1983.

[209] C Woźniak and E Wierzbicki, *Averaging techniques in thermomechanics of composite solids: tolerance averaging versus homogenization*. Częstochowa, Poland: Technical University of Czestochowa Publisher, 2000.

[210] V Kushnevsky, O Morachkovsky, and H Altenbach, "Identification of effective properties of particle reinforced composite materials," *Comput. Mech.* , vol. 22, pp. 317-325, 1988.

[211] H Spohn, *Large scale dynamics of interacting particles*. New York, USA: Springer, 1991.

[212] R Zwanzig, "Collision of a gas atom with a cold surface," *J. Chem. Phys. 1960*, vol. 32, pp. 1173-1177, 1960.

[213] K G Wilson and J Kogut, "The renormalization group and the ε expansion," *Phys. Rep.*, vol. 12, pp. 75-200, 1974.

[214] Z Hashin and S Shtrikman, "A variational approach to the theory of the elastic behaviour of multiphase materials," *J. Mech. Phys. Solids*, vol. 11, pp. 127–140, 1963.

[215] A Bensoussan, J L Lions, and G Papanicolaou, *Asymptotic analysis for periodic structures*. Amsterdam: North-Holland, 1978.

[216] J Fish and W Chen, "Higher order homogenization of initial boundary value problem," *J. Engrg. Mech.*, vol. 127, no. 12, pp. 1223–1230, 2001.

[217] S Ghosh, K Lee, and S Moorthy, "Multiple scale analysis of heterogeneous elastic structures using homogenization theory and Voronoi cell finite element method," *Int. J. Sol. Struct.*, vol. 32, pp. 27-62, 1995.

[218] M Kamiński, *Computational mechanics of composite materials*, 1st ed. London, England: Springer, 2005.

[219] G Somoh, R Toumi, J Renard, and M Monin, "Statistical approach of elastic properties of continuous fiber composite," *Compos. Struct.* , vol. 119, pp. 287-297, 2015.

[220] G W Milton, *The theory of composites*. Cambridge, England: Cambridge University Press, 2002.

[221] S Y Fu, B Lauke, and Y W Mai, *Science and engineering of short fibre reinforced polymer composites*. Boca Raton, Florida: CRC Press, 2009.

[222] E Sanchez-Palencia, *Non-homogeneous media and vibration theory*. Berlin, Germany: Springer-Verlag, 1980.

[223] J D Eshelby, "The determination of the elastic field of an ellipsoidal inclusion, and related problems," *Proc. Math. Phys. Eng. Sci.*, vol. 241, pp. 376–396, 1957.

[224] B A Le, J Yvonnet, and Q He, "Computational homogenization of nonlinear elastic materials using neural networks," *Int. J. Numer. Meth. Eng.*, vol. 104, no. 12, pp. 1061-1084, 2015.

[225] H Shin, J Choi, and M Cho, "An efficient multiscale homogenization modeling approach to describe hyperelastic behavior of polymer nanocomposites," *Compos. Sci. Technol.*, vol. 175, pp. 128-134, 2019.

[226] C C Mei and B Vernescu, *Homogenization methods for multiscale mechanics*. USA: World Scientific, 2010.

[227] J Seguardo and J Llorca, "A numerical approximation to the elastic properties of sphere-reinforced composites," *J. Mech. Phys. Solids*, vol. 50, pp. 2107-2121, 2002.

[228] F Fritzen and T Böhlke, "Periodic three-dimensional mesh generation for particle reinforced composites with application to metal matrix composites," *Int. J. Sol. Struct.*, pp. 706-718, 2011.

[229] G Chen, A Bezold, and C Broeckmann, "Influence of the size and boundary

conditions on the predicted effective strengths of particulate reinforced metal matrix composites (PRMMCs)," *Compos. Struct.*, vol. 189, pp. 300-339, 2018.

[230] T Kanit, S Forest, I Galliet, V Mounoury, and D Jeulin, "Determination of the size of the representative volume element for random composites: Statistical and numerical approach," *Intl J. Solids Struct.*, vol. 40, no. 13-14, pp. 3647-3679, 2003.

[231] D Savvas, G Stefanou, and M Papadrakakis, "Determination of RVE size for random composites with local volume fraction variation," *Comp. Meth. Appl. Mech. Eng.*, vol. 305, pp. 340-358, 2016.

[232] M Majewski, M Kursa, P Holobut, and K Kowalczyk-Gajewska, "Micromechanical and numerical analysis of packing and size effects in elastic particulate composites," *Compos. Part B-Eng.*, vol. 124, pp. 158-174, 2017.

[233] M Ostoja-Starzewski, "Scale effects in plasticity of random media: status and challenges," *Int. J. Plast.*, vol. 21, pp. 1119-1160, 2005.

[234] C L Kuang and G Anindya, "Validity of random microstructures simulation in fiber-reinforced composite materials," *Compos. Part B-Eng.*, vol. 57, pp. 56-70, 2014.

[235] D Pivovarov, "On periodic boundary conditions and ergodicity in computational homogenization of heterogeneous materials with random microstructure," *Comput. Method Appl. Mech. Eng.* , vol. 357, p. 112563, 2019.

[236] P Betsch, F Gruttmann, and E A Stein, "4-node finite shell element for the implementation of general hyperelastic 3D-elasticity at finite strains," *Comput. Method. Appl. Mech. Eng.*, vol. 130, no. 1-2, pp. 57-79, 1996.

[237] M A Bessa et al., "A framework for data-driven analysis of materials under uncertainty: Countering the curse of dimensionality," *Comput. Method. Appl. Mech. Eng.*, vol. 320, pp. 633-667, 2017.

[238] Z Liu and C T Wu, "Exploring the 3D architectures of deep material network in data-driven multiscale mechanics," *J. Mech. Phys. Solids.*, vol. 127, pp. 20-46, 2019.

[239] Z Liu, C T Wu, and M A Koishi, "A deep material network for multiscale topology learning and accelerated nonlinear modeling of heterogeneous materials," *Comput. Method. Appl. Mech. Eng.*, vol. 345, pp. 1138-1168, 2018.

[240] S Bhattacharjee and K Matous, "A nonlinear manifold-based reduced order model for multiscale analysis of heterogeneous hyperelastic materials," *J. Comput. Phys.*, vol. 313, pp. 635–653, 2016.

[241] J Yvonnet and Q He, "The reduced model multiscale method (R3M) for the non-linear homogenization of hyperelastic media at finite strains," *J. Comput. Phys.*, vol. 223, no. 1, pp. 341-368, 2007.

[242] J Yvonnet, E Monteiro, and Q C He, "Computational homogenization method and reduced database model for hyperelastic heterogeneous structures," *Int. J. Multiscale Com.*, vol. 11, no. 3, pp. 201-225, 2013.

[243] C T Wu and M Koishi, "Three-dimensional meshfree-enriched finite element formulation for micromechanical hyperelastic modeling of particulate rubber composites," *Int. J. Numer. Meth. Eng.*, vol. 91, pp. 1137–1157, 2012.

[244] N Triantafyllidis and E C Aifantis, "A gradient approach to localization of deformation. I. Hyperelastic materials," *J. Elasticity*, vol. 16, no. 3, pp. 225-237, 1986.

[245] T De Geus, J Vondrejc, J Zeman, R Peerlings, and M Geers, "Finite strain fft-based non-linear solvers made simple," *Comput. Method. Appl. Mech. Eng.*, vol. 318, pp. 412–430, 2017.

[246] J C Michel and P Suquet, "Computational analysis of nonlinear composite structure using the non-uniform transformation field analysis," *Comput. Meth. Appl. Mech. Engrg*, vol. 193, pp. 5477-5502, 2004.

[247] W Ehlers and S Bidier, "From particle mechanics to micromorphic media. Part I: Homogenisation of discrete interactions towards stress quantities," *Int. J. Solids Struct.*, vol. 187, pp. 23-37, 2018.

[248] Z P Huang and J Wang, "A theory of hyperelasticity of multi-phase media with surface/interface energy effect," *Acta Mech.*, vol. 182, no. 3-4, pp. 195-210, 2006.

[249] M Jahanshahi, H Ahmadi, and A R Khoei, "A hierarchical hyperelastic-based approach for multi-scale analysis of defective nano-materials," *Mech. Mat.*, vol. 140, p. 103206, 2020.

[250] A Masud and T J Truster, "A framework for residual-based stabilization of incompressible finite elasticity: Stabilized formulations and F methods for linear triangles and tetrahedra," *Comput. Method. Appl. Mech. Eng.*, vol. 267, pp. 359-399, 2013.

[251] P Bisegna and R Luciano, "Bounds on the overall properties of composites with debonded frictionless interfaces," *Mech. Mater.*, vol. 28, no. 1-4, pp. 23-32, 1998.

[252] M Dai, P Schiavone, and C F Ga, "Neutral nano-inhomogeneities in hyperelastic materials with a hyperelastic interface model," *Int. J. Nonlin. Mech.* , vol. 87, pp. 38-42, 2016.

[253] X Wang and P Schiavone, "Harmonic three-phase circular inclusions in finite elasticity," *Continuum Mech. Therm.*, vol. 27, no. 4-5, pp. 739-747, 2015.

[254] X Wang and P Schiavone, "Neutral coated circular inclusions in finite plane elasticity of harmonic materials," *Eur. J. Mech. A-Solid.*, vol. 33, pp. 75-81, 2012.

[255] J Ma, S Sahraeem, P Wriggers, and L De Lorenzis, "Stochastic multiscale homogenization analysis of heterogeneous materials under finite deformations with full uncertainty in the microstructure," *Comput. Mech.* , vol. 55, pp. 819-835, 2015.

[256] P Sasikumar, R Suresh, and S Gupta, "Stochastic model order reduction in uncertainty quantification of composite structures," *Compos. Struct.*, vol. 128, pp. 21-34, 2015.

[257] M Kamiński, "Sensitivity and randomness in homogenization of periodic fiber-

reinforced composites via the response function method," *Int. J. Sol. Struct.* , vol. 46, pp. 923-937, 2009.

[258] J Ma, I Temizer, and P Wriggers, "Random homogenization analysis in linear elasticity based on analytical bounds and estimates," *Int. J. Sol. Struct.* , vol. 48, pp. 280-291, 2011.

[259] M Kamiński, "Gaussian uncertainty in homogenization of rubber-carbon black nanocomposites," *Compos. Struct.*, vol. 113, no. 1, pp. 225-235, 2014.

[260] M Kamiński and B Lauke, "Parameter sensitivity and probabilistic analysis of the elastic homogenized properties for rubber filled polymers," *CMES: Comput. Model. Eng. Sci.*, vol. 93, no. 6, pp. 411-440, 2013.

[261] M Kamiński and B Lauke, "Probabilistic homogenization of polymers filled with rubber particles," *Comput. Mat. Sci.*, vol. 82, pp. 483-496, 2014.

[262] M Kamiński, "Multiscale homogenization of n-component composites with semi-elliptical random interface defects," *Int. J. Sol. Struct.*, vol. 42, pp. 3571-3590, 2005.

[263] D Sokołowski and M Kamiński, "Stochastic homogenization of polymeric composites with randomly ellipsoidal reinforcement," in *Presentations at the 9th ICCM2018*, G R Liu and P Trovalusci, Eds. Rome, Italy: ScienTech Publisher, 2018, ch. 3180, pp. 184-197.

[264] D Sokołowski and M Kamiński, "Probabilistic homogenization of hyper-elastic particulate composites with random interface," *Compos. Struct.*, vol. 241, p. 112118, 2020.

[265] D Sokołowski, M Kamiński, and A Wirowski, "Energy fluctuations in the homogenized hyper-elastic particulate composites with stochastic interface defects," *Energies*, no. 13, p. 20112020, 2020.

[266] M Kamiński, "A generalized stochastic perturbation technique for plasticity problems," *Comput. Mech.*, vol. 45, no. 4, pp. 349-361, 2010.

[267] M Kamiński, "Potential problems with random parameters by the generalized perturbation-based stochastic finite element method," *Comput. Struct.*, vol. 88, pp. 437-445, 2010.

[268] M Rabenda and M Kamiński, "Dual probabilistic analysis of the transient heat transfer by the stochastic finite element method with optimized polynomial basis," *J. Civil Eng. Env. Arch.*, vol. 64, pp. 211-225, 2017.

[269] J Szafran and M Kamiński, "Bridges for pedestrians with random parameters using the stochastic finite elements analysis," *Int. J. Appl. Mech. Eng.*, vol. 22, no. 1, pp. 175–197, 2017.

[270] D L Allaix and V I Carbone, "An improvement of the response surface method," *Struct. Saf.*, vol. 33, no. 2, pp. 165-172, 2011.

[271] M R Rajashekhar and B R Ellingwood, "A new look at the response surface approach for reliability analysis," *Struct. Saf.*, vol. 12, pp. 205-220, 1993.

[272] F Jurecka, M Ganser, and K U Bletzinger, "Update scheme for sequential spatial

correlation approximations in robust design optimization ," *Comp. Struct.*, vol. 85, no. 10, pp. 606-614, 2007.

[273] T W Simpson, J D Peplinski, P N Koch, and J K Allen, "Metamodels for computer based engineering design: Survey and recommendations," *Eng. Comput.*, vol. 17, pp. 129-150, 2001.

[274] N Draper and H Smith, *Applied regression analysis*. New York, USA: Wiley, 1998.

[275] R H Myers and D C Montgomery, *Response surface methodology, process and product optimization using designed experiments*, 2nd ed. New York, USA: Wiley, 2002.

[276] U Alibrandi, N Impollonia, and G Ricciardi, "Probabilistic eigenvalue buckling analysis solved through the ratio of polynomial response surface," *Comput. Meth. Appl. Mech. Eng.*, vol. 199, pp. 450-464, 2010.

[277] D Settineri and G Falsone, "An APDM-based method for the analysis of systems with uncertainties," *Comput. Meth. Appl. Mech. Eng.*, vol. 278, pp. 828-852, 2014.

[278] M Kamiński and M Strąkowski, "On sequentially coupled thermo-elastic stochastic finite element analysis of the steel skeletal towers exposed to fire," *Eur. J. Mech. - A/Solid.*, vol. 62, pp. 80-93, 2017.

[279] B Pokusiński and M Kamiński, "Lattice domes reliability by the perturbation-based approaches vs. semianalytical method," *Comput. Struct.*, vol. 221, pp. 179-192, 2019.

[280] G B Dantzig, "Maximization of a linear function of variables subject to linear inequalities," in *Activity analysis of production and allocation*. London, England: Wiley & Chapman-Hall, 1951, pp. 339-347.

[281] M J Panik, "The dual simplex, primal-dual, and complementary pivot methods," in *Linear programming: mathematics, theory and algorithms. Applied optimization*. Boston, USA: Springer, 1996.

[282] G B Dantzig, *Linear programming and extensions*. Princeton, USA: Princeton University Press, 1963.

[283] C E Lemke, "The dual method of solving the linear programming problem," *Nav. Res. Logist. Q.*, vol. 1, pp. 36-47, 1954.

[284] I I Dikin, "Iterative solution of problems of linear and quadratic programming," *Sov. Math., Dokl.*, vol. 8, pp. 674-675, 1967.

[285] J J H Forrest and J A Tomlin, "Vector processing in simplex and interior methods for linear programming," *Ann. Oper. Res.*, vol. 22, pp. 71-100, 1990.

[286] N L Boland, "A dual-active-set algorithm for positive semi-definite quadratic programming," *Math. Programming*, vol. 78, pp. 1-27, 1997.

[287] N I M Gould and P L Toint, "An iterative working-set method for large-scale non-convex quadratic programming," *Appl. Numer. Math.*, vol. 43, pp. 109-128, 2002.

[288] R D C Monteiro and I Adler, "Interior path following primal-dual algorithms, Part II: Convex quadratic programming," *Math. Program.*, vol. 44, pp. 43-66, 1989.

[289] R J Vanderbei, "LOQO: an interior-point code for quadratic programming," *Optim. Methods Soft.*, vol. 11, no. 1-4, pp. 451-484, 1999.

[290] M H Wright , "Interior methods for constrained optimization," *Acta Numer.*, vol. 1, pp. 341 - 407, 1992.

[291] P E Gill, W Murray, D B Ponceleón, and M A Saunders, "Solving reduced KKT systems in barrier methods for linear and quadratic programming," Department of Operations Research, Stanford University, Stanford, Report SOL 91-7, 1991.

[292] P E Gill, W Murray, M A Saunders, J A Tomlin, and M H Wright, "On projected Newton barrier methods for linear programming and an equivalence to Karmarkar's projective method," *Math. Program.*, vol. 36, pp. 183-209, 1986.

[293] A V Fiacco, "Barrier methods for nonlinear programming," in *Operations research support methodology*. New York, USA: Marcel Dekker, 1979, pp. 377–440.

[294] W Murray, "Analytical expressions for the eigenvalues and eigenvectors of the Hessian matrices of barrier and penalty functions," *J. Optim. Theory Appl.*, vol. 7, pp. 189–196, 1971.

[295] S A Vavasis, *Nonlinear optimization: Complexity issues*. Oxford, England: Oxford University Press, 1991.

[296] C Wu and X C Tau, "Augmented Lagrangian method, dual methods, and split Bregman iteration for ROF, vectorial TV, and high order models," *SIAM J. Imag. Sci.*, vol. 3, no. 3, pp. 330-339, 2010.

[297] R Rockafellar and J Tyrrel, "Augmented Lagrange multiplier functions and duality in nonconvex programming," *SIAM J. Control*, vol. 12, no. 2, pp. 268-285, 1974.

[298] A Forsgren, P E Gill, and M H Wright, "Interior methods for nonlinear optimization," *SIAM Review*, vol. 44, no. 4, pp. 525-597, 2002.

[299] M Diehl, H J Ferreau, and N Haverbeke, "Efficient numerical methods for nonlinear MPC and moving horizon estimation," *Lect. Notes Control. Inf. Sci*, vol. 384, pp. 391-417, 2009.

[300] L S Lasdon, A D Waren, A Jain, and M Ratner, "Design and testing of a generalized reduced gradient code for nonlinear programming," *ACM Trans. Math. Softw.*, vol. 4, no. 1, pp. 34-50, 1978.

[301] L S Lasdon, R L Fox, and R W Ratner, "Nonlinear optimization using the generalized reduced gradient method," *Rev. Fr. Autom. Inf. Rech. Oper.*, vol. 8, pp. 73-103, 1974.

[302] G A Gabriele and K M Ragsdell, "The generalized reduced gradient method: A reliable tool for optimal design," *J. Manuf. Sci. Eng.*, vol. 99, no. 2, pp. 394-400, 1977.

[303] K Takamizawa and K Hayashi, "Strain energy density function and uniform strain

hypothesis for arterial mechanics," *J. Biomech.*, vol. 20, pp. 7–17, 1987.

[304] S Hartmann and P Neff, "Polyconvexity of generalized polynomial-type hyperelastic strain energy functions for near-incompressibility," *Int. J. Sol. Struct.*, vol. 40, pp. 2767–2791, 2003.

[305] P Steinmann, M Hossain, and G Possart, "Hyperelastic models for rubber-like materials: consistent tangent operators and suitability for Treloar's data," *Arch. Appl. Mech.*, vol. 82, pp. 1183–1217, 2012.

[306] M Kamiński and B Lauke, "Probabilistic and stochastic aspects of rubber hyperelasticity," *Meccanica*, vol. 53, pp. 2363-2378, 2018.

[307] S I Ranganathan and M Ostoja-Starzewski, "Scaling function, anisotropy and the size of RVE in elastic random polycrystals," *J. Mech. Phys. Solids*, vol. 56, pp. 2773-2791, 2008.

[308] L Lussardi and A Manzin, "Homogenization of random anisotropy properties in polycrystalline magnetic materials," *Physica B* , vol. 407, pp. 1417-1419, 2012.

[309] R Stocki, *Reliability optimization of bar structures for lage displacements - theory and computer program (in Polish)*. Warsaw, Poland: Institute of Fundamental Technological Research Polish Academy of Sciences, 1999.

[310] M Van Dyke, *Perturbation methods in fluid mechanics*. California, USA: Academic Press, 1975.

[311] B Rogowski and M Kamiński, *Technical mechanics (in Polish)*. Łódź, Poland: Lodz University of Technology Publisher, 2009.

[312] M Shinozuka and F Yamazaki, *Stochastic finite element analysis, an introduction. Stochastic structural dynamics*. Amsterdam, Holand: Elsevier, 1988.

[313] B Sudret and A Der Kiureghian, *Stochastic finite element methods and reliability. A state-of-the-art report*. Berkley, England: Department of Civil and Environmental Engineering, University of California, 2000.

[314] K J Bathe, *Finite element procedures*. New York, USA: Prentice-Hall, 1996.

[315] A Nayfeh, *Perturbation methods*. New York, USA: Wiley, 1973.

[316] E J Hinch, *Cambridge texts in applied mathematics: perturbation methods*. Cambridge, USA: Cambridge University Press, 1991.

[317] E W Swokowski, *Calculus with analytic geometry*, 2nd ed. Boston, USA: Prindle, Weber & Schmidt, 1979.

[318] W Feller, *An introduction to probability theory and its applications*. New York, USA: Wiley, 1965.

[319] K Kottegoda and R Rosso, *Applied statistics for civil and environmental engineers*. Chichester, England: Blackwell, 2008.

[320] E Vanmarcke, *Random fields: Analysis and synthesis*. Cambridge, England: MIT Press, 1983.

[321] N V Smirnov and I V Dunin-Barkovskii, *Mathematical statistics in technics (in German)*. Germany: Verlag Wissenschaft, 1969.

[322] M Kamiński and B Lauke, "Probabilistic and stochastic analysis of the effective properties for the particle reinforced elastomers," *Comput. Mat. Sci*, vol. 56, pp. 147-160, 2012.

[323] M Kamiński and J Szafran, "Random eigenvibrations of elastic structures by the response function method and the generalized stochastic perturbation technique," *Arch. Civ. Mech. Eng.*, vol. 9, no. 4, pp. 5-32, 2009.

[324] M Solecka, M Kamiński, and J Szafran, "Comparison of the aluminium versus steel telecommunication towers in stochastic finite element method eigenvibrations analysis," *Int. J. Mech. Eng.*, vol. 15, no. 1, pp. 95-110, 2011.

[325] M Kamiński, "On iterative scheme in determination of the probabilistic moments of the structural response in the stochastic perturbation-based finite element method," *Int. J. Num. Meth. Engrg*, no. 104, p. 1038, 2015.

[326] D H Chung and W R Buessem, "The elastic anisotropy of crystals," *J. Appl. Phys.*, vol. 38, p. 5, 1967.

[327] C Haber, S Ruiz, and D Wirtz, "Shape anisotropy of a single random-walk polymer," *Proc. Nat. Acad. Sci.*, vol. 97, pp. 10792-10795, 2000.

[328] B Xia, H Lu, D Yu, and C Jiang, "Reliability-based design optimization of structural systems under hybrid probabilistic and interval model," *Comput. Struct.*, vol. 160, pp. 126-134, 2015.

[329] M Zhang, H Song, S Lim, M Akyiama, and D M Frangopol, "Reliability estimation of corroded RC structures based on spatial variability using experimental evidence, probabilistic analysis and finite element method," *Eng. Struct.*, vol. 192, pp. 30-52, 2019.

[330] X Q Peng, L Geng, W Liyan, G R Liu, and K Y Yam, "A stochastic finite element method for fatigue reliability analysis of gear teeth subjected to bending," *Comput. Mech.*, vol. 21, pp. 253-261, 1998.

[331] G Falsone, "An extension of the Kazakov relationship for non-Gaussian random variables and its use in the non-linear stochastic dynamics," *Prob. Eng. Mech.*, vol. 20, pp. 45-56, 2005.

[332] M Kamiński, "On the dual iterative stochastic perturbation-based finite element method in solid mechanics with Gaussian uncertainties," *Int. J. Num. Mech. Engrg*, vol. 104, pp. 1038-1060, 2015.

[333] B Xia, D Yu, and J Liu, "Transformed perturbation stochastic finite element method for static response analysis of stochastic structures," *Finite Elem. Anal. Des.*, vol. 79, pp. 9-21, 2014.

[334] H G Kilian, "A molecular interpretation of the parameters of the van der Waals equation of state for real networks," *Polymer Bulletion*, vol. 3, pp. 151-158, 1980.

[335] H G Kilian, "Equation of state of real networks," *Polymer*, vol. 22, no. 2, pp. 209-217, 1981.

[336] H G Kilian, H F Enderle, and K Unseld, "The use of the van der Waals model to elucidate universal aspects of structure-property relationships in simply extended

dry and swollen rubbers," *Colloid Polym. Sci.*, vol. 264, pp. 866-876, 1986.

Norms, catalogues, websites

[N1] PN-EN 1990, *Basis of structural design* (in Polish). Polish Standardization Committee, Warsaw, 2004.

[N2] PN-EN 1993-1-1: 2006 *Eurocode 3: Design of steel structures - Part 1-1: General rules and rules for buildings* (in Polish). Polish Standardization Committee, Warsaw, 2006.

[N3] PN-EN 1993-1-8: *2006 Eurocode 3: Design of steel structures - Part 1-8: Design of joints* (in Polish). Polish Standardization Committee, Warsaw, 2006.

[N4] PN-EN 1993-2: 2010 *Eurocode 3: Design of steel structures - Part 2: Steel bridges* (in Polish). Polish Standardization Committee, Warsaw, 2006.

[N5] http://www.icams.de/content/research/.

[N6] https://www.educative.io/edpresso/overfitting-and-underfitting.

[N7] https://classes.engineering.wustl.edu/2009/spring/mase5513/abaqus/docs/v6.6/books/ stm/default.htm?startat=ch03s02ath61.html.

Figure captions

List of selected notations and abbreviations

$(.)^0$ – mean value of variable $(.)$

$(.)^{eff}$ – effective property/function of the composite

$(.)^{exact}$ – exact measure of variable $(.)$, usually referred here as discrete results at specific points

$(.)^m$ – property/function of the virgin homogeneous material

$(.)^{opt}$ – optimized value for variable $(.)$

$(.)'$ – $(.)$ property/tensor/vector obtained for the homogenized composite

$\dot{(.)}$ – time derivative of variable $(.)$

$a_{i,j}$ – j^{th} coefficient of polynomial for i^{th} effective material coefficient of the composite, different for each hyperelastic potential

a_n – quotient of each Taylor expansion term

$A(\vec{g})$ – 1-periodic coefficient

AB – Arruda-Boyce (constitutive model)

AM – analytical method

AMM – Augmented material model

APP – approximate methods, i.e. AMM or BPO

$\widetilde{A}$ – constant tensor coefficient

$\mathbf{b}$ – Finger tensor (section 3.1) or vector of independent variables (section 3.2)

b – some random variable (section 3.2)

$\mathbf{B}$, $B_{kl\alpha}$ – matrix of the shape functions spatial derivatives

BPO – bivariate polynomial

$\mathbf{C}$ – right Cauchy-Green deformation tensor

C – fourth order elasticity tensor with components C_{ijkl}

CB – carbon black

$C_{i,\xi}^{eff}$ – i^{th} effective material property of potential ξ – AB, MR or NH

$C_{i,\xi}^{int}$ – i^{th} material property of the interphase of potential ξ – AB, MR or NH

$C_{i,\xi}^{m}$ – i^{th} material property of the matrix of potential ξ – AB, MR or NH

$CORR(.)$ – correlation between discrete values of $(.)$ and its continuous

		approximation
CoV	–	coefficient of variation
C-S-H	–	calcium silicate hydrate
$\mathbf{D}$	–	deformation rate tensor
D	–	domain around the mean value of random variable
DDM	–	direct differentiation method
DOF	–	degree of freedom
$D_{\alpha j}$	–	coefficients for the polynomial bases of independent random variable b (in this study volume fraction of interface defects w)
$\mathbf{e}$	–	Eulerian strain tensor
$\mathbf{E}$	–	Langrangian strain tensor
$E(.)$	–	expected value of variable/function (.)
$E_{r,m,\xi}$	–	relative error for m^{th} approximation (FEM, AMM, BPO) for ξ potential
EXP	–	experimental results (section 6.3.3)
$\dot{\mathbf{E}}$	–	time derivative of Langrangian strain tensor
$f(b)$	–	function relating the objective function and random variable b
$f(b, \mathbf{x})$	–	function relating the objective function and random variable b and a vector of other variables $\mathbf{x}$ (random or not)
$\mathbf{F}$	–	deformation gradient
F_{x_i}	–	longitudinal deformation for i^{th} axis
FE	–	finite element
FEM	–	finite element method
FFT	–	fast Fourier transform
f_{ξ}^{U}	–	function of strain energy for ξ potential
$f_{\xi,k}^{\sigma}$	–	function of stress for ξ potential and k^{th} method (FEM, AMM, BPO)
$\mathbf{g}$	–	metric tensor
HDPU	–	high density polyurethane also referred directly as the Laripur LPR 5020
HDPU-CB	–	high density polyurethane reinforced with carbon black
ISPT	–	generalized iterative stochastic perturbation technique
I_i	–	i^{th} invariant of the right Cauchy-Green deformation tensor

$\mathbf{J}$ – derivative of response function for all coefficients $D_{\alpha j}$ (in section 3.2)

J – volumetric change with a reference to material configuration

$\mathbf{K}$ – arbitrary second order tensor

$K_{\alpha\beta}$ – composite global stiffness matrix for α, β indexing all degrees of freedom available in the RVE

$\mathbf{L}$ – velocity gradient

LP – linear programming

LSM – least squares method

M – number of realizations, for example MCS trials

MCS – Monte-Carlo simulation

MR – Mooney-Rivlin (constitutive model)

$\mathbf{N}$, $N_{k\alpha}$ – shape functions

NH – neo-Hookean (constitutive model)

NP – nonlinear programming

$p(b)$ – probability density function of b

PDEs – partial differential equations

PDF – probability density function

QP – quadratic programming

r_i^n – i^{th} radii of n^{th} defect

$R_{(i,j)}$ – Gaussian distribution radius of defects

R3M – reduced model multiscale method

R_n – rest for n^{th} expansion of Taylor function

RFM – response function method

$RMS(.)$ – sum of square errors between discrete values of (.) and its continuous approximation

RSE – representative surface element

RSM – response surface method

RVE – Representative Volume Element

s – order of polynomial

S – weighted residuals functional

$\mathbf{S}$ – second Piola-Kirchhoff stress tensor

$\dot{\mathbf{S}}$ – time derivative of second Piola-Kirchhoff stress tensor

SAM – semi-analytical method

SBEM – stochastic boundary element method

SD – standard deviation also referred as σ in chapter 3

SFEM – stochastic finite element method

SSE – sum of square errors

SPT – stochastic perturbation technique

$\dot{\mathbf{S}}$ – time derivative of the second Piola-Kirchhoff stress tensor

$\mathrm{tr}(.)$ – traction of (.)

TPU – thermoplastic polyurethane

$\mathbf{u}$ – displacement vector

$\mathbf{u}(w)$ – structural response under uncertain variable w

U – strain energy

$U_{iso}^{(.)}$ – isochoric part of strain energy of (.) phase

$U_{v}^{(.)}$ – volumetric part of strain energy of (.) phase

U_{ξ}^{int} – strain energy of the interphase computed for ξ potential (NH, MR or AB)

U_{ξ}^{m} – strain energy of the matrix computed for ξ potential (NH, MR or AB)

$U_{\xi}^{eff,k}$ – effective strain energy of the composite computed for ξ potential (NH, MR or AB) and with use of the k^{th} method (FEM or one of approximations AMM, BPO)

U_{ξ}^{p} – strain energy of the reinforcement computed for ξ potential (NH, MR or AB)

$\mathrm{V}^{(.)}$ – volume of (.) phase

V^{d} – volume of the defects

$\mathrm{V}^{\mathrm{int}}$ – volume of the interphase

V^{m} – volume of the matrix

$\mathrm{VAR}(.)$ – variance between discrete values of (.) and its continuous approximation

w – volume fraction of interface defects, called also the weakening coefficient, an input Gaussian (random) variable

WLSM – weighted least squares method

w.r.t. – with relation to

W_{ξ}^{m} – elastic potential of the virgin homogeneous material according to potential ξ

$\mathbf{x}$ – spatial configuration

$\mathbf{X}$ – reference configuration

$\bar{x}_i^m$ – m^{th} global coordinate of the i-th node

$\alpha(.)$ – coefficient of variation of variable/function (.)

$\beta(.)$ – skewness of variable/function (.)

$\partial\Omega_{\sigma}$, $\partial\Omega_{u}$ – subsets of the outer faces of the given RVE

Δ_j – upper bound on statistical population of the defects radii

Δq_{β} – increment of displacements for β DOF

ΔQ_{α} – external nodal force increment

$\Delta\boldsymbol{\varepsilon}$ – increment of strain

$\boldsymbol{\varepsilon}$ – strain tansor

ε_l – normal strain of axis 1 at l^{th} level of stretch

ε_{ij} – component of strain tensor

ε – positive definite perturbation parameter

ζ_n – first n^{th} stochastic characteristics of the state variable or input variable (1 – expected value, 2 – coefficient of variation, 3 – skewness, 4 – kurtosis), for example ζ_n – expected value and coefficient of variation

$\kappa(.)$ – kurtosis of variable/function (.)

μm – micrometer

$\boldsymbol{\sigma}$ – Cauchy stress tensor

$\boldsymbol{\sigma}^0$ – Truesdell rate of Cauchy stress tensor

σ^d – unidirectional engineering stress of the defects

σ^{int} – unidirectional engineering stress of the interphase

σ^m – unidirectional engineering stress of the matrix

σ_{ξ}^{m} – unidirectional engineering stress of the matrix computed for ξ potential (AB, MR, NH) or ξ laboratory experiments (lab CB 0% or lab CB 5%)

$\sigma_{\xi,k}^{eff}$ – effective unidirectional engineering stress of the composite computed for ξ potential - AB, MR, NH and and with use of the k^{th} method (AMM, BPO)

$\boldsymbol{\tau}$ – Kirchoff stress tensor

λ – stretch ratio

λ_A^m – stretch at which polymer chain networks in matrix becomes locked in Arruda-Boyce constitutive model

μ_m – m^{th} central moment

v_ξ – polynomial coefficient for ξ potential

ξ^i – local normalized coordinate system, i=1,2,3

ξ_k^m – m^{th} global coordinate of the k^{th} node

Ω – full domain of the composite

$\Omega_{(.)}$ – subdomain of the composite

Ω_d – subdomain of the defects

Ω_i – subdomain of hyperelastic interphase

Ω_m – subdomain of hyperelastic matrix

Ω_p – subdomain of linear elastic reinforcing particles

∇ – gradient

$\Re$ – set of real numbers

Appendix A. Hyperelastic constitutive model of the matrix

In an initial phase of numerical experiments it was considered what type of potential to apply for the selected HDPU material to best reflect its uniaxial stretch curve. For this purpose, a single extended stretch was provided for the virgin homogeneous material of Laripur LPR 5020 (the same as in section 4). Its results are presented on Fig. A.1.

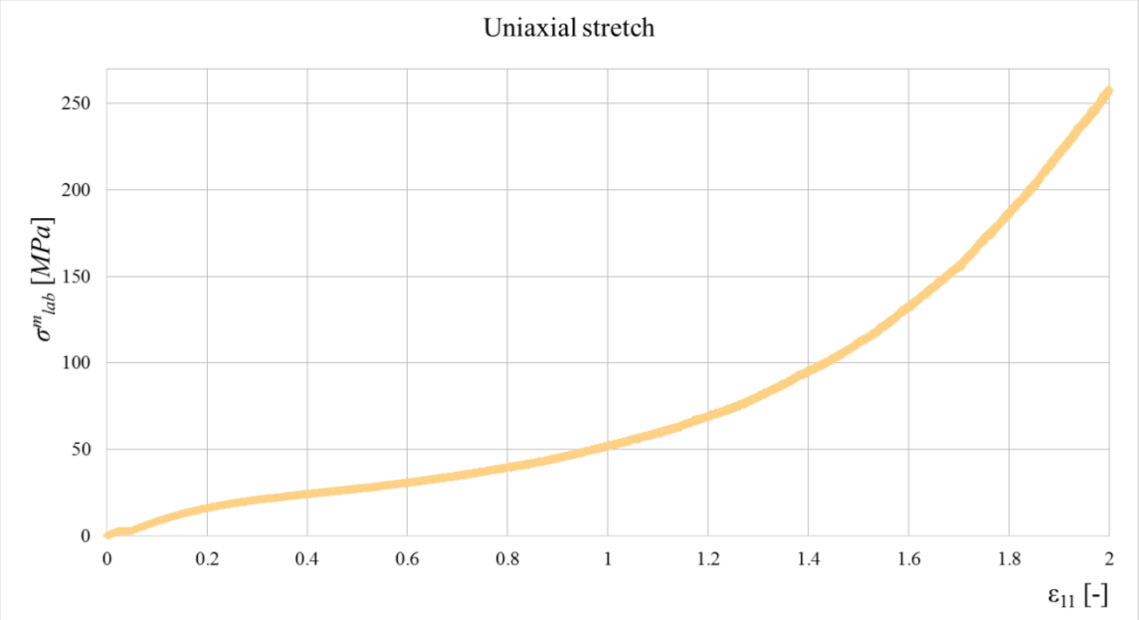

Fig. A.1 Initial stress-strain relation verification.

Course of this function represents a strain hardening typical for hyperelastic materials. Since no test bench for bi-axial or tri-axial test was available for the author, the final selection of the numerical model of the matrix was done among 10 commonly used isotropic hyperelastic potentials. They are following Mooney-Rivlin [46,47], Yeoh [50], Van der Waals [334,335,336], Neo-Hookean [48], reduced polynomial of rank 2 and finally polynomials of the rank 2 till rank 6. Elastic potential of these constitutive models is presented in Table A.1.

Potentials were optimized after the uniaxial stretch laboratory tests presented on Fig. 5.4. Firstly, a mean curve from laboratory tests was calculated and potentials fitted to this curve with use of the least squares method (LSM) with equal weights. Curve was aggregated from the expected values of the stress at each given strain level. They were determined by simple averaging $E[\sigma^m(\varepsilon_{11})]=\frac{1}{M}\sum_{i=1}^{M}\sigma^m(\varepsilon_{11})^{(i)}$; M indicates the number of realizations. It is equal to the number of samples in laboratory tests, which is 10.

Table A.1 Elastic potentials for the selected hyperelastic constitutive models of pure hyperelastic matrix.

Constitutive theory	***Elastic potential W***
Neo-Hookean	$W_{NH}^m = C_{NH}^m \left(I_1 - 3\right), C_{NH}^m = \frac{\mu}{2}$, I_1 – first invariant of the strain tensor, μ – shear modulus
Mooney-Rivlin	$W_{MR}^m = C_{1,\mathrm{MR}}^m \left(\bar{I}_1 - 3\right) + C_{2,\mathrm{MR}}^m \left(\bar{I}_2 - 3\right)$, $C_{1,\mathrm{MR}}^m, C_{1,\mathrm{MR}}^m$ - empirical material constants, $\bar{I}_1, \bar{I}_2$ - first and second invariants of the left Cauchy-Green deformation tensor
Arruda-Boyce	$W_{AB}^m = C_{1,\mathrm{AB}}^m \left\{ \frac{1}{2}\left(I_1 - 3\right) + \frac{1}{20\lambda_m^2}\left(I_1^2 - 9\right) + \frac{11}{5060\lambda_m^4}\left(I_1^3 - 27\right) + \right.$ $\left. + \frac{19}{7000\lambda_m^6}\left(I_1^4 - 81\right) + \frac{519}{673750\lambda_m^8}\left(I_1^5 - 243\right) \right\}$
Yeoh	$W_Y^m = C_{1,Y}^m \left(I_1 - 3\right) + C_{2,Y}^m \left(I_1 - 3\right)^2 + C_{3,\mathrm{Y}}^m \left(I_1 - 3\right)^3$, $C_{1,Y}^m, C_{2,Y}^m, C_{3,\mathrm{Y}}^m$ - material constants
Van der Waals	$W_{VW}^m = \mu \left\{ -\left(\lambda_m^2 - 3\right)\left(\ln\left(1-\theta\right) + \theta\right) - \frac{2}{3}\left(\frac{\tilde{\quad}}{2} \right)^3 \right\}$, $\theta = \sqrt{\frac{\tilde{\quad}}{\lambda_m^2 - 3}}, \tilde{\quad} \quad \left(1-\beta\right) I_2$, β - material parameter
Ogden	$W_O^m = \sum_{p=1}^{N} \frac{\mu_p}{\alpha_p}\left(\lambda_1^{\alpha_p} + \lambda_2^{\alpha_p} + \lambda_1^{-\alpha_p}\lambda_2^{-\alpha_p} - 3\right)$, N, μ_p, α_p – material constants

Optimization of potentials was done by minimization of total LSM error of their stress approximation for all strain levels probing all the material parameters available in each constitutive model. Then, response of this material in different tests, i.e. the bi-axial, pure and simple shear was verified and models with unphysical or questionable stress-

strain curve were eliminated. This was done because laboratory results for these tests were not available and optimized parameters of constitutive model specify entirely matrix behavior. Eliminated constitutive models were polynomial of the second and fourth order and also the Yeoh potential. At the end three best approximating constitutive models were determined by this procedure. They are Neo-Hookean with $C^m_{1,NH}$=1.875·10^7, Arruda-Boyce with parameters of $(\lambda^m_A$=7.00, $C^m_{1,AB}$=3.749·10$^7)$ and Mooney-Rivlin with $C^m_{1,MR}$=1.577·10^7 and $C^m_{2,MR}$=3.648·10^6. Three potentials were chosen instead of one to enable a cross-check of the results of deterministic and probabilistic analysis available in next sections.

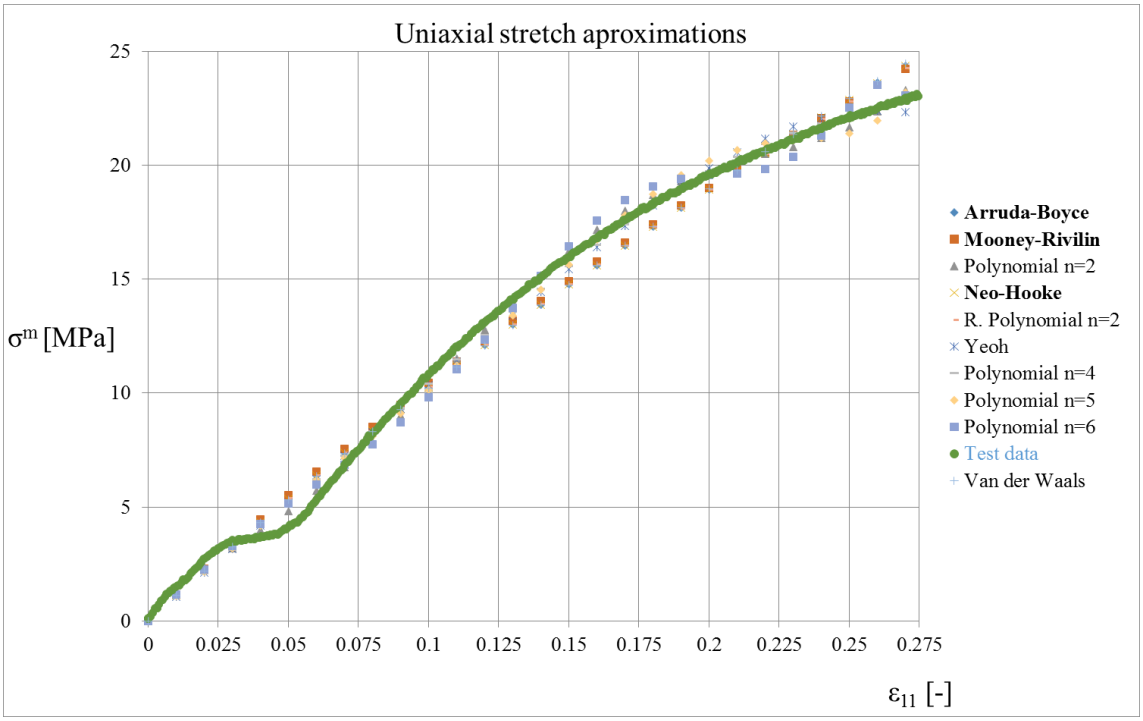

Fig. A.2 Stress approximations and the mean stress curve of the virgin homogeneous material coming from laboratory tests σ^m w.r.t. the uniaxial strain ε_{11}.

All the approximation curves are presented on Fig. A.2 together with the mean stress curve coming directly from the laboratory experiments $E(\sigma^m_{lab}(\varepsilon_{11}))$. On this graph they are marked with different symbols and colors. All potentials ensure a decent approximation of the test curve, especially for $\varepsilon_{11}\in(0.21, 0.26)$ and $\varepsilon_{11}\in(0.0, 0.026)$ corresponding to the matrix elastic range. A small overestimation of stresses is present for the highest strains $\varepsilon_{11}\in(0.26, 0.275)$ but it does not exceed 7% of the stresses in the experimental curve. All potential approximations monotonously increase together with an increase of the strain. Maximum stresses recovered for the three selected

potentials at ε_{11}=0.275 are following: $\sigma^m_{MR}(\varepsilon_{11}=0.275)$=24.58 MPa, $\sigma^m_{AB}(\varepsilon_{11}=0.275)$=24.75 MPa and $\sigma^m_{NH}(\varepsilon_{11}=0.275)$=24.74 and maximum stress of the experimental curve $E\left(\sigma^m(\varepsilon_{11})\right)$ equals to 23.12 MPa. The most precise potential approximation for this extreme strain is ensured by polynomial of the 4th order (difference less than 0.8%, $\sigma^m_{P,4th}(\varepsilon_{11}=0.275)$=22.93 MPa). Some degree of local softening is observed in the experimental curve for $\varepsilon_{11}\in(0.03, 0.07)$. It was not reproduced by the potentials. Recovery of the precise approximation of stress at this region would require splitting the fitting to several regions, using additional parameters in the existing constitutive models or introducing a new potential specific for this matrix. Local effect does not undermine a good overall fitting result, which was the primary goal of the optimization.

Appendix B. Optimization procedure of the response function

The response function used for approximation of the effective composite properties is each time optimized according to the following procedure

- solution of the cell problem solved via the FEM in the domain of $(\varepsilon_{11},w)_{\xi}$ around nine expected values of w $E(w)\in[0.1,\ 0.2,\ \ldots\ 0.9]$ in their 10% vicinity, separately for each selected hyperelastic potential indexed by ξ
- determination of the optimum pairs of effective composite properties and the volume fraction of interface defects $\left(C^{eff}_{i,\xi},w\right)$ with use of linear regression. Optimization is performed with a condition of a minimum total square error of the approximate strain energy $\sum_{k=1}^{n}\left(\sum_{j=1}^{m}\left(U^{eff}_{j,k,\xi}-U^{eff,APP}_{j,k,\xi}\left(C^{eff}_{i,j,k,\xi},w_j,\varepsilon_{11,k}\right)\right)^2\right)=\min$. Each discrete FEM realization serves for calculation of a pair $\left(C^{eff}_{i,\xi},w\right)$
- determination of the continuous representation of the effective material parameters w.r.t. the volume fraction of interface defects $C^{eff}_{i,\xi}(w)$ called further response function; fitting is done with full polynomials of rank 1 till 20. Their coefficients are calculated using the weighted least squares method (WLSM) algorithm with equal weights according to equations included in section 3.2.1
- a triple optimization process minimizing the WLSM RMS error, WLSM variance and maximizing the WLSM correlation.

A triple optimization process aims at finding the lowest possible rank of the polynomial, whose further increase does not significantly improve the correlation, RMS error and variance with respect to the discrete results. Such an approach is applied to exclude overfitting, yet providing a very good approximation of the discrete results. In this approach firstly all ranks with correlation worse than 0.999 are eliminated and then a threshold of 0.1 relative change of *RMS* error and variance is applied so that

$$CORR_{\mathrm{m_{opt}}}\left(C^{eff}_{n,MR}\right)>0.999,$$

$$RMS_{\mathrm{m+1}}\left(C^{eff}_{n,MR}\right)-RMS_{\mathrm{m}}\left(C^{eff}_{n,MR}\right)<0.1, \tag{B.1}$$

$$VAR_{\mathrm{m+1}}\left(C^{eff}_{n,MR}\right)-VAR_{\mathrm{m}}\left(C^{eff}_{n,MR}\right)<0.1,$$

where m denotes the polynomial rank; change of estimators is calculated from the higher to the lower rank. This first step is suitable for prevention of underfitting, but a further visual verification must be applied after its application to eliminate overfitting (as mentioned in section 3.2.2); it must be noted, however, that it is almost always eliminated by introduction of the last criterion of selecting the lowest polynomial rank.

An exemplary optimization process is presented next on the basis of the coefficients for the Mooney-Rivlin potential. It is visualized on the below Figures. They show the weighted least squares RMS error denoted as *RMS*, variance denoted by *VAR* and correlation denoted by *CORR* for both effective material parameters for this constitutive models; they are $C^{eff}_{1,MR}$ (Fig. B.1) and $C^{eff}_{2,MR}$ (Fig. B.2). On these graphs the right vertical axis measures the correlation of the approximating polynomial of the rank m that is presented on the horizontal axis; the left vertical axis marks a relative difference between the RMS and VAR for the polynomial of rank m relative to polynomial with the best results ($RMS_{\min}$, $VAR_{\min}$) so that

$$RMS\left(C^{eff}_{n,MR}\right)=\frac{RMS_{\mathrm{m}}\left(C^{eff}_{n,MR}\right)}{RMS_{\min}\left(C^{eff}_{n,MR}\right)},VAR\left(\mathrm{C^{eff}_{n,MR}}\right)=\frac{VAR_{\mathrm{m}}\left(C^{eff}_{n,MR}\right)}{VAR_{\min}\left(C^{eff}_{n,MR}\right)} \tag{B.2}$$

Both of the graphs show that together with an increase of the rank of the polynomial the correlation *CORR* is only increasing and variance *VAR* together with the *RSM* error is only decreasing; this is valid up to the highest considered polynomial rank, which is 20. It is also visible that the difference of these values between the rank m and m − 1 also decreases together with an increase of m. Additionally, correlation of the response function to the discrete results *CORR* is much better than the considered threshold of 0.999 for polynomials of ranks above the 4th; the *CORR* also converges much before the *RMS* and *VAR*, which are still not very convergent for ranks as high as 15th. With such observations, the proposed approach of optimization may be swiftly verified. The optimized rank for $C^{eff}_{1,MR}$ is the 9th; it is marked by blue horizontal line on Fig. B.1. Its correlation is already almost 0.9999 and both, the *RMS* and *VAR* are less than 10%

worse than for the best fitting polynomial. Interestingly, the polynomials of the rank 11 and above already start to overfit the discrete results.

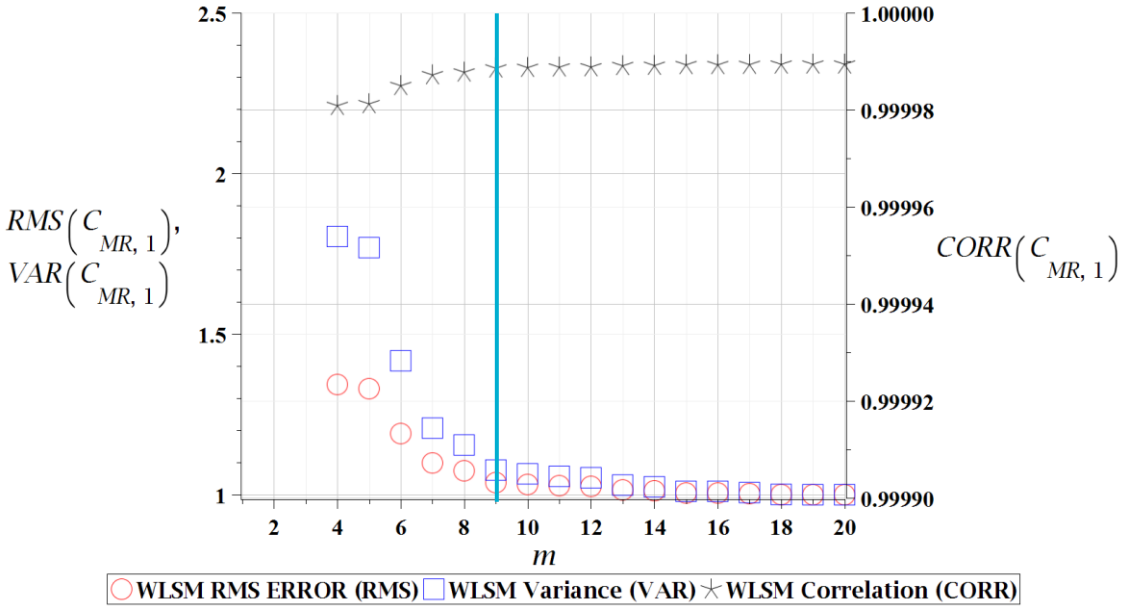

Fig. B.1 Selected plot of error of effective property approximation via the WLSM.

Situation is a little different for the $C^{eff}_{2,MR}$ presented on Fig. B.2. The optimized polynomial rank for this parameter is 8th, but the relative difference of VAR between this an the higher rank is 0.16, so it fails one of the proposed criteria. This rank is still selected because the polynomials from 9th rank and above already overfit the data. This exemplifies, that the strict mathematical criteria are the most objective but not always return the best solution and a human interaction may sometimes be required. An optimization procedure proposed above is applied for all the effective material coefficients that are presented in the next section. Their polynomial representation is further used in eqns (6.6) through (6.7) and (6.15) through (6.17) approximating the effective strain energy and the effective stress of the composite with stochastic interface defects.

The above results prove the Hypothesis 6 (b), because correlation of optimized polynomial to the discrete results is extremely close to 1 and also the WLSM variance of this approximation is low.

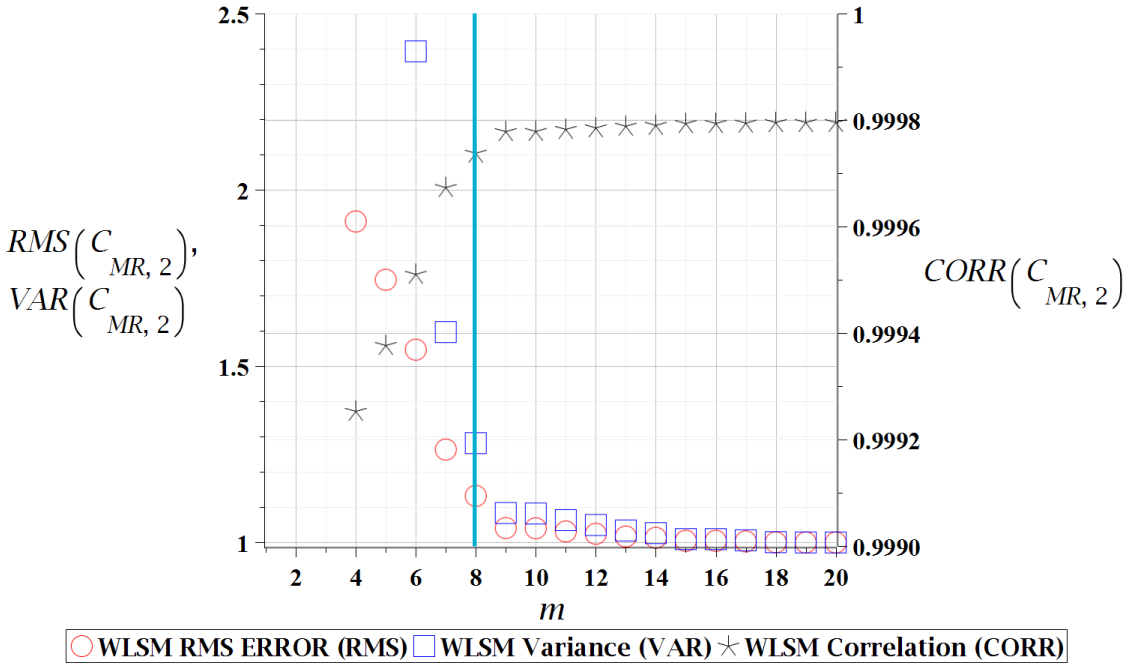

Fig. B.2 Selected plot of error of effective property approximation via the WLSM.

Appendix C. Optimization procedure of the response surface

The response surface is sought from a subset of bivariate polynomials. It is determined in three major steps, which are

1. solution of the cell problem solved via the FEM in the domain of $(\varepsilon_{11},w)_\xi$ around nine expected values of w $E(w)\in[0.1,\ 0.2,\ \dots\ 0.9]$ in their 10% vicinity, separately for each selected hyperelastic potential indexed by ξ
2. determination of the continuous representation of the effective strain energy w.r.t. the mean volume fraction of interface defects and the level of applied strain $U_\xi^{eff}(\varepsilon_{11},w)$ called further response surface; optimization problem is solved with use of the active-set method for full polynomials of rank 1 till 15. Their coefficients are calculated according to equations included in section 3.2.2
3. a double optimization problem to define the best rank of the bivariate polynomial used in further numerical experiments.

Similarly to the optimization applied on the effective material parameters, the double optimization problem consists of finding the lowest rank of polynomial that satisfies the minimum of sum of square errors (*SSE*) and maximum of correlation that does not overfit the discrete dataset. This is preferred over simple application of the very high rank polynomial with minimum SSE because optimization problem increases very quickly together with an increase of polynomial rank; this is also true for complexity of symbolical procedures applied in stochastic calculus. All the symbolic optimization procedures and calculations are programmed in algebra system MAPLE 2018 and are performed in floating point. The proposed approach proves to be suitable for this optimization problem and ensures a very high correlation and low *SSE* of approximation even for low rank polynomials. A selected graph showing the *SSE* and correlation of approximation to the discrete dataset is provided in Fig. C.1. It represents the Arruda-Boyce augmented model. Since the SSE is relatively high, a relative difference is plotted instead of the real error. This gives

$$SSE\left(U_{m,AB}^{eff}\right)=\frac{SSE_{\mathrm{m}}\left(U_{m,AB}^{eff}\right)}{SSE_{\min}\left(U_{m,AB}^{eff}\right)}, \tag{C.1}$$

where $SSE_{\min}\left(U^{eff}_{m,AB}\right)$=3180. A very high correlation of over 0.9999 is returned from optimization algorithm already for ranks above the 1st, but the SSE is 10^8 times bigger than the optimum rank. The sum of square error sharply decreases together with an increase of rank. It is true up to rank 8−9, where it stabilizes around 10 times over the minimum recovered for rank 13. Then it increases again due to a very high amount of decision variables. Please note, that this minimum *SSE* is very low in comparison to the maximum magnitude of strain energy of 10^6 (it represents a sum of 2079 square differences). This holds especially for ranks 9−15. Such relation was observed for all the three augmented material models. The overfit is observed usually at ranks 12 and above for all the selected constitutive models and flattening of the SSE curve begins at ranks 6−7. Taking it into consideration, a final rank selected for Arruda-Boyce augmented model is the 10th. Rank 11 was crossed out because of a relatively low improvement of fitting comparing to and additional computational effort for the stochastic experiments.

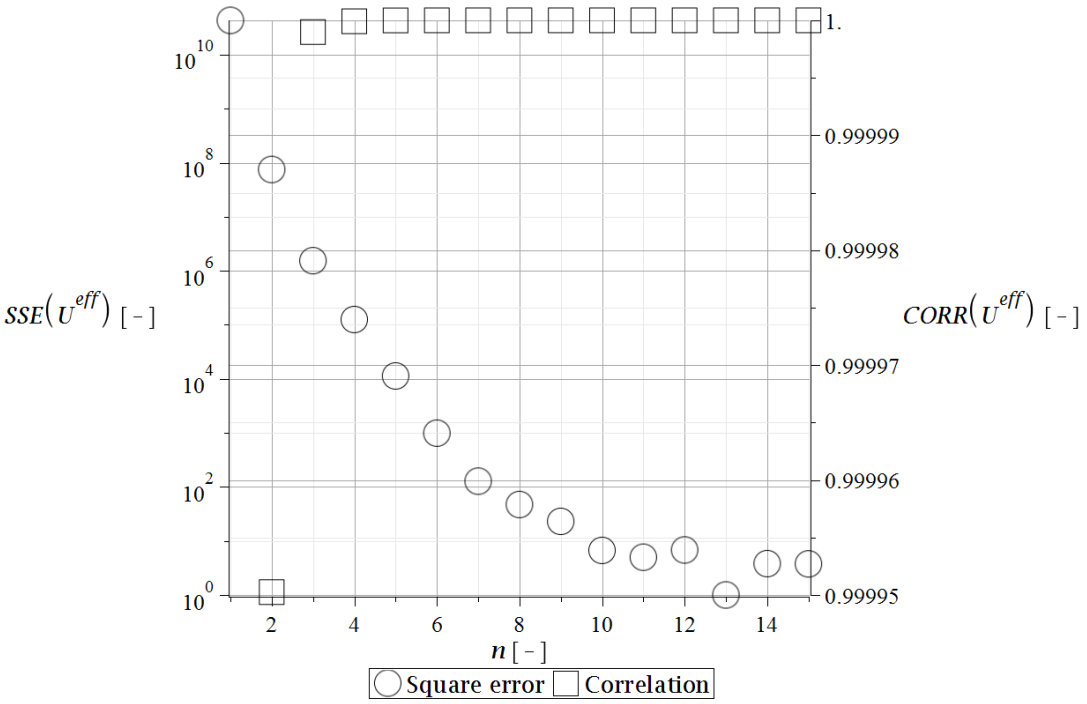

Fig. C.1 Selected sum of square error (*SSE*) and correlation (*CORR*) of the surface method approximation w.r.t. the bivariate polynomial rank.

Apart from a holistic convergence, an error inside the computation domain should also be analyzed. This is especially true for quantities like the effective strain energy, whose variation in strain is very high. In this study it ranges from 0 till over 10^6. In this case a

very small SSE may still allow for local inaccuracies that may be relevant for regions with small magnitudes. Such analysis is provided in section 6.2.2. It covers approximating error of the effective deformation energy for entire domain of the strain and volume fraction of interface defects.

Appendix D. Scheme of probabilistic homogenization algorithm

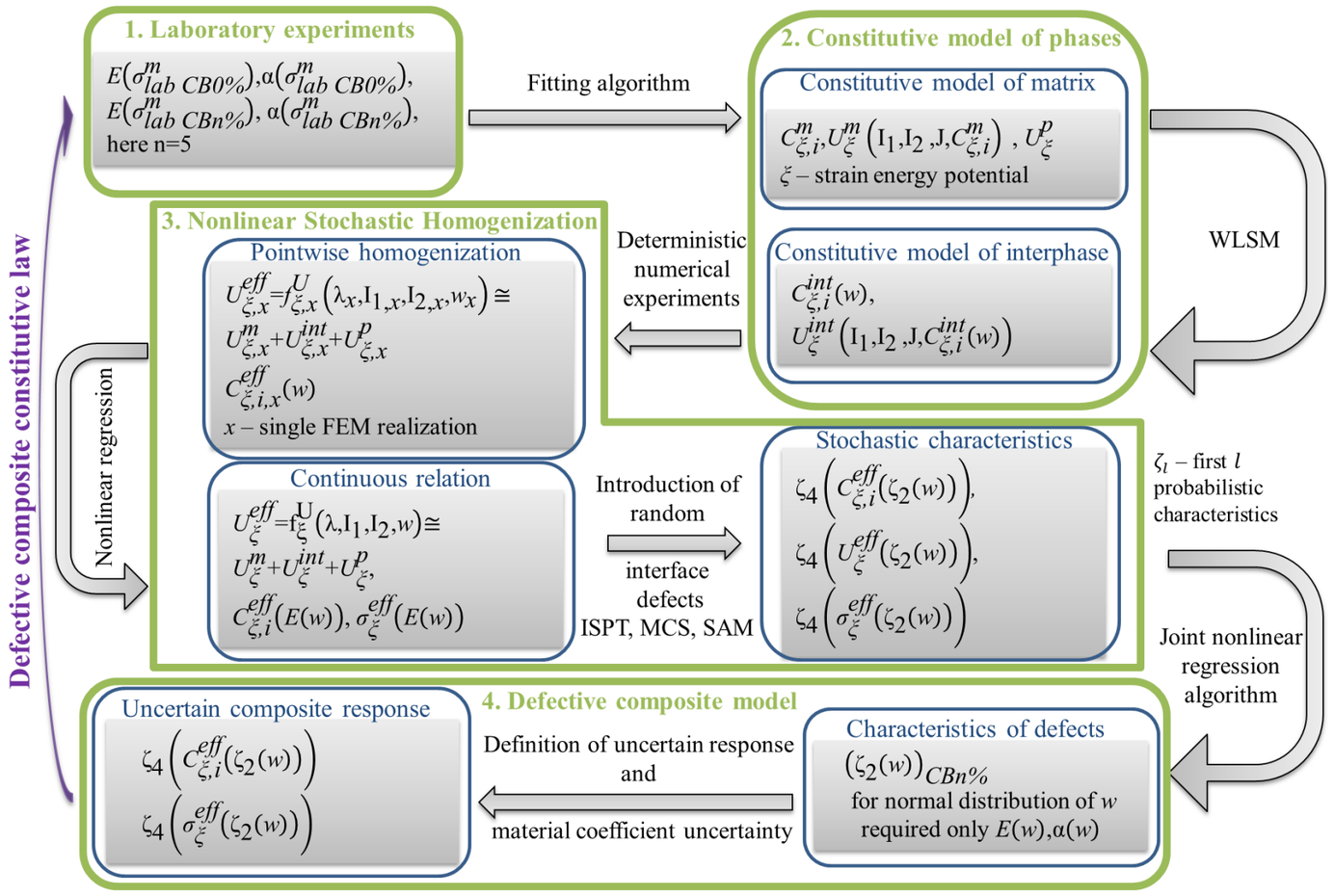

Fig. D.1 Scheme of probabilistic homogenization algorithm.